Università degli Studi di Padova

Dipartimento di Pediatria “Salus Pueri”

SCUOLA DI DOTTORATO DI RICERCA IN
MEDICINA DELLO SVILUPPO E SCIENZE DELLA PROGRAMMAZIONE
Indirizzo Ematooncologia, Immunologia e Genetica

CICLO XXIV

STUDY OF THE MECHANISM OF ACTION OF NEW MOLECULES ENDOWED WITH ANTITUMORAL ACTIVITY

Direttore della Scuola : Ch.mo Prof. Giuseppe Basso
Coordinatore d’indirizzo: Ch.mo Prof. Giuseppe Basso
Supervisore: Dott. Giampietro Viola

Dottoranda: Dott.ssa Roberta Bortolozzi

2009-2011

INDEX

RIASSUNTO

Nelle cellule eucariotiche i microtubuli costituiscono un elemento cruciale nella regolazione di molteplici processi cellulari, tra cui la proliferazione, la formazione del fuso mitotico, il mantenimento della forma cellulare, la regolazione della motilità, il signaling cellulare, i processi di secrezione e trasporto intracellulare. Il ruolo fondamentale di tale struttura citoscheletrica nella progressione mitotica e di conseguenza nella proliferazione cellulare rende i microtubuli un ottimo target per la terapia antitumorale. Molti composti aventi struttura chimica differente sono in grado di legare il sistema tubulina-microtubuli, alterandone la polimerizzazione e la dinamica, in particolare durante la fase mitotica del ciclo cellulare, destabilizzando l'organizzazione del fuso mitotico, ritardando o bloccando la transizione metafase-anafase.

In questo studio è stata valutata l'attività antiproliferativa di sette serie di nuovi inibitori della polimerizzazione della tubulina, derivati da 3 classi di composti che legano i microtubuli a livello del sito di legame della colchicina: combretastatina-A4, calconi e pirrolochinolinoni. In particolare, è stato studiato in modelli *in vitro* e *in vivo* l'effetto di tali inibitori sulla polimerizzazione della tubulina, sul ciclo cellulare e sull'attivazione dell'apoptosi per la descrizione di un possibile meccanismo d'azione. I composti testati hanno mostrato attività antiproliferativa comparabile o superiore rispetto ai composti di riferimento.

Per quanto riguarda il meccanismo d'azione, in generale, l'interazione di tali composti con la tubulina induce un blocco del ciclo cellulare in fase G2/M con l'aumento dell'espressione della ciclina B1 e la fosforilazione di Cdc25c. Tale arresto della progressione mitotica porta all'attivazione del processo apoptotico in modo tempo- e concentrazione- dipendente con la attivazione di caspase-3, il taglio proteolitico di PARP e la riduzione delle proteine Bcl-2 antiapoptotiche.

Inoltre, alcuni composti hanno mostrato elevata efficacia nell'indurre citotossicità in cellule tumorali *multidrug resistant,* esprimenti la glicoproteina-P e le pompe di efflusso MDR*,* resistenti a chemioterapici quali vinblastina, doxorubucina e tassolo.

Esperimenti preliminari, svolti in modelli murini di xenotrapianto, hanno mostrato una significativa riduzione della crescita tumorale, suggerendo una possibile applicazione clinica per alcuni dei composti studiati.

ABSTRACT

The microtubule system of eukaryotic cells is a critical element in a variety of fundamental cellular processes such as cell proliferation, mitotic spindle formation, maintenance of cell shape, regulation of motility, cell signaling, secretion, and intracellular transport. The important role of microtubules dynamic in mitosis progression and thus in cell proliferation, made them an attractive target for cancer therapy. Many chemically diverse compounds bind and affect tubulin-microtubule system, altering polymerization and dynamics during the particularly vulnerable mitotic stage of the cell cycle, causing alteration in the spindle organization with a delay or block at the metaphase-anaphase transition during mitosis.

In this study we evaluated the antiproliferative activity of seven series of novel tubulin polymerization inhibitors deriving from three classes of colchicine site binders: combretastatin-A4, chalcones and pyrroloquinolinones. Furthermore we investigated on the inhibitory effects on tubulin polimerization, cell cycle alteration, and apoptosis induction in *in vitro* and *in vivo* models and described a possible mechanism of action. The studied compounds, showed antiproliferative activity derived from a interference with microtubule assembly similar or higher than the reference compounds. As general mechanisms of action, the interaction of such compounds with tubulin, induces cell cycle arrest in the G2/M phase, with increased expression of cyclin B1 and phosphorylation of cdc25c, that trigger to apoptosis in a time- and concentration-dependent manner with activation of caspase-3 and cleavage of PARP and reduction of Bcl-2 prosurvival protein. Moreover, several compounds was effective against cancer cell lines, characterized by high expression of glycoprotein-P and multidrug resistance-associated protein, resistant to chemotherapy drugs such as vinblastine, doxorubucine and taxol.

Prelimary experiment carried out in vivo models of tumor xenograft showed a significative reduction of tumor growth suggesting a potential clinical applications for these compounds.

1. GENERAL INTRODUCTION

The microtubule system of eukaryotic cells is a critical element in a variety of fundamental cellular processes such as cell proliferation, mitotic spindle formation, maintenance of cell shape, regulation of motility, cell signaling, secretion, and intracellular transport. Their important role in mammalian cell have made them an attractive target for the development of drugs for different purpose such as antiparasitics, pesticides and anticancer drugs[1].

1.1. Microtubule structure and dynamic instability

Microtubules are heterodimerc dynamic structures composed by α- and β-tubulin monomers, and are one of the cytoskeleton structures. Every microtubule consists in 13 linear tubulin polymers, called protofilaments, assembled in hallow tubes approximately 24 nm in diameter, that radiate from the microtubule-organizing centre located in the centrosome[1].

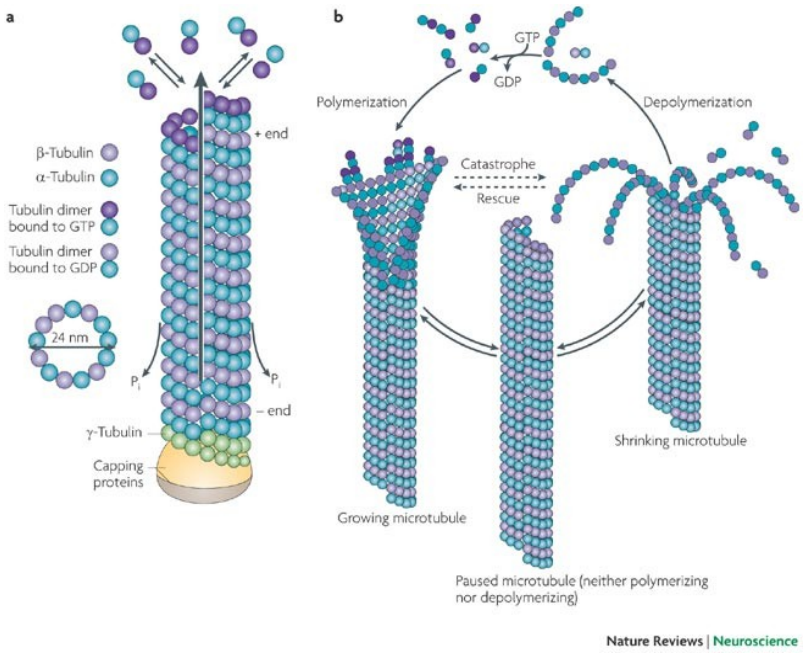

Figure 1.1- Microtubule assembly, organization and dynamics[2]

This cytoskeletal structure has a dynamic behavior known as “dynamic instability” in which microtubules alternate between period of growing and shrinking through the addition or removal of tubulin monomers. This process is mediated by hydrolysis of GTP: β-tubulin has binding site for GTP and microtubule stability depend on the rate of GTP/GDP-bound tubulin. If new GTP

molecules are added more rapidly than GTP is hydrolyzed, the microtubules retain a GTP-cap and growth continues. However, if the rate of polymerization is slow, GTP is hydrolyzed to GDP, GDP-bound tubulin dissociates resulting in a rapid depolymerization of microtubules[3].

Dynamic instability is one of the key events of the cell cycle: during interphase microtubules turnover is slow but becomes rapid at the onset of mitosis with the disassembly of microtubules network, followed by the formation of a new network of spindle microtubules, that can turover 4-100 times more rapidly than interphase microtubules[4].

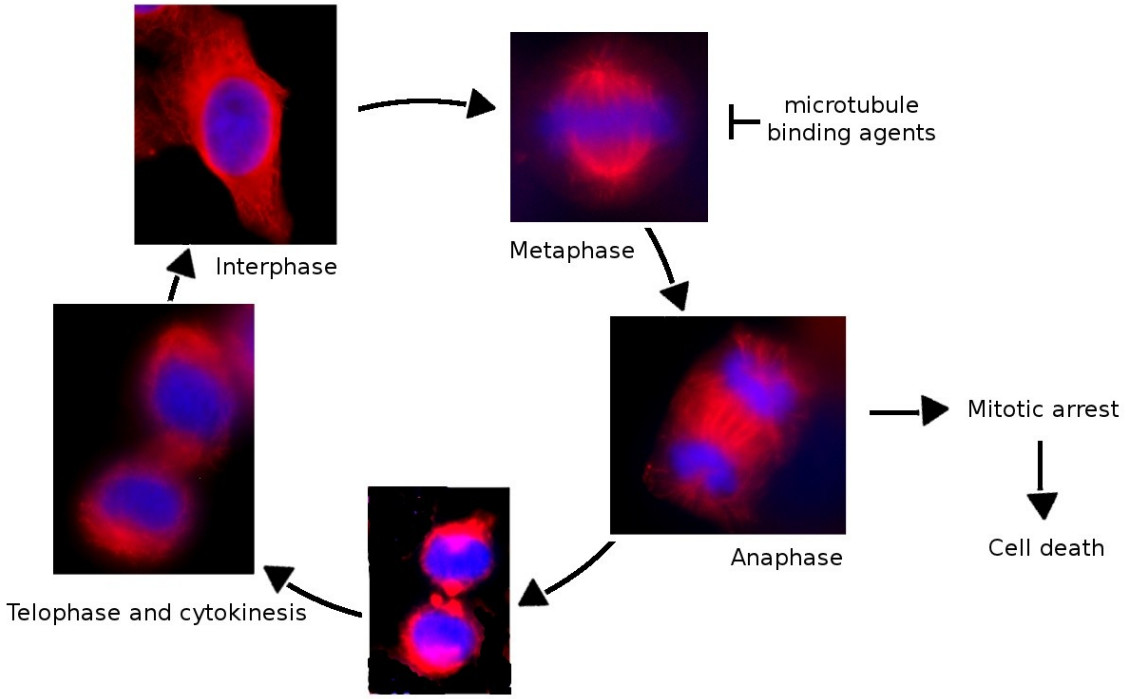

Figure 1.2 Microtubule dynamics during cell cycle progression: immunofluorescences images of HeLa cells stained with anti-β-tubulin antibody TRITC-conjugated and then observed by confocal microscopy.

The regulation of microtubules dynamics, temporal and spatial organization is a tightly regulated mechanisms to ensure the correct spindle formation and segregation of chromosomes during cell division. The main regulators of microtubules dynamics are the microtubule-sequestring protein stathmin (STMN) and microtubules-associated proteins (MAPs). Stathmin is a cytosolic phosphoprotein that regulates mitotic spindle by binding to tubulin heterodimers and inducing microtubule destabilization, while MAPs proteins can bind and stablize microtubules against depolymerization[4].

1.2. Drugs that target tubulin

Because the central role of microtubules dynamic in mitosis progression and thus in cell proliferation, drugs that affect microtubule assembly are important component in combination chemotherapy for the treatment of pediatric and adult cancer.

Many chemically diverse compounds, generally extracted from natural sources, bind and affect tubulin-microtubule system altering polymerization and dynamics during the particularly vulnerable mitotic stage of the cell cycle. Tubulin binding agents (TBAs) can be classified by the mechanism of action into microtubule-destabilizing (such as Vincristine, Vinblastine, Combretastatin-A4) and microtubule-stabilizing drugs (such as Taxanes and epothilones)[1,3,4].

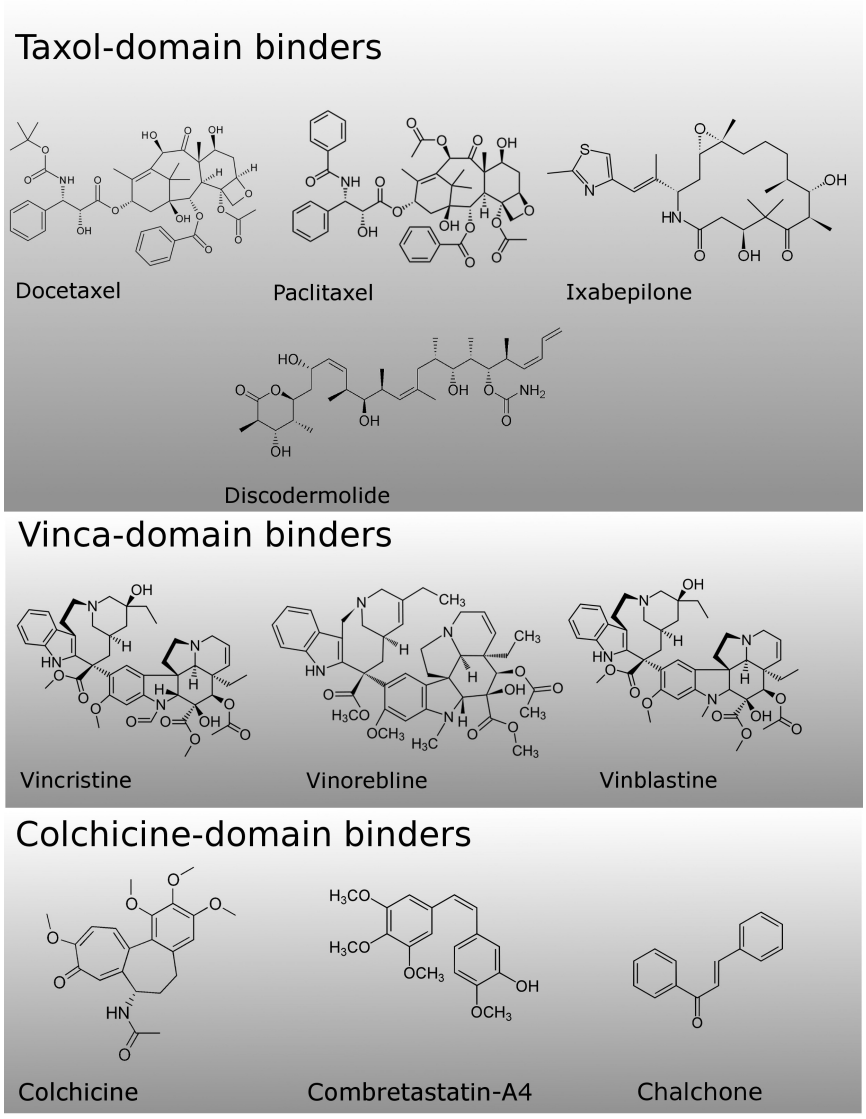

Figure 1.3 Molecular structure of tubulin-binding agents arranged according their binding domain.

Destabilizing agents inhibit microtubule polymerization and most of these agents bind in one of two tubulin domain: the vinca domain or the colchicine domain. Vinca-site binders include the vinca alkaloids, the cryptophycins and the dolastatins; colchicine-site binders include colchicine and its analogues, podophyllotoxin, combretastatins, 2-methoxyoestradiol, phenylahistins, steganacins and curacin.

Vinca alkaloids are used for treating several tumor types, in particular, Vincristine for Non-Hodgkin and Hodgkin lymphoma and certain pediatric cancers and Vinblastine is used for treating testicular, Hodgkin lymphoma, lung, head and neck, and breast cancer. Recently Vinorelbine was approved for the therapy of non small cell lung carcinoma[5].

Colchicine domain binders include Combrestastatin A-4 phosphate, which is in III phase clinical trial in combination with carboplatin for the treatment of anaplastic thyroid cancer, and in other II phase clinical trial as vascular-disrupting agent, and Obrabulin currently in Phase III clinical trials for the treatment of advanced-stage soft-tissue sarcoma[5].

The microtubule-stabilizing agents enhance microtubule polymerization and include taxanes, epothilones, discodermolide, eleutherobins, sarcoddictyns, certain steroids. Most of stabilizing agents bind to the taxoid binding site on β-tubulin located on the inside surface of microtubules[1].

Paclitaxel and docetaxel have been used clinically for many years for treating breast cancer, non small cell lung carcinoma and refractive prostate cancer. Recently Abraxane (a paclitaxel formulation) was approved for the treatment of patient with metastatic breast cancer[5].

Toxicity associated with vinka alkaloids members and each of the taxanes are similar with neutropenia and peripheral neuropathy[5].

1.3. Cytotoxicity of microtubule binding agent

Both classes of drugs suppress microtubule dynamics causing alteration in the spindle organization, with a delay or a block at the metaphase-anaphase transition during mitosis. The activation of spindle assembly checkpoint, and extended mitotic arrest can lead to cell death.

Several works describe that tubulin binding agents induce apoptosis mainly through the intrinsic pathway, and it has been demonstrated that suppression of

microtubule dynamics and alteration of mitochondrial parameters (such as alteration of membrane potential and ROS production) are two early and concomitant events. However, how cell death induction correlates with microtubule destabilization and mitotic arrest still remains unclear and controversial[6].

It has been demonstrated that many microtubules binding agents can induce phophorylation in serine residues of Bcl2 antiapoptotic proteins, in cell that are blocked in G2-M phase, leading to loss of prosurvival function and to destabilization of mitochondrial potential. Moreover Bcl2 phosphorylation decreases its binding to the proapoptotic Bax protein, resulting in an increase of free Bax and apoptosis. This event seems to be specifically linked to microtubule damage as drugs that induce cell death by different mechanisms do not induce Bcl-2 phosphorylation[7].

Wei et al have reported that Bcl-2 phosphorylation promotes the induction of autophagy by disrupting the Bcl-2/Beclin 1 complex, allowing Beclin1 to induce autophagy[8] and many studies associate activation of autophagic process as a protective mechanism against cell death induced by antimitotic agents[9].

Another cell death mechanisms associated with agents that affect microtubule dynamics, by hyperpolymerization, depolymerization or disturbing mitotic process, is “mitotic catastrophe”. Mitotic catastrophe has been described as an aberrant form of mitosis, characterised by multiple spindle assembly, missaggregation of chromosomes and the formation of giant cells. It is still unclear weather mitotic catastrophe is a mode of cell death or it’s a process that leads to apoptosis or necrosis[10].

1.4 Anti-angiogenic and vascular-disrupting effects

Many microtubule depolymerizing agents show vascular disrupting activity at non-toxic doses. Combretastatin A-4 phosphate is the lead microtubule binding agent with vascular disrupting activity and it is in phase II of clinical trials for cancer therapy. Preclinical studies have shown effectiveness of CA-4 in combination with traditional chemotherapeutic agents or radiotherapy. This strategy has as target endothelial cells which are non-tumor cells and thus less susceptible to the development of resistance of these class of drugs.

Vascular disrupting agents have a different behaviour compared to the classical

tubulin binding agents probably due to their instability and the reversibility of their binding to tubulin.[1]

1.5. Microtubules and drug resistance

Microtubule binding agents are selective for cancer cells due to the high rate of proliferation of these cells and their accelerated microtubule dynamics. However, many tumors and cancer cell lines show resistance to microtubule binding agents. Mechanisms of resistance to such agents include alteration in microtubule, drug efflux systems and deficiency in apoptotic signaling.

Drug efflux

The primary resistance system, developed by cancer cell exposed to microtubule-binding agents *in vitro,* is the expression on the cell surface of efflux pumps of the ATP binding cassette (ABC) family. The main transporter responsible of the reduced intracellular concentrations and cytotoxic activity of microtubule binding agents is P-glycoprotein (P-gp), the product of the MDR1 or ABCB1 gene. Moreover vinca alkaloids are actively transported by multidrug resistance-associate protein 1 (MRP1), taxanes are substrates for MRP2 and MRP7, and epothilone B for MRP7.[1]

Despite in many primary tumors the expression MDR protein correlates with a lower response to therapy with microtubule-binding agents, the clinical relevance of efflux pumps in cancer remains controversial[1].

The study and the development of new compounds insensitive to this mechanism of resistance is relevant also to target tumor of central nervous system where brain barrier is characterized by the presence of efflux pump.

Alteration in tubulin-microtubules complex

The efficacy of tubulin-binding agent can be influenced by target-based mechanisms of resistance such as quantitative or qualitative modifications of microtubules. Among them quantitative tubulin isotype composition of microtubules, mutation in tubulin, alteration in level, intracellular localizations, post-translational modification and function on microtubule associated proteins.[4]

Deficient apoptosis signalling

Many proteins involved in regulation of cell cycle and/or apoptosis directly interact with microtubules. Among them, p53 is associated with dynein, while Bcl-2 interact with survivin and other proteins that colocalize with microtubules.
It has been described that cancer cells with mutation in p53 are significantly more resistant to microtubule-targeted drugs (vinca alkaloids and taxanes) then cells with wild type p53. Furthermore has been reported that p53 regulates negatively MAP4 a microtubule-stabilizing protein, survivin, the microtubule-related inhibitor of apoptosis, and the microtubule-sequestring protein stathmin[11].
The overexpression of pro-survival Bcl-2 proteins in cancer cells increases the resistance to cytotoxic effect of tubulin binding compounds[12].
Moreover VanderWeele et al demonstrated Akt activation markedly increases resistance to microtubule-directed agents, including vincristine, colchicine, and paclitaxel. Akt also maintains increased glycolytic metabolism and survival in response to antimicrotubule treatment[13].

1.6. Colchicine domain binders

A **B**

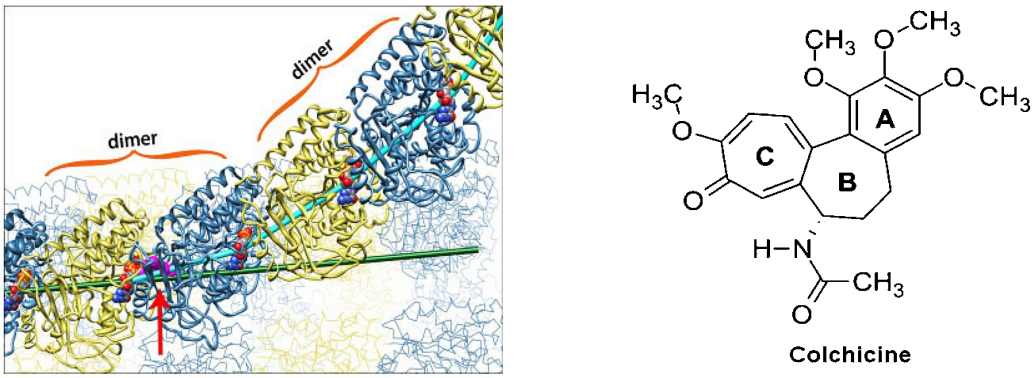

Figure 1.4 A Space filling model of colchicine binding site (highlighted with red arrow) the green axis shows direction of growth of a straight protofilament while the cyan axis connects nucleotides of a peeling protofilament[3] **B** Colchicine molecular structure.

The colchicine-binding site is located in the center of the tubulin dimer, at the interface of α- and β-tubulin monomers and lie in the lumen of the filament. Binding to the colchicine site is followed by a conformational change involving an intradimer bending, where the tubulin monomers undergo twisting around the interface causing the inhibition of the lateral contacts between

protofilaments inducing by this way the microtubule depolymerization[3].

Many microtubules targeting agents bind tubulin in colchicine site, among them combretastatins, chalcones and quinolones.

Colchicine has high affinity to its tubuling binding site, and in our works we used it as reference compound to evaluate the affinity of novel compounds to tubulin. In silico docking models suggest that combretastatin A4 and colchicine bind to β-tubulin in a similar orientation, whereas chalcones binding mode is different from colchicine.

Combretastatins

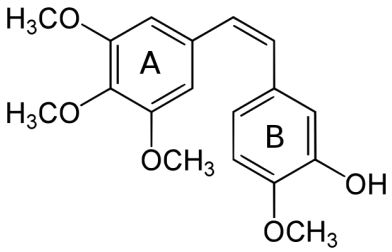

Figure 1.5- Combretastatin-A4 molecular structure

One of the most important antimitotic agents is combretastatin A-4 (CA-4). CA-4, isolated from the bark of the South African tree *Combretum caffrum,* is one of the well-known natural molecules that strongly inhibits tubulin polymerization by binding to the colchicine site. Combretastatin A-4 shows potent cytotoxicity against a wide variety of human cancer cell lines, including those that are multidrug resistant, and is lead compound as vascular disrupting agents probably by its effects on cytosckeleton of endothelial cells. A water-soluble disodium phosphate derivative of CA-4 (named CA-4P) has shown promising results in human cancer clinical trials, thus stimulating significant interest in a variety of CA-4 analogues.[14]

Combretastatin-A4 binds tubulin in the colchicine binding domain with high affiniy probably due to the cis-olefin configuration of the two ring. In addition the trimethoxy substitution in 3'-4'-5' position of A-ring were essential for optimal activity, while some B-ring structural modifications were tolerated by the target.[14]

The *cis*-configuration of CA-4 is prone to isomerize to the thermodynamically more stable *trans*-form during storage and metabolism, resulting in a dramatic decrease of the antitumor activity. [14]

Chalcones

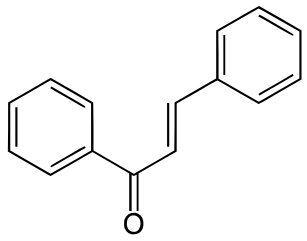

Figure 1.6- Chalcone molecular structure

Chalcones are another class of colchicine domain-binding agents. Chalcones were first isolated from ferns (Pityrogramma calomelanos) and multiple evergreen plants like Calythropsis aurea, Piper aduncum, Fissistigma lanuginosum from the myrtle, matico, and magnolia families, respectively. Chalcones are potent cytotoxic agents and are 300 times more potent than colchicine in arresting cell division thus they are strong antimitotic agents. They display rapid and reversible binding to the colchicine-binding site of β-tubulin at the interface with α-tubulin and cause inhibition of its assembly to microtubules.[3]

Quinolinones

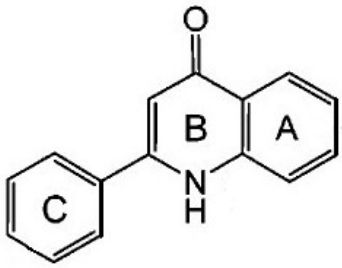

Figure 1.7- 2-phenyl-quinolones molecular structure

Quinolones and flavoquinolones was first identified as antimicrobial agents that inhibit the bacterial DNA gyrase or the topoisomerase II enzymes, blocking DNA replication and transcription. Recently it has been demonstrated the activity of quinolones as antimitotic agents and their effectiveness in inducing cell death in cancer cells lines, due to their ability to bind tubulin in colchicine binding site.

2-Phenylquinolin-4one derivatives are either natural or synthetic small molecules, structurally derived from flavone nucleus. 2-Phenylquinolinones show high antiproliferative activity by the inhibition of tubulin polimerization interacting with the colchicine binding site on tubulin. The presence of a three

ring A-B-C system in the molecular structure of phenyl quinolinones and colchicine, and the position of A and C rings, could explain their ability to bind to tubulin with high affinity in the same binding site.[15]

2. AIM OF THE STUDY

The aim of the study was to evaluate the antiproliferative activity of seven series of novel tubulin polymerization inhibitors deriving from three classes of colchicine site binders, synthesized on the basis of SAR study and molecular modeling; to investigate the inhibitory effects on tubulin polimerization, cell cycle alteration, and apoptosis induction *in vitro* and *in vivo* models, and describe a possible mechanism of action.

In particular, we present the SAR study and suggest the mechanisms of action of five series of combretastatin-A4 derivatives and one series of chalcone derivatives synthesized by Dott. Romagnoli from University of Ferrara, and two series of Pyrroloquinolinones synthesized by Dott.ssa Ferlin from University of Padova.

3. CHALCONE DERIVATIVES

Symmetrical alpha-bromoacryloylamido diaryldienone derivatives as a novel series of antiproliferative agents. Design, synthesis and biological evaluation. Romagnoli R, Baraldi PG, Cruz-Lopez O, Lopez Cara C, Carrion MD, Balzarini J, Hamel E, Basso G, Bortolozzi R, Viola G. **Bioorg Med Chem Lett. 2010 May 1;20(9):2733-9.**[16]

3.1. Symmetrical α-bromoacryloylamido diaryldienone derivatives as a novel series of antiproliferative agents. Design, synthesis and biological evaluation.

Romeo Romagnoli*[a], Pier Giovanni Baraldi[a], Olga Cruz-Lopez[a], Carlota Lopez Cara[a], Maria Dora Carrion[a], Jan Balzarini[b], Ernest Hamel[c], Giuseppe Basso[d], Roberta Bortolozzi[d] and Giampietro Viola[d]

[a]*Dipartimento di Scienze Farmaceutiche, Università di Ferrara, 44100 Ferrara, Italy;*

[b]*Rega Institute for Medical Research, Laboratory of Virology and Chemotherapy, B-3000 Leuven, Belgium;*

[c]*Screening Technologies Branch, Developmental Therapeutics Program, Division of Cancer Treatment and Diagnosis, National Cancer Institute at Frederick, National Institutes of Health, Frederick, Maryland 21702, USA*

[d]*Dipartimento di Pediatria, Laboratorio di Oncoematologia, Università di Padova, 35131 Padova Italy*

Abstract

In a continuing study of hybrid compounds containing the α-bromoacryloyl moiety as potential anticancer drugs, we synthesized a novel series of hybrids **4a-h**, in which this moiety was linked to a 1,5-diaryl-1,4-pentadien-3-one system. Many of the conjugates prepared (**4b**, **4c**, **4e** and **4g**) demonstrated pronounced, submicromolar antiproliferative activity against four cancer cell lines. Moreover, compound **4b** induced apoptosis through the mitochondrial pathway and activated caspase-3 in a concentration-dependent manner.

Results and discussion

Because of their ability to interact with cellular nucleophiles, Michael acceptors are often employed as a powerful tool in the design of anticancer agents.[1] The α,β-unsaturated carbonyl group is capable of undergoing Michael addition, and this moiety may be highly deleterious for malignant cells because it could interfere at multiple points in biological cascades through successive attacks on cellular nucleophiles.[2] Among the α,β-unsaturated ketones, enones and dienones derivatives, the chalcones[3] and the α,α'-bis(arylidene)ketones[4-7], are versatile pharmacophores belonging to the class of Michael acceptors. In previous studies, the 1,5-diaryl-3-oxo-1,4-pentadienyl system was incorporated into various cyclic and acyclic scaffolds with general formula **1a** and **1b**, and these compounds included derivatives that demonstrated promising antiproliferative activities against cancer cell lines.[4, 8] The aromatic symmetrical dienones **1a** and **1b** act as Michael acceptors, suggesting that two successive alkylations of the β-positions of the reactive dienone system by cellular thiols could be one mechanism by which these compounds exert their antiproliferative activity *in vitro.* [9-12]

The α-bromoacryloyl alkylating moiety is present in a series of potent anticancer distamycin-like minor groove binders, including PNU-166196 (brostallicin), which is currently undergoing Phase II clinical trials as a first-line single agent chemotherapy in patients with advanced or metastatic soft tissue sarcoma (Chart 1).[13] It has been hypothesized that the reactivity of the α-bromoacryoyl moiety results from a first-step Michael-type nucleophilic attack, followed by a further reaction of the former vinylic bromo substituent alpha to the carbonyl, leading successively either to a second nucleophilic substitution or to a beta elimination.[14]

In an recent publication, we reported a series of α-bromoacryloylamido chalcones with general structure **2**, containing a pair of Michael acceptors in their structure, corresponding to the α-bromoacryloyl moiety and the α, β-unsaturated ketone system of the chalcone framework.[15] Electron-releasing and electron-withdrawing groups on the phenyl linked to the carbonyl significantly influenced the antiproliferative activity. Of the tested compounds, derivative **2a**

(4-Br) and **2b** (4-OMe) displayed IC_{50} values of 0.62-1.1 and 0.98-1.4 μM, respectively, against a panel of four cancer cell lines (Table 1).

Compound	IC_{50} (μM)[a]			
	L1210	FM3A	CEM	HeLa
2a	0.62 ± 0.20	1.1 ± 0.8	0.99 ± 0.31	1.0 ± 0.0
2b	0.98 ± 0.96	1.2 ± 0.5	1.4 ± 1.2	1.4 ± 0.2
3a	9.3 ± 6.9	40 ± 8	11 ± 4	8.3 ± 0.2
3b	2.4 ± 1.6	2.2 ± 0.5	6.5 ± 0.5	4.4 ± 4.3
6a	7.8 ± 0.7	9.2 ± 0.7	6.1 ± 0.9	4.8 ± 4.4
6b	6.9 ± 0.5	9.1 ± 0.7	1.7 ± 0.1	5.2 ± 3.4
6c	4.8 ± 1.0	8.9 ± 0.8	1.6 ± 0.1	1.8 ± 0.5
6d	35 ± 2	42 ± 0	11 ± 2	30 ± 17
6e	18 ± 7	29 ± 9	8.5 ± 1.9	10 ± 5
6f	6.8 ± 1.0	9.5 ± 1.4	1.9 ± 0.2	5.2 ± 4.7
6g	9.7 ± 0.6	18 ± 6	1.7 ± 0.1	7.6 ± 2.0
6h	9.0 ± 0.0	17 ± 5	1.7 ± 0.05	8.5 ± 0.1
6i	60 ± 14	207 ± 6	168 ± 16	107 ± 91
4a	4.1 ± 3.4	6.5 ± 4.1	2.5 ± 0.9	4.6 ± 4.4
4b	0.32 ± 0.01	0.47 ± 0.10	0.30 ± 0.01	0.70 ± 0.60
4c	0.32 ± 0.03	0.48 ± 0.02	0.41 ± 0.09	0.30 ± 0.02
4d	1.7 ± 1.0	1.7 ± 1.1	1.0 ± 2.0	4.3 ± 3.7
4e	0.38 ± 0.06	0.73 ± 0.00	0.34 ± 0.04	0.35 ± 0.02
4f	1.6 ± 0.7	5.4 ± 1.2	1.6 ± 0.0	0.73 ± 0.63
4g	0.39 ± 0.02	0.79 ± 0.30	0.47 ± 0.17	0.84 ± 0.74
4h	0.62 ± 0.42	1.1 ± 0.9	1.4 ± 0.2	1.6 ± 0.0
melphalan[b]	2.13 ± 0.03	n.d	2.47 ± 0.30	n.d

[a]IC_{50}= compound concentration required to inhibit tumor cell proliferation by 50%. Data are expressed as the mean ± SE from the dose-response curves of at least three independent experiments.
b: These data were previously reported in reference 7.
n.d. not determined

Table 1. In vitro inhibitory effects of compounds **2ab**, **3ab**, **4a-h** and **6a-i** on the proliferation of murine leukemia (L1210), murine mammary carcinoma (FM3A), human T-leukemia (CEM) and human cervix carcinoma (HeLa) cells.

The conversion of α-bromoacryloylamido chalcones **2ab** into the corresponding unsymmetrical dienones **3ab** led to a reduction in activity (0.62-1.1 μM for **2a** *vs.* 8.3-40 μM for **3a**, 0.98-1.4 μM for **2b** *vs.* 2.2-6.5 μM for **3a**).[16]

The observations that both the 1,5-diaryl-3-oxo-1,4-pentadienyl and the α-bromoacryloyl groups can act as trapping agents of cellular nucleophiles led us to prepare and evaluate a novel class of synthetic conjugates with general formulae **4,** incorporating these two moieties within their structures (Chart 1). If such processes occur, the bis-(α-bromoacryloylamidoarylidene) ketone derivatives **4a-h,** characterized by the presence of four potential sites for electrophilic attack on cellular constituents, should be more active than the corresponding 1,5-diaryl-1,4-pentadien-3-one system, containing only two

nucleophilic centers.

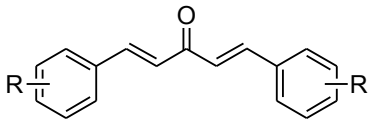

1a

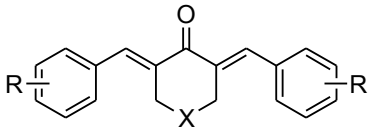

1b

R=electron-releasing or electron-withdrawing groups
X=NH, N-alkyl or N-alkoxycarbonyl
X=(CH_2)n with n from 0 to 4.

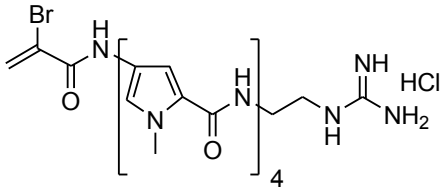

PNU-166196 or Brostallicin

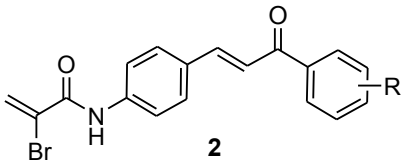

2

R=H, OMe, Me, $N(CH_3)_2$, halogen
R=4-Br, **2a**
R=4-OMe, **2b**

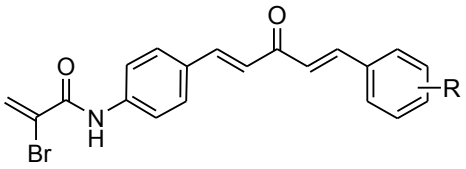

R=4-Br, **3a**
R=4-OMe, **3b**

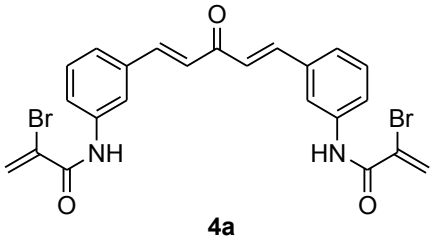

4a

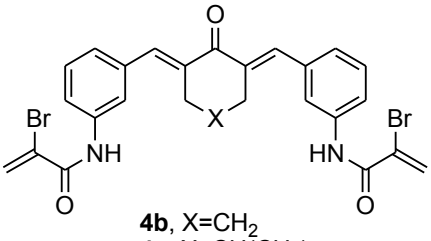

4b, X=CH_2
4c, X=$CH(CH_3)$
4d, X=$(CH_2)_2$
4e, X=$(CH_2)_3$
4f, X=NBn
4g, X=NCO_2CH_3
4h, X=$NCO_2CH_2CH_3$

Chart1

In particular, we have synthesized three different small series of bis-(α-bromoacryloylamidoarylidene) ketone derivatives, corresponding to the acyclic analogue **4a**, the cyclic conjugates **4c-e**, and finally the 4-piperidone derivatives **4f-h**.

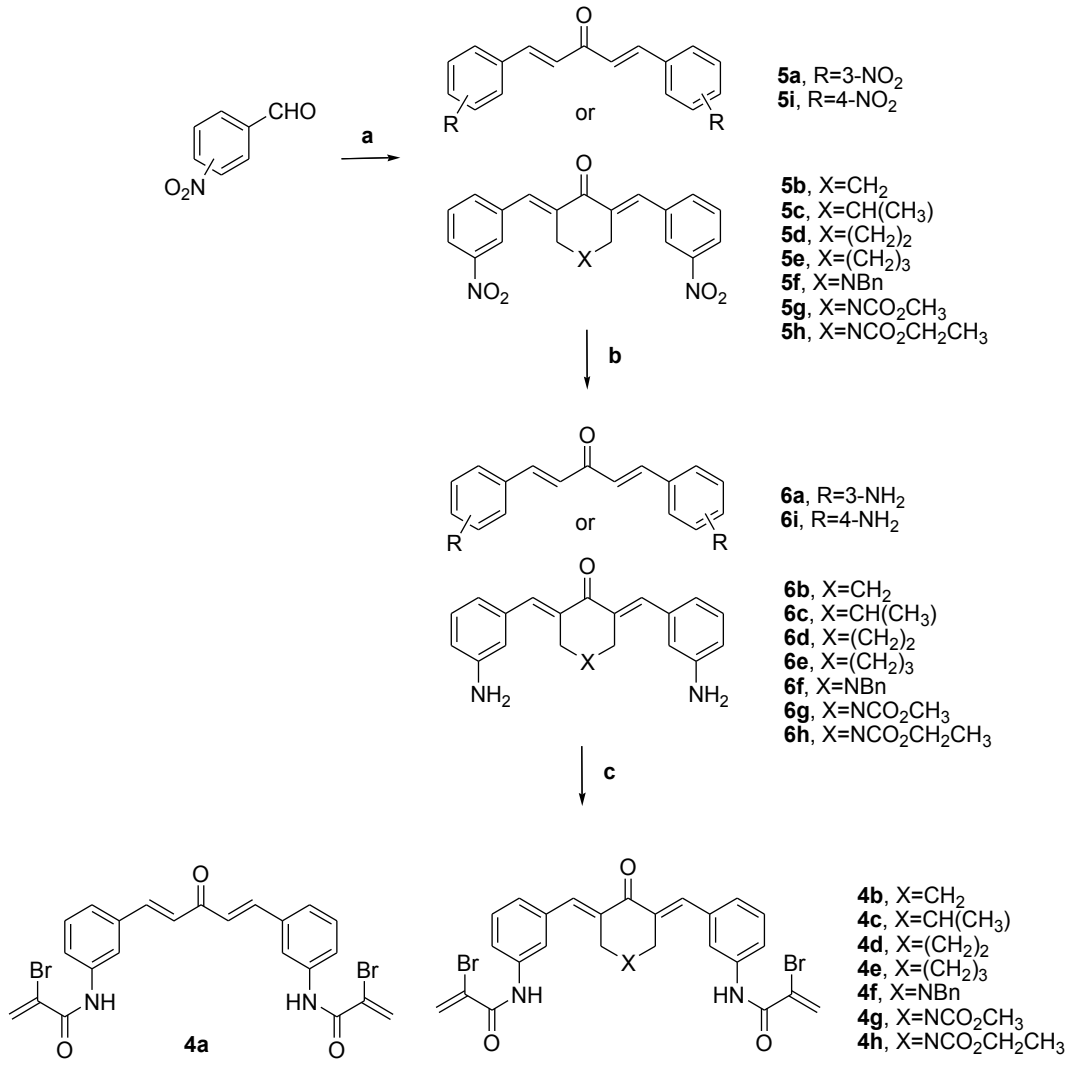

Reagents: **a**. $LiOH{\cdot}H_2O$, cyclic/acyclic ketone, m-nitrobenzaldehyde for the synthesis of **5a-b**, p-nitrobenzaldehyde for the synthesis of **5i** , EtOH, rt, 18h; **b:** Fe, NH_4Cl, H_2O-EtOH, reflux, 2 h; **c**: α-bromoacrylic acid, EDCI, HOBt, DMF, 18h, rt.

Scheme 1 Reagents: (a) LiOHÁH2O, cyclic/acyclic ketone, m-nitrobenzaldehyde for the synthesis of 5a–b, p-nitrobenzaldehyde for the synthesis of 5i, EtOH, rt, 18 h; (b) Fe, NH4Cl, H2O–EtOH, reflux, 2 h; (c) a-bromoacrylic acid, EDCI, HOBt, DMF, 18 h, rt.

The three different series of cyclic ketones **4b** and **4de** were prepared with the aim of evaluating how the size of the ring influenced antiproliferative activity. By the synthesis of compound **4c**, we evaluated the effect of the introduction of a small hydrophobic substituent, corresponding to a methyl group, at the 4-position of the cyclohexanone ring. Hybrid compounds **4a-h** were prepared by the procedure described in Scheme 1. Detailed description of the procedure in the full article published on European Journal of Medicinal Chemistry in 2010 Oct 6.

Table 1 summarizes the inhibitory effects of bis-(α-bromoacryloylamido

arylidene) ketone derivatives **4a-h** on the proliferation of murine leukemia (L1210), murine mammary carcinoma (FM3A), human T-leukemia (CEM) and human cervix carcinoma (HeLa) cells, with bis-(aminobenzylidene)ketones **6a-i,** α-bromoacryloylamido chalcones **2ab** and α-bromoacryloylamido bis-(arylidene)ketones **3ab** as reference compounds. The alkylating agent melphalan was used as a reference drug.

Compounds **6a** and **6i** were synthesized in order to evaluate the influence of the position of amino group on the benzylidene moiety on antiproliferative activity. Changing the location of the amino group from the *para*- in **6i** to the *meta*-position as in **6a**, led to a 10-25-fold increase in antiproliferative activity against all four cancer cell lines. The higher inhibition of cell growth showed by **6a** led us to synthesize α,α'-bis-(*meta*-aminobenzylidene) ketone derivatives **6b-h**.

Comparing the activities of **4a-h** with those of **6a-h** demonstrates that insertion of the two α-bromoacryloyl moieties was an important molecular change leading to a significant increase in antiproliferative activity. The bis-(α-bromoacryloylamido benzylidene) ketones **4a-h** were from 2- to 50-fold more active than the corresponding bis-(anilinomethylidene) precursors **6a-h**. These values are greater or equal to those obtained with the α-bromoacryloylamido enones **2ab**. The greater activity of **4bc**, **4e** and **4gh** compared to that of **3ad** indicated the contribution of a second α-bromoacryloyl moiety to antiproliferative activity.

The compounds displaying the greatest potency were **4b**, **4c** and **4g**, with IC_{50} values of 0.32-0.38, 0.47-0.79, 0.30-0.47 and 0.30-0.84 μM against the L1210, FM3A, CEM and HeLa cell lines, respectively**.** Notably, the acyclic derivative **4a** was significantly less active than its cyclic counterparts **4b-h**. Derivatives **4b-h** were found to have greatest potency to melphalan against tested cancer cell lines.

In the series of compounds **4b-e**, activity decreased when the size of the cyclic ketone was increased from six to seven carbon units, while it increased greatly when the size of the ring increased from seven to eight carbons (compounds **4b, 4d** and **4e**, respectively). Starting from **4b**, the 4-methyl substitution on the cyclohexanone ring, to furnish **4c**, did not improve antiproliferative activity

against L1210, FM3A and CEM cells, but the methyl group doubled potency with respect to HeLa cells.

Comparing the 4-piperidone derivatives **4f-h**, lengthening the alkoxy carbonyl group from methyl to ethyl (compounds **4g** and **4h**, respectively) halved antiproliferative activity.

The more basic *N*-benzyl derivative **4f** showed reduced potency relative to **4g** and **4h** against L1210, FM3A and CEM cells, but **4g** and **4h** were equipotent against HeLa cells.

Next, we examined the effects of increasing concentrations of compounds **4bc**, **4e** and **4g** on cell cycle progression by performing a flow cytometric analysis on HeLa cells (Table 2). Cells were cultured for 24h in the absence or presence of each compound at 0.25, 0.5 or 1 μM, and the cells were stained with propidium iodide (PI). Treatment with **4b**, **4c** or **4e** at 1μM for 24h induced a major shift from the G1 to the G2-M phase compared with control cells, but no concentration, of those tested, of compound **4g** altered cell cycle progression.

Compound	Concentration (μM)	Cell cycle percentage (%)			
		Sub-G1[a]	G1[b]	S[b]	G2-M[b]
Control	NM	1.9 ±0.3	52.9±3.3	29.0 ±3.0	18.1±0.9
4b	0.25	4.7±2.1	44.7±1.1	35.8±4.0	16.1±0.5
4b	0.5	10.5±4.6	50.9±10.1	21.6±6.3	27.8±6.8
4b	1.0	27.2 ±1.2	28.8±6.0	22.7±7.1	51.9±10.4
4c	0.25	3.2±0.6	41.6±5.5	43.5±0.8	14.8±4.7
4c	0.5	4.0±1.1	59.2±9.0	16.1±2.6	27.5±3.8
4c	1.0	4.5±0.9	26.5±1.5	31.3±6.5	41.9±8.0
4e	0.25	2.5±0.9	37.2±8.6	46.2±7.6	16.5±1.0
4e	0.5	6.0±3.0	64.4±1.4	25.0±5.0	10.5±2.5
4e	1.0	15.6±7.5	32.6±10.6	12.9±2.5	54.5±7.8
4g	0.25	8.0±3	49.2±4.0	36.8±6.8	14.5±3.4
4g	0.5	7.2±1.0	51.9±3.9	34.6±11.7	13.4±8.2
4g	1.0	8.2±2.1	57.0±2.5	17.5±2.0	24.9±4.1

Data are expressed as the mean ± SE from the dose-response curves of at least three independent experiments.
a: Percentage of the cell population with hypodiploid DNA content peak (apoptotic cells)
b: The percentage of cells in each phase of the cell cycle was calculated using living cells
NM: not meaningful

Table 2. Cell-cycle distribution of HeLa cells after 24 h of treatment with compounds **4b**, **4c, 4e** or **4g**.

In particular, as shown in Table 2, treatment with 0.25, 0.5 and 1 μM of compound **4b** for 24 h led to a dose-dependent decrease of the G1 peak and a

proportional accumulation of cells in the G2-M phase, accompanied by a concomitant increase in the population of apoptotic cells, as demonstrated by the increase of the sub-G1 peak. Similar effects on the cell cycle progression were observed with **4bc**, **4e** or **4g** after 48h of treatment (see Table 1 in the Supplementary Data section).

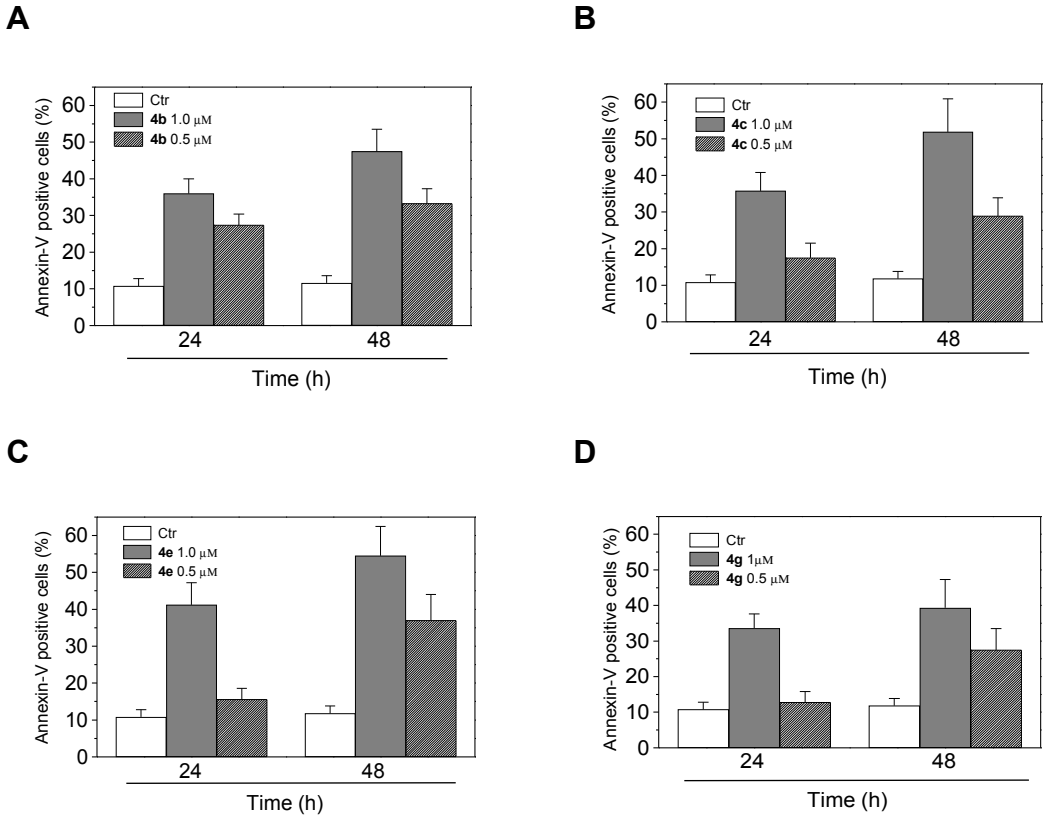

Figure 1. Flow cytometric analysis of apoptotic cells after treatment of HeLa cells with compound 4bc, 4e or 4g. After 24 and 48 h of treatment, cells were harvested and labeled with Annexin-V-FITC and PI and then analyzed by flow cytometry. The data are expressed as mean of percentage of Annexin-V positive cells ± S.E.M. for 3 independent experiments.

The induction of apoptosis in HeLa cells was confirmed by the annexin-V test[18] with compounds **4bc, 4e** and **4g** at various concentrations for 24 or 48 h. Figure 1 shows a time and concentration-dependent increase of the percentage of annexin-V positive cells for all the tested compounds. Only a small percentage (2-5%) of necrotic cells was observed with all compounds and only at the highest concentration employed (data not shown).

Since many compounds that arrest the cell cycle at the G2-M phase are tubulin inhibitors[19], compounds **4bc**, **4e** and **4g** were evaluated for their inhibitory effects on tubulin polymerization. None of tested compounds were effective as inhibitors of tubulin assembly (IC_{50}>40 μM). These data make it unlikely that the

antiproliferative activity of these hybrid compounds results from a direct interaction with tubulin and that they act as microtubule depolymerizing agents.

Impairment of mitochondrial function is an early event in the executory phase of programmed cell death in different cell types, and it occurs as a consequence of a preliminary reduction of the mitochondrial transmembrane potential ($\Delta\psi_{mt}$).[20,21] Early $\Delta\psi_{mt}$ disruption results from an opening of mitochondrial permeability transition pores, and this permeability transition triggers the release of apoptogenic factors, such as apoptosis inducing factor and cytochrome *c*, which in turn lead to later apoptotic events.[20,21]

We used the lipophilic cation 5,5',6,6'-tetrachlo-1,1',3,3'-tetraethylbenzimidazol-carbocyanine (JC-1) to monitor changes in $\Delta\psi_{mt}$ induced by **4b**. The method is based on the ability of this fluorescent probe to enter selectively into the mitochondria, and its color changes reversibly from green to orange as membrane potential increases.[22] This property is due to the reversible formation of JC-1 aggregates upon membrane polarization. Aggregation causes a shift in the emitted light from 530 nm (i.e., emission by JC-1 monomers) to 590 nm (emission by JC-1 aggregates) following excitation at 490 nm.

HeLa cells were treated with compound **4b** for 24, 48 and 72 h at 0.5 and 1 μM. As shown in Figure 2, compound **4b** induces substantial mitochondrial depolarization in a time- and concentration-dependent manner. The disruption of the $\Delta\psi_{mt}$ is associated with the appearance of sub-G1 cells and with the marked increase in the percentage of annexin-V positive cells.

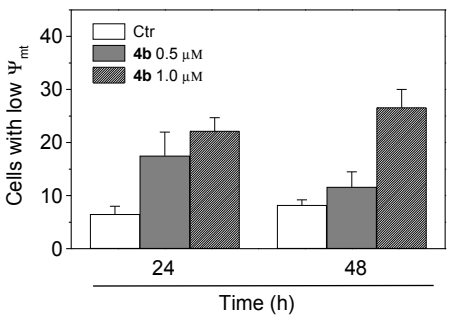

Figure 2. Assessment of mitochondrial potential after treatment with compound **4b.** Induction of loss of mitochondrial membrane potential after 24, 48 and 72 h of incubation of HeLa cells with **4b** at 0.5 or 1.0 μM. Cells were stained with the fluorescent probe JC-1 and analyzed by flow cytometry.

Mitochondrial membrane depolarization is associated with mitochondrial production of reactive oxygen species (ROS).[23,24] ROS are highly reactive molecules with both free radical and non-radical structures, including

superoxide anion, hydrogen peroxide, hydroxyl radical and single oxygen. ROS play a central role as second messengers in a number of signal transduction pathways and cause a wide range of cellular responses ranging from transient to permanent growth arrest, and from apoptosis to necrosis, depending on the level of ROS.

To investigate the effects of **4b** on the production of oxygen species during apoptosis, we utilized two fluorescence probes, hydroethidine (HE) and 2',7'-dichlorodihydrofluorescein diacetate (H_2DCFDA). The fluorescence of these compounds occurs if ROS are generated.[25] As shown in Figure 3 (A and B), there was an increase in cells producing ROS that closely paralleled the increase in cells with low $\Delta\psi_{mt}$, as a function of both the concentration of **4b** and treatment time.

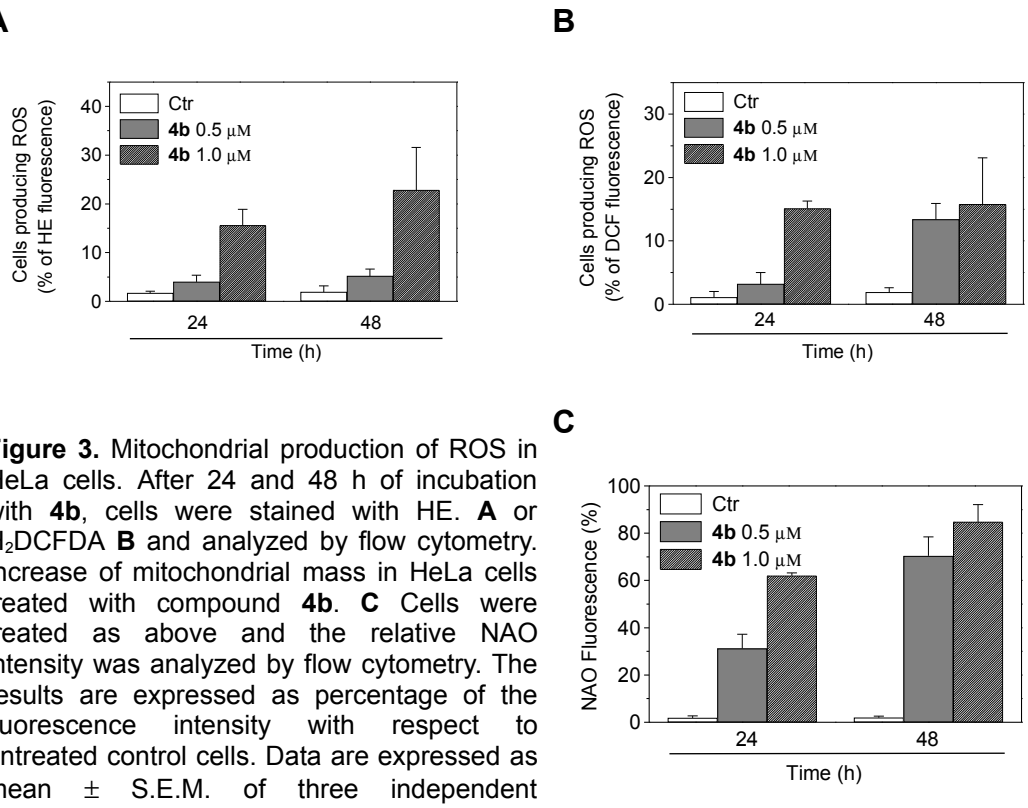

Figure 3. Mitochondrial production of ROS in HeLa cells. After 24 and 48 h of incubation with **4b**, cells were stained with HE. **A** or H_2DCFDA **B** and analyzed by flow cytometry. Increase of mitochondrial mass in HeLa cells treated with compound **4b**. **C** Cells were treated as above and the relative NAO intensity was analyzed by flow cytometry. The results are expressed as percentage of the fluorescence intensity with respect to untreated control cells. Data are expressed as mean ± S.E.M. of three independent experiments

We also evaluated the damage caused by ROS in mitochondria by assessing the oxidation state of cardiolipin, a phospholipid restricted to the inner mitochondrial membrane. We used 10N-nonyl acridine orange (NAO), a fluorescent probe which is independent of the mitochondrial permeability transition.[26] The dye interacts stoichiometrically with intact, non-oxidized cardiolipin.[27] Somewhat unexpectedly, the cells did not show reduction in NAO

fluorescence, but, rather, a marked increase in NAO, especially after 48 h of treatment with **4b** (Figure 3, C). This effect suggests an increase in cardiolipin content as a consequence of increased mitochondrial mass. This has been recently observed by our group in K562 cells following treatment with hybrid α-bromoacryloylamido chalcones[15] but also in other tumor cell lines after treatment with herbimycin A,[28] genistein,[29] and the acronicyne derivative S23906-1[30] and following oxidative stress.[31]

Altogether these results indicated that the cell cycle arrest and apoptosis induced by **4b** in HeLa cells were correlated with a dose- and time-dependent appearance of mitochondrial dysfunction.

The mechanism of apoptosis depends on a cascade of proteolytic enzymes called caspases.[32] They exist in most cells as inactive precursors (zymogens) that, once activated sequentially, lead to irreversible cell death. Within the caspase family, caspase-3 is essential for propagation of the apoptotic signal after exposure of cells to many DNA-damaging agents and other anticancer drugs.[31,33] We therefore determined whether the activation of caspase-3 was involved in the apoptosis induced by compound 4b. We used a monoclonal antibody specific for the active fragment of caspase-3. As shown in Figure 4, with 0.5 and especially 1 μM 4b there was a marked activation of caspase-3 after 24 h of treatment, and no further increase of caspase-3 activity occurred after 48 h.

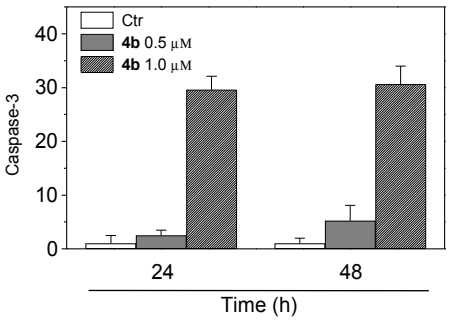

Figure 4. Caspase-3 induced activity by compound **4b**. HeLa cells were incubated in the presence of **4b** at 0.5 or 1.0 μM. After 24 or 48 h of treatment, cells were harvested and stained with an anti-human active Caspase-3 fragment monoclonal antibody conjugated with FITC. Data obtained by flow cytometric analysis are expressed as percentage of caspase-3 active fragment positive cells. Data are expressed as mean ± S.E.M. of three independent experiments

In summary, our plan to optimize the potency of a double Michael acceptor by providing multiple sites of reactivity towards cellular nucleophiles led us to synthesize a series of bis-(α-bromoacryloylamido benzylidene) ketones **4a-h**. Compared to melphalan, an established anticancer agent, derivatives **4b-h**

displayed significantly greater potency. These compounds were derived from the hybridization of two kinds of Michael acceptors, corresponding to the 1,5-diaryl-1,4-pentadien-3-one system of α, α'-bis-(aminobenzylidene) ketones **6a-i** and the α-bromoacryloyl moiety. While compounds **6a-i** showed weak or no antiproliferative activity against five cancer cell lines, the attachment of two α-bromoacryloyl moieties led to significantly increased activity. The greater potency of hybrid compounds **4a-h** than bis-(aminoarylidene) ketones **6a-i** was attributed to the additional electrophilic groups in **4a-h**, enabling these compounds to act potentially as multifunctional Michael acceptors. In the series of cyclic ketones **4b-e**, the six- and the eight-membered cyclic ring was preferred to the seven-membered ring. Compound **4g** had no effect on cycle progression of HeLa cells even at higher concentrations, while compounds **4bc** and **4e** induced cell cycle arrest in a concentration-dependent manner. In particular, treatment with increasing concentrations of **4b** led to cell cycle arrest in the G2-M phase accompanied by an increase in the percentage of apoptotic cells after 24 and 48 h.

As demonstrated with **4b**, the mechanism of action of these compounds appears to be induction of apoptosis mediated by the activation of caspase-3 and by important changes in mitochondrial function, such as dissipation of the transmembrane potential and generation of ROS. Further studies to clarify additional details of the molecular mechanism of action of these compounds and their selectivity in inhibiting the growth of cancer cells are underway.

References

1. Ahn, B.-Z.; Sok, D.-E. *Curr. Pharm. Des.* **1996**, *2*, 247.
2. Dimmock, J.R.; Wong, M. L. C. *Can. J. Pharm. Sci.* **1976**, *11*, 35.
3. Lawrence, N.J.; McGown, A.T. *Curr. Pharm. Des.* **2005**, *11*, 1679.
4. Das, U.; Sharma, R. K.; Dimmock, J. R. *Curr. Med. Chem.* **2009**, *16*, 2001; b) Dimmock, J. R.; Elias, D. W.; Beazely, M. A.; Kandepu, N. M.; *Curr. Med. Chem.* **1999**, *6*, 1125.

5 Dimmock, J.R.; Padmanilayam, M. P.; Zello, G. A.; Nienaber, K. H.; Allen, T. M.; Santos, C. L. De Clercq, E.; Balzarini, J.; Manavathu, E. K.; Stables, J. P. *Eur. J. Med. Chem.* **2003**, *38*, 169.

6 Dimmock, J. R.; Das, U.; Gul, H. I.; Kawase, M.; Sakagami, H.; Barath, Z.; Ocsovsky, I.;

Molnar, J, *Bioorg. Med. Chem. Lett.* **2005**, *15*, 1633.

7. Das, U.; Gul, H. I.; Alcorn, J.; Shrivastav, A.; George, T.; Sharma, R. K.; Nienaber, K. H.; De Clercq, E.; Balzarini, J.; Kawase, M.; Kan, N.; Tanaka, T.; Tani, S.; Werbovetz, K. A.; Yakovich, A. J.; Manavathu, E. K.; Stables, J. P. Dimmock, J. R. *Eur. J. Med. Chem.* **2006**, *41*, 577.
8. Pati, H. N.; Das, U.; Sharma, R. K.; Dimmock, J. R. *Mini-Rev. Med. Chem.* **2007**, *7*, 131.
9. Dimmock, J. R.; Padmanilayam, M. P.; Puthucode, R. N. Nazarali, A. J.; Motaganahalli, N.L.; Zello, G. A.; Quail, J. W.; Oloo, E. O.; Kraatz, H.-B.; Prisciak, J.S.; Allen, T.M.; Santos, C. L.; Balzarini, J.; De Clercq, E.; Manavathu, E.K. *J. Med. Chem*. **2001**, *44*, 586.
10. Baluja, G.; Municio, A. M.; Vega, S. *Chem. Ind.* **1964**, 2053.
11. Mutus, B.; Wagner, J. D.; Talpas, C. J.; Dimmock, J. R.; Phillips, O. A.; Reid, R. S. *Anal. Biochem.* **1989**, *177*, 237.
12. Dimmock, J. R.; Raghavan, S. K.; Logan, B. M.; Bigham, G. E. *Eur. J. Med. Chem.* **1983**, *18*, 248.
13. a) Lorusso, D.; Mainenti, S.; Pietragalla, A.; Ferrandina, G.; Foco, G.; Masciullo, V.; Scambia, G. *Expert Opin. Invest. Drugs* **2009;** *18*, 1939, b) Leahy, M.; Ray-Coquard, I.; Verwei, J.; Le Cesne, A.; Duffaud, F.; Hogendoorn, P. C.; Fowst, C.; De Balincourt, C.; Di Paola, E. D.; Van Glabbeke, M.; Judson, I.; Blay, J. Y. *Eur. J. Cancer* **2007**, *43*, 308.
14. Romagnoli, R.; Baraldi, P. G.; Cruz-Lopez, O.; Lopez-Cara, C.; Preti, D. *Mini-Rev. Med. Chem.* **2009**, *9*, 81.
15. Romagnoli, R.; Baraldi, P.G.; Carrion, M.D.; Cruz-Lopez, O.; Lopez Cara, C.; Balzarini, J.; Hamel, E.; Canella, A.; Fabbri, E.; Gambari R., Basso, G.; Viola, G.; *Bioorg. Med. Chem. Lett.* **2009**, *19*, 2022.
16. For the characterization of compounds **3a** and **3b**, see Supporting Infomation section.
17. Bhagat, S.; Sharma, R.; Chakraborti, A. K. *J. Mol. Catal. A: Chem.* **2006**, *260*, 235.
18. Vermes, I.; Haanen, C.; Steffens-Nakken, H.; Reutelingsperger, C. *J. Imm. Meth*. **1995**, *184*, 39.
19 a) Hamel, E. *Cell Biochem. Biophys.* **2003**, *38*, 1; b) Verdier-Pinard, P.; Lai J.-Y.; Yoo, H.-D.; Yu, J.; Marquez, B.; Nagle D. G.; Nambu, M.; White, J. D.; Falck, J. R.; Gerwick, W. H.; Day, B. W.; Hamel, E. *Mol. Pharmacol.* **1998**, *53*, 62.
20. Ly, J. D.; Grubb, D. R..; Lawen, A. *Apoptosis* **2003** *3*,115.
21. Green, D. R.; Kroemer, G. *Science* **2005**, *305*, 626.
22. Salvioli, S.; Ardizzoni, A.: Franceschi, C.; Cossarizza, A. *FEBS Lett.* **1997**, *411*, 77.
23. a) Hancock, J. T.; Desikan, R.; Neil, S.. *J. Biochem. Sc. Trans.* **2001**, *29*, 245; b) Zamzami, N.; Marchetti, P.; Castedo, M., Decaudin, D.; Macho, A.; Hirsch, T.; Susin, S. A; Petit, P. X.; Mignotte, B.; Kroemer, G. *J. Exp. Med.* **1995**, *182*, 367.
24. a) Nohl, H.; Gille, L.; Staniek, K. *Biochem. Pharmacol.* **2005**, *6,* 719; b) Boonstra, J.; Post, J. A. *Gene* **2004**, *337*, 1.
25. Rothe, G.; Valet, G. *J. Leukoc. Biol.* **1990**, *47,* 440.
26. Petit, J. M.; Maftah, A.; Ratinaud, M. H.; Julien, R. *Eur. J. Biochem.* **1992**, *209*, 267.

27. Gallet, P. F.; Maftah, A.; Petit, J. M.; Denis-Gay, M.; Julien, R. *Eur. J. Biochem.* **1995**, *228*, 113-119.
28. Mancini, M.; Anderson, B.O.; Caldwell, E.; Sedghinasab, M.; Paty, B.P.; Hockenbery, D. M. *J. Cell Biol*. **1997**, *138*, 449.
29. Pagliacci, M.C.; Spinozzi, F.; Migliorati, G.; Fumi, G.; Smacchia, M.; Grignani, F.; Riccardi, C.; Nicoletti, E. *Eur. J. Cancer* **1993**, *29A*, 1573.
30. Kluza, J.; Lansiaux, A.; Wattez, N.; Hildebrand, M. P.; Leonce, S.; Pierre, A.; Hickman, J. A.; Bailly, C. *Biochem. Pharm* **2002**, *63*, 1443.
31. Lee, H. C.; Yin, P. H.; Lu, C. Y.; Chi, C. W.; Wei, Y. H. *Biochem. J*., **2000**, *348*, 425.
32. Kumar, S. *Cell Death Differ.* **2007**, *14*, 32.
33. Selvesen, S.; Dixit, V. M. *Cell* **1997**, *91*, 43.

4. COMBRETASTATIN-A4 DERIVATIVES

Synthesis and antitumor activity of 1,5-disubstituted 1,2,4-triazoles as cis-restricted combretastatin analogues. Romagnoli R, Baraldi PG, Cruz-Lopez O, Lopez Cara C, Carrion MD, Brancale A, Hamel E, Chen L, Bortolozzi R, Basso G, Viola G. **J Med Chem. 2010 May 27;53(10):4248-58.**[17]

Synthesis and biological evaluation of 2-(3',4',5'-trimethoxybenzoyl)-3-aryl/arylaminobenzo[b]thiophene derivatives as a novel class of antiproliferative agents. Romagnoli R, Baraldi PG, Cara CL, Hamel E, Basso G, Bortolozzi R, Viola G. **Eur J Med Chem. 2010 Dec;45(12):5781-91.**[18]

Convergent synthesis and biological evaluation of 2-amino-4-(3',4',5'-trimethoxyphenyl)-5-aryl thiazoles as microtubule targeting agents. Romagnoli R, Baraldi PG, Brancale A, Ricci A, Hamel E, Bortolozzi R, Basso G, Viola G. **J Med Chem. 2011 Jul 28;54(14):5144-53.**[19]

One-Pot Synthesis and Biological Evaluation of 2-Pyrrolidinyl-4-Amino-5-(3',4',5'-Trimethoxybenzoyl)Thiazole: a Unique, Highly Active Antimicrotubule Agent. Romagnoli R, Baraldi PG, Lopez Cara C, Salvador MK, Bortolozzi R, Basso G, Viola G, Balzarini J, Brancale A, Fu XH, Li J, Zhang SZ, Hamel E. **Eur J Med Chem 2011 Dec;46(12):6015-24.**[20]

Synthesis and Evaluation of 1,5-Disubstituted Tetrazoles as Rigid Analogues of Combretastatin A-4 with Potent Antiproliferative and Antitumor Activity Romagnoli R, Baraldi PG, Salvador MK, Preti D, Tabrizi MA, Brancale A, Fu XH, Li J, Zhang SZ, Hamel E, Basso G, Bortolozzi R, and Viola G.. **J. Med. Chem. 2012 Jan 12;55(1):475-88.**[21]

4.1. Synthesis and Antitumor Activity of 1,5-Disubstituted 1,2,4-Triazoles as *cis*-Restricted Combretastatin Analogues.

Romeo Romagnoli*†, Pier Giovanni Baraldi†, Olga Cruz-Lopez†, Carlota Lopez Cara†, Maria Dora Carrion†, Andrea Brancale §, Ernest Hamel‡, Longchuan Chen§§, Roberta Bortolozzi††, Giuseppe Basso†† and Giampietro Viola*††,

†Dipartimento di Scienze Farmaceutiche, Università di Ferrara, Ferrara, Italy

†† Dipartimento di Pediatria, Laboratorio di Oncoematologia, Università di Padova, Padova, Italy

§ The Welsh School of Pharmacy, Cardiff University, Cardiff, UK

§§ Department of Pathology, VA Medical Center, Long Beach, CA

‡ Toxicology and Pharmacology Branch, National Institutes of Health, Frederick, Maryland

Abstract

A series of 1-aryl-5-(3',4',5'-trimethoxyphenyl) derivatives and their related 1-(3',4',5'-trimethoxyphenyl)-5-aryl-1,2,4-triazoles, designed as cis-restricted combretastatin analogues, were synthesized and evaluated for antiproliferative activity, inhibitory effects on tubulin polymerization, cell cycle effects and apoptosis induction. We identified tubulin as the molecular target of most compounds, since those with the greatest inhibitory effects on cell growth strongly inhibited tubulin assembly and the binding of colchicine to tubulin. Their activity was greater than, or comparable with, that of the reference compound CA-4. Flow cytometry studies showed that HeLa and Jurkat cells treated with the most active compounds **4l** and **4o** were arrested in the G2/M phase of the cell cycle in a concentration dependent manner. This effect was accompanied by apoptosis of the cells, mitochondrial depolarization, generation of reactive oxygen species, activation of caspase-3 and PARP cleavage. Compound **4l** was also shown to have potential anti-vascular activity since it induced endothelial cell shape change *in vitro* and disrupted the sprouting of endothelial cells in the chick aortic ring assay.

Introduction

The microtubule system of eukaryotic cells is a critical element in a variety of fundamental cellular processes, such as cell division, formation and maintenance of cell shape, regulation of motility, cell signalling, secretion and intracellular transport.[1] Inhibition of microtubule function using tubulin targeting agents, many of which are natural products, is a validated approach for anticancer therapy.[2] One of the most important antimitotic agents is combretastatin A-4 (CA-4, **1;** Chart 1). CA-4, isolated from the bark of the South African tree *Combretum caffrum,*[3] is one of the well-known natural tubulin-binding molecules affecting microtubule dynamics by binding to the colchicine site.[4] CA-4 shows potent cytotoxicity against a wide variety of human cancer cell lines, including those that are multidrug resistant.[5] A water-soluble disodium phosphate derivative of CA-4 (named CA-4P) has shown promising results in human cancer clinical trials,[6] thus stimulating significant interest in a variety of CA-4 analogues.[7]

It has been established by previous SAR studies that both the 3',4',5'-trimethoxy substitution pattern on the A-ring and the *cis*-olefin configuration at the bridge were essential for optimal activity, while the B-ring structural modifications were tolerated by the target.[7] However, the *cis*-configuration of CA-4 is prone to isomerize to the thermodynamically more stable *trans*-form during storage and administration, producing a dramatic reduction in both antitubulin and antiproliferative activities. Thus, to retain the *cis*-olefin configuration of CA-4 required for bioactivity, several groups have reported that the isomerization from *cis*- to *trans*-olefin can be avoided by incorporating the double bond in five-member aromatic heterocyclic rings, such as pyrazole,[8] imidazole,[9] thiazole[8], isoxazole,[10] 1,2,3-thiadiazole,[11] isomeric triazoles[8, 12, 13] and 1,2,3,4-tetrazole.[8]

Welsh and co-workers reported a series of 3,4-diaryl-1,2,4-triazoles (compounds **3a-c**) with antiproliferative activity, but this was 10-fold reduced relative to the activity of CA-4. Nevertheless, these compounds had similar to that of CA-4 as inhibitors of tubulin polymerization. [13]

Guided by computational molecular modeling, we reconfigured the substitution pattern around the triazole ring by the preparation of two different regioisomeric series of 1,5-diarylsubstituted 1,2,4-triazole derivatives with general structures **3** and **4**. In these two series of designed analogues, obtained by interchanging

the substitution pattern of rings A and B, we fixed one of the aryl groups as a 3',4',5'-trimethoxyphenyl moiety, identical with the A-ring of CA-4, and examined several substitutions with electron-withdrawing (F, Cl and NO_2) ot electron-releasing (Me, MeO and EtO) groups (EWG and ERG, respectively) on the other aryl moiety, corresponding to the B-ring of CA-4.

To compare the effect of *para*-, *meta*- and *ortho*-substitution on compounds with general formula **4**, the methoxy and ethoxy groups were introduced at different positions of the B-phenyl ring, to furnish derivatives **4h-j** and **4l-n**, respectively.

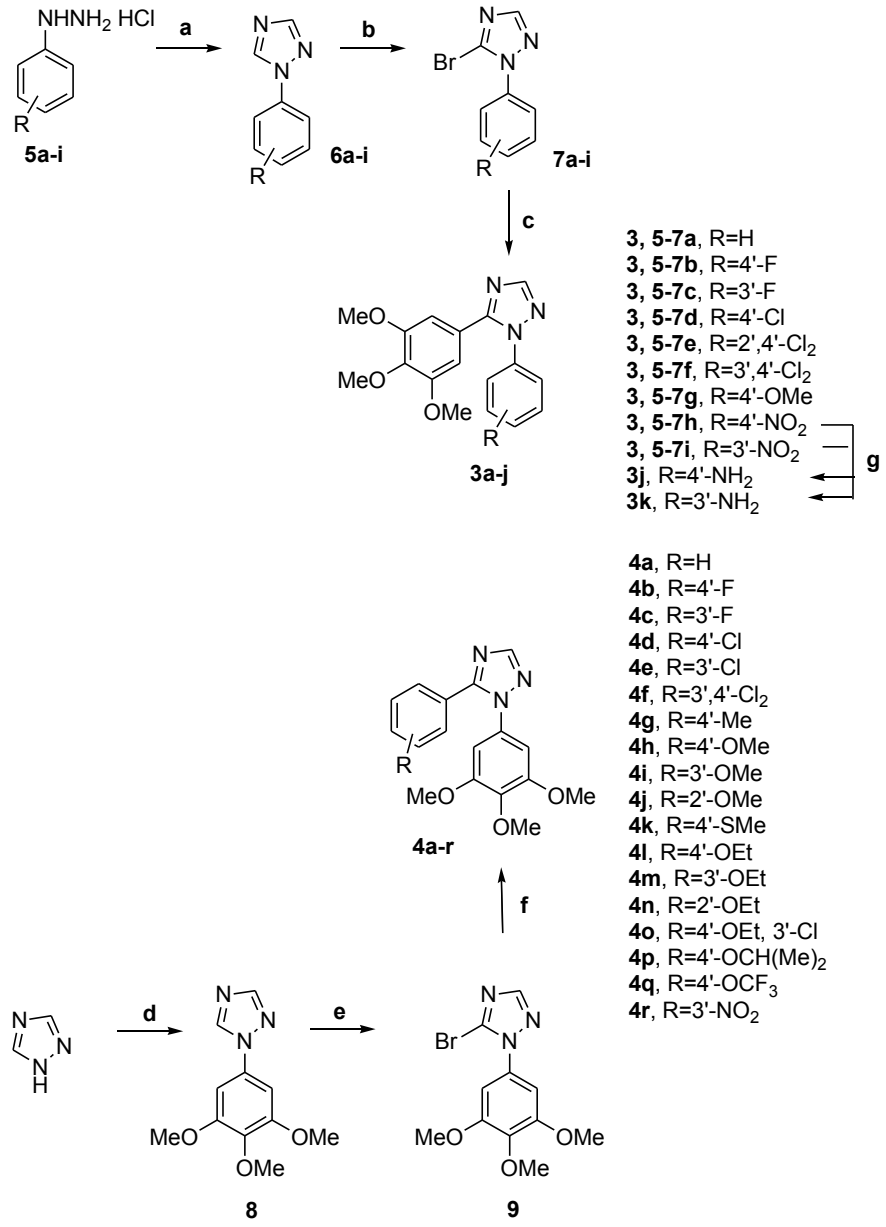

Reagents. **a**: $HCONH_2$, 120°C, 18 h; **b** and **e**: NBS, benzoylperoxide (cat.), CCl_4, rx; **c** and **f**: $Pd(PPh_3)_4$, K_2CO_3, PhMe, rx, 18 h; **d**: 1-bromo-3,4,5-trimethoxybenzene, $CsCO_3$, CuI, DMF, 120 °C, 18 h; **g**: H_2, 10% Pd/C, DMF.

Chart 1. Inhibitors and Potential Inhibitors of Tubulin Polymerization

Chemistry

The target 1,5-diaryl-1,2,4-triazoles **3a-k** and **4a-r** were synthesized as outlined in Scheme 1.

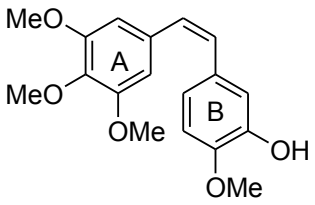

Combretastatin A-4 (CA-4), **1**

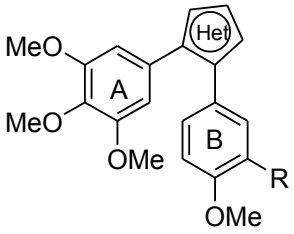

2

R=OH or NH_2
Het=imidazole; pyrazole; thiazole;oxazole; isoxazole; 1,2,3-thiadiazole; 1,2,3- or 1,2,4- or 1,3,4-triazole; 1,2,3,4-tetrazole.

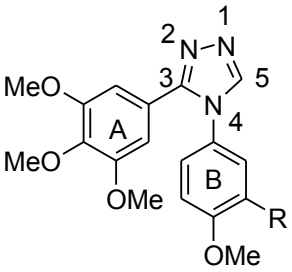

2a, R=H
2b, R=OH
2c, R=F

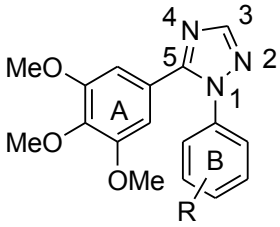

3

3a, R=H
3b, R=4'-F
3c, R=3'-F
3d, R=4'-Cl
3e, R=2',4'-Cl_2
3f, R=3',4'-Cl_2
3g, R=4'-OMe
3h, R=4'-NO_2
3i, R=3'-NO_2
3j, R=4'-NH_2
3k, R=3'-NH_2

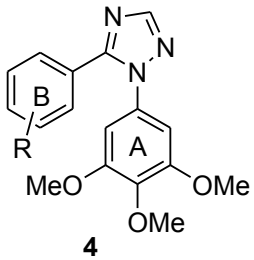

4

4a, R=H
4b, R=4'-F
4c, R=3'-F
4d, R=4'-Cl
4e, R=3'-Cl
4f, R=3',4'-Cl_2
4g, R=4'-Me
4h, R=4'-OMe
4i, R=3'-OMe
4j, R=2'-OMe
4k, R=4'-SMe
4l, R=4'-OEt
4m, R=3'-OEt
4n, R=2'-OEt
4o, R=4'-OEt, 3'-Cl
4p, R=4'-OCH(Me)$_2$
4q, R=4'-OCF_3
4r, R=3'-NO_2

Scheme 1

Detailed description of the synthesis procedure is reported in the full article published on Journal of Medicinal Chemistry (2010 May 27).

Results and Discussion

***In vitro* antiproliferative activities.** The series of 1-aryl-5-(3',4',5'-trimethoxyphenyl) and their related 1-(3',4',5'-trimethoxyphenyl)-5-aryl-1,2,4-triazoles, corresponding to compounds **3a-k** and **4a-r**, respectively, were evaluated for their antiproliferative activity against a panel of six different human tumor cell lines and compared with the reference compound CA-4 (**1**). Data for inactive compounds (IC_{50}>10 μM) are not shown in Table 1. Two of the synthesized compounds, **4l** and **4o**, had the best antiproliferative activities against these cell lines and, overall, were as active as CA-4. In particular, the 3'-chloro-4'-ethoxyphenyl derivative **4o** exhibited IC_{50} values ranging from 3 to 20 nM against the cell lines, as compared with the range of 4-370 nM obtained with CA-4. It was less active than CA-4 only against the K-562 cells.

Compd	IC_{50} [a](nM)					
	HeLa	A549	HL-60	Jurkat	K562	MCF-7
3g	>10,000	>10,000	6200±1200	93±30	3600±900	7400±1200
4g	250±50	1100±100	90±6	300±80	>10,000	540±20
4h	280±60	520±90	120±10	50±10	950±40	360±50
4k	150± 20	800±50	500±20	50±10	340±50	390±90
4l	15±4	100±20	20±3	5±0.2	20±8	50±9
4o	6±2	10±5	3±0.2	3±0.6	20±10	17±1
4p	600±20	>10,000	700±200	650±60	800±100	610±10
CA-4	4±1	180±50	1±0.2	5±0.6	5±0.1	370±100

[a]IC_{50}= compound concentration required to inhibit tumor cell proliferation by 50%. Data are expressed as the mean ± SE from the dose-response curves of at least three independent experiments.

Table 1. In vitro cell growth inhibitory effects of compounds 3g and 4g and CA-4 (1)

Apparently, the relative positions of the two aromatic rings on the 1,2,4-triazole moiety seemed not to be critical for antiproliferative activity. With the exception of the weak activity observed with the *p*-methoxyphenyl derivative **3g**, all the 1-aryl-1,2,4-triazole derivatives **3a-k** were inactive (IC_{50}>10 μM). Switching the position of the two aryls on the 1,2,4-triazole ring (**3a** vs. **4a**, **3b** vs. **4b**, **3c** vs. **4c**, **3d** vs. **4d**, **3f** vs. **4f** and **3i** vs. **4r**) did not yield active compounds, except that there was a considerable difference in potency observed between the regioisomeric 4'-methoxyphenyl derivatives **3g** and **4h** (the latter was considerably more active than the former in four out of the six cell lines).

In the series of 1-(3',4',5'-trimethoxyphenyl)-1,2,4-triazole analogues **4h-j** and **4l-n**, the position of methoxy or ethoxy substituent on the 5-phenyl ring had a profound influence on antiproliferative activity. Starting from compound **4h**, moving the methoxy group from the *para*- to the *meta*- and *ortho*-positions (compounds **4i** and **4j**, respectively), led to a dramatic drop of potency. The same effect was observed for the ethoxy substituent (**4l** *vs.* **4m** and **4n**). The *para*-ethoxy derivative **4l** was 4- to 40-fold more potent than its methoxy counterpart **4h**.

Replacement of the *para*-methoxy group with a weak electron-releasing thiomethyl group, resulted in derivative **4k**, which overall had activity similar to that of **4h** against Jurkat and MCF-7 cells. Similarly, except with the K562 cells, replacing the 4'-methoxy of **4h** with a 4'-methyl group (**4g**) overall had only minor effects on antiproliferative activities.

Since the 4'-ethoxy group of **4l** was favorable for potency, it is important to point out that introduction of an additional EWG chlorine group at the 3'-position of 4'-ethoxyphenyl ring, resulting in compound **4o**, produced from 2- to 15-fold increase of antiproliferative activity against four of the six cell lines, while **4l** and **4o** were equipotent against the Jurkat and K562 cells.

Finally, among the antiproliferative compounds, replacing 4'-ethoxy group of **4l** with the bulky isopropoxy moiety (**4p**) caused a sharp drop in antiproliferative activity in all cell lines, suggesting that an increase in steric bulk at this position causes a decrease in potency.

Inhibition of tubulin polymerization and colchicine binding. To investigate whether the antiproliferative activities of compounds **3g**, **4gh**, **4kl** and **4op** derived from an interaction with tubulin, they were evaluated for their inhibition of tubulin polymerization and for effects on the binding of [^{3}H]colchicine to tubulin (Table 2).[15,16]

For comparison, CA-4 was examined in contemporaneous experiments. In the assembly assay, compound **4l** was found to be the most active (IC50, 0.76 μM), and it was almost twice as potent as CA-4 (IC50,.1.2 μM). While **4l** was generally less potent than **4o** as an antiproliferative agent, **4l** was about twice as active as **4o** as an inhibitor of tubulin assembly. Derivative **4o** was also slightly less active than CA-4 as an inhibitor of tubulin assembly. Compound **4h**

was the next most active agent as inhibitor of tublin assembly (about half as potent as CA-4). The remaining compounds with lower antiproliferative effects on cancer cells, were still less active as inhibitors of tubulin assembly. For these seven compounds and CA-4, the order of activity was **4l**>**CA-4>4o**>**4h>4k>4g>4p>>3g**.

Compound	Tubulin assembly[a] IC_{50}±SD (μM)	Colchicine binding [b] % ±SD
3g	16±1	n.d.
4g	3.9±0.4	33±6
4h	2.3±0.0	55±1
4k	3.6±0.1	38±3
4l	0.76±0.1	86±2
4o	1.5±0.2	75±0.1
4p	5.1±0.8	37±3
CA-4 (**1**)	1.2±0.1	87±3

[a] Inhibition of tubulin polymerization. Tubulin was at 10 μM.
[b] Inhibition of [^{3}H]colchicine binding. Tubulin, colchicine and tested compound were at 1, 5 and 1 μM, respectively. N.d.=not done

Table 2. Inhibition of tubulin polymerization and colchicine binding by compounds 3g, 4g-h, 4k-l, 4o-p and CA-4.

In the colchicine binding studies, derivative **4l** was as potent as CA-4, which in these experiments inhibited colchicine binding by 87%, while **4o** was slightly less potent (75% inhibition). The potent inhibition observed with the two compounds, indicates that **4l** and **4o** bind to tubulin at a site overlapping the colchicine site. Inhibition of colchicine binding by compounds **4gh**, **4k** and **4p** fell into the 33-55% range. In this series of seven compounds, inhibition of [^{3}H]colchicine binding correlated more closely with inhibition of tubulin assembly than with antiproliferative activity. In conclusion, we note that CA-4 is one of the most potent colchicine compounds yet described. It is thus significant that two agents in the present series have activities comparable to that CA-4 as inhibitors of tubulin assembly and, less frequently observed, as inhibitors of colchicine binding to tubulin.

Analysis of cell cycle. The effects of different concentrations of compounds **4l** and **4o** on cell cycle progression were examined with HeLa and Jurkat cells (Figure 1).

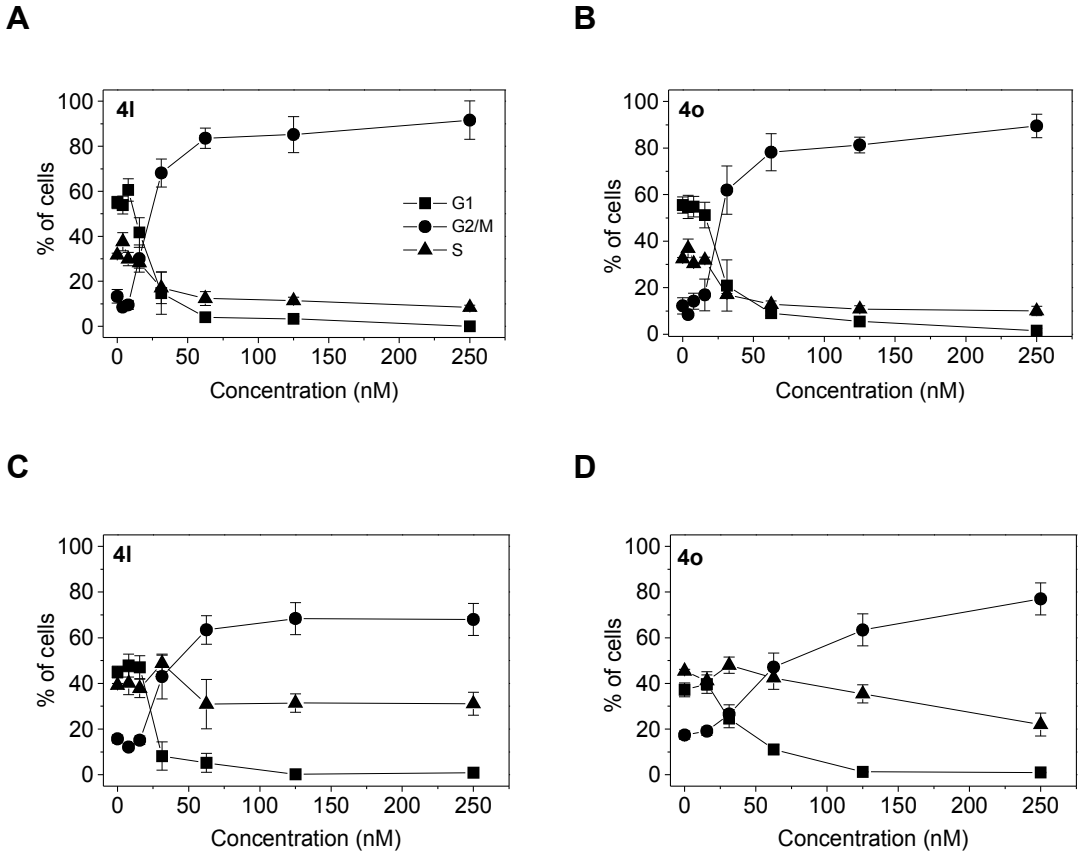

Figure 1. A e **B** Effect of **4l** and **4o**-induced G2/M phase arrest in Hela and Jurkat cells **C** e **D**. Cells were treated with different concentrations ranging from 7 to 250 nM for 24 h. Then the cells were fixed and stained with PI to analyze DNA content by flow cytometry. Data are presented as mean ± SEM of three independent experiments.

Untreated HeLa cells showed a classical pattern of proliferating cells distributed in the G1 (55.2%), S (32.4%) and G2/M (12.4%) phases. Both **4l** and **4o** caused a clear G2/M arrest pattern in a concentration-dependent manner, with a concomitant decrease of cells in phases of the cell cycle (Figure 1). In particular, as shown in Figure 2 (A e B), the G2/M cell population increased from 12% in the control to over 70% with 30 nM compounds **4l** and **4o** at 48 h.

In the leukemia T-cell Jurkat line, both compounds also induced a significant block in the G2/M phase. With both cell lines, the accumulation of G2/M cells increased to varying extents in a time-dependent manner (Figure 2). In addition, treatment of cells with **4l** or **4o** caused the appearance of a hypodiploid peak (sub-G1) indicative of apoptosis (data not shown).

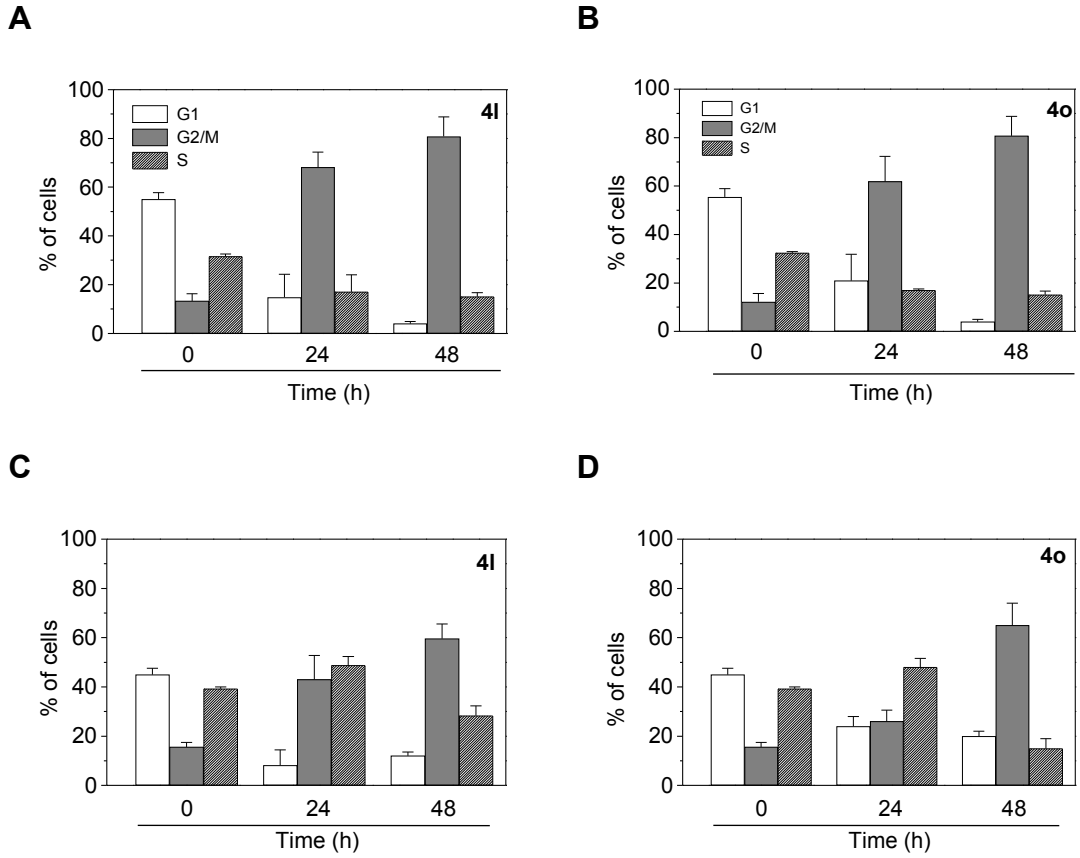

Figure 2. Effect of 4l and 4o-induced G2/M phase arrest in Hela **A** e **B** and Jurkat cells **C** e **D**. Cells were treated with the concentration of 30 nM for 24 and 48 h. Then the cells were fixed and stained with PI to analyze DNA content by flow cytometry. Data are presented as mean ± SEM of three independent experiments.

Loss of plasma membrane asymmetry during apoptosis. To better characterize drug-induced apoptosis, we performed a biparametric cytofluorimetric analysis using propidium iodide (PI) and annexin-V-FITC, which stain DNA and phosphatidylserine (PS) residues, respectively.[17] Annexin-V is a Ca^{2+}-dependent phospholipid binding protein with high affinity for PS. Annexin-V staining precedes the loss of membrane integrity that accompanies the latest stages of cell death resulting from either apoptotic or necrotic processes. Because the externalization of PS occurs in the earlier stages of apoptosis, annexin-V staining identifies apoptosis at an earlier stage than the appearance of sub-G1 cells. These cells appear at a later stage of cell death and indicate the occurrence of nuclear changes such as DNA fragmentation.

After treatment with **4l** and **4o** at the concentration of 50 nM for different times, Jurkat cells were labelled with the two dyes and the resulting red (PI) and green (FITC) fluorescence was monitored by flow cytometry. It can be observed from

Figure 3 that **4l** and **4o** provoked a significant induction of apoptotic cells after 24 h of treatment. The percentage of annexin-V positive cells then further increase at 48 and 72 h. These findings prompted us to further investigate the apoptotic process after treatment with the two compounds.

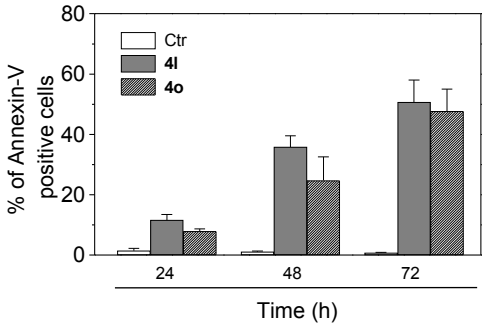

Figure 3. Flow cytometric analysis of apoptotic cells after treatment of Jurkat cells with **4l** and **4o**. After different times of treatment cell were harvested and labeled with Annexin-V-FITC and PI and then analyzed by flow cytometry. The data are expressed as mean of percentage of Annexin-V positive cells ± S.E.M. for 4 independent experiments

Induction of mitochondrial depolarization. Mitochondria play an essential role in the propagation of apoptosis.[18] It is well established that, at an early stage, apoptotic stimuli alter the mitochondrial transmembrane potential ($\Delta\psi_{mt}$). $\Delta\psi_{mt}$ was monitored by the fluorescence of the dye JC-1.[19] With normal cells (high $\Delta\psi_{mt}$), JC-1 displays a red fluorescence (590 nm). This is caused by spontaneous and local formation of aggregates that are associated with a large shift in the emission. In contrast, when the mitochondrial membrane is depolarized (low $\Delta\psi_{mt}$), JC-1 forms monomers which emit at 530 nm. Treated Jurkat cells in the presence of derivatives **4l** and **4o** (50 nM) exhibited a remarkable shift in fluorescencecompared with control cells, indicating depolarization of the mitochondrial membrane potential (Figure 4, A). The percentage of cells with low $\Delta\psi_{mt}$ following treatment increases in a time-dependent fashion (figure 4, B). The disruption of $\Delta\psi_{mt}$ is associated with the appearance of annexin-V positivity in the treated cells when they are in an early apoptotic stage. In fact, the dissipation of $\Delta\psi_{mt}$ is characteristic of apoptosis and has been observed with both microtubule stabilizing and destabilizing agents, including CA-4, in different cell types.[20]

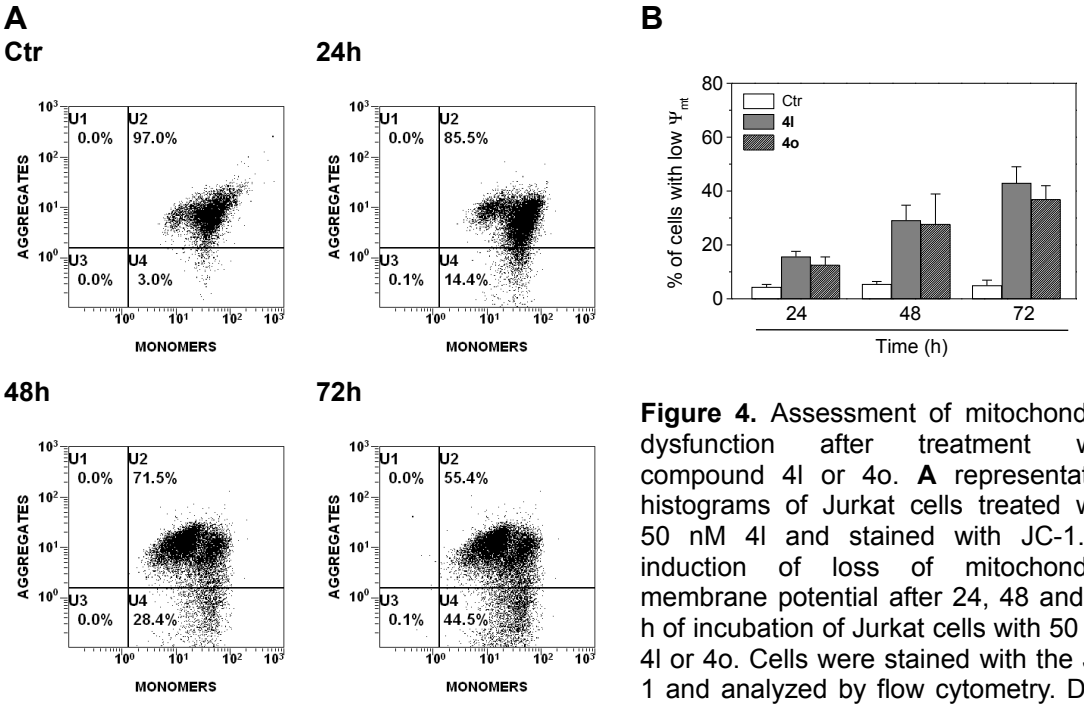

Figure 4. Assessment of mitochondrial dysfunction after treatment with compound 4l or 4o. **A** representative histograms of Jurkat cells treated with 50 nM 4l and stained with JC-1. **B** induction of loss of mitochondrial membrane potential after 24, 48 and 72 h of incubation of Jurkat cells with 50 nM 4l or 4o. Cells were stained with the JC-1 and analyzed by flow cytometry. Data are expressed as mean ± S.E.M. for 3 independent experiments.

Mitochondrial generation of reactive oxygen species (ROS). Mitochondrial membrane depolarization is associated with mitochondrial production of ROS.[21] Therefore, we investigated whether ROS production increased after treatment with the test compounds. We utilized the fluorescence indicator hydroethidine (HE), whose fluorescence appears if ROS are generated.[22] HE is oxidized by superoxide anion into the ethidium ion, which fluoresces red. Superoxide is produced by mitochondria due to a shift from the normal 4-electron reduction of O_2 to a 1-electron reduction when cytochrome c is released from mitochondria. ROS generation was also measured with the dye 2,7-dichlorodihydrofluorescein diacetate (H_2-DCFDA), which is oxidized to the fluorescent compound dichlorofluorescein (DCF) by a variety of peroxides including hydrogen peroxide. [22]

The results are presented in Figure 5 , where it can be observed that **4l** and **4o** induce the production of large amounts of ROS in comparison with control cells, which agrees with the previously described dissipation of Dy_{mt}, The amount of ROS produced increased over the entire 72 h treatment time.

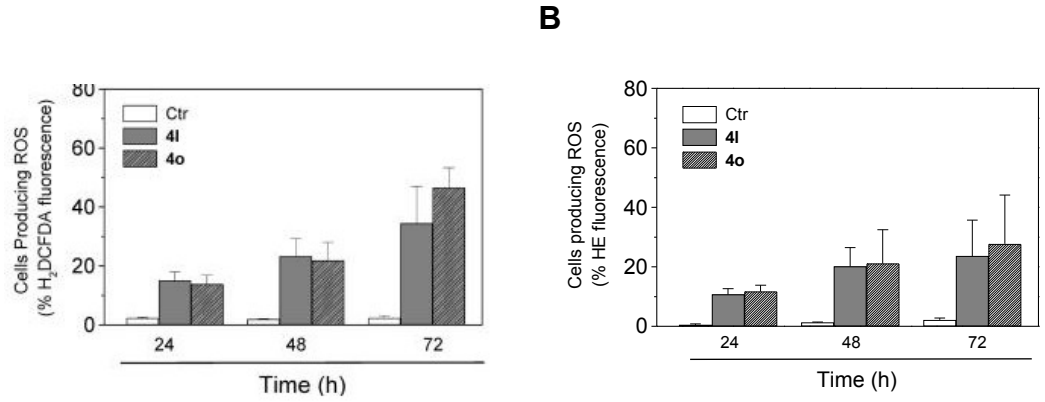

Figure 5. Mitochondrial production of ROS in Jurkat cells. After 24, 48 and 72 h of incubation with **4l** or **4o**, cells were stained with H^2-DCFDA **A** or HE **B** and analyzed by flow cytometry. Data are expressed as mean ± S.E.M. of three independent experiments.

Caspase-3 activation, polyADP-ribose polymerae (PARP) cleavage and Bcl-2 downregulation. Caspases are the central executioners of apoptosis mediated by various inducers.[23] Caspases are synthesized as proenzymes that are activated by cleavage. Caspases-2, -8, -9, and -10 are termed apical caspases and are usually the first to be stimulated in the apoptotic process. Their activation in turn leads to their activation of effector caspases, in particular caspase-3.[24] Exposure of Jurkat cells to the two compound **4l** or **4o** resulted in the activation of caspase-3 in a time-dependent manner, as shown in Figure 6.

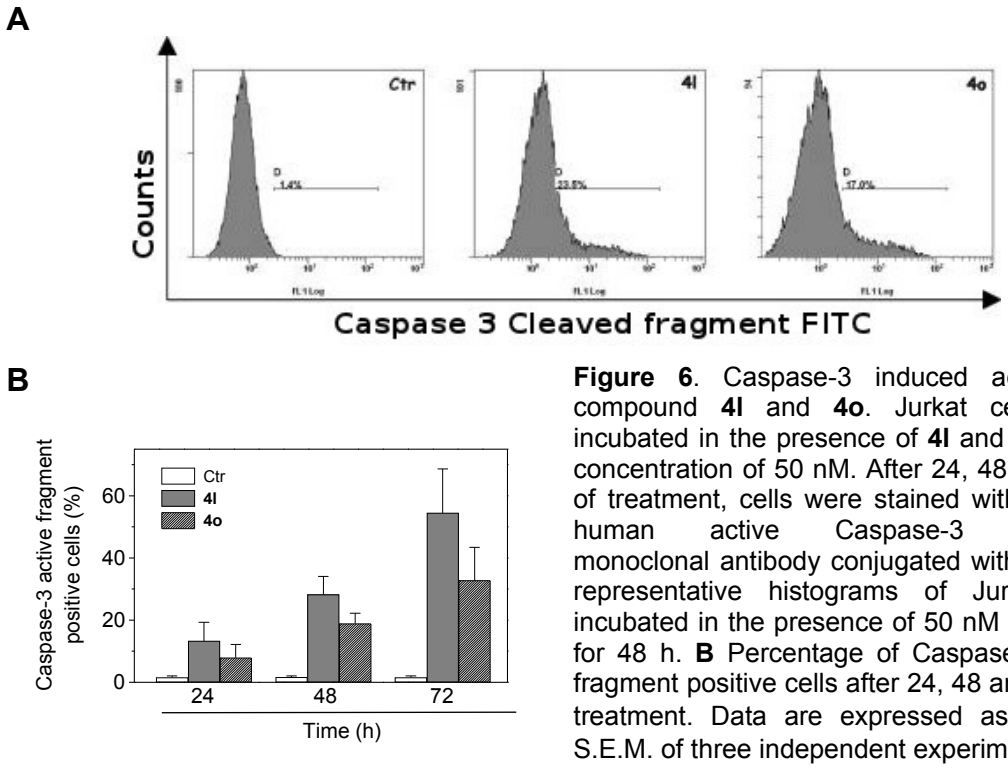

Figure 6. Caspase-3 induced activity by compound **4l** and **4o**. Jurkat cells were incubated in the presence of **4l** and **4o** at the concentration of 50 nM. After 24, 48 and 72 h of treatment, cells were stained with an anti-human active Caspase-3 fragment monoclonal antibody conjugated with FITC. **A** representative histograms of Jurkat cells incubated in the presence of 50 nM **4l** and **4o** for 48 h. **B** Percentage of Caspase-3 active fragment positive cells after 24, 48 and 72 h of treatment. Data are expressed as mean ± S.E.M. of three independent experiments.

PARP is a 116 kDa nuclear protein that appears to be involved in apoptosis.[25] This protein is one of the main cleavage targets of caspase-3 both *in vitro* and *in vivo*.[25] As shown in Figure 7 (top panel), immunoblot analysis demonstrated extensive formation of the typical 89 kDa fragment of PARP following a 24 h treatment with either 50 nM **4l** or 50 nM **4o**. There was a further increase, especially with **4o**, after treatment for another 24 h, most noticeable through disappearance of uncleaved PARP. Similar results were obtained with CA-4 in HeLa cells.[20b]

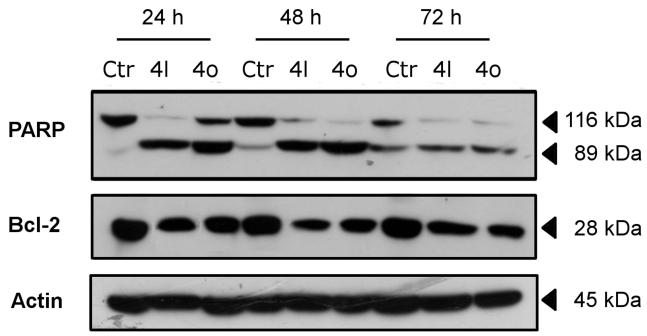

Figure 7. Western blot analysis for the cleavage of PARP and the expression of Bcl-2 in Jurkat cells. Control lanes (Ctr) refer to untreated cells. In the other lanes the cell were treated with 50 nM compounds **4l** or **4o** for the indicated times. Whole cell lysates were subjected to SDS-PAGE, followed by blotting with an anti-PARP, anti-Bcl-2 or anti-actin antibody.

Bcl-2 is a protein that has been extensively investigated as a modulating agents of apoptosis and plays a major role as an inhibitor of apoptosis. It does this by regulating the mitochondrial membrane potential, thus avoiding release of cytochrome *c* and caspase activation.[26] Therefore, we examined whether the induction of apoptosis by **4o** and **4l** is associated with changes in the expression of this protein. As depicted in Figure 7 (middle panel), immunoblot analysis showed that treatment with either compound resulted in decreased expression of Bcl-2. Altogether these data indicate that the induction of apoptosis by these new derivative is associated with Bcl-2 down regulation and caspase-3 activation that in turn stimulate PARP cleavage.

Anti-vascular activity. CA-4 and its analogues in clinical development have been shown to quickly and selectively shut down the blood flow of tumors.[6a,6b] This family of drugs is therefore called anti-vascular or vascular disrupting agents. The effect is thought to be mediated by inducing endothelial cell shape change, possibly through disrupting microtubule dynamics.[27] We tested the derivative **4l** for its ability to induce rapid endothelial cell shape changes using a human umbilical vein endothelial cell (HUVEC) culture assay and a chick aortic

ring assay.[28] The HUVEC line expressed green fluorescent protein (GFP). In these model systems, we found that changes occurred rapidly and were extensive 30 min after drug addition, corresponding to the quick *in vivo* effect of shutting down tumor circulation. Like CA-4, **4l** caused spreading HUVECs to retract and form blebs on their membranes at a concentration as low as 0.5 μM, and the effect was prominent at 10 μM. The area of GFP positive HUVECs was reduced to 30% of the area measured before treatment (Figure 8).

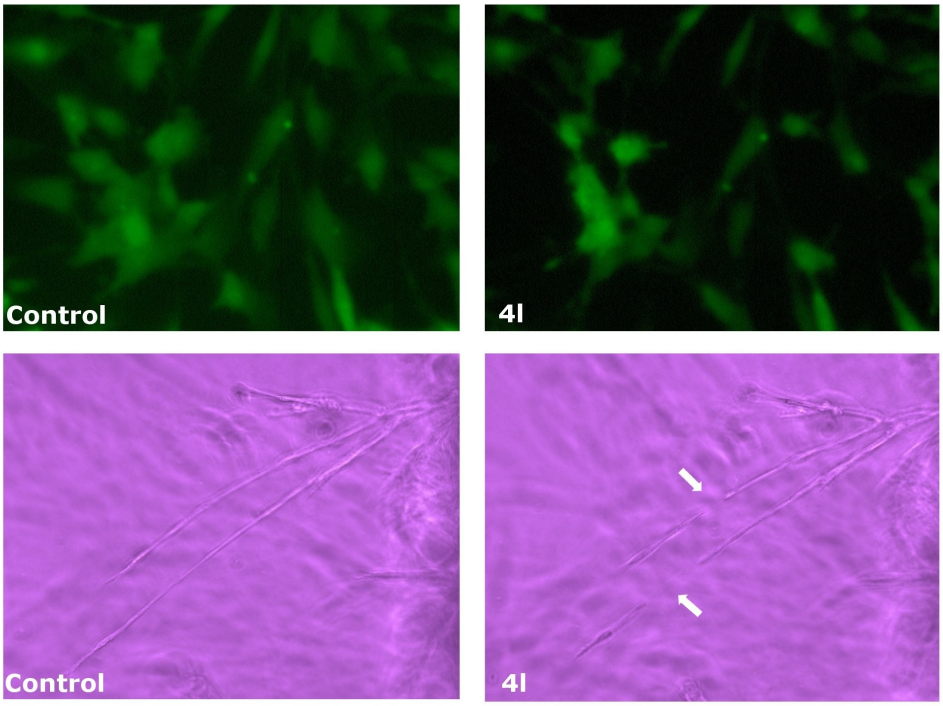

Figure 8. Effect of compound **4l** on endothelial cell shape in cultured HUVECs (top panels) and chick aortic vascular sprouts (lower panels). Cells or aortic arches from 14 day chick embryos were treated with **4l** and analyzed by confocal microscopy. The left hand panels are cells prior to compound addition, and the right hand panels show cells before after 30 min of treatment with 10 μM **4l**. In the lower panels the arrow indicate the disruption of the aortic vascular sprout induced by drug treatment.

Compound **4l** also disrupted formation of vascular sprouts from chick aortic ring after only 30 min incubation. These observations suggest that **4l**, like CA-4, would most likely cause severe vascular disruption *in vitro* and it could be considered as a new vascular disrupting agent.

Molecular modeling studies. To rationalize the experimental data obtained, a set of molecular docking studies was performed on this series of compounds. The docking pose observed for **4l** showed a very similar binding mode to the co-crystallised DAMA-colchicine[29] with the trimethoxyphenyl ring in close

contact to Cys 241 (residue numbering derived from the crystal structure used) and the other aromatic moiety placed deep in the binding pocket (Figure 9).

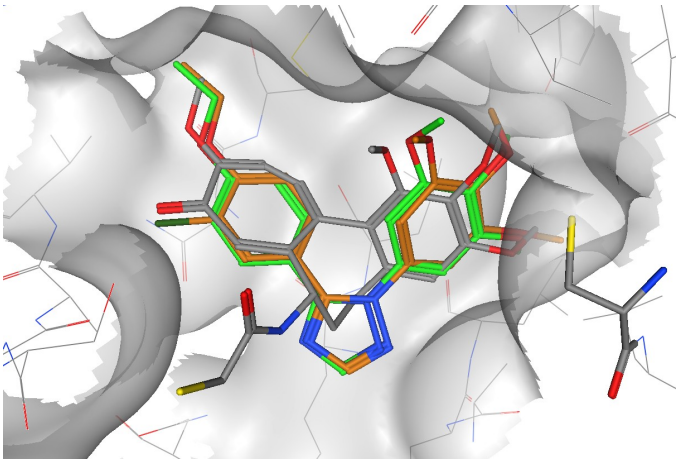

Figure 9. Putative binding mode of compound **4l** (green) and compound **4o** (orange). DAMA-colchicine is shown in gray, and Cys 241 is shown on the right are in stick representation.

These results are in accordance with the observed experimental results, in particular, the ethoxy group is placed in a tight hydrophobic region, which does not seem able to accommodate a bulkier group, explaining the loss in activity of compound **4p**. Furthermore, in the case of **4o**, the chlorine atom in position 3 of the aromatic ring is placed in the same position as the carbonyl group of DAMA-colchicine and, also in this case, only relatively small groups should be tolerated in this position. In further support of this model is the inactivity of compounds **4i** and **4m**, which have a methoxy group and an ethoxy group, respectively, at position 3 of the aromatic ring. These compounds could not be docked successfully in the colchicine binding site.

Conclusions

In conclusion, we proposed that 1,5-diarylsubstituted 1,2,4-triazole ring could serve as a suitable mimic to retain the bioactive configuration afforded by the *cis*-double bond present in CA-4. In the present study, we fixed one of the aryl groups as a 3',4',5'-trimethoxyphenyl moiety, and the modification were mainly focused on variation of the substituents on the second phenyl ring. It is clear that the substitution pattern on the phenyl at the 5-position of the 1,2,4-triazole ring plays an important role for antitubulin and antiproliferative activities, and

this was supported by the molecular docking studies. The results demonstrated that either the 4'-ethoxy (**4l**) substituent or the 4'-ethoxy and 3'-chloro (**4o**) substituents on the second phenyl ring could replace the B-ring of CA-4, at least with a triazole ring as the bridge. Both these derivatives exhibited potent tubulin polymerization inhibitory activity as well as antiproliferative activity, comparable to that of CA-4. Compound **4l** was the most potent inhibitor of tubulin polymerization and one of the most potent inhibitors of colchicine binding (IC_{50}=0.76 μM for assembly, 86% inhibition of the binding of [^{3}H]colchicine, We also showed by flow cytometry that **4l** and **4o** had cellular effects typical for microtubule-interacting agents, causing accumulation of cells in the G2/M phase of the cell cycle. Further studies show that **4l** and **4o** are potent inducers of apoptosis in the Jurkat cell line. Apoptosis induced by antimitotic agents has been associated with alteration in a variety of cellular signalling pathway. As many antimitotic drugs, compounds **4l** and **4o** are able to induce Bcl-2 down-regulation just after 24 h of treatment. The Bcl-2 prevents the initiation of the cellular programme by stabilizing mitochondrial permeability. The loss of $\Delta\psi_{mt}$ results in an uncoupling of the respiratory chain and the efflux of small molecules such as caspase-9 and the apoptosis-inducing factor (AIF) which in turn can stimulate proteolytic activation of caspase-3. Our results confirm that the induction of apoptosis by **4l** and **4o** is associated with down-regulation of Bcl-2, dissipation of the mitochondrial transmembrane potential and activation of caspase-3, which is coupled with terminal events of apoptosis such as PARP cleavage.

Finally, preliminary experiments have assessed the potential antivascular activity of compound **4l**. The ability of this compound to inhibit vascular sprouting is consistent with antivascular agent utility and warrants further testing in preclinical in vivo cancer models.

Experimental Section

Antiproliferative assays. Human T-leukemia (Jurkat), human promyelocytic leukemia (HL-60) and human chronic myelogenous leukemia (K562) cells were grown in RPMI-1640 medium, (Gibco Milano Italy). Breast adenocarcinoma

(MCF7), human non-small lung carcinoma (A549) and human cervix carcinoma (HeLa) cells were grown in DMEM medium (Gibco, Milano, Italy), all supplemented with 115 units/mL of penicillin G (Gibco, Milano, Italy), 115 μg/mL streptomycin (Invitrogen, Milano, Italy) and 10% fetal bovine serum (Invitrogen, Milano, Italy). Individual wells of a 96-well tissue culture microtiter plate were inoculated with 100 μL of complete medium containing $8x10^3$ cells. The plates were incubated at 37 °C in a humidified 5% CO_2 incubator for 18 h prior to the experiments. After medium removal, 100 L of the drug solution, dissolved in complete medium at different concentrations, was added to each well and incubated at 37 °C for 72 h. Cell viability was assayed by the (3-(4,5-dimethylthiazol-2-yl)-2,5-diphenyl tetrazolium bromide (MTT) test as previously described.[30] The IC_{50} was defined as the compound concentration required to inhibit cell proliferation by 50%.

Effects on tubulin polymerization and on colchicine binding to tubulin. To evaluate the effect of the compounds on tubulin assembly[15] *in vitro,* varying concentrations of compounds were preincubated with 10 μM bovine brain tubulin in glutamate buffer at 30 ˚C and then cooled to 0 ˚C. After addition of 0.4 mM GTP, the mixtures were transferred to 0°C cuvettes in a recording spectrophotometer and warmed to 30 °C. Tubulin assembly was followed turbidimetrically at 350 nm. The IC_{50} was defined as the compound concentration that inhibited the extent of assembly by 50% after a 20 min incubation. The capacity of the test compounds to inhibit colchicine binding to tubulin was measured as described,[16] except that the reaction mixtures contained 1 μM tubulin, 5 μM [^{3}H]colchicine and 1 μM test compound.

Flow cytometric analysis of cell cycle distribution and apoptosis. For flow cytometric analysis of DNA content, $5x10^5$ HeLa or Jurkat cells in exponential growth were treated with different concentrations of the test compounds for 24 and 48 h. After an incubation period, the cells were collected, centrifuged and fixed with ice-cold ethanol (70%). The cells were then treated with lysis buffer containing RNAse A and 0.1% Triton X-100, and then stained with PI. Samples were analyzed on a Cytomic FC500 flow cytometer (Beckman Coulter). DNA

histograms were analyzed using MultiCycle® for Windows (Phoenix Flow Systems).

Annexin-V assay. Surface exposure of PS on apoptotic cells was measured by flow cytometry with a Coulter Cytomics FC500 (Beckman Coulter) by adding Annexin-V-FITC to cells according to the manufacturer's instructions (Annexin-V Fluos, Roche Diagnostic). Simultaneously the cells were stained with PI. Excitation was set at 488 nm, and the emission filters were at 525 nm and 585 nm, respectively.

Assessment of mitochondrial changes. The mitochondrial membrane potential was measured with the lipophilic cation 5,5',6,6'-tetrachlo-1,1',3,3'-tetraethylbenzimidazolcarbocyanine (JC-1, Molecular Probes), as described.[19,30] Briefly, after different times of treatment, the cells were collected by centrifugation and resuspended in Hank's Balanced Salt Solution (HBSS) containing 1 μM JC-1. The cells were then incubated for 10 min at 37 °C, centrifuged and resuspended in HBSS. The production of ROS was measured by flow cytometry using either HE (Molecular Probes) or H_2DCFDA (Molecular Probes).

After different times of treatment, cells were collected by centrifugation and resuspended in HBSS containing the fluorescence probes HE or H_2DCFDA at the concentrations of 2.5 and 0.1 μM, respectively. The cells were then incubated for 30 min at 37 °C, centrifuged and resuspended in HBSS. The fluorescence was directly recorded with the flow cytometer, using as excitation wavelength 488 nm and emission at 585 nm and 530 nm for HE and H_2DCFDA, respectively.

Caspase-3 assay. Caspase-3 activation in Jurkat cells was evaluated by flow cytometry using a human active caspase-3 fragment antibody conjugated with FITC (BD Pharmingen). Briefly, after different incubation times in the presence of test compounds, the cells were collected by centrifugation and resuspended in Cytofix™ (BD Pharmingen) buffer for 20 min, washed with Perm/Wash™ (BD Pharmingen) and then incubated for 30 min with the antibody. After this period, cells were washed and analyzed by flow cytometry. Results qre expressed as

percentage of caspase-3 active fragment positive cells.

Western Blot Analysis. Jurkat cells were incubated in the presence of test compounds and, after different times, were collected, centrifuged and washed two times with ice cold phosphate-buffered saline (PBS). The pellet was then resuspended in lysis buffer. After the cells were lysed on ice for 30 min, lysates were centrifuged at 15000 x g at 4 °C for 10 min. The protein concentration in the supernatant was determined using BCA protein assay reagents (Pierce, Italy). Equal amounts of protein (20 μg) were resolved using sodium dodecyl sulfate polyacrylamide gel electrophoresis (SDS-PAGE) (7.5-15 % acrylamide gels) and transferred to PVDF Hybond-p membrane (GE Healthcare). Membranes were blocked with I-block (Tropix) the membrane being gently rotated overnight at 4 °C. Membranes were then incubated with primary antibodies against, Bcl-2, PARP, (all rabbit, 1:1000, Cell Signaling), or β-actin (mouse, 1:10,000, Sigma) for 2 hr at room temperature. Membranes were next incubated with peroxidase-labeled goat anti-rabbit IgG (1:100,000, Sigma), peroxidase-labeled goat anti-mouse IgG (1:100,000, Sigma) for 60 min. All membranes were visualized using ECL Advance (GE Healthcare) and exposed to Hyperfilm MP (GE Healthcare). To ensure equal protein loading, each membrane was stripped and reprobed with anti-b-actin antibody.

Endothelial cell shape change assays. HUVEC cells expressing GFP (Green Fluorescence Protein) were cultured in EGM-2 media with endothelial cell growth supplment and plated into 18-well μ-Slide coated with collagen one day before assay. Cell morphology and GFP fluorescence were recorded by a Nikon confocal microscope with an imaging system before and after drug additions at different time points. The area of HUVEC cells with GFP was further analyzed by imaging software MetaMorph (Molecular Device). Chick aortic ring assay was performed as described in reference 28. Briefly, aortic arches were dissected from day 14 chick embryos, cut into cross-sectional slices and implanted in 10 μl Matrigel (Becton Dickinson) in 8 well Lac-Tek chamber slides with complete media. Endothelial cell sprouts or channels were formed in 24-48 h. Various concentrations of 4l were added and images of the vascular channels were captured by digital camera before and 30 min after drug

addition.

Molecular modeling. All molecular modeling studies were performed on a MacPro dual 2.66GHz Xeon running Ubuntu 8. The tubulin structure was downloaded from the PDB data bank (http://www.rcsb.org/ - PDB code: 1SA0).[30] Hydrogen atoms were added to the protein, using Molecular Operating Environment (MOE),[31] and minimized keeping all the heavy atoms fixed until a RMSD gradient of 0.05 kcal mol^{-1} $Å^{-1}$ was reached. Ligand structures were built with MOE and minimized using the MMFF94x forcefield until a RMSD gradient of 0.05 kcal mol^{-1} $Å^{-1}$ was reached. The docking simulations were performed using PLANTS.[32]

Supporting information available.

Spectroscopic data for compounds **6a-f, 6hi, 7a-f, 7hi,**. **3a-f, 3h-k, 4a-f**, **4ij**, **4mn** and **4r**. This material is available free of charge via the Internet at http://pubs.acs.org.

References

1. a) Amos, L. A. Microtubule structure and its stabilisation. *Org. Biomol. Chem.* **2004**, *2*, 2153-2160; b) Walczak, C.E. Microtubule dynamics and tubulin interacting proteins. *Curr. Opin. Cell. Biol.* **2000**, *12*, 52-56;

2. a) Mahindroo, N; Liou, J.P.; Chang, J.Y.; Hsieh, H.P. Antitubulin agents for the treatment of cancer. A medicinal chemistry update. *Exp. Opin. Ther. Pat.* **2006**, *16*, 647-691; b) Jordan, M. A.; Wilson, L. Microtubules as a target for anticancer drugs. *Nat. Rev. Cancer* **2004**, *4*, 253-265; c) Hadfield, J. A.; Ducki, S.; Hirst, N.; McGown, A. T. Tubulin and microtubules as targets for anticancer drugs. *Prog. Cell Cycle Res.* **2003**, 5, 309-325; d) Honore, S.; Pasquier, E.; Braguer, D. Understanding microtubule dynamics for improved cancer therapy. *Cell. Mol. Life. Sci*. **2005**, *62*, 3039-3065; e) Pellegrini, F.; Budman, D.R. Review: tubulin function, action of antitubulin drugs, and new drug development. *Cancer Invest.* **2005**, *23*, 264-273. f) Attard, G.; Greystoke, A.; Kaye, S.; De Bono, J. Update on tubulin binding agents. *Pathol. Biol.*, **2006**, *54*, 72-84; g) Lawrence, N.J.; McGown, A.T. The chemistry and biology of antimitotic chalcones and related enone systems. *Curr. Pharm. Des.* **2005**, *11*, 1679-1693;

3. Pettit, G.R.; Singh, S.B.; Hamel, E.; Lin, C.M.; Alberts, D.S.; Garcia-Kendall, D. Isolation and structure of the strong cell growth and tubulin inhibitor combretastatin A-4. *Experentia* **1989**, *45*, 209-211.

4. Lin, C.M.; Ho, H.H.; Pettit, G.R.; Hamel, E. Antimitotic natural products combretastatin A-4 and combretastatin A-2: studies on the mechanism of their inhibition of the binding of colchicine to tubulin. *Biochemistry* **1989**, *28*, 6984-6991.

5. Mc Gown, A. T.; Fox, B. W. Differential cytotoxicity of combretastatins A1 and A4 in two daunorubucin-resistant P388 cell lines. *Cancer Chemother. Pharmacol.* **1990**, *26*, 79-81.

6. a) Grosios, K.; Holwell, S. E.; McGown, A. T.; Pettit, G. R.; Bibby, M. C. In vivo and in vitro evaluation of combretastatin A-4 and its sodium phosphate prodrug. *Br. J. Cancer* **1999**, *81*, 1318-1327; b) Vincent, L.; Kermani, P.; Young, L. M.; Cheng, J.; Zhang, F.; Shido, K.; Lam, G.; Bompais-Vincent, H.; Zhu, Z.; Hicklin, D. J.; Bohlen, P.; Chaplin, D. J.; May, C.; Rafii, S. Combretastatin A4 phosphate induces rapid regression of tumor neovassels and growth through interference with vascular endothelial-cadherin signaling. *J. Clin. Invest.* **2005**, *115*, 2992-3006; c) Chaplin, D. J.; Hill, S. A. The development of combretastatin A4 phosphate as a vascular targeting agent. *Int. J. Radiat. Oncol. Biol. Phys.* **2002**, *54:* 1491-1496; d) Young, S. L.; Chaplin, D. J. Combretastatin A-4 phosphate: background and current clinical status. *Expert Opin. Invest. Drugs* **2004**, *13*, 1171-1182; e) Bilenker, J. H.; Flaherty, K. T.; Rosen, M.; Davis, L.; Gallagher, M.; Stevenson, J. P.; Sun, W.; Vaughn, D.; Giantonio, B.; Zimmer, R.; Scnall, M.; O'Dwyer, P. J. Phase I trial of combretastatin A-4 phospate with carboplatin. *Clin. Cancer Res.* **2005**, *11*, 1527-1533.

7. a) Nam, N.H. Combretastatin A-4 analogues as antimitotic antitumor agents. *Curr. Med. Chem.* **2003**, *10*, 1697-1722; b) Chaudari, A.; Pandeya, S. N.; Kumar, P.; Sharma, P. P.; Gupta, S.; Soni, N.; Verma, K. K.; Bhardwaj, G. Combretastain A-4 analogues as anticancer agents. *Mini Rev. Med. Chem.* **2007**, *12*, 1186–1205; c) Tron, G.C.; Pirali, T.; Sorba, G.; Pagliai, F.; Busacca, S.; Genazzani, A. A. Medicinal chemistry of combretastatin A4: present and future directions. *J. Med. Chem.* **2006**, *49*, 3033-3044; d) Gaukroger, K.; Hadfield, J. A.; Lawrence, N. J.; Nlan, S.; McGown, A. T. Structural requirements for the interaction of combretastatins with tubulin: how important is the trimethoxy unit? *Org. Biomol. Chem.* **2003**, *1*, 3033-3037; e) Hatanaka, T.; Fujita, K.; Ohsumi, K.; Nakagawa, R.; Fukuda, Y.; Nihei, Y.; Suga, Y.; Akiyama, Y.; Tsuji, T. Novel B-ring modified combretastatin analogues: synthesis and antineoplastic activity. *Bioorg. Med. Chem. Lett.* **1998**, *8*, 3371-3374.

8. Ohsumi, K.; Hatanaka, T.; Fujita, K.; Nakagawa, R.; Fukuda, Y.; Nihai, Y.; Suga, Y.; Morinaga, Y.; Akiyama, Y.; Tsuji, T. Synthesis and antitumor activity of cis-restricted combretastatins 5-membered heterocyclic analogues. *Bioorg. Med. Chem. Lett.* **1988**, *8*, 3153-3158.

9. a) Bellina, F.; Cauteruccio, S.; Monti, S.; Rossi, R. Novel imidazole-based combretastatin A-4 analogues. Evaluation of their in vitro antitumor activity and molecular modeling study of their binding to the colchicine site of tubulin. *Bioorg. Med. Chem. Lett.* **2000**, *16*, 5757-5762; b) Wang, L.; Woods, K. W.; Li, Q.; Barr, K. J.; McCroskey, R. W.; Hannick, S. M.; Gherke, L.; Credo, R. B.; Hui, Y.-H.; Marsh, K.; Warner, R.; Lee, J. Y.; Zielinski-Mozng, N.; Frost, D.; Rosenberg, S. H.; Sham, H. L. Potent, orally active heterocycle-based combretastatin A-4 analogues: synthesis, structure-activity relationship, pharmaokinetics, and in vivo antitumor activity evaluation. *J. Med. Chem.* **2002**, *45*, 1697-1711.

10. Kaffy, J.; Pontikis, R.; Carrez, D.; Croisy, A.; Monneret, C.; Florent, J.-C. Isoxazole-type derivatives related to combretastatin A-4, synthesis and biological evaluation. *Bioorg. Med. Chem.* **2006**, *14*, 4067-4077.

11. Wu, M.; Li, W.; Yang, C.; Chen, D.; Ding, J.; Chen, Y.; Lin, L.; Xie, Y. Synthesis and activity of combretastatin A-4 analogues: 1,2,3-thiadiazoles as potent antitumor agents. *Bioorg. Med. Chem. Lett.* **2007**, *17*, 869-873.

12. Odlo, K.; Hntzen, J.; Fournier dit Chabert, J.; Ducki, S.; Gani, O. A. B. S. M.; Sylte, I. Skrede, M.; Florenes, V. A.; Hansen, T. V. 1,5-Disubstituted 1,2,3-triazoles as cis-restricted analogues of combretastatin A-4: synthesis, molecular modeling and evaluation as cytotoxic agents and inhibitors of tubulin. *Bioorg. Med. Chem.* **2008**, *16*, 4829-4838.

13. Zhang, Q.; Peng, Y.; Wang, X. I.; Keeman, S. M.; Aurora. S.; Welsh, W. J. Highly potent triazole-based tubulin polymerization inhibitors. *J. Med. Chem.* **2007**, *50*, 749-754.

14. Zhu, L.; Guo, P.; Li, G.; Lan, J.; Xie, R.; You, J. Simple copper sal-catalyzed N-arylation of nitrogen-cntaining heterocycles with aryl and heteroaryl halides. *J. Org. Chem.* **2007**, *72*, 8535-8538.

15. Hamel, E. Evaluation of antimitotic agents by quantitative comparisons of their effects on the polymerization of purified tubulin. *Cell Biochem. Biophys.* **2003**, *38*, 1-21.

16. Verdier-Pinard, P.; Lai J.-Y.; Yoo, H.-D.; Yu, J.; Marquez, B.; Nagle D.G.; Nambu, M.; White, J.D.; Falck, J.R.; Gerwick, W.H.; Day, B.W.; Hamel, E. Structure-activity analysis of the interaction of curacin A, the potent colchicine site antimitotic agent, with tubulin and effects of analogs on the growth of MCF-7 breast cancer cells. *Mol. Pharmacol.* **1998**, *53*, 62-67.

17. Vermes, I.; Haanen, C.; Steffens-Nakken, H.; Reutelingsperger, C. A novel assay for apoptosis. Flow cytometric detection of phosphatidylserine expression on early apoptotic cells using fluorescein labelled annexin V. *J. Immunol. Methods* **1995**, *184*, 39–51.

18. a) Ly, J.D., Grubb D.R., Lawen A. The mitochondrial membrane potential ($\Delta\Psi_m$) in apoptosis: an update. *Apoptosis* **2003,** 3, 115-128; b) Green, D. R.; Kroemer, G. The pathophysiology of mitochondrial cell death. *Science* **2005**, *305*, 626–629.

19. Salvioli S.; Ardizzoni A.: Franceschi C.; Cossarizza A JC-1 but not DiOC6(3) or rhodamine 123 is a reliable fluorescent probe to asses $\Delta\Psi$ changes in intact cells: implications for studies on mitochondrial functionality during apoptosis. *FEBS Lett.* **1997** *411*, 77-82.

20. a) Mollinedo, F.; Gajate, C. Microtubules, microtubule-interfering agents and apoptosis. *Apoptosis* **2003**, 8:413-450; b) Vitale, I..; Antoccia, A.; Cenciarelli, C.; Crateri, P.; Meschini, S.; Arancia, G.; Pisano, C.; Tanzarella, C. Combretastatin CA-4 and combretastatin derivative induce mitotic catastrophe dependent on spindle checkpoint and caspase-3 activation in non-small cell lung cancer cells. *Apoptosis* **2007**, *12*, 155-166.

21. c) Zamzami, N.; Marchetti, P.; Castedo, M.; Decaudin, D.; Macho, A.; Hirsch, T.; Susin, S. A.; Petit, P. X.; Mignotte, B.; Kroemer, G. Sequential reduction of mitochondrial transmembrane potential and generation of reactive oxygen species in early programmed cell death. *J. Exp. Med.* **1995**, *182*, 367–377.

22. a) Rothe, G.; Valet, G. Flow cytometric analysis of respiratory burst activity in phagocytes with hydroethidine and 2′,7′-dichlorofluorescein. *J. Leukocyte Biol.* **1990**, *47*, 440–448; b) Cai, J.; Jones, D. P. Superoxide in apoptosis. Mitochondrial generation triggered by cytochrome *c* loss. *J Biol Chem* **1998**, *273*,11401-11404; c) Nohl, H.; Gille, L.; Staniek, K. Intracellular generation of reactive oxygen species by mitochondria. *Biochem Pharmacol* **2005**, *69*, 719–723.

23. a) Thomberry, A. N.; Lazebnik, Y. Caspases: enemies within. *Science* **1998**, *281*, 1312–1316; b) Earshaw, W. C.; Martins, L. M.; Kaufmann, S. H. Mammalian caspases: Structure, activation, substrates and functions during apoptosis. *Annu. Rev. Biochem.* **1999**, *68*, 383–424; c) Reed, J. C. Apoptosis-Based Therapies. *Nat. Rev. Drug Discovery* **2002**, *1*, 111-121; d) Denault, J.-B.; Salvesen, G. S. Caspases: keys in the ignition of cell death. *Chem. Rev.* **2002**, *102*, 4489-4499.

24. Porter, A. G.; Janicke, R. U. Emerging role of caspase-3 in apoptosis *Cell Death Differ* **1999,** *6*, 99-104.

25. Soldani, C.; Scovassi, A. I. Poly(ADP-ribose) polymerase-1 cleavage during apoptosis: an update. *Apoptosis*. **2002,** *7*, 321-328.

26. a) Kluck, R. M.; Bossy-Wetzel, E.; Green, D. R. The release of cytochrome c from mitochondria: a primary site for Bcl-2 regulation of apoptosis. *Science* **1997**, *275*,1132-1136. b) Knudson, C. M.; Korsmeyer, S.. J. Bcl-2 and Bax function independently to regulate cell death *Nature Genet* **1997**, *16*, 358-363.

27. Satchi-Fainaro R.; Puder, M.; Davies, J.; Tran, H.; Greene, A. K.; Corfas, G.; Folkman,

J. Targeting angiogenesis with a conjugate of HPMA copolymer and TNP-470, *Nature Medicine* **2004**, *10*, 255-261.

28. Galbraith, S. M.; Chaplin, D. J.; Lee, F.; Stratford, M. R.; Locke, R. J.; Vojnovic, B.; Tozer, G. M: Effects of combretastatin A4 phosphate on endothelial cell morphology in vitro and relationship to tumour vascular targeting activity in vivo. *Anticancer Res.* **2001,** *21*, 93-102.

29. Ravelli, R. B. G.; Gigant, B.; Curmi, P. A.; Jourdain, I.; Lachkar, S.; Sobel, A.; Knossow, M. Insight into tubulin regulation from a complex with colchicine and a stathmin-like domain. *Nature* **2004**, *428*, 198-202.

30. Viola G.; Fortunato E.; Cecconet L.; Del Giudice L., Dall'Acqua F.; Basso G. Central role of p53 and mitochondrial damage in PUVA-induced apoptosis in human keratinocytes *Toxicol. Appl. Pharm.* **2008**, *227*, 84-96.

31. Molecular Operating Environment (MOE 2008.10). Chemical Computing Group, Inc. Montreal, Quebec, Canada. http://www.chemcomp.com.

32. Korb, O.; Stützle, T.; Exner, T. E. PLANTS: Application of ant colony optimization to structure-based drug design. In *Ant Colony Optimization and Swarm Intelligence*, 5th International Workshop, ANTS 2006, Brussels, Belgium, Sep 4−7, 2006; Dorigo, M.; Gambardella, L. M.; Birattari, M.; Martinoli, A.; Poli, R.; Sttzle, T., Eds.; Springer: Berlin, 2006; LNCS 4150, pp 247− 258.

4.2. Synthesis and Biological Evaluation of 2-(3',4',5'-Trimethoxybenzoyl)-3-Aryl/ArylaminoBenzo[*b*]thiophene Derivatives as a Novel Class of Antiproliferative Agents.

Romeo Romagnoli[*a], Pier Giovanni Baraldi[a], Carlota Lopez Cara[a], Ernest Hamel[b], Giuseppe Basso[c], Roberta Bortolozzi[c] and Giampietro Viola[*c]

[a]*Dipartimento di Scienze Farmaceutiche, Università di Ferrara, Via Fossato di Mortara 17-19, 44100 Ferrara, Italy*

[b]*Screening Technologies Branch, Developmental Therapeutics Program, Division of Cancer Treatment and Diagnosis, National Cancer Institute at Frederick, National Institutes of Health, Frederick, Maryland 21702, USA*

[d]*Dipartimento di Pediatria, Laboratorio di Oncoematologia, Università di Padova, 35131 Padova Italy*

Abstract

The biological importance of microtubules in mitosis, as well as in interphase, makes them an interesting target for the development of anticancer agents. Small molecules such as benzo[*b*]thiophenes are attractive as inhibitors of tubulin polymerization. Thus, a new class of compounds that incorporated the structural motif of the 2-(3',4',5'-trimethoxybenzoyl)-3-aryl/arylamino benzo[*b*]thiophene molecular skeleton, with electron-donating (Me, OMe, SMe or OEt) or electron-withdrawing (F and Cl) substituents on the B-ring, was synthesized and evaluated for antiproliferative activity, inhibition of tubulin polymerization and cell cycle effects. The most promising compound in this series was 2-(3',4',5'-trimethoxybenzoyl)-3-(4'-ethoxyphenyl)-benzo[*b*]thiophene (**4e**), which significantly inhibited cancer cell growth at submicromolar concentrations, especially against HeLa and Jurkat cells, and interacted with tubulin. As determined by flow cytometric analysis, **4e** caused G2/M phase arrest and apoptosis in a time- and concentration-dependent manner. The block in G2/M was correlated with increased expression of cyclin B1 and phosphorylation of cdc25c. Moreover, **4e** perturbed mitochondrial membrane potential and caused activation of caspase-3 and cleavage of poly(ADP-rybose)polymerase (PARP), events that are involved in **4e-**induced apoptosis.

Introduction

The microtubule system of eukaryotic cells plays important roles in regulating cell architecture, and it has an essential role in cell division, since microtubules are a key component of the mitotic spindle[1,2]. Microtubules are a dynamic cellular compartment in both neoplastic and normal cells. This dynamicity is characterized by the continuous turnover of αβ-tubulin heterodimers in the polymeric microtubules. They are involved in a variety of fundamental cellular processes, such as regulation of motility, cell signalling, formation and maintenance of cell shape, as well as transport of material within the cell[3-5]. Numerous chemically diverse antimitotic agents, many of which are derived from natural products, have been found to interact specifically with tubulin[6-13].

Among the natural microtubule depolymerizing agents, combretastatin A-4 (CA-4, **1;** Chart 1) is one of the more studied compounds. CA-4, isolated from the bark of the South African tree *Combretum caffrum*[14]*,* strongly inhibits the polymerization of tubulin by binding to the colchicine site[15]. Because of its structural simplicity, a wide number of CA-4 analogues have been developed and evaluated in structure-activity relationship (SAR) studies [16-18].

Although many synthetic tubulin inhibitors have been synthesized in the last few years, there is still a need to identify novel molecules that target microtubules. Such compounds would ideally be characterized by relatively simple structures and be easy to prepare in a cost-effective way. Among such compounds, the benzo[*b*]thiophene molecular skeleton is the core structure of a series of derivatives with general structure **2** described by Pinney and co-workers [19]. These compounds are based on the 2-aryl-3-(3',4',5'-trimethoxybenzoyl)-benzo[*b*]thiophene ring system and showed antiproliferative activity ranging from 0.5 to 2 μM against human Burkitt lymphoma, CA46 and human breast carcinoma MCF-7 cells. Compound **2a** showed partial effect on tubulin polymerization at a concentration of 40 μM, while **2b** was active at a lower concentration (IC_{50}=3.5 μM) [19,20]. These findings prompted us to study this class of compounds in more detail.

In this article we present a flexible, concise and highly convergent protocol for the preparation of two new series of derivatives with general structure **3** and **4**, characterized by the presence of a substituted aryl or arylamino moiety,

respectively, on the 3-position of the 2-(3',4',5'-trimethoxybenzoyl)benzo[*b*]thiophene core.

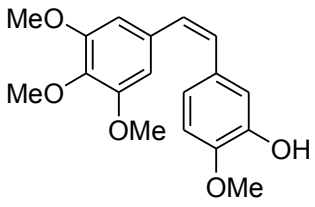

Combretastatin A-4 (CA-4), **1**

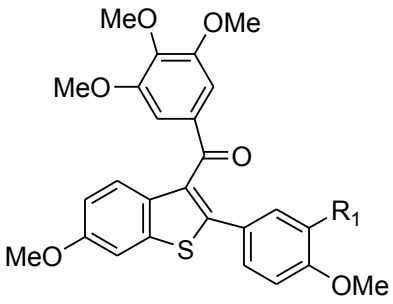

2

R_1=H, **2a**
IC_{50}=2 μM on CA46 cells
IC_{50}=0.64 μM on MCF-7 cells

R_1=OH, **2b**
IC_{50}=0.50 μM on CA46 cells
IC_{50}=0.52 μM on MCF-7 cells

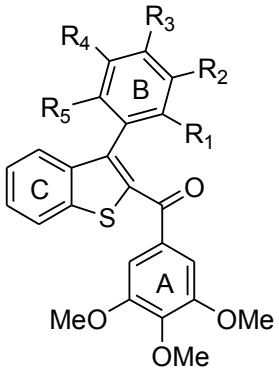

3a-k

R_{1-5}=H, **3a**
R_3=F, $R_{1-2,\ 4-5}$=H, **3b**
R_3=Cl, $R_{1-2,\ 4-5}$=H, **3c**
R_3=Me, $R_{1-2,\ 4-5}$=H, **3d**
R_3=OMe, $R_{1-2,\ 4-5}$=H, **3e**
R_3=SMe, $R_{1-2,\ 4-5}$=H, **3f**
R_1=OMe, R_{2-5}=H, **3g**
$R_{1,3}$=OMe, $R_{2,4\ 5}$=H, **3h**
$R_{1,4}$=OMe, $R_{2-3,\ 5}$=H, **3i**
R_2=Me, R_3=OMe, $R_{1,\ 4-5}$=H, **3j**
R_3=OEt, $R_{1-2,\ 4-5}$=H, **3k**

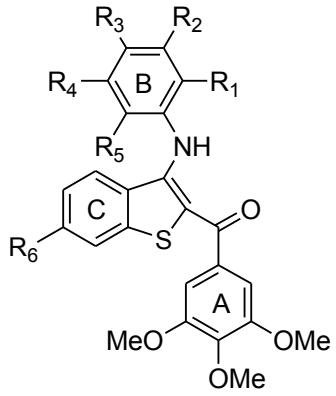

4a-g

R_{1-6}=H, **4a**
R_3=Cl, $R_{1-2,\ 4-6}$=H, **4b**
R_3=Me, $R_{1-2,\ 4-6}$=H, **4c**
R_3=OMe, $R_{1-2,\ 4-6}$=H, **4d**
R_3=OEt, $R_{1-2,\ 4-6}$=H, **4e**
$R_{3,6}$=Me, $R_{1-2,\ 4-5}$=H, **4f**
R_3=OEt, R_6=Me, $R_{1-2,\ 4-5}$=H, **4g**

Chart 1. Inhibitors of Tubulin Polymerization

In the present investigation, the 3',4',5'-trimethoxyphenyl group on the 2-benzoyl moiety was kept unchanged because it is the characteristic structural requirement for activity in a numerous inhibitors of tubulin polymerization, such

as colchicine, CA-4 and podophyllotoxin [21-23]. The pharmacological evaluation of compounds **3a-k** and **4a-e** allowed us to investigate SAR when electron-withdrawing (F and Cl) or electron-releasing (Me, MeO, MeS and EtO) substituents were placed on the B-ring at the 3-position of the benzo[*b*]thiophene ring.

Finally, by the synthesis of compounds **4f-g** we evaluated the effect of the introduction of the electron–releasing methyl group at the 6-position of the C-ring of the benzo[*b*]thiophene nucleus.

Chemistry

The 2-(3',4',5'-trimethoxybenzoyl)-3-aryl/arylamino benzo[*b*]thiophene derivatives **3a-k** and **4a-g** were synthesized by the procedure reported in Scheme 1.

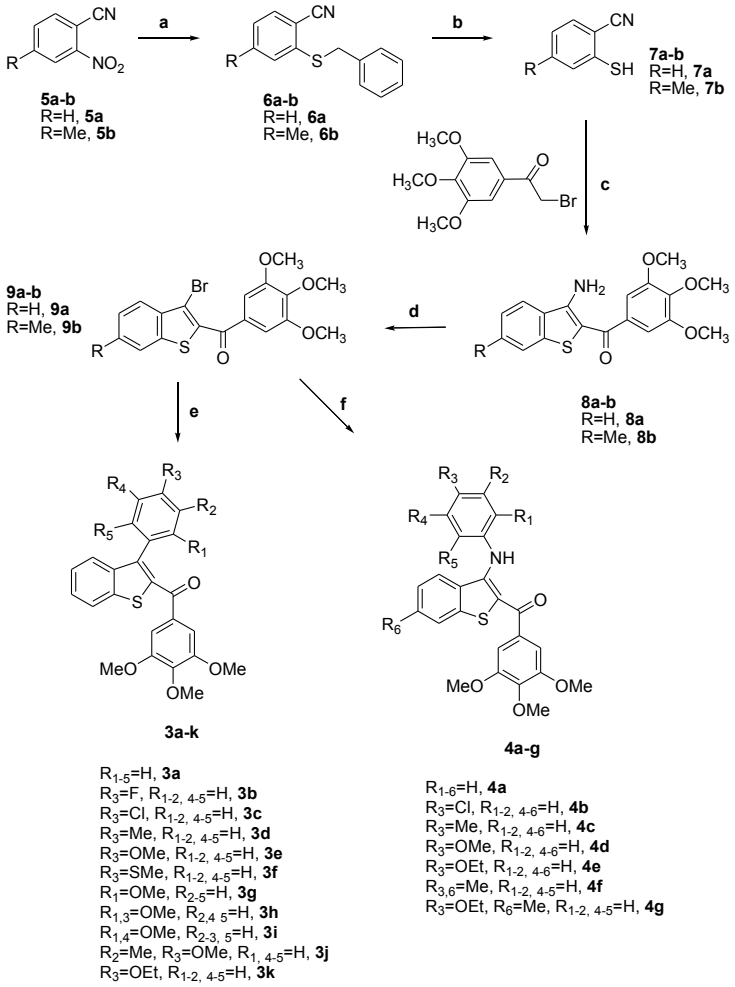

Reagents. **a**: $C_6H_5CH_2SH$, KOH, DMF; **b**: $AlCl_3$, C_6H_6; **c**: 3,4,5-trimethoxphenyl-2-bromoethanone, K_2CO_3, $(CH_3)_2CO$, rx, 18 h; **d**: t-BuONO, $CuBr_2$, CH_3CN, 65 °C; **e**: **9a**. $ArB(OH)_2$, $Pd(PPh_3)_4$, K_2CO_3, PhMe, rx, 18 h, **f**: **9a** or **9b**, $ArNH_2$, $Pd(OAc)_2$, BINAP, $CsCO_3$, PhMe, 100 °C, 16 h.

Scheme 1 synthesis procedure of 2-(3',4',5'-trimethoxybenzoyl)-3-aryl/arylamino benzo[*b*]thiophene

Detailed description of the procedure is reported in the full article published on European Journal of Medicinal Chemistry (2010 Oct 6).

Biological Results and Discussion

Table 1 summarizes the growth inhibitory effects of 2-(3',4',5'-trimethoxy)benzo[*b*]thiophene derivatives **3a-j** and **4a-g** against a panel of five human cell lines, which were derived from different cancer types, including cervix carcinoma (HeLa), non-small lung carcinoma (A549), promyelocytic leukemia (HL-60), T-leukemia (Jurkat) and chronic myelogenous leukemia (K562) cells. All of the compounds showed a considerable growth inhibitory effect and were active in the micromolar range, although the difference between the different cell lines are not significative. Of all tested compounds, the 3-(4'-ethoxyphenylamino) derivative **4e** possessed the highest potency, inhibiting the growth of HeLa, A549, HL-60, Jurkat and K562 cells with IC_{50} values of 0.7, 1.4, 0.5, 0.3 and 0.2 μM, respectively. These values are from 2- to 15-fold lower than those obtained with the 3-(4-ethoxyphenyl) derivative **3k**. Starting from **4e**, the introduction of a C-6 methyl on the C-ring (compound **4g**) has a detrimental effect on activity, with **4g** being 4- to 20-fold less potent than **4e**.

Compound	IC_{50} [a](mM)				
	HeLa	A549	HL-60	Jurkat	K562
3a	1.9±0.9	5.0±0.9	1.7±0.3	1.5±0.5	2.1±0.4
3b	3.0 ± 0.3	3.2±0.4	3.2±0.8	2.3±0.9	2.1±0.4
3c	5.2 ± 2.6	7.5±0.7	3.3±0.7	3.7±0.8	4.2±0.3
3d	3.7 ± 1.0	7.8±0.8	1.4±0.5	3.3±1.0	3.5±0.3
3e	4.2 ± 1.3	4.4±0.5	1.6±0.5	1.6±0.6	1.7±0.3
3f	3.5 ± 0.4	5.4±0.5	1.3±0.6	1.9±0.2	1.8±0.3
3g	5.0±0.7	>10	2.9±0.2	2.9±0.3	3.4±0.5
3h	3.9±0.5	5.8±0.5	4.6±0.2	4.0±0.2	4.1±0.2
3i	>10	>10	>10	>10	>10
3j	>10	>10	>10	>10	>10
3k	3.0±0.2	3.1±0.05	3.5±0.5	4.1±0.5	3.1±0.2
4a	2.7 ± 0.1	3.0±0.2	5.2±0.8	1.6±0.8	2.3±0.1
4b	3.7 ± 0.05	3.1±0.1	5.4±0.5	1.9±0.1	1.1±0.2
4c	3.5 ±0.8	2.6±0.3	4.6±0.8	1.7±0.5	1.6±0.2
4d	7.7±0.8	9.3±0.9	3.7±0.3	3.5±0.8	2.9±0.5
4e	0.7 ± 0.2	1.4±0.2	0.5±0.1	0.3 ± 0.1	0.2±0.05
4f	0.98 ± 0.2	1.9±0.4	1.9±0.5	2.5±0.8	1.4± 0.3
4g	4.3 ± 0.2	5.8±0.2	4.0±0.6	5.0±0.4	4.3± 0.5

[a]IC_{50}= compound concentration required to inhibit tumor cell proliferation by 50%. Data are expressed as the mean ± SE from the dose-response curves of at least three independent experiments.

Table 1. In vitro antiproliferative effects of compounds 3a-k and 4a-g

In comparing compounds with the same substituent on the B-ring (**3a** *vs.* **4a**, **3c** *vs.* **4b**, **3d** *vs.* **4c**, **3e** *vs.* **4d**, **3k** *vs.* **4e**) in terms of the average IC_{50}, in two cases (the unsubstituted **3a** and the *para*-methoxy substituted **3e**) the aryl derivative was more active than the 3-anilino derivative. In contrast, the 3-anilino derivatives **4b**, **4c** and **4e**, with *para*-chloro, *para*-methyl and *para*-ethoxy substituents, respectively, were more active than the corresponding aryl derivatives.

In the series of 3-aryl analogues **3b-k**, the *para*-substituted phenyl derivatives with either electron-withdrawing groups, such as fluorine (**3b**) or chlorine (**3c**), or an electron-donating group, like methyl (**3d**), methoxy (**3e**), thiomethyl (**3f**) or ethoxy (**3k**), exhibited good antiproliferative activities, with average IC_{50} values of 2.7-4.8 μM. Introducing an electron-withdrawing fluorine (**3b**) or chlorine (**3c**) led to reduction in antiproliferative activity in comparison with the unsubstituted derivative **3a**, with the chlorine having a greater effect than the fluorine atom. Electron-donating groups also caused a loss of activity relative to **3a**, with the least effects occurring with *para* thiomethyl and methoxy groups (**3e** and **3f**, respectively).

Moving the methoxy group from *para*- (**3f**) to the *ortho*-position (**3g**) caused about a 50% loss in average antiproliferative activity, as did addition of a second methoxy group at the *ortho* position (**4h**). Still larger losses in activity occurred with addition of a *meta*-methyl group (**3j**) or with two methoxy groups in the *ortho* and *meta* positions (**3i**).

In the series of 3-anilino derivatives **4a-g**, average antiproliferative activity was more dependent on the substituent on the B-phenyl ring at the 3-position, there being a 9-fold difference between **4e**, the most active compound in the group, and **4d**, the least active.

Relative to the unsubstituted **4a**, the electron withdrawing chlorine (**4b**), had essentially no effect, while the different electron-donating groups had variable effects. Thus, the *para* methyl group (**4c**) had minimal effect, the *para* methoxy group (**4d**) led to almost a 50% loss in activity, and the *para* ethoxy group (**4e**) to a 5-fold increase in activity. One further modification we explored in the 3-anilino derivatives was addition of a methyl substituent in ring C, at the 6-position of the benzo[*b*]thiophene skeleton. Again the effect was variable. With a *para* methyl substituent on the B ring, the C ring methyl enhanced activity (cf. **4f**

with **4c**). In contrast, with the *para* ethoxy substituent, the C ring methyl group led to almost a 3-fold loss of activity (cf. **4g** with **4e**).

To investigate whether the antiproliferative activities of these compounds were related to an interaction with the microtubule system, the compounds **4e**, **4f** and **4g**, were evaluated for their effects on tubulin polymerization [30]. For comparison, CA-4 was examined in contemporaneous experiments as a reference compound. The benzo[*b*]thiophene derivatives **4e** and **4f** inhibited the assembly reaction with IC_{50} values of 7.2 and 15 μM, respectively, considerably higher than the value obtained with CA-4 (IC_{50}=1.0 μM). Compound **4g**, however, did not inhibit the reaction by 50% even 40 μM. These results indicate that tubulin may be the intracellular target of compounds **4e** and **4f**. Nevertheless, we could not exclude the possibility that these compounds may affect other molecular targets in addition to microtubules resulting in the enhanced cytotoxicity.

4e induces G2/M phase arrest and changes the expression of G2/M regulatory proteins. Because molecules exhibiting effects on tubulin assembly should cause alteration of cell cycle parameters with preferential G2/M blockade, flow cytometric analysis was performed to determine the effect of different concentrations of the most active compound **4e** on leukemia T-cell Jurkat (Figure1A) and HeLa cells (Figure 1B). Cellular DNA was stained with propidium iodide (PI) for these studies.

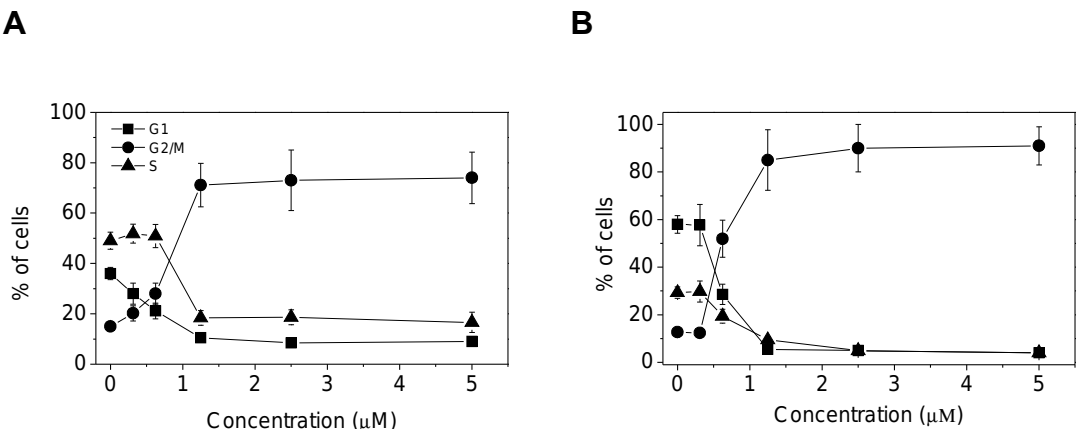

Figure 1. Effect of 4e-induced G2/M phase arrest in Jurkat (panel A) and HeLa cells (panel B). Cells were treated with different concentrations ranging from 0.312 to 5 μM for 24 h. The cells were fixed and stained with PI to analyze DNA content by flow cytometry. Data are presented as mean ± SEM of two independent experiments.

Untreated Jurkat cells showed a classic pattern of proliferating cells distributed between the G1 (58%), S (36%) and G2/M (15%) phases. With **4e** treatment, a clear G2/M arrest pattern occurred in a concentration-dependent manner, with a concomitant decrease of cells in the other phases of the cell cycle. In particular, as showed in Figure 1 (panel A), the G2/M cell population increased from 15 % in the control to 70% with compound **4e** at 1.25 μM. Under the same conditions, the G1 cells decreased from 58 in the control to 10% and the S phase cellsdecreased from 36 to 18%.

In the HeLa cells, the G2/M block induced by **4e** was even more pronounced (Figure 1 panel B). At 0.625 μM, 52% of the cells were blocked in G2/M, and this increased further to 85% at 1.25 μM, with accompanying reductions of cells in the G1 and S phases. After 48 h of treatment, a hypodiploid peak (sub-G1) indicative of apoptosis, appeared in both cell lines (data not shown).

We next studied the association between **4e**-induced G2/M arrest and alterations in expression of proteins that regulate cell division. Generally, antimitotic drugs directed against tubulin, cause cell arrest at the prometaphase/metaphase to anaphase transition, which is normally regulated by the mitotic checkpoint [31]. In eukaryotic cells, cyclin B and cdc25c kinase regulate the onset of the G2/M phase. Phosphorylation of cdc25c directly stimulates its phosphatase activity, and this is necessary to activate cyclin B kinase on entry into mitosis [32].

As shown in Figure 2 in HeLa cells, **4e** causes a concentration-dependent increase in cyclin B1 expression, while slower migrating forms of phosphatase cdc25c were present, indicating changes in the phosphorylation state of this protein.

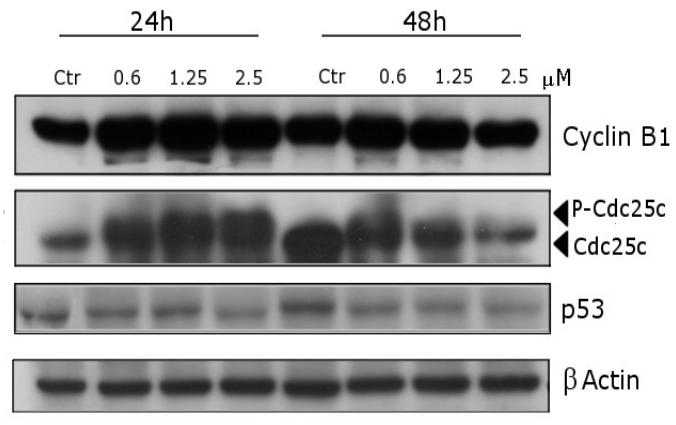

Figure 2. Effect of **4e** on the expression of cell cycle protein regulators. HeLa cells were treated for 24 or 48 h with the indicated concentration of the compound. The cells were harvested and lysed for the detection of cyclin B1, cdc25c and p53 expression by western blot analysis. To ensure equal protein loading, each membrane was stripped and reprobed with anti-b-actin antibody

These changes are consistent with the observed cell cycle arrest in mitosis.

The tumor suppressor protein p53 acts as a DNA binding transcription factor, regulating specific target genes to arrest the cell cycle and initiate apoptosis. However, with increasing concentrations of **4e,** there was no difference in the expression of p53. This suggests that cell growth inhibition and apoptosis induced by **4e** may be through a p53-independent pathway.

Analysis of cell death. To characterize the mode of cell death induced by **4e**, a biparametric cytofluorimetric analysis was performed using PI, which stains DNA and is permeable only to dead cells, and fluorescent immunolabeling of the protein annexin-V, which binds to the phospholipid phosphatidylserine (PS) in a highly selective manner[33,34].

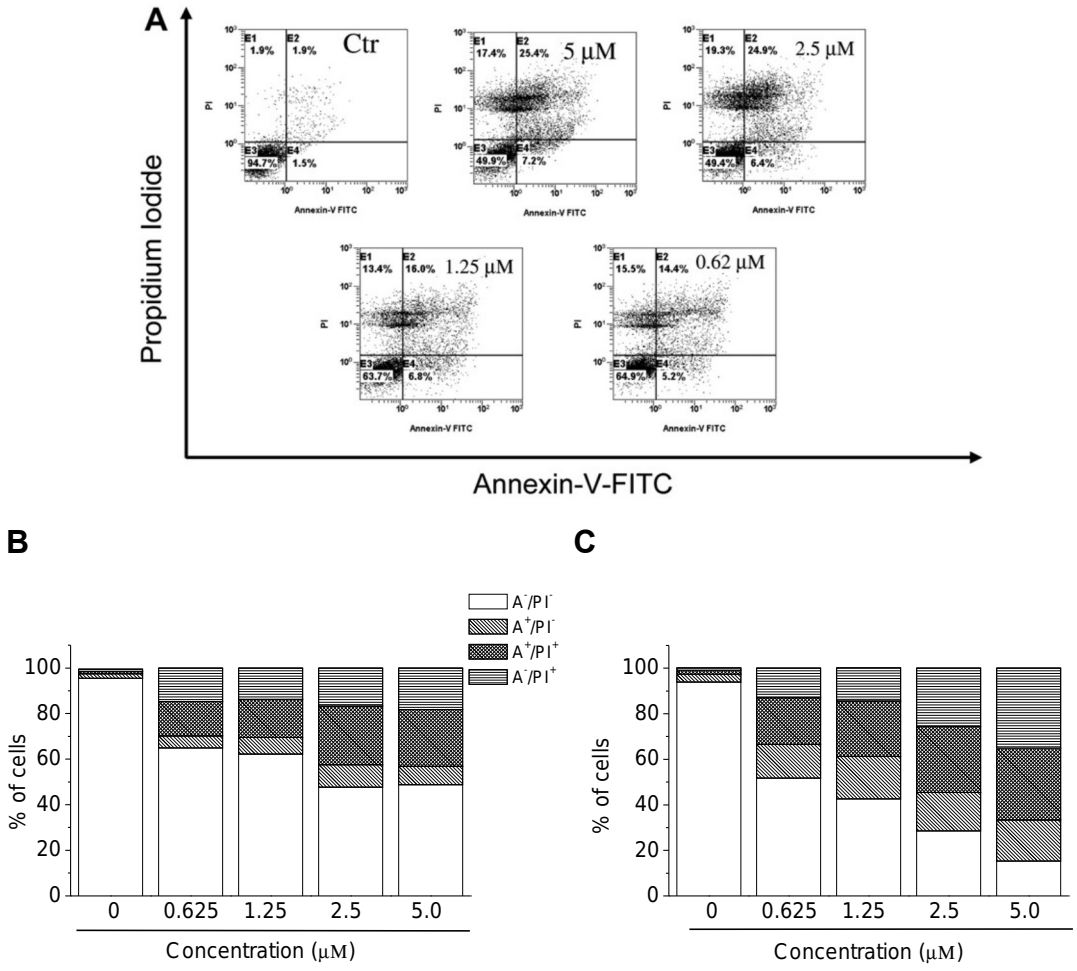

Figure 3. Flow cytometric analysis of apoptotic cells after treatment of HeLa cells with 4e. The cells were labeled with annexin-V-FITC and PI and analyzed by flow cytometry. **A** Representative biparametric histograms obtained after 24 h of incubation at the indicated concentration of 4e. In these histograms, the lower left-hand segment represents the annexin-V^-/PI^- cells, the lower right-hand segment the annexin-V^+/PI^- cells, the upper right-hand segment the annexin-V^+/PI^+ cells, and the upper left-hand segment the annexin-V^-/PI^+ cells. **B** and **C**. Percentage of cells found in the different regions of the biparametric histograms shown in panel A, after incubation with 4e for 24 h (**B**) and 48 h (**C**).

This phospholipid flips from the inner to the outer leaflet of the plasma membrane during apoptosis. Positive staining with annexin-V correlates with the loss of plasma membrane polarity, but this staining precedes the complete loss of membrane integrity that accompanies the later stages of cell death, resulting from either apoptosis or necrosis. In contrast, PI can only enter cells after complete loss of membrane integrity. Thus, dual staining for annexin-V and with PI permits discrimination between unaffected cells (annexin-V^-/PI^-), early apoptotic cells (annexin-V^+/PI^-), late apoptotic cells (annexin-V^+/PI^+) and necrotic cells (annexin-V^-/PI^+)[34]. Figure 3 (panel A) shows representative, biparametric histograms demonstrating the effects of different concentrations of **4e** on HeLa cells after 24 h of treatment. Compound **4e** at 24 h had already induced an accumulation of annexin-V positive cells in comparison with the control, and this accumulation was concentration dependent. There was a further increase in these apoptotic and necrotic cells at 48 h.

These findings led us to us to investigate further apoptotic pathways following treatment with 4e.

Mitochondrial depolarization and generation of reactive oxygen species (ROS). Mitochondria play a key role in the apoptotic process, and it is well established that at an early stage apoptotic stimuli alter the mitochondrial potential ($\Delta\Psi_{mt}$) [35,36]. Rhodamine 123 (Rho 123) was used as an indicator of mitochondrial membrane potential [37] analyzing, by flow cytometry, HeLa cells after treatment with compound **4e**. As shown in Figure 4 (panel A), the test compound induced in a concentration and time dependent manner a reduction of Rho123 fluorescence intensity, which reflects the collapse of $\Delta\Psi_{mt}$.

Mitochondrial membrane depolarization is associated with mitochondrial production of ROS[38]. Therefore, we investigated whether ROS production increased after treatment with the test compounds. We utilized the fluorescence indicator hydroethidine (HE), whose fluorescence appears if ROS are generated[39,40]. HE is oxidized by superoxide anion into the ethidium ion, which fluoresces red. Superoxide is produced by mitochondria due to a shift from the normal 4-electron reduction of O_2 to a 1-electron reduction when cytochrome c is released from mitochondria. ROS generation was also measured with the dye 2,7-dichlorodihydrofluorescein diacetate (H_2-DCFDA), which is oxidized to the

fluorescent compound dichlorofluorescein (DCF) by a variety of peroxides including hydrogen peroxide[40].

The results are presented in Figure 4 (panels B and C), where it can be observed that **4e** induces the production of large amounts of ROS in comparison with control cells, which agrees with the previously described dissipation of $\Delta\psi_{mt}$.

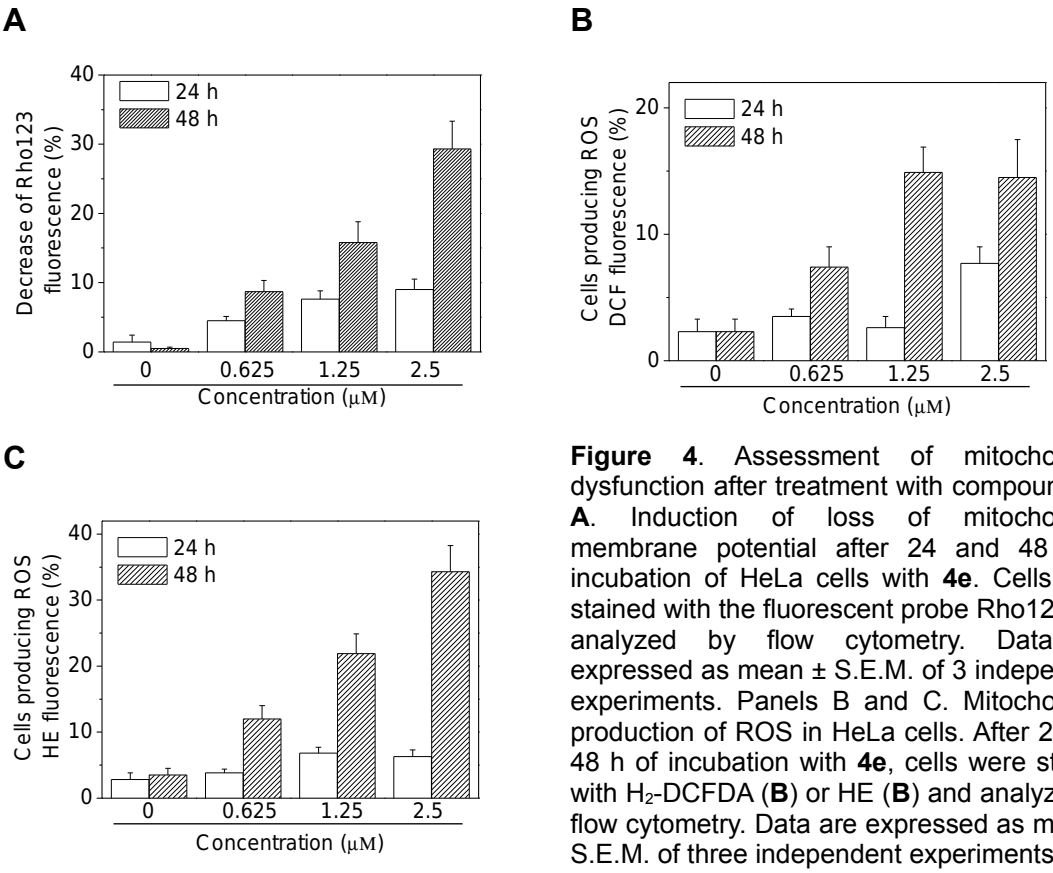

Figure 4. Assessment of mitochondrial dysfunction after treatment with compound **4e**. **A**. Induction of loss of mitochondrial membrane potential after 24 and 48 h of incubation of HeLa cells with **4e**. Cells were stained with the fluorescent probe Rho123 and analyzed by flow cytometry. Data are expressed as mean ± S.E.M. of 3 independent experiments. Panels B and C. Mitochondrial production of ROS in HeLa cells. After 24 and 48 h of incubation with **4e**, cells were stained with H_2-DCFDA (**B**) or HE (**B**) and analyzed by flow cytometry. Data are expressed as mean ± S.E.M. of three independent experiments.

Caspase activation and PARP cleavage. The mechanism by which apoptosis is induced by antimitotic drugs is not completely understood [31]. The activation of caspases represent a crucial step in the induction of drug induced apoptosis and cleavage of poly(ADP-ribose)polymerase (PARP) by caspase-3 is considered to be one of the hallmarks of apoptosis[41-44]. As shown in Figure 5 (panel A), incubation of HeLa cells with compound **4e** resulted in the activation of caspase-3 in a time- and concentration dependent manner. In agreement with this finding, immunoblot analysis (Figure 5, panel B) showed that the typical 89 kDa cleaved fragment of PARP increased in treated cells with compound **4e** after 24 h and especially after 48 h of treatment.

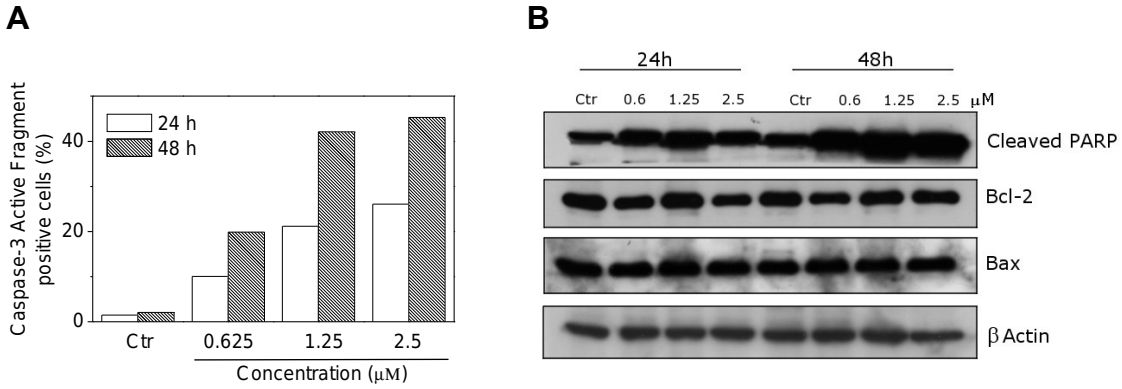

Figure 5. A Caspase-3 induced activity by compound 4e. HeLa cells were incubated in the presence of **4e**. After 24 and 48 h of treatment, cells were stained with an anti-human active caspase-3 fragment monoclonal antibody conjugated with FITC. Data are expressed as percentage of Caspase-3 active fragment positive cells. **B** Western blot analysis for the cleavage of PARP and the expression of Bcl-2 and Bax in HeLa cells after treatment with 4e for 24h and 48h.

Bcl-2 is a protein that has been extensively investigated as a modulating agent of apoptosis and plays a major role as an inhibitor of apoptosis. It does this by regulating the mitochondrial membrane potential, thus avoiding release of cytochrome *c* and caspase activation[45]. Another protein involved in the apoptosis pathways is Bax, which has been shown to promote apoptosis and increases the sensitivity of cancer cells to a variety of antineoplastic agents[46]. Therefore, we examined whether the induction of apoptosis by **4e** was associated with changes in the expression of these proteins. As shown in Figure 6 (panel B) by immunoblot analysis, treatment with **4e** resulted in a slight decrease in the expression of Bcl-2 while the expression of Bax remained unchanged.

Altogether these data indicate that the induction of apoptosis by **4e** is associated with Bcl-2 down regulation and caspase-3 activation, which in turn stimulates PARP cleavage.

Conclusions

In this report we have described a procedure that gives access to a range of substitution patterns at the 3-position of the benzo[*b*]thiophene ring, making it an ideal process for SAR studies of biologically active molecules. In the series of 3-aryl derivatives **3a-k**, the introduction both of electron-releasing or electron withdrawing groups on the B-ring did not have a profound effect on the activity

in comparison with the unsubstituted 3-aryl derivative **3a**. This study revealed that 2-(3',4',5'-trimethoxybenzoyl) 3-substituted benzo[*b*]thiophenes are an interesting class of compounds, and our SAR study showed that **4e** was the most active agent among those synthesized, since **4e** had antiproliferative activity in the submicromolar range against HeLa, HL-60, Jurkat and K562 cells. The introduction of a methyl group at the C-6 position of benzo[*b*]thiophene core was detrimental to antiproliferative activity. We also showed that the antiproliferative activity of **4e** and **4f** may derived from a interference with microtubule assembly, although at this stage we cannot exclude that other molecular targets could be involved in the mechanism of action of these compounds. The interaction with tubulin leads to cell cycle arrest in the G2/M phase. Consistent with the mitotic block, treatment of HeLa cells led to increased expression of cyclin B1, which then phosphorylated cdc25c. We also found that mitotic arrest caused by **4e** was associated with the induction of apoptosis, as manifested by loss of mitochondrial membrane potential, generation of ROS and activation of caspase-3 with typical cleavage of PARP.

Experimental protocols

Chemistry. Detailed methods and protocols described in the full article published on European Journal of Medicinal Chemistry in 2010 Oct 6

Antiproliferative assays. Human T-leukemia (Jurkat), human promyelocytic leukemia (HL-60) and human chronic myelogenous leukemia (K562) cells were grown in RPMI-1640 medium, (Gibco, Milano Italy). Human non-small lung carcinoma (A549) and human cervix carcinoma (HeLa) cells were grown in DMEM medium (Gibco, Milano, Italy) Both media were supplemented with 115 units/mL of penicillin G (Gibco, Milano, Italy), 115 μg/mL streptomycin (Invitrogen, Milano, Italy) and 10% fetal bovine serum (Invitrogen, Milano, Italy). Individual wells of a 96-well tissue culture microtiter plate were inoculated with 100 μL of complete medium containing $8x10^3$ cells. The plates were incubated at 37 °C in a humidified 5% CO_2 incubator for 18 h prior to the experiments. After medium removal, 100 μL of the drug solution, dissolved in complete

medium at different concentrations, was added to each well and incubated at 37 °C for 72 h. Cell viability was assayed by the (3-(4,5-dimethylthiazol-2-yl)-2,5-diphenyl tetrazolium bromide (MTT) test as previously described[47]. The IC_{50} was defined as the compound concentration required to inhibit cell proliferation by 50%.

Effects on tubulin polymerization. To evaluate the effect of the compounds on tubulin assembly *in vitro*[30], varying concentrations were preincubated with 10 μM tubulin in glutamate buffer at 30 ˚C and then cooled to 0 ˚C. After addition of GTP, the mixtures were transferred to 0 °C cuvettes in a recording spectrophotometer and warmed to 30 °C, and the assembly of tubulin was observed turbidimetrically. The IC_{50} value was defined as the compound concentration that inhibited the extent of assembly by 50% after a 20 min incubation.

Flow cytometric analysis of cell cycle distribution. For flow cytometric analysis of DNA content, $5x10^5$ HeLa or Jurkat cells in exponential growth were treated with different concentrations of the test compounds for 24 and 48 h. After the incubation, the cells were collected, centrifuged and fixed with ice-cold ethanol (70%). The cells were then treated with lysis buffer containing RNAse A and 0.1% Triton X-100 and then stained with PI. Samples were analyzed on a Cytomic FC500 flow cytometer (Beckman Coulter). DNA histograms were analyzed using MultiCycle® for Windows (Phoenix Flow Systems).

Annexin-V assay. Surface exposure of PS on apoptotic cells was measured by flow cytometry with a Coulter Cytomics FC500 (Beckman Coulter) by adding Annexin-V-FITC to cells according to the manufacturer's instructions (Annexin-V Fluos, Roche Diagnostic). Simultaneously the cells were stained with PI. Excitation was set at 488 nm, and the emission filters were at 525 nm and 585 nm, respectively.

Assessment of mitochondrial changes. The mitochondrial membrane potential was measured with the fluorescent dye rhodamine 123 (Rho 123, Pierce, Rockford IL, USA), as described[37]. Briefly, after different times of

treatment, the cells were collected by centrifugation and resuspended in Hank's Balanced Salt Solution (HBSS) containing 0.1 μM Rho123. The cells were then incubated for 20 min at 37 °C, centrifuged and resuspended in HBSS. The production of ROS was measured by flow cytometry using either HE (Molecular Probes) or H_2DCFDA (Molecular Probes). After different times of treatment, cells were collected by centrifugation and resuspended in HBSS containing the fluorescence probes HE or H_2DCFDA at the concentrations of 2.5 and 0.1 M, respectively. The cells were then incubated for 30 min at 37 °C, centrifuged and resuspended in HBSS. The fluorescence was directly recorded with the flow cytometer, using as excitation wavelength 488 nm and emission at 585 nm and 530 nm for HE and H_2DCFDA, respectively.

Caspase-3 assay. Caspase-3 activation in Jurkat cells was evaluated by flow cytometry using a human active caspase-3 fragment antibody conjugated with FITC (BD Pharmingen). Briefly, after different incubation times in the presence of test compounds, the cells were collected by centrifugation and resuspended in Cytofix™ (BD Pharmingen) buffer for 20 min, washed with Perm/Wash™ (BD Pharmingen) and then incubated for 30 min with the antibody. After this period, cells were washed and analyzed by flow cytometry. Results are expressed as percentage of caspase-3 active fragment positive cells.

Western Blot Analysis. Jurkat cells were incubated in the presence of test compounds and, after different times, were collected, centrifuged and washed two times with ice cold phosphate-buffered saline (PBS). The pellet was then resuspended in lysis buffer. After the cells were lysed on ice for 30 min, lysates were centrifuged at 15000 x g at 4 °C for 10 min. The protein concentration in the supernatant was determined using BCA protein assay reagents (Pierce, Italy). Equal amounts of protein (20 μg) were resolved using sodium dodecyl sulfate polyacrylamide gel electrophoresis (SDS-PAGE) (7.5-15% acrylamide gels) and transferred to a PVDF Hybond-p membrane (GE Healthcare). Membranes were blocked with I-block (Tropix), the membrane being gently rotated overnight at 4 °C. Membranes were then incubated with primary antibodies against, Bcl-2, PARP, Cdc25C, Bax, and p53 (all rabbit, 1:1000, Cell Signalling, Milano, Italy), Cyclin B1 (mouse, 1:1000, BD, Milano Italy) or β-actin

(mouse, 1:10,000, Sigma-Aldrich, Milano, Italy) for 2 h at room temperature. Membranes were next incubated with peroxidase-labeled goat anti-rabbit IgG (1:100,000, Sigma-Aldrich) or peroxidase-labeled goat anti-mouse IgG (1:100,000, Sigma-Aldrich) for 60 min. All membranes were visualized using ECL Advance (GE Healthcare) and exposed to Hyperfilm MP (GE Healthcare). To ensure equal protein loading, each membrane was stripped and reprobed with anti-β-actin antibody.

References

1. L. A. Amos. Microtubule structure and its stabilisation. Org. Biomol. Chem. 2 (2004) 2153-2160.
2. C. E. Walczak. Microtubule dynamics and tubulin interacting proteins. Curr. Opin. Cell. Biol. 12 (2000) 52-56.
3. K. H. Downing, E. Nogales. Tubulin structure: insights into microtubule properties and functions. Curr. Opin. Struct. Biol. 8 (1998) 785-791.
4. K. H. Downing. Structural basis for the interaction of tubulin with proteins and drugs that affect microtubule dynamics. Annu. Rev. Cell. Dev. Biol. 16 (2000) 89-111.
5. P. K. Sorger, M. Dobles, R. Tournebize, A. A. Hyman. Coupling cell division and cell death to microtubule dynamics. Curr. Opin. Cell. Biol. 9 (1997) 807-814.
6. N. Mahindroo, J. P. Liou, J. Y. Chang, H. P. Hsieh. Antitubulin agents for the treatment of cancer. A medicinal chemistry update. Exp. Opin. Ther. Pat. 16 (2006) 647-691.
7. M. A. Jordan, L. Wilson. Microtubules as a target for anticancer drugs. Nat. Rev. Cancer 4 (2004) 253-265.
8. J. A. Hadfield, S. Ducki, N. Hirst, A. T. McGown. Tubulin and microtubules as targets for anticancer drugs. Prog. Cell Cycle Res. 5 (2003) 309-325.
9. S. Honore, E. Pasquier, D. Braguer. Understanding microtubule dynamics for improved cancer therapy. Cell. Mol. Life. Sci. 62 (2005) 3039-3065.
10. F. Pellegrini, D. R. Budman. Review: tubulin function, action of antitubulin drugs, and new drug development. Cancer Invest. 23 (2005) 264-273.
11. G. Attard, A. Greystoke, S. Kaye, J. De Bono Update on tubulin binding agents. Pathol. Biol. 54 (2006) 72-84.
12. T. Beckers, S. Mahboobi. Natural semisynthetic and synthetic microtubule inhibitors for cancer therapy. Drugs Future 28 (2003) 767-785.
13. B. R. Hearn, S. J. Shaw, D. C. Myles. Microtubule targeting agents. Comprehensive Medicinal Chemistry II 7 (2007) 81-110.
14. G. R. Pettit, S. B. Singh, E. Hamel, C. M. Lin, D. S. Alberts, D. Garcia-Kendall. Isolation and structure of the strong cell growth and tubulin inhibitor combretastatin A-4. Experentia 45 (1989) 209-211.
15. C. M. Lin, H. H. Ho, G. R. Pettit, E. Hamel. Antimitotic natural products combretastatin A-4 and combretastatin A-2: studies on the mechanism of their inhibition of the binding of colchicine to tubulin. Biochemistry 28 (1989) 6984-6991.

16. N. H. Nam. Combretastatin A-4 analogues as antimitotic antitumor agents. Curr. Med. Chem. 10 (2003) 1697-1722.

17. A. Chaudari, S. N. Pandeya, P. Kumar, P. P. Sharma, S. Gupta, N. Soni, K. K. Verma, G. Bhardwaj. Combretastain A-4 analogues as anticancer agents. Mini Rev. Med. Chem. 12 (2007) 1186–1205.

18. G. C. Tron, T. Pirali, G. Sorba, F. Pagliai, S. Busacca, A. Genazzani. A. Medicinal chemistry of combretastatin A4: present and future directions. J. Med. Chem. 49 (2006) 3033-3044.

19. K. G. Pinney, A. D. Bounds, K. M. Dingerman, V. P. Mocharla, G. R. Pettit, R. Bai, E. Hamel. A new anti-tubulin agent containing the benzo[b]thiophene ring system. Bioorg. Med. Chem. Lett. 9 (1999) 1081-1086.

20. B. L. Flynn, P. Verdier-Pinard, E. Hamel. A novel palladium-mediated coupling approach to 2,3-disubstituted benzo[b]thiophenes and its application to the synthesis of tubulin binding agents. Org. Lett. 3 (2001) 651-654.

21. A. Chaudari, S. N. Pandeya, P. Kumar, P. P. Sharma, S. Gupta, N. Soni, K. K. Verma, G. Bhardwaj. Combretastain A-4 analogues as anticancer agents. Mini Rev. Med. Chem. 12 (2007) 1186–1205.

22. K. Gaukroger, J. A. Hadfield, N. J. Lawrence, S. Nlan, A. T. McGown Structural requirements for the interaction of combretastatins with tubulin: how important is the trimethoxy unit? Org. Biomol. Chem. 1 (2003) 3033-3037.

23. T. Hatanaka, K. Fujita, K. Ohsumi, R. Nakagawa, Y. Fukuda, Y. Nihei, Y. Suga, Y. Akiyama, T. Tsuji. Novel B-ring modified combretastatin analogues: synthesis and antineoplastic activity. Bioorg. Med. Chem. Lett. 8 (1998) 3371-3374.

24. D. E. L. Carrington, K. Clarke, R. M. Scrowston 1,2-Benzisothiazoles. Part I. Reaction of 3-chloro-1,2-benzisothiazole with nucleophiles. J. Chem. Soc. 1971 3262-3265.

25. J. R. Beck. A facile synthesis of 2-phenylbenzo[b]thiophene-3-amine and the corresponding S-oxide. J. Heterocycl. Chem. 15 (1978) 513-514.

26. M. P. Doyle, B. Siegfried, J. F. Jr. Dellaria. Alkyl nitrite-metal halide deamination rections. 2. Substitutive deamination of arylamines by alkyl nitrites and copper (II) halides. A direct and remarkably efficient conversion of arylamines to aryl halides. J. Org. Chem. 42 (1977) 2426-2431.

27. W. C. Shieh, J. A. Carlson. A simple asymmetric synthesis of 4-arylphenylalanines via palladium-catalyzed cross-coupling reaction of arylboronic acids with tyrosine triflate. J. Org. Chem. 57 (1992) 379-381.

28. M.-J. R. Queiroz, A. Begouin, I. C. F. R. Ferreira, G. Kirsch, R. C. Calhelha, S. Barbosa, L. M. Estevinho. Palladium-catalysed amination of electron-deficient or relatively electron-rich benzo[b]thienyl bromids-Preliminary studies of antimicrobial activity and SARs. Eur. J. Org. Chem. 2004 3679-3685.

29. M. W. Hooper, M. Utsunomiya, J. F. Hartwig. Scope and mechanism of palladium-catalyzed amination of five-membered heterocyclic halides. J. Org. Chem. 68 (2003) 2861-2873.

30. E. Hamel. Evaluation of antimitotic agents by quantitative comparisons of their effects on the polymerization of purified tubulin. Cell Biochem. Biophys. 38 (2003) 1-21.

31. F. Mollinedo, C. Gajate. Microtubules, microtubule-interfering agents and apoptosis. Apoptosis 8 (2003) 413-450.

32. P.R. Clarke, L. A. Allan. Cell-cycle control in the face of damage- a matter of life or death. Trends Cell Biol. 19 (2009) 89-98.

33. S. J. Martin, C. P Reutelingsperger, A. J. McGahon, J. A. Rader., R. C. van Schie, D. M. Laface, D. R Green. Early redistribution of plasma membrane phosphatidylserine is a

general feature of apoptosis regardless of the initiating stimulus: inhibition by overexpression of Bcl-2 and Abl. J. Exp. Med. 182 (1995) 1545-1556.

34. I. Vermes, C. Haanen, H. Steffens-Nakken, C. Reutelingsperger. A novel assay for apoptosis. Flow cytometric detection of phosphatidylserine expression on early apoptotic cells using fluorescein labelled annexin V. J. Immunol. Methods 184 (1995) 39–51.

35. D. R. Green, G. Kroemer. The pathophysiology of mitochondrial cell death. Science 305 (2005) 626–629.

36. J.D. Ly, D.R. Grubb, A. Lawen. The mitochondrial membrane potential ($\Delta\Psi_m$) in apoptosis: an update. Apoptosis 3 (2003**)** 115-128.

37. A. Baracca, G. Sgarbi, G. Solaini, G. Lenaz. Rhodamine 123 as a probe of mitochondrial membrane potential: evaluation of proton flux through F0 during ATP synthesis. Biochim. Biophys. Acta. Bioenergetics 1606 (2003) 137-145.

38. N. Zamzami, P. Marchetti, M. Castedo, D. Decaudin, A. Macho, T. Hirsch, S. A. Susin, P. X. Petit, B. Mignotte, G. Kroemer. Sequential reduction of mitochondrial transmembrane potential and generation of reactive oxygen species in early programmed cell death. J. Exp. Med. 182 (1995) 367–377.

39. H. Nohl, L. Gille, K. Staniek. Intracellular generation of reactive oxygen species by mitochondria. Biochem. Pharmacol. 69 (2005) 719–723.

40. G. Rothe, G. Valet. Flow cytometric analysis of respiratory burst activity in phagocytes with hydroethidine and 2′,7′-dichlorofluorescein. J. Leukocyte Biol. 47 (1990) 440–448.

41. W. C. Earshaw, L. M. Martins, S. H. Kaufmann. Mammalian caspases: Structure, activation, substrates and functions during apoptosis. Annu. Rev. Biochem. 68 (1999) 383–424.

42. J.-B. Denault, G. S. Salvesen. Caspases: keys in the ignition of cell death. Chem. Rev. 102 (2002) 4489-4499.

43. A. G. Porter, R. U. Janicke, Emerging role of caspase-3 in apoptosis Cell Death Differ. 6 (1999) 99-104.

44. C. Soldani, A. I. Scovassi. Poly(ADP-ribose) polymerase-1 cleavage during apoptosis: an update. Apoptosis 7 (2002) 321-328.

45. R. M. Kluck, E. Bossy-Wetzel, D. R. Green. The release of cytochrome *c* from mitochondria: a primary site for Bcl-2 regulation of apoptosis. Science 275 (1997) 1132-1136.

46. C. M. Knudson, S. J. Korsmeyer. Bcl-2 and Bax function independently to regulate cell death. Nature Genet. 16 (1997) 358-363.

47. G. Viola, E. Fortunato, L. Cecconet, L. Del Giudice, F. Dall'Acqua, G. Basso. Central role of p53 and mitochondrial damage in PUVA-induced apoptosis in human keratinocytes. Toxicol. Appl. Pharm. 227 (2008) 84-96.

4.3. Convergent Synthesis and Biological Evaluation of 2-Amino-4-(3',4',5'-trimethoxyphenyl)-5-Aryl Thiazoles as Microtubule Targeting Agents.

Romeo Romagnoli*†, Pier Giovanni Baraldi†, Andrea Brancale§, Antonio Ricci§, Ernest Hamel‡, Roberta Bortolozzi††, Giuseppe Basso†† and Giampietro Viola*††

†Dipartimento di Scienze Farmaceutiche, Università di Ferrara, 44100 Ferrara, Italy; §The Welsh School of Pharmacy, Cardiff University, King Edward VII Avenue, Cardiff, CF10 3NB, UK;

‡Screening Technologies Branch, Developmental Therapeutics Program, Division of Cancer Treatment and Diagnosis, National Cancer Institute at Frederick, National Institutes of Health, Frederick, Maryland 21702, USA;

††Dipartimento di Pediatria, Laboratorio di Oncoematologia, Università di Padova, 35131 Padova, Italy

Abstract

Based on combretastatin A-4, a potent tubulin polymerization inhibitor, a novel series of 2-amino-4-(3',4',5'-trimethoxyphenyl)-5-aryl thiazoles was synthesized. to evaluate the effect of electron-releasing or electron-withdrawing substituents on the phenyl at the 5-position of the thiazole skeleton on biological activities. The ethoxy group was the optimal substituent at the para-position of C5-phenyl group, with IC_{50} values in the range of 0.03-0.9 nM against five of seven cancer cell lines. Furthermore, our data show that the most active compounds are effective against multidrug resistant cancer cells. As determined by flow cytometry, cells treated are arrested in the G2/M phase of the cell cycle. Annexin-V and propidium iodide staining indicate that cell death proceeds through an apoptotic pathway, although this was only partially caspase-dependent. Our results suggest that, in addition to cell death by apoptosis, cells can be killed via mitotic catastrophe as an alternative cell death mechanism.

Introduction

The microtubule system of eukaryotic cells is a critical element in a variety of fundamental cellular processes, such as cell division, formation and maintenance of cell shape, regulation of motility, cell signalling, secretion and intracellular transport.[1] Among the various strategies developed to block mitosis, microtubules represent an attractive target for numerous small natural and synthetic molecules that inhibit the formation of the mitotic spindle.[2] One of the most important antimitotic agents is combretastatin A-4 (CA-4, **1;** Chart 1). CA-4, isolated from the bark of the South African tree *Combretum caffrum,*[3] is one of the well-known natural molecules that strongly inhibits tubulin polymerization by binding to the colchicine site.[4] CA-4 shows potent cytotoxicity against a wide variety of human cancer cell lines, including those that are multidrug resistant,[5] and CA-4 is also a vascular disrupting agent.[6] A water-soluble disodium phosphate derivative of CA-4 (named CA-4P) has shown promising results in human cancer clinical trials,[7] thus stimulating significant interest in a variety of CA-4 analogues.[8]

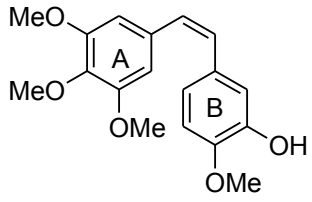

Combretastatin A-4 (CA-4), **1**

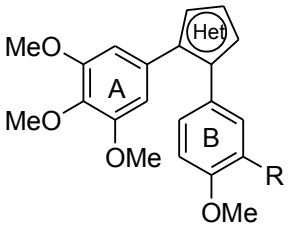

2

R=OH or NH_2
Het=imidazole; pyrazole; thiazole;oxazole; isoxazole; 1,2,3-thiadiazole; 1,2,3- or 1,2,4- or 1,3,4-triazole; 1,2,3,4-tetrazole, furazan.

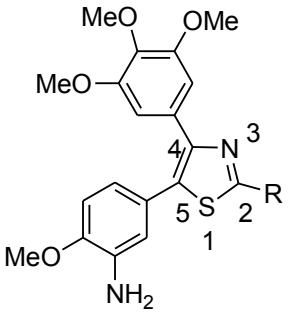

2a, R=H
2b, R=Me
2c, R=NH_2
2d, R=$NHNH_2$

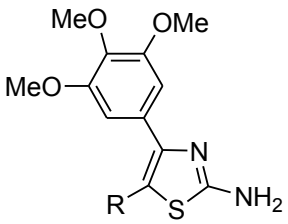

3

Chart 1. Lead structures of tubulin polymerization inhibitors

Previous SAR studies have demonstrated that both the 3',4',5'-trimethoxy substitution pattern on the A-ring and the *cis*-olefin configuration at the bridge were fundamental requirements for optimal activity, while some B-ring structural modifications were tolerated by the target.[8,9] However, the *cis*-configuration of CA-4 is prone to isomerize to the thermodynamically more stable *trans*-form during storage and metabolism, resulting in a dramatic decrease in antitumor activity. Thus, to retain the appropriate geometry of the two adjacent aryl groups required for a potent bioactivity, chemically stable *cis*-restricted derivatives of CA-4 were obtained by incorporating the olefinic double bond with vicinal diaryl-substituted five-member aromatic heterocyclic rings, such as pyrazole,[10] imidazole,[11] thiazole,[12] furazan (1,2,5-oxadiazole),[13] isoxazole,[14] oxazole,[10] 1,2,3-thiadiazole,[15] triazole[16] and 1,2,3,4-tetrazole.[12]

In a previous study, Ohsumi and co-workers reported a linear synthetic approach for the preparation of a small series of molecules based on the thiazole ring (compounds **2a-d**) substituted at the 2-position with a hydrogen (**2a**), methyl (**2b**), amino (**2c**) or hydrazino (**2d**) group.[12] The 2-amino derivative **2c** retains activity similar to that of CA-4 as an inhibitor of tubulin polymerization, but it is inferior to CA-4 with respect to antiproliferative activity against colon cancer cells.

In our efforts to discover new potent antimitotic agents, we developed an efficient and versatile convergent synthetic procedure for the preparation of a new series of 2-amino-4-(3',4',5'-trimethoxyphenyl)-5-aryl thiazoles with general structure **3**, starting with a common 2-amino protected-4-(3',4',5'-trimethoxyphenyl)-5-bromo thiazole intermediate. In this series of designed analogues, we maintained one of the aryl groups as a 3',4',5'-trimethoxyphenyl moiety, identical with the A-ring of CA-4, which was considered essential for maximal tubulin binding activity.[8] Modifications were focused on varying the other aryl moiety at the 5-position of the thiazole skeleton, corresponding to the B-ring of CA-4, by adding electron-withdrawing (CF_3) or electron-releasing (Me, Et, MeO and EtO) substituents (EWG and ERG, respectively) In addition, the B-ring was replaced with naphth-1-yl, naphth-2-yl or benzo[b]thienyl moieties. Since the methoxy and ethoxy groups proved to be favorable for bioactivity, we maintained one of these substituents at the *para*-position and introduced additional substituents (F, Cl, Me and MeO) at the *meta*-position of the phenyl

ring.

We examined the efficacy of the newly synthesized compounds on a panel of human cancer cell lines, including multidrug resistant lines overexpressing the 170-kDa P-glycoprotein (P-gp) drug efflux pump . Moreover, a possible mechanism of action for these compounds is described.

Chemistry

The synthetic protocol employed for the preparation of 2-amino-4-(3',4',5'-trimethoxyphenyl)-5-aryl thiazoles **3a-o** is shown in Scheme 1. Detailed description of the procedure is reported in the full article published on Journal of Medicinal Chemistry (2011 Jul 28)

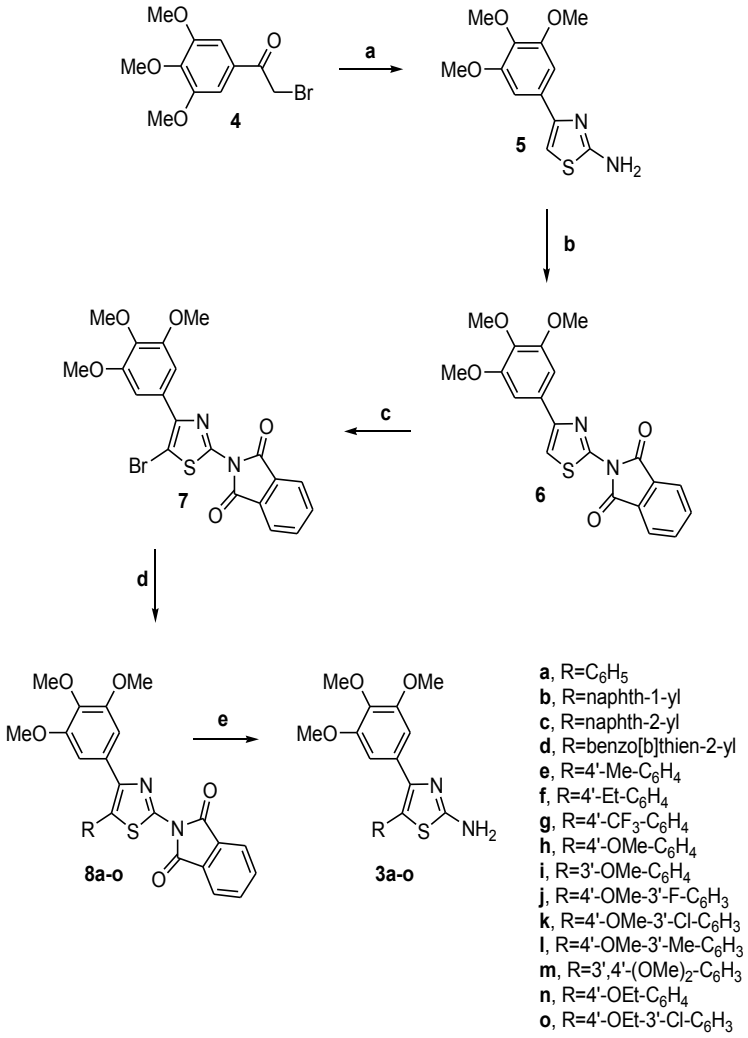

Reagents. **a**: thiourea, EtOH, reflux; **b**: phthalic anhydride, AcOH, reflux; **c**: NBS, $CHCl_3$, room temperture; **d**: $PdCl_2(DPPF)$, $ArB(OH)_2$, CsF, 1,4-dioxane, 65 °C; **e**: NH_2NH_2, EtOH, reflux.

Scheme 1.

Biological Results and Discussion

***In vitro* antiproliferative activities.** The 2-amino-4-(3',4',5'-trimethoxyphenyl)-5-aryl thiazoles **3a-o** were evaluated for their antiproliferative activity against a panel of seven human tumor cell lines and compared with the reference compound CA-4 (**1**). The data shown in Table 1 indicated the importance of the aryl substitution at the 5-position of the thiazole system for activity and selectivity against different cancer cell lines. In general, the introduction of electron-withdrawing or electron-releasing substituents increased activity compared with the unsubstituted phenyl derivative **3a**, with no clear difference in effect on potency between EWG and ERG. The antiproliferative activity of the most potent compounds was generally greater against the cervical carcinoma HeLa cells as compared with the other cell lines.

The 4'-ethoxyphenyl derivative **3n** displayed the strongest growth-inhibitory against HeLa, A549, and K562 cells, with IC_{50} values of 0.03, 0.09 and 0.07 nM, respectively. Compounds **3g** (4'-CF_3 substituent) and **3j** (4'-OMe and 3'-F substitutents) were the most active molecules against MCF-7 and HT-29 cells, respectively (IC_{50}'s of 0.4 and 5.7 nM, respectively). With the exception of compounds **3a**, **3b**, **3g**, **3i** and **3m**, the tested compounds were distinctly more potent than CA-4, with IC_{50} concentrations in the double-digit nanomolar range in the CA-4 resistant HT-29 cells. Compound **3n** was the only compound more active than CA-4 against the whole panel of cancer cell lines.

The phenyl (**3a**) and naphth-1-yl (**3b**) derivatives were the least active compounds in the whole series, with IC_{50}'s over 3 μM against all cell lines. Replacement of the naphth-1-yl moiety (**3b**) with the naphth-2-yl group (**3c**) resulted in a marked increase in activity, since **3c** was more active than CA-4 in five of the seven cell lines. Since the electronic properties of the **3b** and **3c** substituents are similar, the inactivity of **3b** is presumably due to steric factors caused by the naphthyl ring (see modeling section below). Replacement of the naphth-2-yl ring (**3c**) by the bioisosteric benzo[b]thien-2-yl moiety (**3d**) had relatively minor effects on antiproliferative activity in all cell lines.

Comparing the 4'-methylphenyl (**3e**) and 4-ethylphenyl (**3f**) with each other and with **3c** and **3d**, there were only minor differences in IC_{50} values, except that **3f** was the least active against the A549 cells and **3e** against the MCF-7 cells**.** Replacement of methyl (**3e**) with the methoxy group (**3h**) increased

antiproliferative activity in five of the cell lines, with a 10-fold increase in the A549 and K562 cells.

The number and position of methoxy substituents on the C5-phenyl ring had a major influence on antiproliferative activity. Moving the methoxy group from the *para*- (**3h**) to the *meta*-position (**3i**) or the insertion of an additional methoxy group (3',4'-dimethoxy derivative **3m**) led to a drop in potency. As noted above, the 4'-ethoxy homologue **3n** generally had the greatest antiproliferative activity of all compounds in the series. Specifically comparing it with the 4'-methoxy compound **3h**, **3n** was less active only in the HT-29 cells. The greatest differences in activity were 77-fold in the HeLa cells, 224-fold in the A549 cells, and 73-fold in K562 cells.

In comparing the effects of strong ERGs and EWGs on the phenyl at the C-5 thiazole position, no consistent difference in effects on antiproliferative activity occurred. For example, replacement of the ERG methoxy group with the EWG and bulkier trifluoromethyl moiety (compounds **3h** and **3g**, respectively) resulted in an 18- and 20-fold reduction in activity against A-549 and HT-29 cells, while **3h** and **3g** showed comparable potencies against HeLa, HL-60, Jurkat and K562 cells, but **3g** was 150-fold more active than **3h** against MCF-7 cells and was the most active compound of the series against this cancer cell line.

Relative to the activity of **3h**, the insertion of an additional EWG or ERG group on the 3'-position of the 4'-methoxyphenyl ring affected antiproliferative activity. In general, compounds **3j** and **3k**, with the EWG fluorine and chlorine atoms, showed stronger antiproliferative activities as compared with compounds with electron-releasing methyl (**3l**) and, especially, methoxy (**3m**) groups. Specific effects, however, seemed to vary with the cell line tested. Thus, with compounds **3h**-**l**, **3h** had the greatest activity with Jurkat and K562 cells, **3j** with A549, MCF-7 and HT-29 cells, and **3k** with HeLa and HL-60 cells.

Comparing the highly active 4'-ethoxy derivative **3n** with **3o**, which has additional 3'-chloro substituent on the phenyl ring, activity was increased with **3o** by 2-20 fold against HL-60, Jurkat, MCF-7 and HT-29 cells, but sharply reduced (30- to 125-fold) against HeLa, A549 and K562 cells.

Compd	IC_{50} [a](nM)						
	HeLa	A549	HL-60	Jurkat	K562	MCF-7	HT-29
3a	3094±126	9600±1490	3642±132.5	3834±443	8502±840	>10,000	7922±1820
3b	3865±335	6321±2882	8657±2403	4691±325	9031±891	>10,000	>10,000
3c	1.6±0.6	3.8±0.6	2.7±0.3	3.3±0.9	22.1±7.5	51.2±9.2	23.9±3.9
3d	2.8±0.5	16.0±2.1	0.9±0. 1	0.6±0.01	19.6±9.1	47.0±2.6	19.1±9.0
3e	0.73±0.2	42.8±5.7	3.9±1.1	3.9±0.6	58.7±37.1	279.5±69.8	12.4±5.1
3f	1.0±0.4	238±88	1.1±0.3	4.1±1.1	49.7±9.5	117±38	54.1±15.0
3g	3.2±0.4	357±65	5.1±1.1	8.5±1.2	7.6±2.1	0.4±0.1	221±50
3h	2.3±0.2	20.2±1.7	3.2±1.2	2.1±0.4	5.1±1.1	60.9±8.4	11.7±3.9
3i	209±0.2	2374±594	118±30	48.4±7.1	728±122	476±30	239±44
3j	2.0±0.2	3.1±0.6	6.1±2.1	7.3±1.1	6.0±2.0	18.6±6.2	5.7±1.5
3k	1.6±0.3	37.7±5.0	2.8±0.4	2.9±1.5	36.1±18.6	27.3±9.6	12.8±5.0
3l	2.6±0.4	305±87	4.0±0.3	21.5±7.5	67.6±28.3	58.7±4.7	24.0±10.4
3m	249±13	1797±231	301±17	319±80	829±181	1170±222	432±79
3n	0.03±0.005	0.09±0.01	0.9±0.3	0.14±0.05	0.07±0.004	44.0±6.3	38.2±11.4
3o	0.91±0.32	11.2±1.5	0.27±0.02	0.06±0.01	8.8±1.0	14.1±6.3	15.6±7.9
CA-4	4±1	180±50	1±0.2	5±0.6	5±0.1	370±100	3100±100

[a]IC_{50}= compound concentration required to inhibit tumor cell proliferation by 50%. Data are expressed as the mean ± SE from the dose-response curves of at least three independent experiments.

Table 1. In vitro cell growth inhibitory effects of compounds 3a-o and CA-4 (1)

Inhibition of tubulin polymerization and colchicine binding. To investigate whether the antiproliferative activities of compounds **3c-h**, **3j-l** and **3n-o** derived from an interaction with tubulin, these agents evaluated for their inhibition of tubulin polymerization and for effects on the binding of [^{3}H]colchicine to tubulin (Table 2).[18]

Compound	Tubulin assembly[a]	Colchicine binding [b]
	IC_{50}±SD (μM)	% ±SD
3c	0.74±0.0	94±0.7
3d	2.0±0.2	86±2
3e	0.44±0.0	88±1
3f	1.1±0.0	73±3
3g	4.0±0.5	25±0.7
3h	1.1±0.0	79±0.3
3j	1.2±0.1	81±0.2
3k	0.88±0.1	77±0.2
3l	1.1±0.1	72±3
3n	0.61±0.07	95±1
3o	0.89±0.05	87±1
CA-4 (**1**)	1.2±0.1	98±0.6

[a] Inhibition of tubulin polymerization. Tubulin was at 10 μM.
[b] Inhibition of [^{3}H]colchicine binding. Tubulin, colchicine and tested compound were at 1, 5 and 1 μM, respectively.

Table 2. Inhibition of tubulin polymerization and colchicine binding by compounds **3c-h**, **3j-l**, **3n-o** and CA-4

For comparison, CA-4 was examined in contemporaneous experiments. In the assembly assay, compound **3e** was found to be the most active (IC_{50}, 0.44 μM), and it was almost three-fold more potent than CA-4 (IC_{50},1.2 μM). With the

exception of compounds **3d** and **3g**, all tested molecules strongly inhibited tubulin assembly, with activity superior to (**3c**, **3k**, **3n** and **3o**) or comparable with (**3e**, **3f**, **3h**, **3j** and **3l**) that of CA-4. Compound **3d** was half as active and **3g** about one-fourth as active as CA-4, although **3d** and **3g** were more potent than CA-4 as antiproliferative agents against MCF-7 and HT-29 cells.

When comparing inhibition of tubulin polymerization versus the growth inhibitory effect, we found a good correlation for most, but not all, of the active compounds. While **3e** was generally less potent than **3d** as an antiproliferative agent, **3d** was about five times less active than **3e** as inhibitor of tubulin assembly.

In the colchicine binding studies, derivatives **3c-e** and **3n-o** were almost (86-95% inhibition) as potent as CA-4, which in these experiments inhibited colchicine binding by 98%. The potent inhibition observed indicates that **3c-e** and **3n-o** bind to tubulin at a site overlapping the colchicine site. Inhibition of colchicine binding by compounds **3f**, **3h** and **3j-l** was slightly lower (72-81%), while **3g** inhibited colchicines binding by only 25%. It is thus significant that many agents in the present series have activities superior to that CA-4 as inhibitors of tubulin assembly and are also highly active as inhibitors of colchicine binding to tubulin.

While this group of compounds were all potent in the biological assays (inhibition of cell growth, tubulin assembly and colchicine binding), correlations between the three assay types were imperfect. Thus, while **3e** was 5-fold more potent than **3d** in the tubulin assembly assay, these two molecules were equipotent as inhibitors of colchicine binding.

We further examined the effect of **3n**, one of the most active compounds, on the cellular microtubule network by immunofluorescence analysis. As shown in Figure 1, the microtubule network exhibited normal arrangement and organization in HeLa cells in the absence of drug treatment. In contrast, 24 or 48 h of exposure to 10 nM **3n** caused microtubule disassembly, with induction of a spherical morphology. Exposure to the compound at 100 nM resulted in an almost complete loss of microtubules. Nuclear changes were also observed. Exposure of the cells to **3n** resulted in the appearance of giant interphase cells with multiple nuclei of different sizes. In contrast to the dramatic changes in cellular microtubules, cells treated with **3n** showed minimal effects in the

arrangement and amount of F-actin (Figure 1, panel B), consistent with a preferential effect on microtubules.

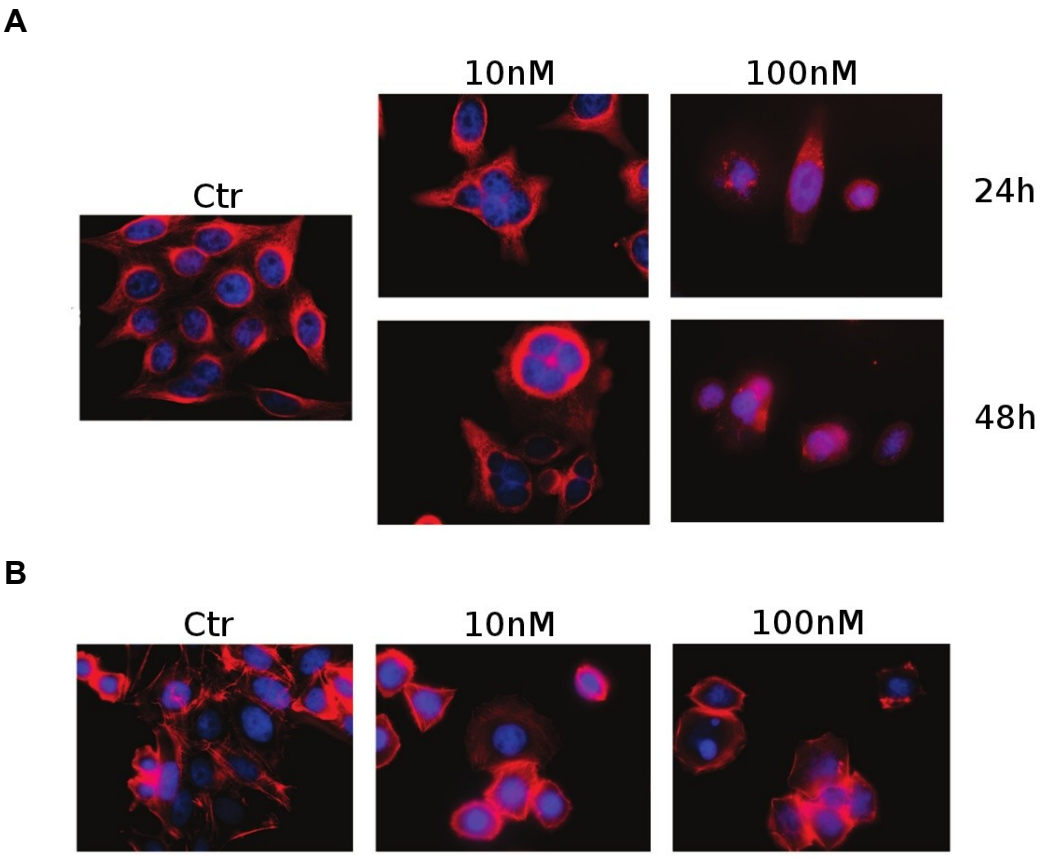

Figure1. Immunofluorescences images of HeLa cells stained with anti- β-tubulin antibody TRITC-conjugated and then observed by confocal microscopy. **A**Cells were exposed to 10 or 100 nM 3n for 24 or 48 h, fixed and analyzed by fluorescence microscopy. Magnification 60Â. **B** Representative images of HeLa cells stained with phalloidin tetramethylrhodamine B isothiocyanate conjugate after a 24 h incubation in the presence of 3n. Cells were also counterstained with DAPI to visualize the nuclei.

Molecular Modeling. To rationalize our experimental findings, a series of molecular docking simulations on β-tubulin were performed, using a procedure reported previously.[16c] The binding mode observed for this series of compounds is very similar to the one observed for the co-crystallized DAMA-colchicine (Figure 2).[19]

The trimethoxyphenyl group occupies the same position as the corresponding moiety of the colchicine analogue, while the aromatic ring in the 5 position of the thiazole ring establishes a π-π interaction with Asn258 and a series of non-polar interactions with Met259 and Lys352. Also consistent with our experimental data, while the 2-naphthyl analogue **3c** binds in the way described above (Figure 2), the different orientation of the naphthyl ring of **3b** does not allow a suitable docking for this compound. Also, in the cases of compounds **3i** and **3m**,

steric hindrance by the methoxy substituent in the *meta* position of the aromatic ring does not allow a successful docking, while smaller groups like F, Cl and CH_3 in the same position (**3j**, **3k** and **3l**) can be accommodated in the binding pocket. This observation is in accordance with the experimental data obtained for these compounds, as well as with the results obtained previously with another series of compounds.[16c]

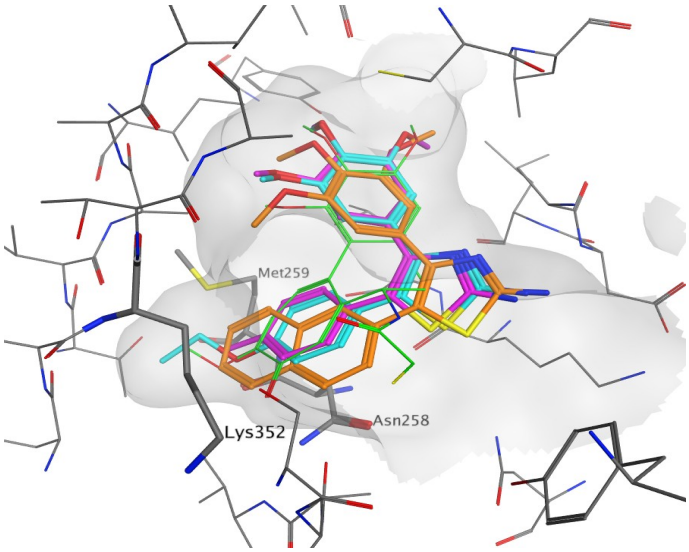

Figure 2. Docked pose of **3c** (orange), **3e** (magenta) and **3n** (cyan) overlapped with DAMA-colchicine (green) in the tubulin binding-site.

Effects of compounds 3h, 3n and 3o on multidrug resistant cell lines. Although many anticancer drugs in clinical use are effective in the treatment of different kinds of tumors, their potential is limited by the development of drug resistance.[20] Resistance can be intrinsic or acquired but, in either case, tumors become refractory to a variety of structurally different drugs. Thus, the antiproliferative effects of **3h**, **3n** and **3o** were evaluated in two human cancer cell lines derived from a lymphoblastic leukemia ($CEM^{Vbl\text{-}100}$) and a colon carcinoma ($Lovo^{Doxo}$) both expressing high levels of the 170-kDa P-glycoprotein (P-gp) drug efflux pump.[21,22] As shown in Table 3, the examined compounds were equally potent toward parental cells and cells resistant to vinblastine or doxorubicin.

Resistance to microtubule inhibitors is also mediated by changes in the levels of expression of different β-tubulin isotypes and by tubulin gene mutations that result in modified tubulin with impaired polymerization properties. A-549-T12 is a cell line with an *α*-tubulin mutation with increased resistance to taxol.[23] The data shown in Table 3 suggested that **3h**, **3n** and **3o** might be useful in the treatment of drug refractory tumors, in particular those with resistance to other

antitubulin drugs.

Compd	IC_{50} [a](nM)					
	LoVo	$LoVo^{Doxo}$	CEM	CEM ^{Vbl100}	A549	A549-T12
3h	3.1±1.0	0.8±0.06 (0.25)[b]	7.7±3.7	1.2±0.6 (0.1)	20.2±1.7	11.4±2.3 (0.6)
3n	0.7±0.08	0.6±0.05 (0.9)	0.9±0.2	0.8±0.09 (0.9)	0.09±0.01	0.2±0.05 (2.2)
3o	2.0±1.0	1.7±0.7 (0.9)	1.4±0.6	0.7±0.08 (0.5)	11.2±2.5	8.5±1.2 (0.8)
Doxorubicine	120±30	13150±210 (109.6)	n.d.	n.d.	n.d.	n.d.
Vinblastine	n.d.	n.d.	4.1 ±0.2	230 ± 32 (56.1)	n.d.	n.d.
Taxol	n.d.	n.d.	n.d.	n.d.	7.2 ± 0.1	75.2±12.5 (10.4)

[a]IC_{50}= compound concentration required to inhibit tumor cell proliferation by 50%. Data are expressed as the mean ± SE from the dose-response curves of at least three independent experiments. n.d. not determined

[b]Values in brackets are fold resistance, indicating reduced potency of the compounds in the resistant cell lines

Table 3. In vitro cell growth inhibitory effects of compounds **3h, 3n** and **3o** on drug resistant cell lines

Analysis of cell cycle. The effects of different concentrations of compound **3n** on cell cycle progression were examined in HeLa and Jurkat cells (Figure 3, panels A and B). Compound **3n** caused a clear G2/M arrest pattern in a concentration-dependent manner, starting at a concentration of 5 nM for both cell lines, a concentration higher than that induce cytotoxicity. In parallel we observed a concomitant decrease of cells in the G1 phase of the cell cycle (Figure 3, panels A and B), while the percentage of S phase cells declined slightly at 100 nM for HeLa cells and extensively for Jurkat cells. Analogous behavior was also observed after 48 h of treatment (data not shown).

The apparent discrepancy between the different concentrations that induce cell cycle arrest and the cytotoxic efficacy of **3n** could be explained by the crucial role of microtubules play in maintaining normal cellular functions. Most antimitotic drugs have an all or nothing effect on cell division in a sense that they have no observable effect at low concentrations but induce a significant mitotic arrest above critical concentrations and may induce cell death without an apparent block of the cell cycle. [24,25]

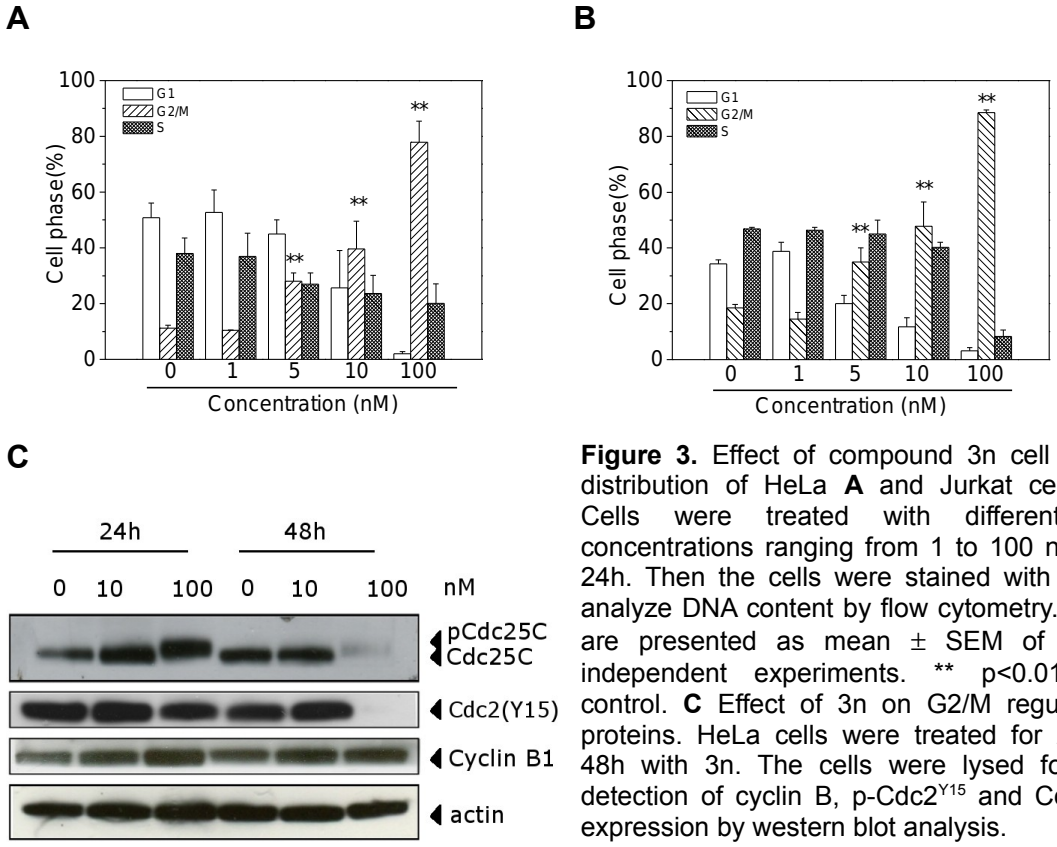

Figure 3. Effect of compound 3n cell cycle distribution of HeLa **A** and Jurkat cells **B**. Cells were treated with different 3n concentrations ranging from 1 to 100 nM for 24h. Then the cells were stained with PI to analyze DNA content by flow cytometry. Data are presented as mean ± SEM of three independent experiments. ** $p<0.01$ *vs*. control. **C** Effect of 3n on G2/M regulatory proteins. HeLa cells were treated for 24 or 48h with 3n. The cells were lysed for the detection of cyclin B, p-Cdc2^{Y15} and Cdc25c expression by western blot analysis.

We next studied the association between **3n**-induced G2/M arrest and alterations in expression of proteins that regulate cell division. Cell arrest at the prometaphase/metaphase to anaphase transition is normally regulated by the mitotic checkpoint.[26] In eukaryotic cells the activation of Cdc2 kinase is necessary for occurrence of the G2/M transition of the cell cycle. Activation of the kinase requires accumulation of the cyclin B1 protein and its dephosphorylation at Tyr15 and Thr14.[26] As shown in Figure 3 (panel C) in HeLa cells, **3n** caused a concentration- and time-dependent increase in cyclin B1 expression and a decreased expression of p-Cdc2^{Y15}, in particular after 48 h of treatment.

In addition, slower migrating forms of phosphatase Cdc25c were present, especially at the concentration of 100 nM, indicating changes in the phosphorylation state of this protein. The phosphorylation of Cdc25c directly stimulates its phosphatase activity, and this is necessary to activate Cdc2/Cyclin B on entry into mitosis.[26] These results indicate that arrest at G2/M induced by **3n** is accompanied by an increased expression of cyclin B1 and at later times (48h) for the highest concentration (100 nM) by a remarkable decrease of Cdc25c and p-Cdc2^{Y15}.

Compound 3n induces apoptosis that is partially caspase-dependent. To characterize the mode of cell death induced by **3n**, a biparametric cytofluorimetric analysis was performed using PI, which stains DNA and is permeable only to dead cells, and fluorescent immunolabeling of the protein annexin-V, which binds to PS in a highly selective manner. [27]

Dual staining for annexin-V and with PI permits discrimination between live cells (annexin-V^-/PI^-), early apoptotic cells (annexin-V^+/PI^-), late apoptotic cells (annexin-V^+/PI^+) and necrotic cells (annexin-V^-/PI^+),[28] as showed in Figure S1 (see Supporting informations). As depicted in Figure 4 (panel A), compound **3n** at 24 h had already induced an accumulation of annexin-V positive cells in comparison with the control, and this accumulation was concentration dependent. After a 48 h incubation, we observed a further decrease of cell viability along with a marked increase in PI positive cells.

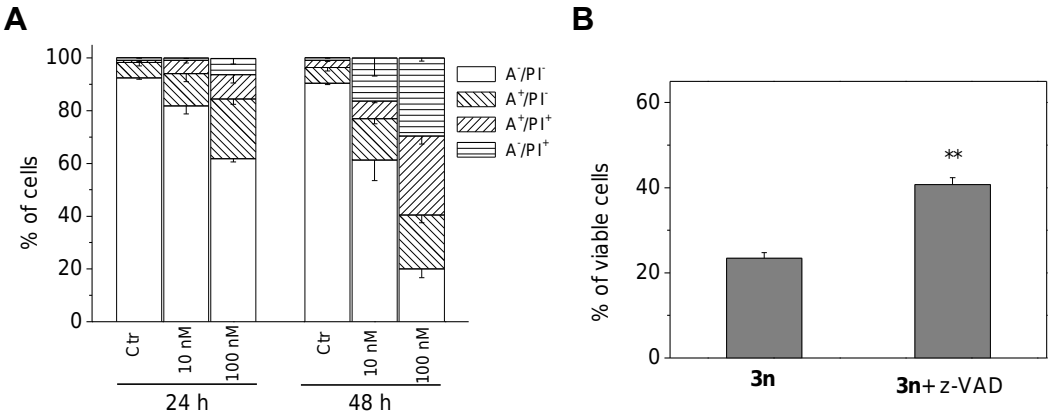

Figure 4. Flow cytometric analysis of apoptotic cells after treatment of HeLa cells with **3n.** The cells were harvested and labeled with annexin-V-FITC and PI and analyzed by flow cytometry. **A**. Percentage of cells found in the different regions of the biparametric histograms obtained from cytofluorimetric analysis, after incubation with **3n** for 24 h or 48 h. **B**. Percentage of cell viability after 48 h of incubation of HeLa cells with **3n** (100 nM) in the presence or in the absence of z-VAD.fmk (100 µM). Mean ± SEM of three independent experiments. **P<0.01 *vs*. **3n** treated cells.

To evaluate if the cell death induced by **3n** is caspase-dependent, HeLa cells were treated with **3n** in the absence or presence of the pan-caspase inhibitor z-VAD.fmk. Inhibition of caspases significantly increased cell viability (Figure 4, panel B), but this caspase inhibition had only a partial impact on **3n**-induced cell death. The caspase inhibitor increased cell survival from about 20% to 40%, suggesting that other mechanism(s) may lead to cell death following treatment with **3n**.

Effect of 3n on the activation of caspases. To have better insight into the mechanism of cell death induced by compound **3n**, we analyzed the mitochondrial potential ($\Delta\Psi_{mt}$) after cell treatment with the compound. No changes in $\Delta\Psi_{mt}$ were observed after treatment with 3n as depicted in figure S2 (Supporting information). We also evaluated the mitochondrial production of ROS by two fluorescent probes, HE and H_2DCFDA, by flow cytometry.[29] In agreement with the $\Delta\Psi_{mt}$ results, only a slight increase of ROS production was observed for cells treated with **3n** (Supporting informations, Figure S2).

Next, we analyzed the effect of **3n** on the expression of two members of the Bcl-2 family, the anti-apoptotic Bcl-2 and the proapototic Bax. The proteins of the Bcl family play a major role in controlling apoptosis through the regulation of mitochondrial processes and the release of mitochondrial proapoptotic molecules important for the cell death pathway.[26a] As shown in Figure 5 (panel B), **3n** did not significantly affect the expression of these two proteins, except for a marked decrease at 48 h following the death of a large number of cells. Altogether these data indicate that mitochondria were not involved in the mechanism of cell death induced by **3n**.

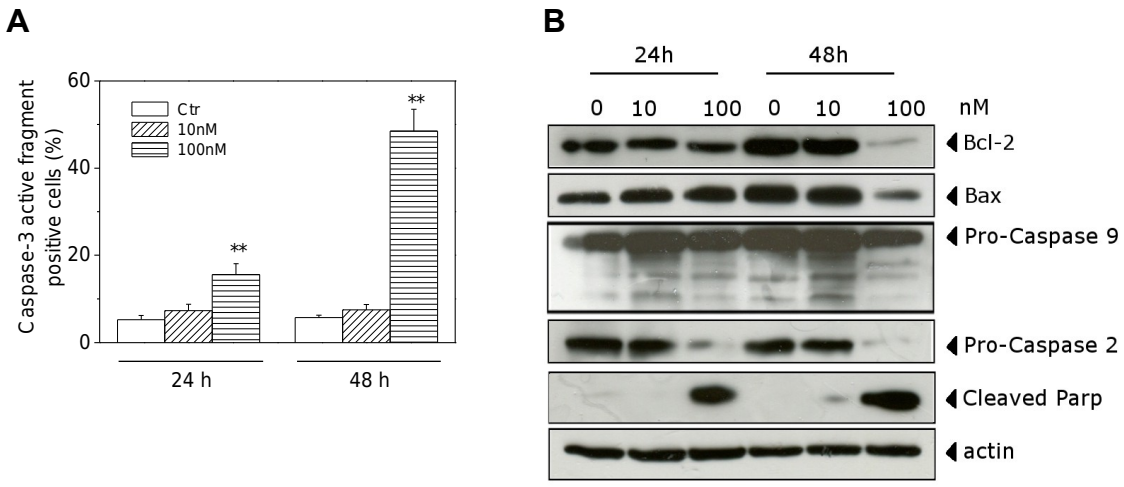

Figure 5. A Induction of caspase-3 activity by compound 3n. HeLa cells were incubated in the presence of 3n at the indicated concentration. After a 24 or 48 h treatment, cells were stained with an anti-human active caspase-3 fragment monoclonal antibody conjugated with FITC. Data are expressed as percentage of caspase-3 active fragment positive cells. ** $p<0.01$ vs. control. **B** Western blot analysis for the cleavage of PARP and the expression of Bcl-2, Bax, pro-caspase-9 and pro-caspase-2 in HeLa cells treated with **3n** for 24h and 48h.

As shown before, apoptosis is only partially caspase-dependent. To determine which caspases were involved in **3n**-induced cell death, the expression of

caspases was evaluated by immunoblot analysis and flow cytometry. We observed a clear activation in a time-dependent manner, especially at 100 nM, of the effector caspase-3 and cleavage of its substrate PARP (Figure 5, panel A and B). Compound **3n** did not induce activation of caspase-9, the major initiator caspase of the mitochondrial apoptotic pathway (Figure 5, panel B). Following treatment with **3n**, caspase-2 seems to be activated upstream of caspase-3. Recent evidences about the functions and activation mechanisms of the caspases have indicated that caspase-2 is unique among these enzymes, displaying features of both initiator and executioner.[30] Many recent studies indicate that activation of caspase-2 is fundamental for the induction of apoptosis induced by antimitotic drugs.[31]

Compound 3n induces mitotic catastrophe. It was recently demonstrated that antimitotic drugs, including CA-4, induce an alternative form of cell death to that of apoptosis. This has been called mitotic catastrophe or cell death occurring during metaphase.[32] Mitotic catastrophe is a type of cell death that usually occurs during mitosis in response to DNA damage or antimitotic agents.[33] Unlike apoptosis, which is basically dependent on caspase activation, mitotic catastrophe may be mediated in a caspase-independent or caspase-dependent fashion. In some cases mitotic catastrophe shares the same signaling pathways with apoptosis. Cells undergoing mitotic catastrophe are characterized by multi-nucleation, incomplete DNA synthesis and premature chromosome condensation.[32c,d]

Morphological alterations were observed in both HeLa and Jurkat cells after 24 and 48 h of exposure to **3n** (Figure 6, panels A and B). These changes consisted mainly of DNA condensation, abnormal mitotic figures, multinucleation and formation of large cells. Furthermore, large cytoplasmic vacuoles were also observed in Jurkat cells.

To determine whether cell death was induced because of DNA damage, we examined the expression of phospho-γH2A.X, a well known marker for cellular DNA double strand breaks. As shown in Figure 6 (panel C), a dramatic increase in expression of phospho-γH2A.X was observed after both 24 h and 48 h treatments, suggesting that DNA damage did occur after its replication was stalled by compound **3n**. In this context, p53 and $p21^{waf/cip1}$ play an essential role

in inducing cell cycle arrest.[33] The p53 protein levels did not show any variation relative to the untreated cells, except at 48 h when expression was reduced in the presence of **3n** (Figure 6 panel C), bypassing the G2/M checkpoint stage to enter mitotic catastrophe. Cells may proceed to mitosis again by the degradation of p21. Our results showed that p21 expression was strongly reduced after both 24 and 48 h treatments with 100 nM **3n**. Downregulation of $p21^{waf/cip1}$ protein by **3n** might have contributed to the formation of multinucleated cells, as previously reported.[34]

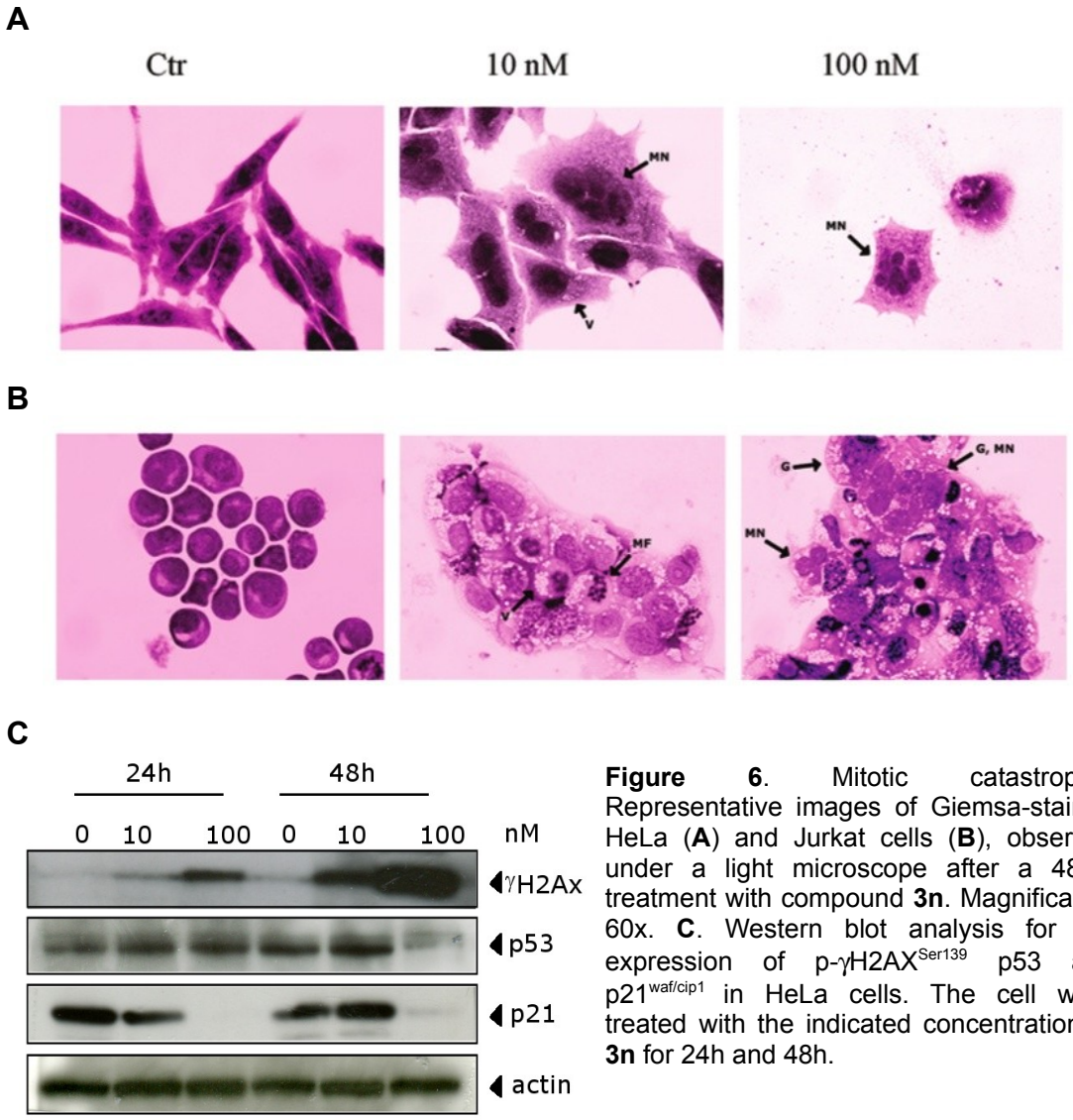

Figure 6. Mitotic catastrophe. Representative images of Giemsa-stained HeLa (**A**) and Jurkat cells (**B**), observed under a light microscope after a 48 h treatment with compound **3n**. Magnification 60x. **C**. Western blot analysis for the expression of p-γH2AX^{Ser139} p53 and $p21^{waf/cip1}$ in HeLa cells. The cell were treated with the indicated concentration of **3n** for 24h and 48h.

Conclusions

An efficient convergent synthesis and biological evaluation of a new series of rigid analogues of CA-4 were described. The new compounds contain the 2-amino thiazole ring system in place of the ethylene bridge present in CA-4. We fixed one of the aryl groups as a 3',4',5'-trimethoxyphenyl moiety throughout the present investigation, and the modifications were mainly focused on variation of the substituents on the second aryl ring. Change in this second aryl moiety had unpredictable effects on biological activity. The screening antiproliferative studies revealed that most of the synthesized compounds strongly inhibited the growth of all cancer cell lines examined, but specific effects were highly dependent on the aryl substituent at the 5-position of the thiazole ring, with no clear influence on activity observed by comparing the effects of ERG's and EWG's. It is clear that the substitution pattern on the phenyl moiety at the 5-position of the 2-amino thiazole ring plays an important role for antitubulin and antiproliferative activities, and this was supported by the molecular docking studies. As shown in Table 1, human cervical carcinoma HeLa cells were, in general, more sensitive toward tested compounds than the other cancer cell lines, with IC_{50} values in the low nanomolar range. Among the evaluated compounds, one of the most active analogues was found to be the 2-amino-4-(3',4',5'-trimethoxyphenyl)-5-(4'-ethoxyphenyl) thiazole analogue **3n**. This compound displayed antiproliferative activity at subnanomolar concentration (IC_{50}=0.03-0.9 nM) against all tested cancer cell lines, with the exception of HT-29 and MCF-7 cells (IC_{50}=39 and 44 nM, respectively). Compounds **3c**-**h**, **3j-k** and **3n-o** exhibited the strongest growth inhibition activity, with some of their IC_{50} values much lower than that of the reference compound CA-4. More importantly, these compounds were also found to be active in cells overexpressing P-gp, suggesting that these derivatives might be useful in treating drug-refractory patients. We identified tubulin as the molecular target of all compounds examined. With most of them, tubulin polymerization was more potently inhibited than occurred with the reference compound CA-4. Like CA-4, however, all compounds inhibited colchicine binding to tubulin.

Compound **3e** was the most potent inhibitor of tubulin polymerization and one of the most potent inhibitors of colchicine binding (IC_{50}=0.44 μM for assembly, 88%

inhibition of the binding of [^{3}H]colchicine). We also showed by flow cytometry that **3n** induced apoptosis and that apoptosis induced by **3n** was only partially dependent on caspase activation. Apoptosis induced by **3n** did not involve mitochondrial depolarization. Preliminary experiments suggested that, in addition to apoptosis, cells were killed by mitotic catastrophe, as indicated by morphological changes including formation of giant cells and multinucleated cells. These observations were corroborated at molecular level by analysis of the expression of some proteins associated with mitotic catastrophe. The ability of **3n** to induce different modes of cell death may contribute to its efficacy in different types of cancer cells, and its properties warrant its further testing in preclinical *in vivo* cancer models.

Supporting information

Detailed characterization of synthesized compounds **8a**-**o** and **3a-o**. Experimental procedures for biological assays and computational methodology. This material is available free of charge via the Internet at http://pubs.acs.org.

Reference

1. a) Amos, L. A. Microtubule structure and its stabilisation. *Org. Biomol. Chem.* **2004**, *2*, 2153-2160; b) Downing, K.H.; Nogales, E. Tubulin structure: insights into microtubule properties and functions. *Curr. Opin. Struct. Biol.* **1998**, *8*, 785-791; c) Honore, S.; Pasquier, E.; Braguer, D. Understanding microtubule dynamics for improved cancer therapy. *Cell. Mol. Life Sci.* **2005**, *62*, 3039-3056.

2. a) Bhattacharyya, B.; Panda, D.; Gupta, S.; Banerjee, M. Antimitotic activity of colchicine and the structural basis for its interaction with tubulin. *Med. Res. Rev.* **2008**, *28*, 155-183; b) Hearn, B. R.; Shaw, S. J.; Myles, D. C. Microtubule targeting agents. *Comprehensive Medicinal Chemistry II* **2007**, *7*, 81-110; c) Mahindroo, N; Liou, J.P.; Chang, J.Y.; Hsieh, H.P. Antitubulin agents for the treatment of cancer. A medicinal chemistry update. *Exp. Opin. Ther. Pat.* **2006**, *16*, 647-691; d) Jordan, M. A.; Kamath, K. How do microtubule-targeted drugs works? An overview. *Curr. Cancer Drug Targets* **2007**, *7*, 730-742; e) Risinger, A. L.; Giles, F. J.; Mooberry, S. L. Microtubule dynamics as a target in oncology. *Cancer Treat. Rev.* **2008**, *35*, 255-261; f) Carson, R. O. New tubulin targeting agents currently in clinical development. *Expert Opin. Investig. Drugs* **2008**, *17*, 707-722.

3. Pettit, G.R.; Singh, S.B.; Hamel, E.; Lin, C.M.; Alberts, D.S.; Garcia-Kendall, D. Isolation and structure of the strong cell growth and tubulin inhibitor combretastatin A-4. *Experentia* **1989**, *45*, 209-211.

4. Lin, C.M.; Ho, H.H.; Pettit, G.R.; Hamel, E. Antimitotic natural products combretastatin A-4 and combretastatin A-2: studies on the mechanism of their inhibition of the binding of colchicine to tubulin. *Biochemistry* **1989**, *28*, 6984-6991.

5. McGown, A. T.; Fox, B. W. Differential cytotoxicity of combretastatins A1 and A4 in two daunorubucin-resistant P388 cell lines. *Cancer Chemother. Pharmacol.* **1990**, *26*, 79-81.

6. Lippert, J. W., III. Vascular Disrupting Agents. *Bioorg. Med. Chem.* **2007**, *15*, 605-615.

7. a) Cooney, M. M.; Ortiz, J.; Bukowski, R. M.; Remick, S. C. Novel vascular targeting disrupting agents: combretastatin A4 phosphate and related compounds. *Curr. Oncol. Rep.* **2005**, *7*, 90-95; b) Vincent, L.; Kermani, P.; Young, L. M.; Cheng, J.; Zhang, F.; Shido, K.; Lam, G.; Bompais-Vincent, H.; Zhu, Z.; Hicklin, D. J.; Bohlen, P.; Chaplin, D. J.; May, C.; Rafii, S. Combretastatin A4 phosphate induces rapid regression of tumor neovessels and growth through interference with vascular endothelial-cadherin signaling. *J. Clin. Invest.* **2005**, *115*, 2992-3006; c) Chaplin, D. J.; Hill, S. A. The development of combretastatin A4 phosphate as a vascular targeting agent. *Int. J. Radiat. Oncol. Biol. Phys.* **2002**, *54:* 1491-1496; d) Young, S. L.; Chaplin, D. J. Combretastatin A-4 phosphate: background and current clinical status. *Expert Opin. Invest. Drugs* **2004**, *13*, 1171-1182; e) Bilenker, J. H.; Flaherty, K. T.; Rosen, M.; Davis, L.; Gallagher, M.; Stevenson, J. P.; Sun, W.; Vaughn, D.; Giantonio, B.; Zimmer, R.; Scnall, M.; O'Dwyer, P. J. Phase I trial of combretastatin A-4 phospate with carboplatin. *Clin. Cancer Res.* **2005**, *11*, 1527-1533.

8. a) Nam, N.H. Combretastatin A-4 analogues as antimitotic antitumor agents. *Curr. Med. Chem.* **2003**, *10*, 1697-1722; b) Chaudari, A.; Pandeya, S. N.; Kumar, P.; Sharma, P. P.; Gupta, S.; Soni, N.; Verma, K. K.; Bhardwaj, G. Combretastain A-4 analogues as anticancer agents. *Mini Rev. Med. Chem.* **2007**, *12*, 1186–1205; c) Tron, G.C.; Pirali, T.; Sorba, G.; Pagliai, F.; Busacca, S.; Genazzani, A. A. Medicinal chemistry of combretastatin A4: present and future directions. *J. Med. Chem.* **2006**, *49*, 3033-3044; d) Gaukroger, K.; Hadfield, J. A.; Lawrence, N. J.; Nlan, S.; McGown, A. T. Structural requirements for the interaction of combretastatins with tubulin: how important is the trimethoxy unit? *Org. Biomol. Chem.* **2003**, *1*, 3033-3037;

9. a) Hatanaka, T.; Fujita, K.; Ohsumi, K.; Nakagawa, R.; Fukuda, Y.; Nihei, Y.; Suga, Y.; Akiyama, Y.; Tsuji, T. Novel B-ring modified combretastatin analogues: synthesis and antineoplastic activity. *Bioorg. Med. Chem. Lett.* **1998**, *8*, 3371-3374; b) Gaukroger, K.; Hadfield, J. A.; Lawrence, N. J.; Nlan, S.; McGown, A. T. Structural requirements for the interaction of combretastatins with tubulin: how important is the trimethoxy unit? *Org. Biomol. Chem.* **2003**, *1*, 3033-3037.

10. Wang, L.; Woods, K. W.; Li, Q.; Barr, K. J.; McCroskey, R. W.; Hannick, S. M.; Gherke, L.; Credo, R. B.; Hui, Y.-H.; Marsh, K.; Warner, R.; Lee, J. Y.; Zielinski-Mozng, N.; Frost, D.; Rosenberg, S. H.; Sham, H. L. Potent, orally active heterocycle-based combretastatin A-4 analogues: synthesis, structure-activity relationship, pharmaokinetics, and in vivo antitumor activity evaluation. *J. Med. Chem.* **2002**, *45*, 1697-1711.

11. a) Schobert, R.; Biersack, B.; Dietrich, A.; Effenberger, K.; Knauer, S.; Mueller, T. 4-(3-Halo/amino-4,5-dimethoxyphenyl)-5-aryloxazoles and N-methylimidazoles that are cytotoxic against combretastatin A resistant tumor cels and vascular disrupting in a cis platin resistant germ cell tumor model. *J.Med. Chem.* **2010**, *53*, 6595-66002; b) Bonezzi, K.; Taraboletti, G.; Borsotti, P.; Bellina, F.; Rossi, R.; Giavazzi, R. Vascular disrupting activity of tubulin-binding 1,5-diaryl-1*H*-imidazoles. *J. Med. Chem.* **2009**, *52*, 7906-7910.

12. Ohsumi, K.; Hatanaka, T.; Fujita, K.; Nakagawa, R.; Fukuda, Y.; Nihai, Y.; Suga, Y.; Morinaga, Y.; Akiyama, Y.; Tsuji, T. Synthesis and antitumor activity of cis-restricted combretastatins 5-membered heterocyclic analogues. *Bioorg. Med. Chem. Lett.* **1988**, *8*, 3153-3158.

13. Tron, G. C.; Pagliai, F.; Sel Grosso, E.; Genazzani, A. A.; Sorba, G.; Synthesis and cytotoxic evaluation of combretafurazans. *J. Med. Chem.* **2005**, *48*, 3260-3258.

14. Liu, T.; Dong, X.; Xue, N.; Wu, R.; He, Q.; Yang, B.; Hu, Y. Synthesis and biological evaluation of 3,4-biaryl-5-aminoisoxazole derivatives. *Bioorg. Med. Chem.* **2009**, *17*,

6279-6285.

15. Wu, M.; Li, W.; Yang, C.; Chen, D.; Ding, J.; Chen, Y.; Lin, L.; Xie, Y. Synthesis and activity of combretastatin A-4 analogues: 1,2,3-thiadiazoles as potent antitumor agents. *Bioorg. Med. Chem. Lett.* **2007**, *17*, 869-873.

16. a) Odlo, K.; Hntzen, J.; Fournier dit Chabert, J.; Ducki, S.; Gani, O. A. B. S. M.; Sylte, I. Skrede, M.; Florenes, V. A.; Hansen, T. V. 1,5-Disubstituted 1,2,3-triazoles as cis-restricted analogues of combretastatin A-4: synthesis, molecular modeling and evaluation as cytotoxic agents and inhibitors of tubulin. *Bioorg. Med. Chem.* **2008**, *16*, 4829-4838; b) Zhang, Q.; Peng, Y.; Wang, X. I.; Keeman, S. M.; Aurora. S.; Welsh, W. J. Highly potent triazole-based tubulin polymerization inhibitors. *J. Med. Chem.* **2007**, *50*, 749-754; c) Romagnoli, R.; Baraldi, P. G.; Cruz-Lopez, O.; Lopez-Cara, C.; Carrion, M. D.; Brancale, A.; Hamel, E.; Chen, L.; Bortolozzi, R.; Basso, G.; Viola, G. Synthesis and antitumor activity of 1,5-disubstituted 1,2,4-triazoles as cis-restricted combretastatin analogs, *J. Med. Chem.* **2010**, *53*, 4248-4258.

17. For a general review on palladium cross-coupling reactions see: Miyaura, N.; Suzuki, A. Palladium-catalyzed cross-coupling reactions of organoboron compounds. *Chem. Rev.* **1995**, *95*, 2457-2483.

18. a) Hamel, E. Evaluation of antimitotic agents by quantitative comparisons of their effects on the polymerization of purified tubulin. *Cell Biochem. Biophys.* **2003**, *38*, 1-21; b) Verdier-Pinard, P.; Lai J.-Y.; Yoo, H.-D.; Yu, J.; Marquez, B.; Nagle D.G.; Nambu, M.; White, J.D.; Falck, J.R.; Gerwick, W.H.; Day, B.W.; Hamel, E. Structure-activity analysis of the interaction of curacin A, the potent colchicine site antimitotic agent, with tubulin and effects of analogs on the growth of MCF-7 breast cancer cells. *Mol. Pharmacol.* **1998**, *53*, 62-67.

19. Ravelli, R. B. G.; Gigant, B.; Curmi, P. A.; Jourdain, I.; Lachkar, S.; Sobel, A.; Knossow, M. Insight into tubulin regulation from a complex with colchicine and a stathmin-like domain. *Nature* **2004**, *428*, 198-202.

20. Baguley B.C. Multidrug resistance mechanism in cancer *Mol. Biotechnol.* **2010**, *46*, 308-316.

21. Dupuis, M.; Flego, M.; Molinari, A.; Cianfriglia, M. Saquinavir induces stable and functional expression of the multidrug transporter P-glycoprotein in human CD4 T-lymphoblastoid CEM rev cells. *HIV Medicine* **2003,** *4*, 338–345.

22. Toffoli, G.; Viel, A.; Tuimoto, I.; Bisconti, G.; Rossi, G.; Baoiocchi, M. Pleiotropic-resistant phenotype is a multifactorial phenomenon in human colon carcinoma cell lines. *Br J Cancer* **1991**, *63*, 51–56.

23. Martello, L.A.; Verdier-Pinard, P.; Shen, H. J.; He, L.; Torres, K.; Orr, G. A.; Horwitz, S. B. Elevated level of microtubule destabilizing factors in a taxol-resistant/ dependent A549 cell line with an alpha-tubulin mutation *Cancer Res.* **2003**, *63*, 448-454.

24. Chen, J.G.; Horwitz, S.B. Differential mitotic responses to microtubule-stabilizing and –destabilizing drugs *Cancer Res.* **2002**, *62*, 1935-1938.

25. Gascoigne, K.E., Taylor S.S. Cancer cells display profound intra and interline variation following prolonged exposure to antimitotic drugs *Cancer Cell* **2008**, *14*, 111-122

26. a) Mollinedo, F.; Gajate, C. Microtubules, microtubule-interfering agents and apoptosis. *Apoptosis* **2003**, 8:413-450; b) Clarke, P. R.; Allan, L. A. Cell-cycle control in the face of damage- a matter of life or death. *Trends Cell Biol.* **2009**, *19*, 89-98.

27. Vermes, I.; Haanen, C.; Steffens-Nakken, H.; Reutelingsperger, C. A novel assay for apoptosis. Flow cytometric detection of phosphatidylserine expression on early apoptotic cells using fluorescein labelled annexin V. *J. Immunol. Methods* **1995**, *184*, 39–51.

28. Martin, S. J.; Reutelingsperger, C. P.; McGahon, A. J.; Rader, J. A.; van Schie, R. C.; Laface, D. M.; Green, D. R. Early redistribution of plasma membrane

phosphatidylserine is a general feature of apoptosis regardless of the initiating stimulus: inhibition by overexpression of Bcl-2 and Abl. *J. Exp. Med.* **1995**, *182*, 1545.

29. a) Rothe, G.; Valet, G. Flow cytometric analysis of respiratory burst activity in phagocytes with hydroethidine and 2′,7′-dichlorofluorescein. *J. Leukocyte Biol.* **1990**, *47*, 440–448; b) Cai, J.; Jones, D. P. Superoxide in apoptosis. Mitochondrial generation triggered by cytochrome *c* loss. *J. Biol. Chem*. **1998**, *273*,11401-11404; c) Nohl, H.; Gille, L.; Staniek, K. Intracellular generation of reactive oxygen species by mitochondria. *Biochem. Pharmacol.* **2005**, *69*, 719–723.

30. Vakifahmetoglu-Norberg, H.; Zhivotovsky, B. The unpredictable caspase-2: what can it do? *Trends Cell Biol* **2010**, *20*, 150-159.

31. a) Mhaidat, N. M.; Wang, Y.; Kiejda, K. A.; Zang, X. D.; Hersey, P. Docetaxel-induced apoptosis in melanoma cells is dependent on activation of caspase-2 *Mol. Cancer Ther.* **2007**, *6*, 752-761. b) Ho, L. H.; Read, S. H.; Dorstyn, L.; Lambrusco L.; Kumar, S. Caspase-2 is required for cell death induced by cytosketal disruption *Oncogene* **2008**, *27*, 3393-3404.

32. a) Vitale, I., Antoccia, A.; Cenciarelli, C.; Crateri, P.; Meschini, S.; Arancia, G.; Pisano, C.; Tanzarella, C. Combretastatin CA-4 and combretastatin derivative induce mitotic catastrophe dependent on spindle checkpoint and caspase-3 activation in non-small cell lung cancer cells. *Apoptosis*. **2007**, *12*, 155-66. b) Cenciarelli, C.; Tanzarella, C.; Vitale, I.; Pisano, C.; Crateri, P.; Meschini. S.; Arancia, G.; Antoccia, A. The tubulin-depolymerising agent combretastatin-4 induces ectopic aster assembly and mitotic catastrophe in lung cancer cells H460. *Apoptosis* **2008**, *13*, 659-69. c) Castedo, M.; Perfettini, J. L.; Roumier, T.; Andreau, K.; Medema, R.; Kroemer, G. Cell death by mitotic catastrophe: a molecular definition *Oncogene* **2004**, *23*, 2825-2837. d) Vakifahmetoglu, H.; Olsson M.; Zhivotovsky B. Death trough a tragedy: mitotic catastrophe *Cell Death Diff.* **2008**, *15*, 1153-1162.

33. Portugal, J.; Mansilla, S.; Bataller, M. Mechanisms of drug-induced mitotic catastrophe in cancer cells. *Curr. Pharm Des.* **2010**, *16*, 69-78.

34. Mantel, C.; Braun, S.E.; Reid, S.; Henegariu, O.; Liu, L.; Hangoc, G.; Broxmeyer H.E. p21(cip^1/waf^1) deficiency causes deformed nuclear architecture, centriole overduplication, polyploidy, and relaxed microtubule damage checkpoints in human hematopoietic cells. *Blood* **1999** *15*, 1390-1398.

4.4. One-Pot Synthesis and Biological Evaluation of 2-Pyrrolidinyl-4-Amino-5-(3',4',5'-Trimethoxybenzoyl)Thiazole: a Unique, Highly Active Antimicrotubule Agents.

Romeo Romagnoli [a, *], Pier Giovanni Baraldi [a], Carlota Lopez Cara [a], Ernest Hamel [b], Giuseppe Basso [c], Roberta Bortolozzi [c], Giampietro Viola [c, **]

[a] *Dipartimento di Scienze Farmaceutiche, Università di Ferrara, Via Fossato di Mortara 17-19, 44100 Ferrara, Italy*

[b] *Screening Technologies Branch, Developmental Therapeutics Program, Division of Cancer Treatment and Diagnosis, National Cancer Institute at Frederick, National Institutes of Health, Frederick, MD 21702, USA*

[c] *Dipartimento di Pediatria, Laboratorio di Oncoematologia, Università di Padova, 35131 Padova, Italy*

Abstract

A wide variety of small molecules with diverse molecular scaffolds inhibit microtubule formation. In this article we report a one-pot procedure for the preparation of a novel 2-(*N*-pyrrolidinyl)-4-amino-5-(3',4',5'-trimethoxybenzoyl)thiazole in which the size of the substituent at the C-2 position of the thiazole ring plays an essential role in compound activity. The most active agent (**3f**) compound inhibited at submicromolar concentrations the growth of tumor cell lines. It also inhibited tubulin polymerization with an activity quantitatively similar to that of CA-4, and treatment of HeLa cells resulted in their arrest at the G2-M phase of the cell cycle. Furthermore, **3f** was effective against multidrug resistant cancer cells and reduced *in vivo* the growth of the HT-29 xenograft in a nude mouse model. This indicated that **3f** is a promising new antimitotic agent with clinical potential.

Introduction

Antimitotic agents are one of the major classes of cytotoxic drugs for cancer treatment, and tubulin is the target for numerous small natural and synthetic molecules that inhibit the formation of the mitotic spindle.[1] Besides mitosis, the microtubule system of eukaryotic cells is a critical element in a variety of essential cellular processes, including formation and maintenance of cell shape, regulation of motility, cell signalling, secretion and intracellular transport.[2] One of the most important antimitotic agents is combretastatin A-4 (CA-4, **1;** Chart 1).[3] CA-4, isolated from the bark of the South African tree *Combretum caffrum,* is one of the well-known natural tubulin-binding molecules affecting microtubule dynamics by binding to the colchicine site.[4] Because of its simple structure, a wide number of CA-4 analogues have been developed and evaluated in SAR studies.[5]

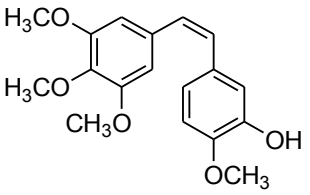

Combretastatin A-4 (CA-4), **1**

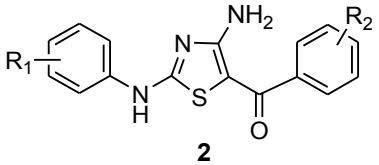

2

R_1=H, F, Cl, Me and OMe
R_2=H, OMe, Cl, Br and NO_2

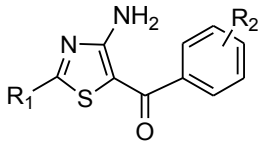

3a-o

3a, R_1=NH_2, R_2=3',4',5'-$(OCH_3)_3$
3b, R_1=$N(CH_3)_2$, R_2=3',4',5'-$(OCH_3)_3$
3c, R_1=$N(C_2H_5)_2$, R_2=3',4',5'-$(OCH_3)_3$
3d, R_1=$NCH_3(n\text{-}C_4H_9)$, R_2=3',4',5'-$(OCH_3)_3$
3e, R_1=$NCH_3(CH_2C_6H_5)$, R_2=3',4',5'-$(OCH_3)_3$
3f, R_1=pyrrolidin-1-yl, R_2=3',4',5'-$(OCH_3)_3$
3g, R_1=piperidin-1-yl, R_2=3',4',5'-$(OCH_3)_3$
3h, R_1=morpholin-4-yl, R_2=3',4',5'-$(OCH_3)_3$
3i, R_1=pyrrolidin-1-yl, R_2=3',4'-$(OCH_3)_2$
3j, R_1=pyrrolidin-1-yl, R_2=4'-OCH_3
3k, R_1=pyrrolidin-1-yl, R_2=3'-OCH_3
3l, R_1=pyrrolidin-1-yl, R_2=2'-OCH_3
3m, R_1=pyrrolidin-1-yl, R_2=4'-Cl
3n, R_1=pyrrolidin-1-yl, R_2=4'-Br
3o, R_1=pyrrolidin-1-yl, R_2=H

Chart 1. Inhibitors of Tubulin Polymerization

Among the synthetic inhibitors of tubulin polymerization, we have recently described a series of 2-arylamino-4-amino-5-aroylthiazoles with general structure **2** that showed strong antiproliferative activity against tumor cell lines and inhibited tubulin polymerization by interfering with the colchicine site.[6] These compounds also caused cancer cells to arrest in the G2-M phase of the cell cycle, and all possessed a 4-aminothiazole nucleus in which substitution either at the C-2 or C-5 position played an essential role in potency.

As a part of our continuing search for novel antimitotic agents, these findings prompted us to synthesize by a one-pot four-step procedure a new series of 2-alkylamino-4-amino-5-aroylthiazole derivatives with general structure **3** in which the 2-anilino moiety of compounds **2** was replaced by an amino moiety or various cyclic or acyclic alkyl amino substituents. SAR between the substitutions at the C-2 and C-5 positions of the thiazole core were evaluated.

Since it is well known that the trimethoxyphenyl group is the characteristic structural requirement to maximize the potent activity in a large series of inhibitors of tubulin polymerization, such as colchicine, CA-4 and podiphyllotoxin,[7] we prepared compounds **3a-h**, all of which retain the 3',4',5'-trimethoxybenzoyl group at the C-5 position of the thiazole ring, allowing us to evaluate the effect of substitution at the C-2 position by cyclic and acyclic alkyl amines. The pyrrolidin-1-yl substituent (**3f**) resulted in a compound that was superior to the others. The potent activity of **3f** led us to synthesize a second series of derivatives **3i-o** in which we maintained the pyrrolidin-1-yl group at the C-2 position, but replaced the 5-(3',4',5'-trimethoxybenzoyl) moiety of **3f** with other benzoyl groups.

Chemistry

The synthetic protocol employed for the preparation of 2-Pyrrolidinyl-4-Amino-5-(3',4',5'-Trimethoxybenzoyl)Thiazole 3a-o is shown in Scheme 1.

Detailed description of the procedure is reported in the full article published on European Journal of Medicinal Chemistry (2011 Dec)

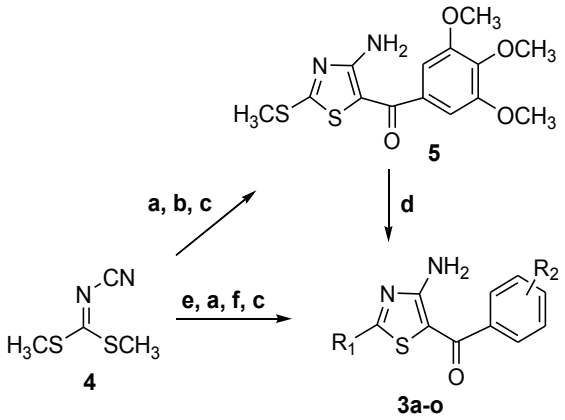

Reagents. **a**: $Na_2S{\cdot}9H_2O$, DMF, 70 °C, 2 h; **b**: 1-(3',4',5'-trimethoxyphenyl)-2-bromoethanone, 50 °C, 2 h; **c**: K_2CO_3, 1 h; **d**. NH_3 for **3a**, $(CH_3)_2NH$ in EtOH for **3b**, $(C_2H_5)NH$ for **3c**; **e**: appropriate secondary amine, DMF, 70 °C, 1 h; **f:** appropriate α-bromoacetophenone, 2 h, 50 °C.

Scheme1 synthesis procedure of 2-Pyrrolidinyl-4-Amino-5-(3',4',5'-Trimethoxybenzoyl)Thiazole.

Results and Discussion

Table 1 summarizes the antiproliferative effects of derivatives **3a-o** against a panel of three human and two rodent cancer cell lines. These are murine leukemia (L1210) and mammary carcinoma (FM3A) lines and the human T-leukemia lines Molt/4 and CEM and the human cervix carcinoma HeLa line. Only **3f** showed submicromolar antiproliferative activity against all tested lines, while other derivatives generally had little activity, with IC_{50}'s usually greater than 10 μM. Derivative **3f** was 10- to 100-fold less active than the reference compound CA-4.

Extensive exploration of SAR of this novel series of compounds showed that the presence of pyrrolidin-1-yl and 3',4',5'-trimethoxybenzoyl at the C-2 and C-5 positions of the 4-aminothiazole scaffold were essential for the biological activity of **3f**. Considering substitutions at the C-2 position, ever minor modifications, such as expanding the pyrrolidine (**3f**) to a piperazine (**3g**) ring, caused a large reduction in antiproliferative activity.

Comparing **3f** with **3i-o**, all with a pyrrolidin-1-yl moiety at the C-2 position of the thiazole skeleton, demonstrated that the 3',4',5'-trimethoxbenzoyl moiety at the C-5 position (**3f**) was essential for activity. Its replacement with a 3',4'-dimethoxybenzoyl (**3i**), several isomeric methoxybenzoyl (**3j-l**), 4'-chloro- and 4'-bromobenzoyl (derivatives **3m** and **3n**, respectively) or the unsubstituted benzoyl (**3o**) moiety all led to inactive compounds.

Compd	IC_{50} [a] (μM)				
	L1210	FM3A	Molt4	CEM	HeLa
3a	48±7.2	63±11	n.d.	42±0.0	31±6.3
3b	11±2.4	12±3.2	n.d.	11±0.2	8.2±1.1
3c	62±5.4	115±43	n.d	78±1.7	38±11
3d	53±0	47±0	32±15	42±18	31±1.8
3e	>200	>200	>200	>200	>200
3f	0.37±0.07	0.18±0.02	0.26±0.09	0.32±0.04	0.34±0.02
3g	43±10	39±16	16±3.2	22±12	11±5.1
3h	38±23	24±2.2	22±17	25±1.3	8.8±1.1
3i	60±20	112±38	31±6.2	19±1.3	36±6.2
3j	>200	>200	>200	>200	>200
3k	>200	>200	>200	>200	>200
3l	>200	>200	>200	171±74	185±4
3m	>200	>200	>200	>200	>200
3n	>200	>200	>200	>200	>200
3o	>200	>200	>200	>200	>200
CA-4	0.003±0.001	0.042±0.006	0.016±0.001	0.002±0.001	0.002±0.001

[a] IC_{50}= compound concentration required to inhibit tumor cell proliferation by 50%.

Table 1. In vitro inhibitory effects of compounds **3a-o** and **CA-4**

Conversely, when the 3',4',5'-trimethoxbenzoyl group was at the C-5 position of the thiazole skeleton (derivatives **3a-f** and **3gh**), significant loss of activity occurred upon changing the pyrrolidin-1-yl ring at the C-2 position to any other substituent that we have evaluated. Alternate groups examined were the amine (**3a**), dimethylamine (**3b**), diethylamine (**3c**), *N*-methyl-*N'*-*n*-butyl amine (**3d**), *N*-methyl-*N'*-benzylamine (**3e**),), piperidin-1-yl (**3g**) and morpholin-4-yl (**3h**). Thus, we speculate that the tubulin binding pocket for this portion of the molecule is quite small and allowed the presence only of the pyrrolidin-1-yl moiety.

This hypothesis was supported by molecular docking experiments that we performed on this series of compounds.

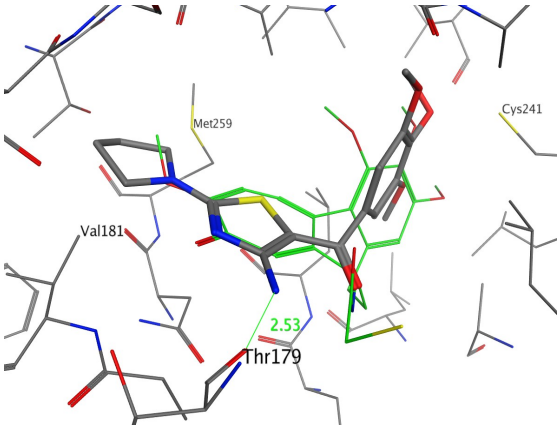

Figure 1 Docked pose of 3f overlapped with DAMA-colchicine (green) in the β-tubulin binding site.

Figure 1 shows how compound **3f** is placed with the trimethoxyphenyl ring in proximity to Cys241, while the amino group establishes a hydrogen bond with

Thr179. Furthermore, the pyrrolidine ring can be placed in close contact with Val181 and Met259 deep in the binding pocket. This hydrophobic region does not seem able to accommodate more voluminous substituents, and, as expected, the docking results for **3g** and **3h** did not produce a satisfactory binding pose.

To further characterize the interaction with the microtubule system of this novel series of 4-aminothiazole derivatives, a selected series of compounds (**3a-c** and **3f-h**) were evaluated for their *in vitro* inhibition of tubulin polymerization. For comparison, CA-4 was examined in contemporaneous experiments. In this assembly assay, compound **3f** was slightly less active than the reference compound CA-4, with IC_{50} values of 1.3±0.1 and 1.0±0.1 μM, respectively. In agreement with the antiproliferative data, compounds **3a-c** and **3g-h** were inactive as inhibitors of tubulin polymerization and did not inhibit tubulin assembly at concentrations as high as 20 μM.

Compound **3f** was also evaluated for inhibitory effects on the binding of [^{3}H]colchicine to tubulin. In this assay, 67% inhibition occurred with equimolar concentrations of **3f** and radiolabeled colchicine (5 μM each) in the reaction mixture. Compound **3f** was somewhat less potent than CA-4, which inhibited colchicine binding by 99%. These results are consistent with the conclusion that the antiproliferative activity of **3f** derives from an interaction with the colchicine site of tubulin, and this results in interference with microtubule assembly.

Because only compound **3f** had submicromolar activity as an antiproliferative agent against cancer cell lines, further evaluation was limited to this agent.

Effects of 3f on multidrug resistant cell lines. Drug resistance is an important therapeutic problem caused by the emergence of tumor cells possessing different mechanisms which confer resistance against a variety of anticancer drugs.[9,10] Among the more common mechanisms are those related to the overexpression of glycoproteins capable of mediating the efflux of various drugs.[9,10] Therefore, we investigated whether **3f** inhibited the growth of two drug-resistant cell lines, one derived from a lymphoblastic leukemia ($CEM^{Vbl\text{-}100}$), the other derived from a colon carcinoma ($Lovo^{Doxo}$). Both these lines express high levels of the 170-kDa P-glycoprotein (P-gp) drug efflux pump.[11,12] As shown in Table 2, compound **3f** was equally potent toward parental cells and cells

resistant to vinblastine or doxorubicin.

Compd	IC_{50} [a] (μM)					
	LoVo	$LoVo^{Doxo}$	CEM	CEM^{Vbl100}	A549	A549-T12
3f	0.10 ±0.04	0.43±0.19 (4.3)[b]	0.02 ±0.006	0.01±0.002 (0.2)	0.037 ±0.013	0.16±0.09 (4.3)
Doxorubicine	0.12 ±0.03	13.1±0.21 (109.6)	n.d.	n.d.	n.d.	n.d.
Vinblastine	n.d.	n.d.	0.004 ±0.0002	0.23 ± 0.032 (56.1)	n.d.	n.d.
Taxol	n.d.	n.d.	n.d.	n.d.	0.0072 ± 0.0001	0.075±0.012 (10.4)

[a] IC_{50}= compound concentration required to inhibit tumor cell proliferation by 50%.
[b] Values in parentheses are fold resistance, indicating reduced potency of the compounds in the resistant cell lines.
Data are expressed as the mean ± SE from the dose-response curves of at least three independent experiments. n.d. not determined

Table 2. In vitro cell growth inhibitory effects of **3f** on drug resistant cell lines

Resistance to microtubule inhibitors is also mediated by changes in the levels of expression of different β-tubulin isotypes and by tubulin gene mutations that result in modified tubulin with impaired polymerization properties. A-549-T12 is a cell line with an *α*-tubulin mutation with increased resistance to taxol.[13] Compound **3f** had greater relative activity than taxol in this cell line, suggesting that **3f** might be useful in the treatment of drug refractory tumors resistant to other antitubulin drugs.

Analysis of cell cycle effects. The effects of different concentrations of compound **3f** after 24h of treatment on cell cycle progression were examined in HeLa cells (Figure 2, panel A). Compound **3f** caused a remarkable G2/M arrest pattern in a concentration-dependent manner, starting at 0.125 μM. In parallel we observed a concomitant decrease of cells in the G1 phase of the cell cycle (Figure 2, panel A), while the percentage of S phase cells declined only at the highest concentration used (0.5 μM).

More importantly, we observed a concentration-dependent increase of the cell population with a hypodiploid DNA content peak (subG1), representing those cells with a DNA content less than G1, which are usually considered to be apoptotic cells (Figure 2, panel B). This suggests that **3f** may induce apoptosis.

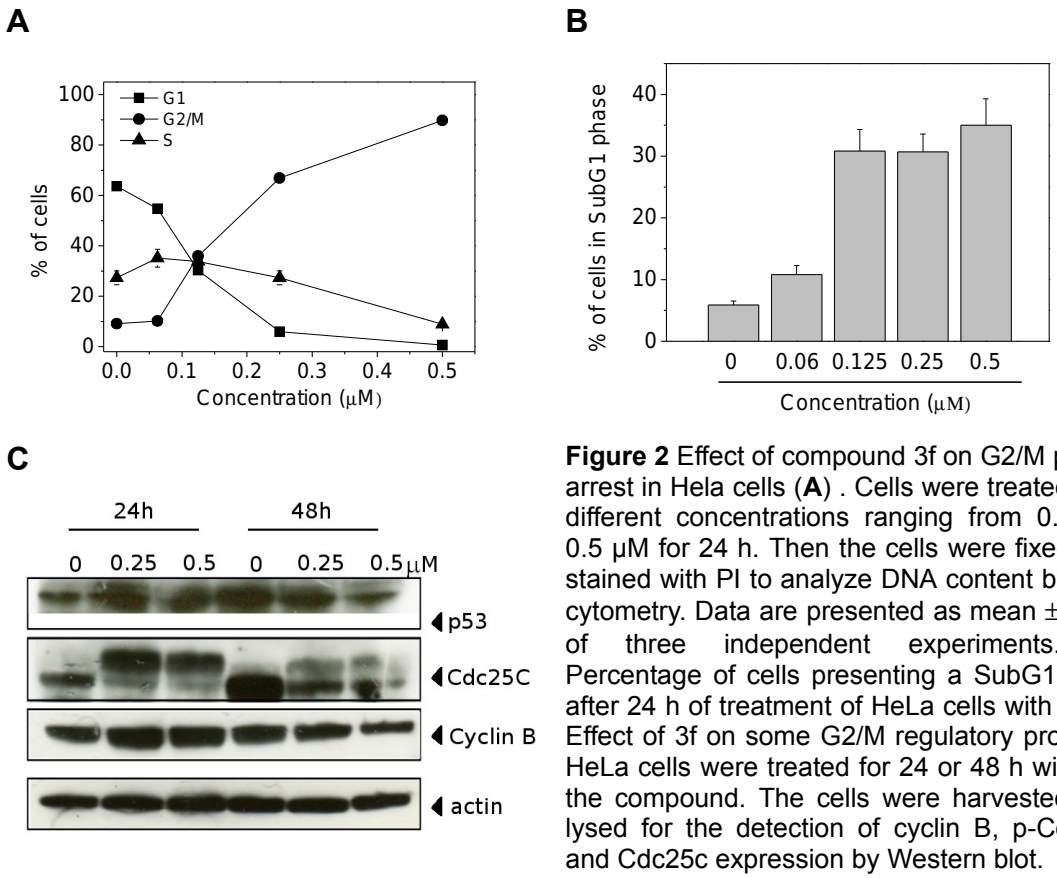

Figure 2 Effect of compound 3f on G2/M phase arrest in Hela cells (**A**) . Cells were treated with different concentrations ranging from 0.06 to 0.5 μM for 24 h. Then the cells were fixed and stained with PI to analyze DNA content by flow cytometry. Data are presented as mean ± SEM of three independent experiments. **B**. Percentage of cells presenting a SubG1 peak after 24 h of treatment of HeLa cells with 3f. **C**. Effect of 3f on some G2/M regulatory proteins. HeLa cells were treated for 24 or 48 h with the the compound. The cells were harvested and lysed for the detection of cyclin B, p-Cdc2^{Y15} and Cdc25c expression by Western blot.

We next studied the association between **3f**-induced G2/M arrest and alterations in expression of proteins that regulate cell division. Cell arrest at the prometaphase/metaphase to anaphase transition is normally regulated by the mitotic checkpoint.[14] In eukaryotic cells the activation of Cdc2 kinase is necessary for occurrence of the G2/M transition of the cell cycle. Activation of the kinase requires accumulation of the cyclin B1 protein and its dephosphorylation at Tyr15 and Thr14.[14] As shown in Figure 2 (panel C) in HeLa cells, **3f** caused an increase in cyclin B1 expression after 24 h of treatment that then decreased by 48h. At the same time, there was a marked reduction in Tyr15 phosphorylation at 24 h, with partial recovery by 48 h.

In addition, slower migrating forms of phosphatase Cdc25c appeared at 24 h, followed by partial disappearance at 48 h, indicating changes in the phosphorylation state of this protein. The phosphorylation of Cdc25c directly stimulates its phosphatase activity, and this is necessary to activate Cdc2/cyclin B on entry into mitosis.[14]

Compound 3f induces apoptosis. To characterize the mode of cell death

induced by **3f**, a biparametric cytofluorimetric analysis was performed using PI, which stains DNA and enters only dead cells, and fluorescent immunolabeling of the protein annexin-V, which binds to PS in a highly selective manner.[15] Dual staining for annexin-V and with PI permits discrimination between live cells (annexin-V^-/PI^-), early apoptotic cells (annexin-V^+/PI^-), late apoptotic cells (annexin-V^+/PI^+) and necrotic cells (annexin-V^-/PI^+).[16]

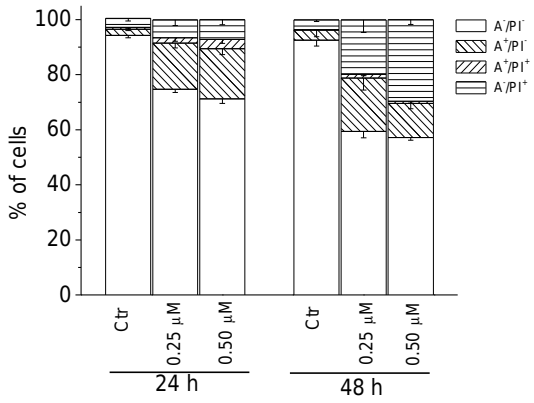

Figure 3. Flow cytometric analysis of apoptotic cells after treatment of HeLa cells with **3f.** The cells were harvested and labeled with annexin-V-FITC and PI and analyzed by flow cytometry. Percentage of cells found in the different regions of the biparametric histograms after incubation with **3f** for 24 h or 48 h. Data are expressed as mean ± S.E.M. for four independent experiments.

As depicted in Figure 3, compound **3f** at 24 h had already induced an accumulation of annexin-V positive cells in comparison with the control, and this accumulation was concentration dependent, in good agreement with the appearance of the sub-G1 cells described above. After a 48 h incubation, we observed a further decrease of cell viability along with a marked increase in PI positive cells.

Effect of 3f on mitochondrial depolarization. Mitochondria play an essential role in the propagation of apoptosis.[17] It is well established that, at an early stage, apoptotic stimuli alter the mitochondrial transmembrane potential ($\Delta\psi_{mt}$). $\Delta\psi_{mt}$ was monitored by the fluorescence of the dye JC-1.[18] With normal cells (high $\Delta\psi_{mt}$), JC-1 displays a red fluorescence (590 nm). This is caused by spontaneous and local formation of aggregates that are associated with a large shift in the emission. In contrast, when the mitochondrial membrane is depolarized (low $\Delta\psi_{mt}$), JC-1 forms monomers that emit at 530 nm. As shown in Figure 4 (panel A), **3f** induced a time and concentration–dependent increase in cells with depolarized mitochondria.

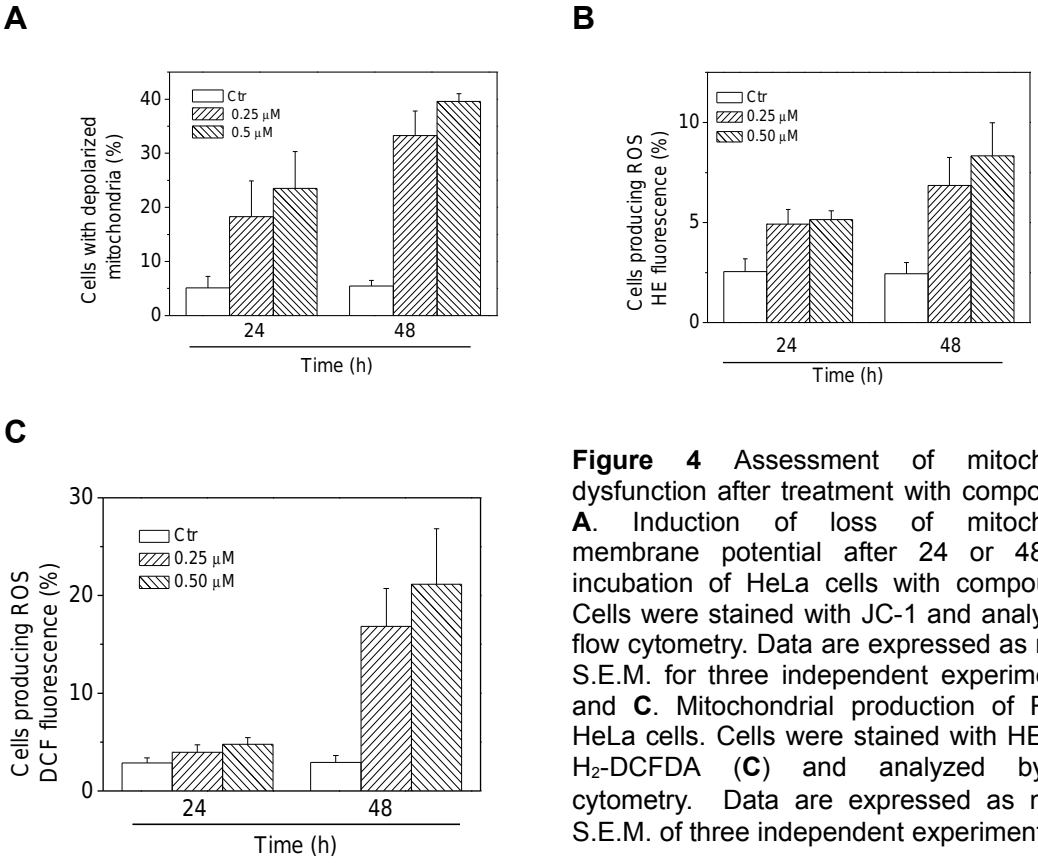

Figure 4 Assessment of mitochondrial dysfunction after treatment with compound 3f. **A**. Induction of loss of mitochondrial membrane potential after 24 or 48 h of incubation of HeLa cells with compound 3f. Cells were stained with JC-1 and analyzed by flow cytometry. Data are expressed as mean ± S.E.M. for three independent experiments. **B** and **C**. Mitochondrial production of ROS in HeLa cells. Cells were stained with HE (**B**) or H_2-DCFDA (**C**) and analyzed by flow cytometry. Data are expressed as mean ± S.E.M. of three independent experiments

Mitochondrial membrane depolarization is associated with mitochondrial production of ROS.[19] Therefore, we investigated whether ROS production increased after treatment with **3f**. We utilized two fluorescence indicators: HE, whose fluorescence appears if ROS are generated[19a] and the dye H_2-DCFDA, which is oxidized to the fluorescent compound DCF by a variety of peroxides, including hydrogen peroxide. [19a]

The results presented in Figure 4 (panels B and C show that **3f** induced the production of large amounts of ROS in comparison with control cells, which agrees with the previously described dissipation of $\Delta\psi_{mt}$. Altogether, these results indicate that compound **3f** induced apoptosis through the mitochondrial pathway.

Effect of 3f on Bcl-2, Bax expression and caspase-3 activation. Next, we analyzed the effect of **3f** on the expression of two members of the Bcl-2 family, the anti-apoptotic Bcl-2 and the pro-apototic Bax. The proteins of the Bcl family play a major role in controlling apoptosis through the regulation of mitochondrial processes and the release of mitochondrial proapoptotic molecules important

for the cell death pathway.[20] As shown in Figure 5 (panel B), **3f** did not significantly affect the expression of these two proteins, except for a marked decrease at 48 h of the anti-apoptotic protein Bcl-2.

To determine if caspases were involved in **3f**-induced cell death, the expression of caspase-3 was evaluated by flow cytometry. We observed a clear activation in a time-dependent manner, of caspase-3 and cleavage of its substrate PARP (Figure 5, panels A and B).

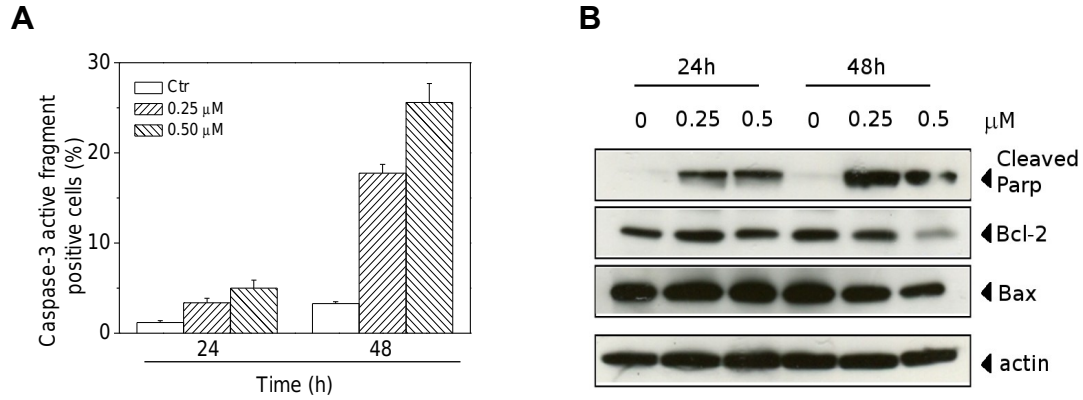

Figure 5 A. Caspase-3 induced activity by compound 3f. HeLa cells were incubated in the presence of 3f. After 24 or 48 h of treatment, cells were harvested and stained with an anti-human active caspase-3 fragment monoclonal antibody conjugated with FITC. Data are expressed as percentage of caspase-3 active fragment positive cells. **B**. Western blot analysis for the cleavage of PARP and the expression of Bcl-2 and Bax, in HeLa cells.

***In vivo* antitumor activity of compound 3f.** To evaluate the *in vivo* antitumor activity of **3f**, human colon adenocarcinoma xenografts were established by subcutaneous injection of HT29 cells in the backs of nude mice. Once the HT-29 xenografts reached a size of ~300 mm^3, eighteen mice were randomly assigned to one of the three groups. In two of the groups, compound **3f** or CA-4, prepared in DMSO, were injected intraperitoneally at doses of 100 mg/kg. All drugs, as well as a vehicle control, were administered three times a week for one week. As shown in Figure 6, compound **3f** caused a significant reduction in tumor growth (58%) as compared with administration of vehicle only. The effect on tumor volume reduction by **3f** was better than the effect of CA-4, which caused a 43.7 % of reduction day 24, despite the greater antiproliferative and antitubulin activities of CA-4. During the whole treatment period, no significant weight changes occurred in the treated animals (Figure 6, panel B).

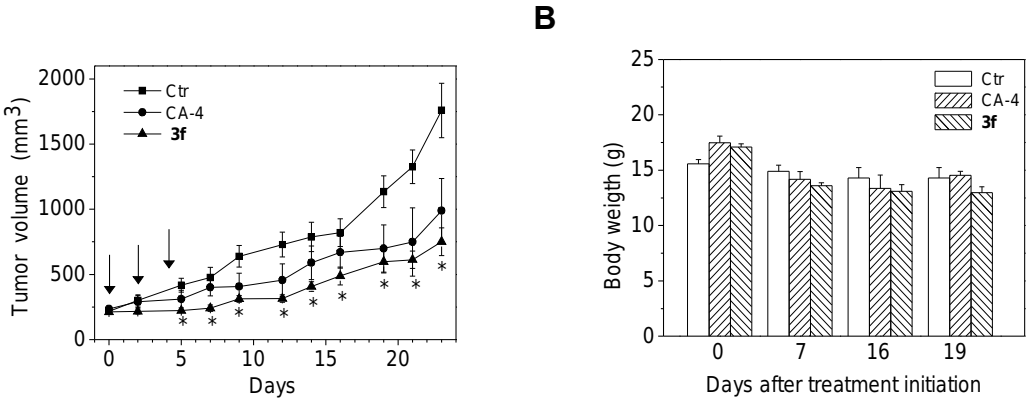

Figure 6. Inhibition of human xenograft growth *in vivo* by compound 3f. **A**. HT29 tumor-bearing nude mice were administered with vehicle control or 100 mg/kg of 3f or CA-4 intraperitoneally on days 0, 2 and 4 (indicated by an arrow). The figure shows the tumor volume (**A**) and body weight (**B**) recorded at the indicated days after treatments. Data are expressed as mean ± SEM of tumor volume and body weight at each time point for six animals per group. *p<0.01 *vs*. control.

However, in the CA-4 group two animal died on day 7 and one animal died in the **3f** on day 19. Thus, **3f** is potentially less toxic than CA-4 despite equivalent or superior *in vivo* activity.

Conclusions

In conclusion, a series of 2-alkylamino-4-amino-5-aroylthiazoles was synthesized by a one-pot procedure. This efficient method afforded a readily accessible compound, 2-(pyrrolidinin-1-yl)-4-amino-5-(3',4',5'-trimethoxybenzoyl)thiazole, displaying submicromolar IC_{50} values in all cancer cell lines examined. Compound **3f** was comparable to CA-4 as an inhibitor of tubulin polymerization through an interaction at the colchicine site. SAR studies demonstrated that an appropriate combination of C-2 and C-5 substitutions at the thiazole ring was essential for the activity. Of all substituents examined, the pyrrolidin-1-yl moiety at the C-2 position was required. These results suggested a strict spatial requirement for the substituent at the C-2 position on the thiazole scaffold at the tubulin binding site, which was confirmed in molecular docking studies. A similar phenomenon was observed with the substituent at the C-5 position, where the 3',4',5'-trimethoxybenzoyl moiety was the only tolerated group of all those examined and was crucial for potent biological activity.

Compound **3f** was also active in suppressing the growth of drug resistant cells, and. even more importantly, it had significant *in vivo* activity in a colon cancer

xenograft. These findings suggest that **3f** is a promising new antimitotic compound for the potential treatment of cancer.

Biological assay and computational study

Growth inhibitory activity. Murine leukemia L1210, murine mammary carcinoma FM3A, human T-lymphocyte Molt 4 and CEM cells and human cervix carcinoma (HeLa) cells were suspended at 300,000-500,000 cells/mL of culture medium, and 100 μL of a cell suspension was added to 100 μL of an appropriate dilution of the test compounds in wells of 96-well microtiter plates. After incubation at 37 °C for two days, the cell number was determined using a Coulter counter. The IC_{50} was defined as the compound concentration required to inhibit cell proliferation by 50%. Data are expressed as the mean ± SE from the dose-response curves of at least three independent experiments.

Effects on tubulin polymerization and on colchicine binding to tubulin. Bovine brain tubulin was purified as described previously.[9] To evaluate the effect of the compounds on tubulin assembly *in vitro,*[10] varying concentrations were preincubated with 10 μM tubulin in glutamate buffer at 30 ˚C and then cooled to 0 ˚C. After addition of GTP, the mixtures were transferred to 0 °C cuvettes in a recording spectrophotometer and warmed-up to 30 °C, and the assembly of tubulin was observed turbidimetrically. The IC_{50} was defined as the compound concentration that inhibited the extent of assembly by 50% after a 20 min incubation. The capacity of the test compounds to inhibit colchicine binding to tubulin was measured as described, [11] except that the reaction mixtures contained 1 μM tubulin, 5 μM [^{3}H]colchicine and 1 μM test compound.

Antiproliferative assays. Human non-small lung carcinoma (A549), human cervix carcinoma (HeLa) and human colon adenocarcinoma (HT-29) cells were grown in DMEM medium (Gibco, Milano, Italy), all supplemented with 115 units/mL of penicillin G (Gibco, Milano, Italy), 115 μg/mL streptomycin (Invitrogen, Milano, Italy) and 10% fetal bovine serum (Invitrogen, Milano, Italy). $LoVo^{Doxo}$ are doxorubicin resistant subclone of LoVo cells[22] and were grown in

complete HAM'S F12 medium supplemented with doxorubicin (0.1 μg/ml). $CEM^{Vbl-100}$ are a multidrug-resistant line selected against vinblastine[21]. A549-T12 are non-small cell lung carcinoma cells exhibiting resistance to taxol[23]. They were grown in complete DMEM medium supplemented with taxol (12 nM). Individual wells of a 96-well tissue culture microtiter plate were inoculated with 100 μL of complete medium containing $8x10^3$ cells. The plates were incubated at 37 °C in a humidified 5% CO_2 incubator for 18 h prior to the experiments. After medium removal, 100 μL of the drug solution, dissolved in complete medium at different concentrations, was added to each well and incubated at 37 °C for 72 h. Cell viability was assayed by the (3-(4,5-dimethylthiazol-2-yl)-2,5-diphenyl tetrazolium bromide (MTT) test as previously described.[32] The IC_{50} was defined as the compound concentration required to inhibit cell proliferation by 50%.

Flow cytometric analysis of cell cycle distribution. For flow cytometric analysis of DNA content, $5x10^5$ HeLa cells in exponential growth were treated with different concentrations of the test compounds for 24 and 48 h. After an incubation period, the cells were collected, centrifuged and fixed with ice-cold ethanol (70%). The cells were then treated with lysis buffer containing RNAse A and 0.1% Triton X-100, and then stained with PI. Samples were analyzed on a Cytomic FC500 flow cytometer (Beckman Coulter). DNA histograms were analyzed using MultiCycle for Windows (Phoenix Flow Systems).

Annexin-V assay. Surface exposure of PS on apoptotic cells was measured by flow cytometry with a Coulter Cytomics FC500 (Beckman Coulter) by adding Annexin-V-FITC to cells according to the manufacturer's instructions (Annexin-V Fluos, Roche Diagnostic). Simultaneously the cells were stained with PI. Excitation was set at 488 nm, and the emission filters were at 525 nm and 585 nm, respectively.

Assessment of mitochondrial changes. The mitochondrial membrane potential was measured with the lipophilic cation 5,5',6,6'-tetrachlo-1,1',3,3'-tetraethylbenzimidazolcarbocyanine (JC-1, Molecular Probes), as described.[32] Briefly, after different times of treatment, the cells were collected by centrifugation and resuspended in Hank's Balanced Salt Solution (HBSS)

containing 1 μM JC-1. The cells were then incubated for 10 min at 37 °C, centrifuged and resuspended in HBSS. The production of ROS was measured by flow cytometry using either HE (Molecular Probes) or H_2DCFDA (Molecular Probes). After different times of treatment, cells were collected by centrifugation and resuspended in HBSS containing the fluorescence probes HE or H_2DCFDA at the concentrations of 2.5 and 0.1 μM, respectively. The cells were then incubated for 30 min at 37 °C, centrifuged and resuspended in HBSS. The fluorescence was directly recorded with the flow cytometer, using as excitation wavelength 488 nm and emission at 585 nm and 530 nm for HE and H_2DCFDA, respectively.

Caspase-3 assay. Caspase-3 activation in Jurkat cells was evaluated by flow cytometry using a human active caspase-3 fragment antibody conjugated with FITC (BD Pharmingen). Briefly, after different incubation times in the presence of test compounds, the cells were collected by centrifugation and resuspended in Cytofix™ (BD Pharmingen) buffer for 20 min, washed with Perm/Wash™ (BD Pharmingen) and then incubated for 30 min with the antibody. After this period, cells were washed and analyzed by flow cytometry. Results are expressed as percentage of caspase-3 active fragment positive cells.

Western Blot Analysis. HeLa cells were incubated in the presence of test compounds and, after different times, were collected, centrifuged and washed two times with ice cold phosphate-buffered saline (PBS). The pellet was then resuspended in lysis buffer. After the cells were lysed on ice for 30 min, lysates were centrifuged at 15000 x g at 4 °C for 10 min. The protein concentration in the supernatant was determined using BCA protein assay reagents (Pierce, Italy). Equal amounts of protein (20 μg) were resolved using sodium dodecyl sulfate polyacrylamide gel electrophoresis (SDS-PAGE) (7.5-15 % acrylamide gels) and transferred to PVDF Hybond-p membrane (GE Healthcare). Membranes were blocked with I-block (Tropix) the membrane being gently rotated overnight at 4 °C. Membranes were then incubated with primary antibodies against, Bcl-2, Bax cleaved PARP, (all rabbit, 1:1000, Cell Signaling), Cyclin B, p-Cdc2^{Tyr15}, Cdc25c, p53, p21$^{waf/cip1}$, or β-actin (mouse, 1:10,000, Sigma) for 2 hr at room temperature. Membranes were next incubated with

peroxidase-labeled goat anti-rabbit IgG (1:100,000, Sigma), peroxidase-labeled goat anti-mouse IgG (1:100,000, Sigma) for 60 min. All membranes were visualized using ECL Advance (GE Healthcare) and exposed to Hyperfilm MP (GE Healthcare). To ensure equal protein loading, each membrane was stripped and reprobed with anti-b-actin antibody.

Antitumor activity *in vivo.* 4 weeks old, Female BALB/c-nu nude mice (15–18g) were obtained from Shanghai SLAC Laboratory Animal Co.Ltd(Shanghai, China). The animals were maintained under specific pathogen-free conditions with food and water supplied ad libitum in Zhejiang University of Traditional Chinese Medicine Laboratory Animal Center. Human colon adenocarcinoma, HT-29 cells in the logarithmic growth phase, were resuspend in FBS-free RPMI 1640, at the cell concentration of 1×10^7cells/ mL, and inoculate (0.2mL) in the hypodermis of the pars dorsalis of each mouse. Once the HT-29 xenografts reached a size of ~300 mm^3, eighteen mice were randomly assigned to three groups: Compound TR624 and Ca4 were prepared in DMSO and injected intraperitoneally at volumes of 0.01 ml/g body weight to give a dose of 100 mg/kg, respectively. All drugs were administered three times a week for one week. After completing the treatment schedule, tumor-bearing mice were euthanized. Tumor volume was calculated by the formula: $V=\times(L \times W^2)/2$ where L is the length and W is the width of the tumor nodules measured by vernier caliper. The study was approved by the Institutional Animal Ethical Committee of the second affiliated hospital, school of medicine, Zhejiang University (PRC).

Statistical analysis. Unless indicated differently, the results are presented as mean ± S.E.M. The differences between different treatments were analysed, using the two-sided Student's *t* test. P values lower than 0.05 were considered significant

References

1. Risinger, A. L.; Giles, F. J.; Mooberry, S. L. Microtubule dynamics as a target in oncology. *Cancer Treat. Rev.* **2008**, *35*, 255-261.

2. Honore, S.; Pasquier, E.; Braguer, D. Understanding microtubule dynamics for improved cancer therapy. *Cell. Mol. Life Sci.* **2005**, *62*, 3039-3056.

3. Pettit, G.R.; Singh, S.B.; Hamel, E.; Lin, C.M.; Alberts, D.S.; Garcia-Kendall, D. Isolation and structure of the strong cell growth and tubulin inhibitor combretastatin A-4. *Experientia* **1989**, *45*, 209-211.

4. Lin, C.M.; Ho, H.H.; Pettit, G.R.; Hamel, E. Antimitotic natural products combretastatin A-4 and combretastatin A-2: studies on the mechanism of their inhibition of the binding of colchicine to tubulin. *Biochemistry* **1989**, *28*, 6984-6991.

5. Chaudari, A.; Pandeya, S. N.; Kumar, P.; Sharma, P. P.; Gupta, S.; Soni, N.; Verma, K. K.; Bhardwaj, G. Combretastain A-4 analogues as anticancer agents. *Mini Rev. Med. Chem.* **2007**, *12*, 1186–1205.

6. Romagnoli, R.; Baraldi, P. G.; Carrion, M. D.; Cruz-Lopez, O.; Lopez-Cara, C.; Basso, G.; Viola, G.; Khedr, M.; Balzarini, J.; Mahboobi, S.; Sellmer, A.; Brancale, A.; Hamel, E.. 2-Arylamino-4-Amino-5-Aroylthiazoles. “One-Pot” Synthesis and Biological Evaluation of a New Class of Inhibitors of Tubulin Polymerization. *J. Med. Chem.* **2009**, *52*, 5551-5555.

7. 7.Gaukroger, K.; Hadfield, J. A.; Lawrence, N. J.; Nlan, S.; McGown, A. T. Structural requirements for the interaction of combretastatins with tubulin: how important is the trimethoxy unit? *Org. Biomol. Chem.* **2003**, *1*, 3033-3037.

8. a) Thomae, D.; Perspicace, E.; Hesse, S.; Kirsch, G.; Seck, P. Synthesis of substituted [1,3]thiazolo[4,5-d][1,2.3]triazines. *Tetrahedron*, **2008**, *64*, 9306-9314; b) Thomae, D.; Perspicace, E.; Xu, Z.; Henryon, D.; Schneider, S.; Hesse, S.; Kirsch, G.; Seck, P. One-pot synthesis of new 2,4,5-trisubstituted 1,3-thiazoles and 1,3-selenazoles. *Tetrahedron*, **2009**, *65*, 2982-2988.

9. Szakács, G.; Paterson, J.K.; Ludwig, J.A.; Booth-Genthe, C.; Gottesman, M.M. Targeting multidrug resistance in cancer *Nat. Rev. Drug Discov*. **2006**, 5, 219-234.

10. Baguley B.C. Multidrug resistance mechanism in cancer *Mol. Biotechnol.* **2010**, *46*, 308-316.

11. Dupuis, M.; Flego, M.; Molinari, A.; Cianfriglia, M. Saquinavir induces stable and functional expression of the multidrug transporter P-glycoprotein in human CD4 T-lymphoblastoid CEM rev cells. *HIV Medicine* **2003,** *4*, 338–345.

12. Toffoli, G.; Viel, A.; Tuimoto, I.; Bisconti, G.; Rossi, G.; Baoiocchi, M. Pleiotropic-resistant phenotype is a multifactorial phenomenon in human colon carcinoma cell lines. *Br. J. Cancer* **1991**, *63*, 51–56.

13. Martello, L.A.; Verdier-Pinard, P.; Shen, H. J.; He, L.; Torres, K.; Orr, G. A.; Horwitz, S. B. Elevated level of microtubule destabilizing factors in a taxol-resistant/ dependent A549 cell line with an alpha-tubulin mutation *Cancer Res.* **2003**, *63*, 448-454.

14. Mollinedo, F.; Gajate, C. Microtubules, microtubule-interfering agents and apoptosis. *Apoptosis* **2003**, 8:413-450;

15. Vermes, I.; Haanen, C.; Steffens-Nakken, H.; Reutelingsperger, C. A novel assay for apoptosis. Flow cytometric detection of phosphatidylserine expression on early apoptotic cells using fluorescein labelled annexin V. *J. Immunol. Methods* **1995**, *184*, 39–51.

16. Martin S. J., Reutelingsperger C. P., McGahon A. J., Rader J. A., van Schie R. C., Laface D. M., Green D. R. (1995). Early redistribution of plasma membrane phosphatidylserine is a general feature of apoptosis regardless of the initiating stimulus: Inhibition by overexpression of Bcl-2 and Abl. *J. Exp. Med. 182*,1545-1556.

17. a) Ly, J.D., Grubb D.R., Lawen A. The mitochondrial membrane potential ($\Delta\Psi_m$) in apoptosis: an update. *Apoptosis* **2003,** 3, 115-128; b) Green, D. R.; Kroemer, G. The pathophysiology of mitochondrial cell death. *Science* **2005**, *305*, 626–629.

18. Viola, G.; Fortunato, E.; Cecconet, L.; Del Giudice, L., Dall’Acqua, F.; Basso, G. Central role of mitochondria and p53 in PUVA-induced apoptosis in human keratinocytes cell

line NCTC-2544. *Toxicol. Appl. Pharm.* **2008**, *227*, 84-96.

19. a) Rothe, G.; Valet, G. Flow cytometric analysis of respiratory burst activity in phagocytes with hydroethidine and 2′,7′-dichlorofluorescein. *J. Leukocyte Biol.* **1990**, *47*, 440–448; b) Cai, J.; Jones, D. P. Superoxide in apoptosis. Mitochondrial generation triggered by cytochrome *c* loss. *J. Biol. Chem.* **1998**, *273*,11401-11404; c) Nohl, H.; Gille, L.; Staniek, K. Intracellular generation of reactive oxygen species by mitochondria. *Biochem. Pharmacol.* **2005**, *69*, 719-723.

20. a) Kluck, R. M.; Bossy-Wetzel, E.; Green, D. R. The release of cytochrome c from mitochondria: a primary site for Bcl-2 regulation of apoptosis. *Science* **1997**, *275*,1132-1136. b) Knudson, C. M.; Korsmeyer, S. J. Bcl-2 and Bax function independently to regulate cell death *Nature Genet.* **1997**, *16*, 358-363.

4.5. Synthesis and Evaluation of 1,5-Disubstituted Tetrazoles as Rigid Analogues of Combretastatin A-4 with Potent Antiproliferative and Antitumor Activity.

Romeo Romagnoli[†], Pier Giovanni Baraldi[†], Maria Kimatrai Salvador[†], Delia Preti[†], Mojgan Aghazadeh Tabrizi[†], Andrea Brancale[‡], Xian-Hua Fu[§], Jun Li[§], Su-Zhan Zhang[§], Ernest Hamel[⊥], Roberta Bortolozzi[‖], Giuseppe Basso[‖], and Giampietro Viola[‖].

† Dipartimento di Scienze Farmaceutiche, Università di Ferrara, 44100 Ferrara, Italy

‡ The Welsh School of Pharmacy, Cardiff University, King Edward VII Avenue, Cardiff, CF10 3NB, U.K.

§ Cancer Institute, Key Laboratory of Cancer Prevention and Intervention, China National Ministry of Education, The Second Affiliated Hospital, School of Medicine, Zhejiang University, Hangzhou, Zhejiang Province 310009, People's Republic of China

⊥Screening Technologies Branch, Developmental Therapeutics Program, Division of Cancer Treatment and Diagnosis, National Cancer Institute at Frederick, National Institutes of Health, Frederick, Maryland 21702, United States

‖ Laboratorio di Oncoematologia, Dipartimento di Pediatria, Università di Padova, 35131 Padova, Italy

Abstract

Tubulin, the major structural component of the microtubules, is the target for the development of anticancer agents. Two series of 1,5-diaryl substituted-1,2,3,4-tetrazoles were concisely synthesized using a palladium-catalyzed cross coupling reaction, and identified as potent antiproliferative agents and novel tubulin polymerization inhibitors that act at the colchicines binding site. The SAR information indicated that 4-ethoxy phenyl group at the N-1 or C-5 position of 1,2,3,4-tetrazole ring exhibited maximal activity. Several compounds have also potent activity in the growth inhibition of multidrug resistant cells. These compounds clearly induces apoptosis through mitochondrial pathway and caspase-9 and -3 activation. Furthermore, compound **4l** significantly reduced *in vivo* the growth of the HT-29 xenograft in a nude mouse model, suggesting that **4l** is a promising new antimitotic agent with clinical potential.

Introduction

Microtubules are the key components of cytoskeleton and they are involved in a wide range of cellular functions, such as regulation of motility, cell division, organelle transport, cytokinesis, maintenance of cell morphology and signal transduction.[1] The essential role of microtubules in mitotic spindle formation and proper chromosomal separation makes them one of the most attractive targets for the design and development of many small natural and synthetic antitumor drugs.[2] Many of them exert their effects by inhibiting non-covalent polymerization of tubulin to microtubules. Therefore, there has been great interest in identifying and developing novel anti-microtubule molecules. Among the naturally occurring compounds, combretastatin A-4 (CA-4, **1;** Chart 1) is one of the best characterized antimitotic agents.

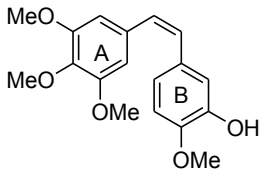

Combretastatin A-4 (CA-4), **1**

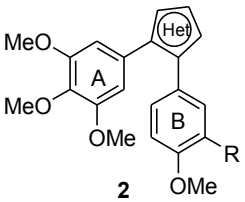

2

R=OH or NH_2
Het=thiophene, furan, imidazole; pyrazole; thiazole;oxazole; isoxazole; 1,2,3-thiadiazole; triazole, tetrazole..

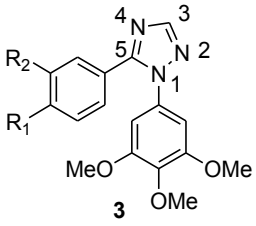

3

3a, R_1=OEt, R_2=H
3b, R_1=OEt, R_2=Cl

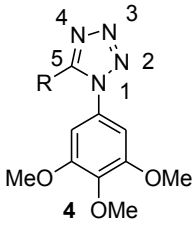

4

4a, R=C_6H_5
4b, R=2-thienyl
4c, R=p-$COCH_3$-C_6H_4
4d, R=p-CH_3-C_6H_4
4e, R=p-CH_2CH_3-C_6H_4
4f, R=p-OCH_3-C_6H_4
4g, R=R=m,p-$(OCH_3)_2$-C_6H_3
4h, R=m,m',p-$(OCH_3)_3$-C_6H_2
4i, R=p-OCH_3, m-F-C_6H_4
4j, R=p-OCH_3, m-Cl-C_6H_4
4k, R=p-OCH_3, m-CH_3-C_6H_4
4l, R=p-OCH_2CH_3-C_6H_4
4m, R=p-OCH_2CH_3, m-Cl-C_6H_4
4n, R=p-$O(CH_2)_2CH_3$-C_6H_4
4o, R=p-$O(CH_2)_3CH_3$-C_6H_4
4p, R=p-$O(CH_2)_4CH_3$-C_6H_4

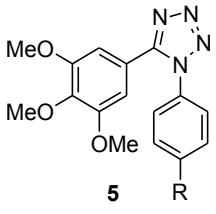

5

5a, R=OMe
5b, R=OEt

Chart 1. Inhibitors and Potential Inhibitors of Tubulin Polymerization

CA-4, isolated from the bark of the South African tree *Combretum caffrum,*[3] is one of the highly effective natural tubulin-binding molecules affecting microtubule dynamics by binding to the colchicine site.[4] CA-4 shows potent cytotoxicity against a wide variety of human cancer cell lines, including those that are multidrug resistant.[5] A water-soluble disodium phosphate derivative of CA-4 (named CA-4P) has shown promising results in human cancer clinical trials,[6] thus stimulating significant interest in a variety of CA-4 analogues.[7]

Previous SAR studies showed that both the 3',4',5'-trimethoxy substitution pattern on the A-ring and the *cis*-olefin configuration at the bridge were essential for optimal activity, while B-ring structural modifications were tolerated by the target.[7] Despite the remarkable anticancer activity of CA-4, the *cis*-configurated double bond is prone to isomerize to the chemically more stable *trans*-form during storage and metabolism, resulting in a dramatic loss in antitumor activity. Thus, to retain the appropriate configuration of the two adjacent aryl groups required for bioactivity, heterocombretastatin derivatives with general structure **2** were obtained replacing the stilbene core of CA-4 with 1,2-diarylsubstituted five-member aromatic heterocyclic rings, such as thiophene,[8] furan,[8] pyrazole,[9] imidazole,[9, 10] thiazole[9a], isoxazole,[11] 1,2,3-thiadiazole [12] and isomeric triazoles.[9, 13]

Recently we described a series of 1,5-diaryl-1,2,4-triazoles with general structure **3**, as potent inhibitors of cell growth and antimitotic agents.[13c] Among the synthesized compounds, derivatives **3a** and **3b** resulted the most active analogues for their ability to inhibit the growth of various human human tumor cell lines at low nanomolar concentrations (IC_{50} values ranging from 5-100 and 3-20 nM for **3a** and **3b**, respectively). In addition, these molecules exhibited inhibition of tubulin polymerization at concentration comparable to that of CA-4.

These results led us to start a pharmacophore exploration and optimization effort around the 1,2,4-triazole nucleus, replacing the CH at its C-3 position with a nitrogen, to afford the bioisosteric 1,2,3,4-tetrazole derivatives with general structure **4**.[14] A noteworthy point was that the preparation of most derivatives for this series was carried out via an efficient and flexible one-step procedure, starting from a common *N*-1-(3',4',5'-trimethoxyphenyl)tetrazole intermediate.

For compounds **4a-p**, modifications were focused on varying the aryl moiety at the C-5 position of the tetrazole skeleton, corresponding to the B-ring of CA-4,

by adding electron-withdrawing ($COCH_3$) or electron-releasing (alkyl and alkoxy) substituents (EWG and ERG, respectively) In addition, the B-ring was replaced with thien-2-yl moiety. Since the methoxy and ethoxy groups proved to be favourable for bioactivity, we maintained one of these substituents at the *para*-position and introduced additional substituents (F, Cl, Me and MeO) at the *meta*-position of the phenyl ring.

In order to understand the positional effect of the 3',4',5'-trimethoxyphenyl moiety on tetrazole ring, interchanging the 4'-alkoxyaryl and 3',4',5'-trimethoxyphenyl moieties at the *N*-1 and C-5 positions of compounds **4f** and **4l,** we have also synthesized the corresponding regioisomeric analogues **5a** and **5b**, respectively. Compounds **4a-p** and **5ab** were characterized by the presence of 3',4',5'-trimethoxyphenyl moiety, identical with the A-ring of CA-4, which was considered essential for maximal tubulin binding activity.[15]

We examined the efficacy of the newly synthesized compounds on a panel of human cancer cell lines, including multidrug resistant lines overexpressing the 170-kDa P-glycoprotein (P-gp) drug efflux pump and preliminary *in vivo* on murine xenograft nude mouse model indicated high activity in growth tumor suppression. In addition the mechanism of action of the most active compounds was investigated in detail.

Chemistry

1,5-Aryl tetrazoles **4a-p** and **5ab** were prepared following the procedure reported in Scheme 1.

The detailed procedure of synthesis is described on the full article published on Journal of Medicinal Chemistry (2012 Jan 12).

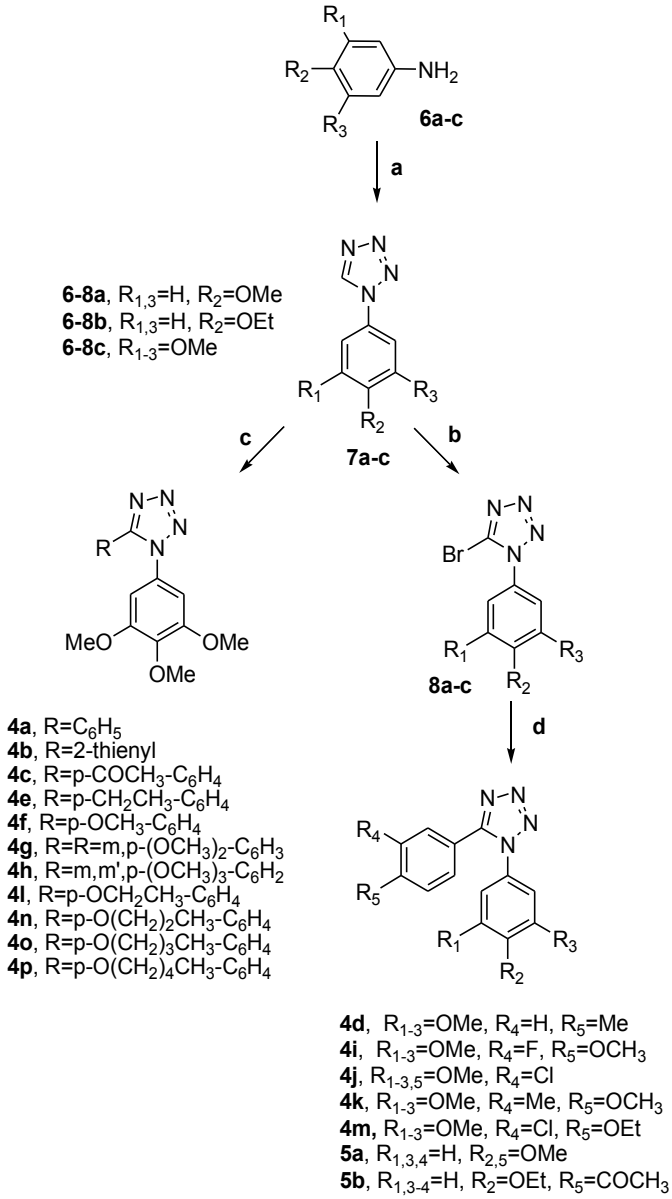

Reagents. **a**: NaN_3, $HC(OEt)_3$, CH_3CO_2H, rx; **b:** NBS, benzoylperoxide (cat.), CCl_4, rx; **c**: ArI, $Pd(OAc)_2$, CuI, TFP, $CsCO_3$, CH_3CN, 40 °C; **d**: $ArB(OH)_2$, $Pd(PPh_3)_4$, Na_2CO_3, PhMe-H_2O-EtOH, rx.

Scheme 1 synthesis procedure of 1,5-Aryl tetrazoles 4a-p and 5ab

Results and Discussion

In vitro **antiproliferative activities.** The 1-(3',4',5'-trimethoxyphenyl)-5-aryl-tetrazoles **4a-p** and the corresponding regioisomeric analogues **5ab** were evaluated for their inhibition of cell growth activity against a panel of six different human cancer cell lines and compared with the 1,2,4-triazole derivative **3a** and the reference compound CA-4. (**1**). In general, the antiproliferative activities of the tested compounds were less pronounced against A549 cells than the other

cell lines. Compound **4l**, bearing a 4'-ethoxy phenyl at the C-5 position of tetrazole ring, and its isomeric derivative **5b** exhibited the greatest antiproliferative activity among the tested compounds, with IC_{50} values of 1.3-8.1 nM and 0.3-7.4 nM, respectively.

Compd	IC_{50} [a](nM)					
	HeLa	A549	HL-60	Jurkat	MCF-7	HT-29
4a	4097±333	>10,000	903±123	3.8±0.7	>10,000	>10,000
4b	>10,000	>10,000	>10,000	>10,000	>10,000	>10,000
4c	648±211	>10,000	596±121	325±28	>10,000	6033±1527
4d	255±32.3	3420±127	329±41	222±17	1785±653	673±43
4e	29.0±5.6	3383±659	53.1±10	55.1±4.4	12.6±6.7	182±60
4f	2.6±0.0	222±59	2.9±0.6	2.6±0.1	38.5±5.8	4.6±0.6
4g	259±36.0	3574±280	488±71	345±28	2716±625	355±55
4h	>10,000	>10,000	>10,000	>10,000	>10,000	>10,000
4i	2.8±0.7	332±17	7.3±2.2	1.3±0.1	29.7±5.9	2.7±0.7
4j	2.3±0.5	402±84	3.6±0.6	10.0±0.9	25.2±3.4	35.9±4.4
4k	2.1±0.7	37.7±5.0	2.0±0.7	4.1±0.2	15.4±6.5	5.6±1.5
4l	1.9±0.7	8.1±3.2	1.3±0.3	0.16±0.06	2.3±0.8	2.8±0.7
4m	2.6±0.8	28.8±5.6	0.8±0.09	0.23±0.06	1.8±0.6	1.6±0.6
4n	11.1±3.2	495±24	43.3±14.5	47.0±0.06	66.2±13.4	105±47
4o	>10,000	>10,000	>10,000	>10,000	>10,000	>10,000
4p	6404±1906	>10,000	>10,000	>10,000	>10,000	>10,000
5a	952±122	>10000	40.3±16.6	209±86	27.1±8.2	265±26
5b	0.3±0.09	7.4±2.2	0.7±0.09	0.26±0.08	2.8±0.9	3.1±1.2
3a	15±4	100±20	20±3	5±0.2	50±9	n.d.
CA-4	4±1	180±50	1±0.2	5±0.6	370±100	3100±100

[a]IC_{50}= compound concentration required to inhibit tumor cell proliferation by 50%. Data are expressed as the mean ± SE from the dose-response curves of at least three experiment.

Table 1. In vitro cell growth inhibitory effects of compounds **3a**, **4a-p, 5ab** and CA-4 (**1**)

These values were similar to those obtained with CA-4 against HL-60, while **4l** and **5b** were from 2- to-1000-fold more active than CA-4 against the others five cell lines. While there not was any difference in activity between **4l** and **5b** against each cancer cell line, the same effect was not observed for the two isomeric 4'-methoxyphenyl derivatives **4f** and **5a**. This latter compound was from 4- to 50-fold less active than **4f** in five of the six cancer cell lines, exception being the MCF-7 cells in which **4f** and **5a** are equiactive.

Notably, comparing **3a** and **4l** which shared common 3',4',5'-trimethoxyphenyl and 4'-ethoxyphenyl moieties at their N-1 and C-5 positions, 1,2,3,4-tetrazole **4l** was from 8- to 31-fold more active than 1,2,3-triazole congener **3a**, while the regioisomeric derivative **5b** was from 15- to 50-fold more active than **3a**.

The unsubstituted C-5 phenyl derivative **4a** was weakly active (IC_{50}>1 μM)

against all the cell lines screened, with the notable exception of Jurkat cells in which it showed significant antiproliferative activity at low nanomolar concentration (IC_{50}=3.8 nM). The activity against Jurkat cells was completely lost replacing the phenyl with the bioisosteric 2-thienyl ring (compound **4b**). Further structural optimization was conducted with variation in the ERG or EWG on phenyl group at the 5-position of tetrazole ring. With the exception of Jurkat cells, the introduction of a weak electron-withdrawing acetyl group (**4c**) produced a slight increase of activity with respect to **4a.**

Comparing the two *para*-alkylphenyl derivatives **4d** and **4e**, replacing of the methyl (**4d**) with an ethyl (**4e**) resulted in an almost 10-, 6-, 4-, 150- and 3-fold enhancement of the potency against HeLa, HL-60, Jurkat, MCF-7 and HT-29 cells, respectively, while **4d** and **4e** were equipotent at low micromolar concentrations (IC_{50}=3.3 μM) against A549 cells. The replacement of the *para*-methyl with a para-methoxy (**4f**) has a beneficial effect, causing a 10- to 150-fold increase in antiproliferative activity.

Relative to the activity of **4f**, the insertion of an additional EWG or ERG group on the 3'-position of the 4'-methoxyphenyl ring affected variably the antiproliferative activity, suggesting that steric than electronic factors account for the potency of these compounds. While the strong electron-releasing methoxy group (**4g**) caused a decrease in potency of two orders of magnitude relative to **4f**, in general compound **4k** with the weak electron-releasing methyl group was more potent than compounds **4i** and **4j**, with the electron-withdrawing fluorine and chlorine atoms. Specific effects, however, seemed to vary with the cell line tested. On A549 cells, fluorine and chlorine addition was more disfavoured than methyl, with **4k** which displayed six-fold improvement in activity as compared with the parent compound **4f**. Thus, with compounds **4fgijk**, **4k** had the greatest activity with HeLa, A549, HL-60 and MCF-7 cells, **4i** with Jurkat cells and **4i** with HT-29 cells. Starting from the dimethoxy derivative **4g**, the introduction of a third methoxy group (compound **4h**) led to a complete loss of antiproliferative activity.

SAR information indicated that the introduction of an ethoxy group located at the *para*-position of phenyl at C-5 or *N*-1 positions of the tetrazole ring (compounds **4l** and **5b**, respectively) plays an important role in maximizing activity. With A549 cells, a 3-fold reduction in potency was observed comparing **4l** with its 3'-chloro analogue **4m**, but only minor changes in antiproliferative

activity occurred with the other five cell lines.

In an effort to further understand the bulk tolerance at the para-position of the C-5 phenyl ring, the methoxy or ethoxy were substituted with alkoxy groups of varying straight alkyl chain. As the length of the alkoxy group increased from ethoxy to *n*-propoxy (*n*-PrO*,* **4n**), the activity decrease by one or two order of magnitude in all cell lines relative to **4l** . The reduction in potency was more pronounced (IC_{50}>6 μM) with the *n*-butoxy (*n*-BuO) and *n*-penthoxy (*n*-PeO) analogues **4o** and **4p**, respectively. This indicated that in the series of *para*-alkoxy derivatives **4flnop**, the ethoxy substitution was the optimal requisite for activity.

Inhibition of tubulin polymerization and colchicine binding. To investigate whether the antiproliferative effect of compounds **4ef**, **4i-n** and **5ab** was related to tubulin interactions, they were evaluated for their inhibition of tubulin polymerization and for effects on the binding of [^{3}H]colchicine to tubulin (Table 2).[20] For comparison, CA-4 and **3a** were examined in contemporaneous experiments. In the assembly assay, compound **4l** was found to be the most active (IC_{50}, 1.1 μM), with activity being in the range of CA-4 and **3a** (IC_{50}, 1.3 and 0.76 μM, respectively). The remaining compounds were good inhibitors of tubulin polymerization, with IC_{50} values ranging from 2 to 4 μM, somewhat less active than CA-4.

While this group of compounds was highly potent in inhibition of cell growth and tubulin assembly, correlation between these two assay types was imperfect. Thus, while compound **4l** was the best inhibitor of tubulin assembly, it was two fold more potent that isomeric derivative **5b** in this assay, while **4l** and **5b** were equipotent as inhibitors of cell growth.

In the colchicine binding studies, derivatives **4l** and **5ab** have quantitatively similar effects, varying within a narrow range (70-78% inhibition) and they were slightly less potent than CA-4, which in these experiments inhibited colchicine binding by 99%. For compounds **4ef**, **4jk** and **4mn**, the inhibition of colchicines binding ranged from 46 to 58%, resulting almost half as active as CA-4 in this assay. In this series of ten compounds, inhibition of [^{3}H]colchicine binding correlated more closely with inhibition of tubulin assembly than with antiproliferative activity.

Compound	Tubulin assembly[a] IC_{50}±SD (μM)	Colchicine binding [b] % ±SD
4e	3.7±0.5	47±3
4f	2.5±0.3	54±0.3
4i	2.1±0.2	60±0.7
4j	3.5±0.2	50±1
4k	2.5±0.1	59±3
4l	1.1±0.1	78±3
4m	2.0±0.2	58±2
4n	3.1±0.4	46±4
5a	2.1±0.3	70±0.1
5b	2.0±0.1	71±2
3a	0.76±0.1	86±2
CA-4 (**1**)	1.3±0.1	99±0.4

[a] Inhibition of tubulin polymerization. Tubulin was at 10 μM.
[b] Inhibition of [^{3}H]colchicine binding. Tubulin, colchicine and tested compound were at 1, 5 and 5 μM, respectively. N.d.=not done

Table 2. Inhibition of tubulin polymerization and colchicine binding by compounds **3b**, **4ef, 4i-n, 5ab** and CA-4

Molecular Modelling. A series of molecular docking simulations were performed on this series of compounds to understand the role of the tetrazole ring in the binding with tubulin, using the same procedure reported previously.[13c] From the results obtained (Figure 1), it is possible to observe how the proposed binding is very similar to the pose of the co-crystallised DAMA-colchicine, with trimethoxyphenyl ring placed in proximity of Cys241. Furthermore, the tetrazole is placed toward the external part of the pocket and it does not seem to establish any specific interaction. Indeed, the binding pose of the two isomers **4l** and **5b** is virtually identical. Another important consideration is that the tetrazole analogues binding mode is very similar to the one observed for the triazole compounds **3a-b**,[13c] and even in this case only relatively small substitution are tolerated in the *meta* position of the second phenyl ring (e.g **4i-k**), while analogues with larger groups, both in the *meta* and *para* position (e.g **4g-h** and **4o-p**) do not dock successfully, probably because of a steric clash with the binding pocket. These results correlate well with the biological data observed for these compounds.

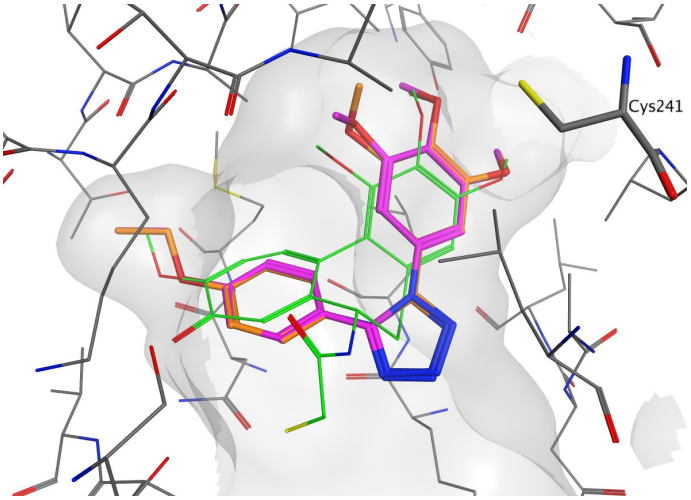

Figure 1. Proposed binding mode of 4l (purple) and 5b (orange) with DAMA-colchicine (green) in the tubulin binding site.

Effects of 4l, 4m and 5b on multidrug resistant cell lines. Drug resistance is an important therapeutic problem caused by the emergence of tumor cells possessing different mechanisms which confer resistance against a variety of anticancer drugs.[21,22] Among the more common mechanisms are those related to the overexpression of a cellular membrane protein called P-glycoprotein capable of mediating the efflux of various structurally unrelated drugs.[21,22] In this context, we evaluated sensitivity to the most active compounds (**4l**, **4m** and **5b)** in two multidrug-resistant cell lines, one derived from a lymphoblastic leukemia ($CEM^{Vbl\text{-}100}$), the other derived from a colon carcinoma ($Lovo^{Doxo}$). Both these lines express high levels of the 170-kDa P-glycoprotein (P-gp) drug efflux pump.[23,24] As shown in Table 3, the three compounds were equally potent toward parental cells and cells resistant to vinblastine or doxorubicin.

Resistance to microtubule inhibitors may be also mediated by changes in the levels of expression of different β-tubulin isotypes and by tubulin gene mutations that result in modified tubulin with impaired polymerization properties. A-549-T12 is a cell line with an *α*-tubulin mutation with increased resistance to taxol.[25] Compounds **4l, 4m** and **5b** had greater relative activity than taxol in this cell line, suggesting that these compounds might be useful in the treatment of drug refractory tumors resistant to other antitubulin drugs.

Compd	IC_{50} [a](nM)					
	LoVo	$LoVo^{Doxo}$	CEM	CEM ^{Vbl100}	A549	A549-T12
4l	1.1±0.9	0.7±0.06 (0.6)[b]	3.1±1.0	0.7±0.09 (0.2)	8.1±3.27	8.2±5.0 (1.0)
4m	12.5±2.1	15.7±6.5 (1.2)	0.7±0.1	0.7±0.2 (1.0	28.8±5.6	31.5±11.4 (1.1)
5b	118.2±60.5	96.9±42.6 (0.8)	3.8±1.4	0.5±0.1 (0.1)	7.4±2.2	4.2±1.8 (0.6)
Doxorubicine[c]	120±30	13150±210 (109.6)	n.d.	n.d.	n.d.	n.d.
Vinblastine[c]	n.d.	n.d.	4.1 ±0.2	230 ± 32 (56.1)	n.d.	n.d.
Taxol[c]	n.d.	n.d.	n.d.	n.d.	7.2 ± 0.1	75.2±12.5 (10.4)

[a]IC_{50}= compound concentration required to inhibit tumor cell proliferation by 50%. Data are expressed as the mean ± SE from the dose-response curves of at least three independent experiments.
[b]Values in brackets are fold resistance, indicating reduced potency of the compounds in the resistant cell lines
[c]Data taken from ref.13c n.d. not determined

Table 3. In vitro cell growth inhibitory effects of compounds on drug resistant cell lines

Analysis of cell cycle effects. The effects of different concentrations of compounds **4l, 4m** and **5b** after 24h of treatment on cell cycle progression were examined in HeLa cells (Figure 2, panel A, B, C). The two isomers **4l** and **5b** caused a significant G2/M arrest in a concentration-dependent manner, already at low concentration (30 nM) where at higher concentrations more than 80% of the cells are blocked in this phase reaching a plateau at 60 nM. At the same time we observed a concomitant decrease of all the other phases of the cell cycle (G1 and S).

Compound **4m** showed an analogous behavior although it is less efficacious in inducing G2/M arrest than the other two compounds.

We next studied the association between **4l**-induced G2/M arrest and alterations in expression of proteins that regulate cell division. Cell arrest at the prometaphase/metaphase to anaphase transition is normally regulated by the mitotic checkpoint.[26] The major regulator of the G2 to M transition is M phase-promoting factor (MPF), a complex made up of the catalytic sub-unit of cdc2 and the regulatory subunit of cyclin B. These complexes are activated at different checkpoints after certain intervals during the cell cycle and can also be regulated by several exogenous factors. Cyclin B/Cdc2 complexes are held in an inactive state by phosphorylation of Cdc2 at two negative regulator sites

(Thr14 and Tyr15). Dephosphorylation of these negative regulatory sites is needed to activate the Cdc2/cyclin B complex. Cdc25C is a major phosphatase that dephosphorylates both sites on Cdc2 to activate them.[27,28]

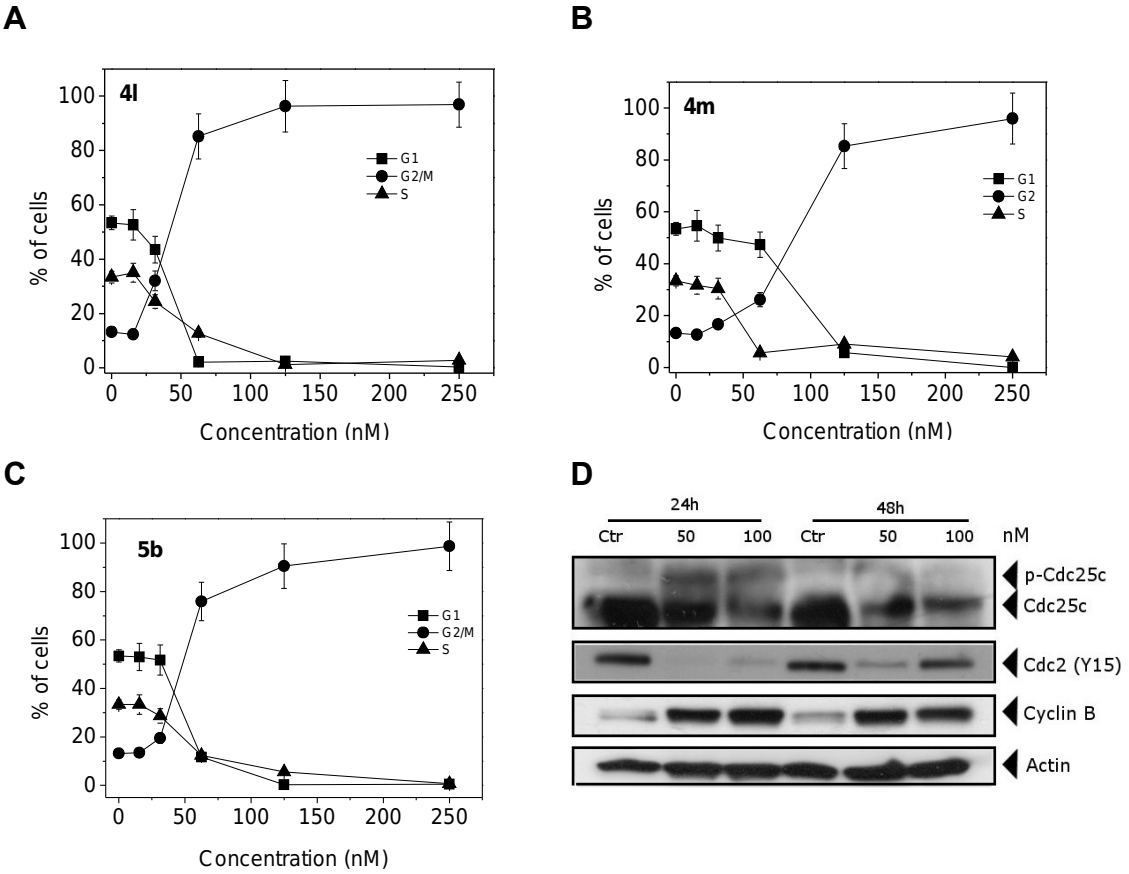

Figure 2 Effect of compounds **4l** (**A**), **4m** (**B**) and **5b** (**C**) on cell cycle distribution of HeLa. Cells were treated with different concentrations of the compounds ranging from 15 to 250 nM for 24 h. Then the cells were fixed and stained with PI to analyze DNA content by flow cytometry. Data are presented as mean ± SEM of three independent experiments. **D**. Effect of **4l** on G2/M regulatory proteins. HeLa cells were treated for 24 or 48 h with the of the compound. The cells were harvested and lysed for the detection of cyclin B, p-Cdc2^{Y15} and Cdc25c expression by western blot analysis.

As shown in Figure 2 (panel D) in HeLa cells, **4l** caused a remarkable increase in cyclin B1 expression both after 24 h and 48 h of treatment. In addition, slower migrating forms of phosphatase Cdc25c appeared at 24 h, indicating changes in the phosphorylation state of this protein followed by partial disappearance of the total form of the protein at 48 h,. The phosphorylation of Cdc25c directly stimulates its phosphatase activity, and this is necessary to activate Cdc2/cyclin B on entry into mitosis.[27,28] In well agreement we observed the de-phosphorylation of Cdc2 (Tyr15) resulting in inhibition of the cdc2/cyclinB complex formation.

Compounds 4l and 5b induces apoptosis. To characterize the mode of cell death induced by **4l** and **5b**, a biparametric cytofluorimetric analysis was performed using PI, which stains DNA and enters only dead cells, and fluorescent immunolabeling of the protein annexin-V, which binds to PS in a highly selective manner.[29] Dual staining for annexin-V and with PI permits discrimination between live cells (annexin-V^-/PI^-), early apoptotic cells (annexin-V^+/PI^-), late apoptotic cells (annexin-V^+/PI^+) and necrotic cells (annexin-V^-/PI^+) . As depicted in Figure 3 (panels A-C), both compounds induced an accumulation of annexin-V positive cells in comparison with the control, in a concentration and time-dependent manner.

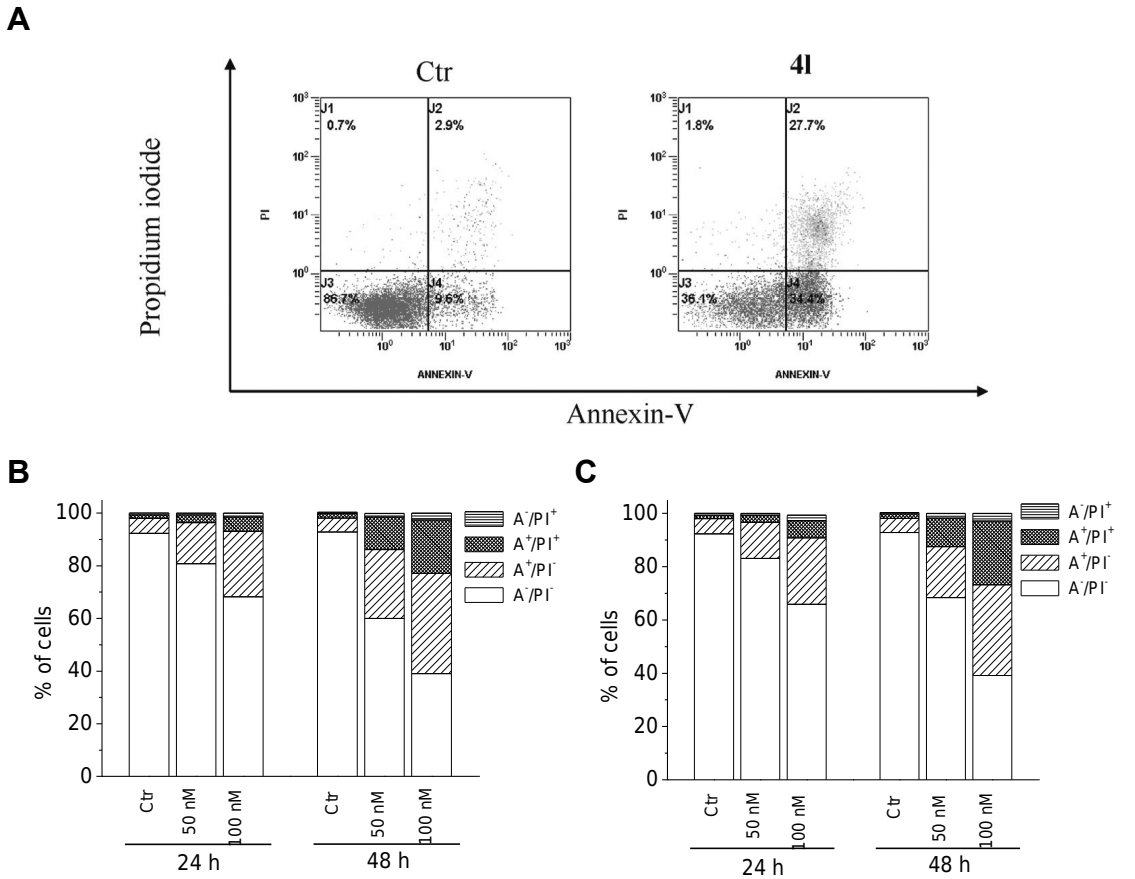

Figure 3. Panel A. Representative histograms of HeLa cells treated with **4l** (100 nM) for 48 h and analyzed by flow cytometry after double staining of the cells with Annexin-V-FITC and PI. Panel B. Percentage of cells found in the different regions of the biparametric histograms obtained from cytofluorimetric analysis, after incubation with **4l** (**B**) and **5b** (**C**) for 24 h or 48 h as indicated.

Effect of 4l and 5b on mitochondrial depolarization. Mitochondria play an essential role in the propagation of apoptosis.[30] It is well established that, at an early stage, apoptotic stimuli alter the mitochondrial transmembrane potential ($\Delta\psi_{mt}$). $\Delta\psi_{mt}$ was monitored by the fluorescence of the dye JC-1. With normal

cells (high $\Delta\psi_{mt}$), JC-1 displays a red fluorescence (590 nm). This is caused by spontaneous and local formation of aggregates that are associated with a large shift in the emission. In contrast, when the mitochondrial membrane is depolarized (low $\Delta\psi_{mt}$), JC-1 forms monomers that emit at 530 nm. As shown in Figure 4 (panels A-C), both **4l** and **5b** induced a time and concentration–dependent increase in cells with depolarized mitochondria.

Mitochondrial membrane depolarization is associated with mitochondrial production of ROS.[31] Therefore, we investigated whether ROS production increased after treatment with **4l** and **5b**. We utilized two fluorescence indicators: hydroethydine (HE), whose fluorescence appears if ROS are generated[32] and the dye H_2-DCFDA, which is oxidized to the fluorescent compound DCF by a variety of peroxides, including hydrogen peroxide. [32]

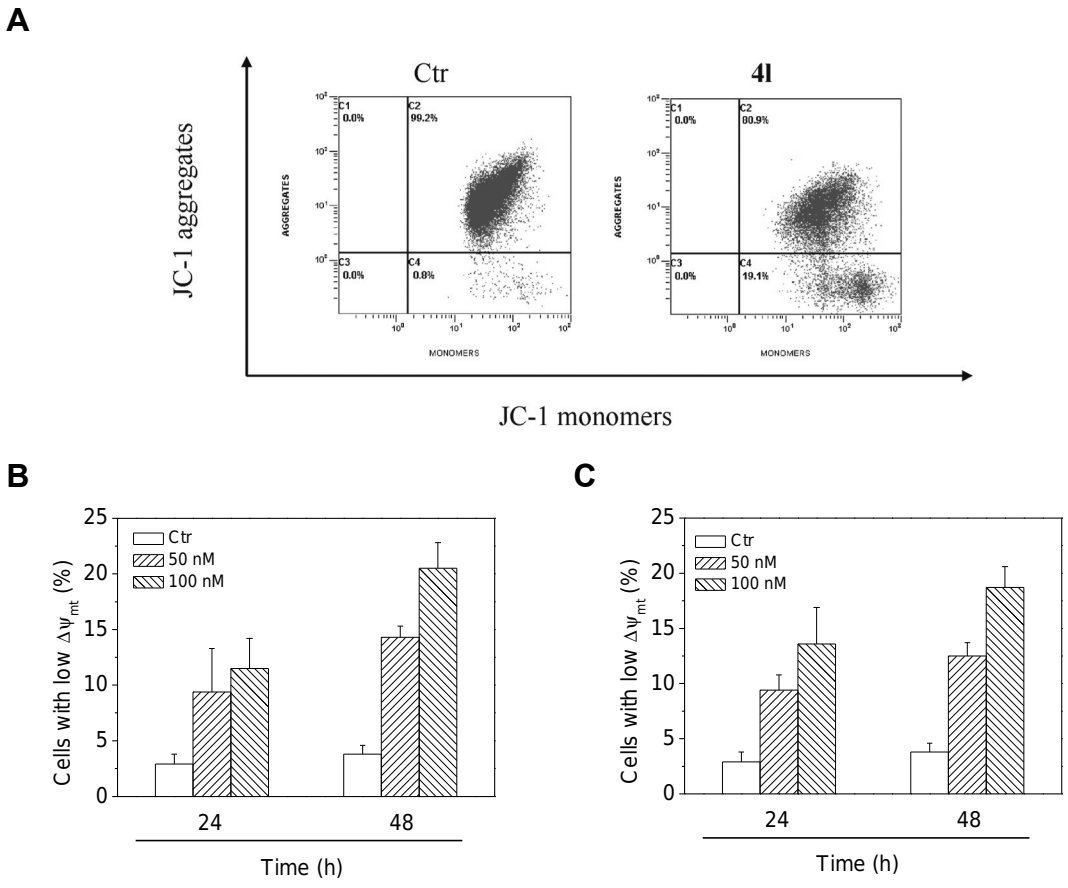

Figure 4. Assessment of mitochondrial potential after treatment with compounds **4l** and **5b**. Panel **A** shows as representative histograms of the cells incubated in the presence of **4l**, and stained with the fluorescent probe JC-1 after 48 h of treatment. The horizontal axis shows fluorescence intensity of JC-1 monomer and vertical axis show fluorescence of JC-1 aggregates. Panels B and C. Induction of loss of mitochondrial membrane potential after 24 or 48 h of incubation of HeLa cells with compound **4l** (**B**) and **5b** (**C**). Data are expressed as mean ± S.E.M. for three independent experiments.

The results presented in Figure 5 (panels B and C) show that both **4l** and **5b** induced the production of significant amounts of ROS in comparison with control cells, which agrees with the previously described dissipation of $\Delta\psi_{mt}$. Altogether, these results indicate that these compounds induced apoptosis through the mitochondrial pathway. In this context also triazole derivative **3a** has showed to induce apoptosis following the intrinsic pathway.[13c]

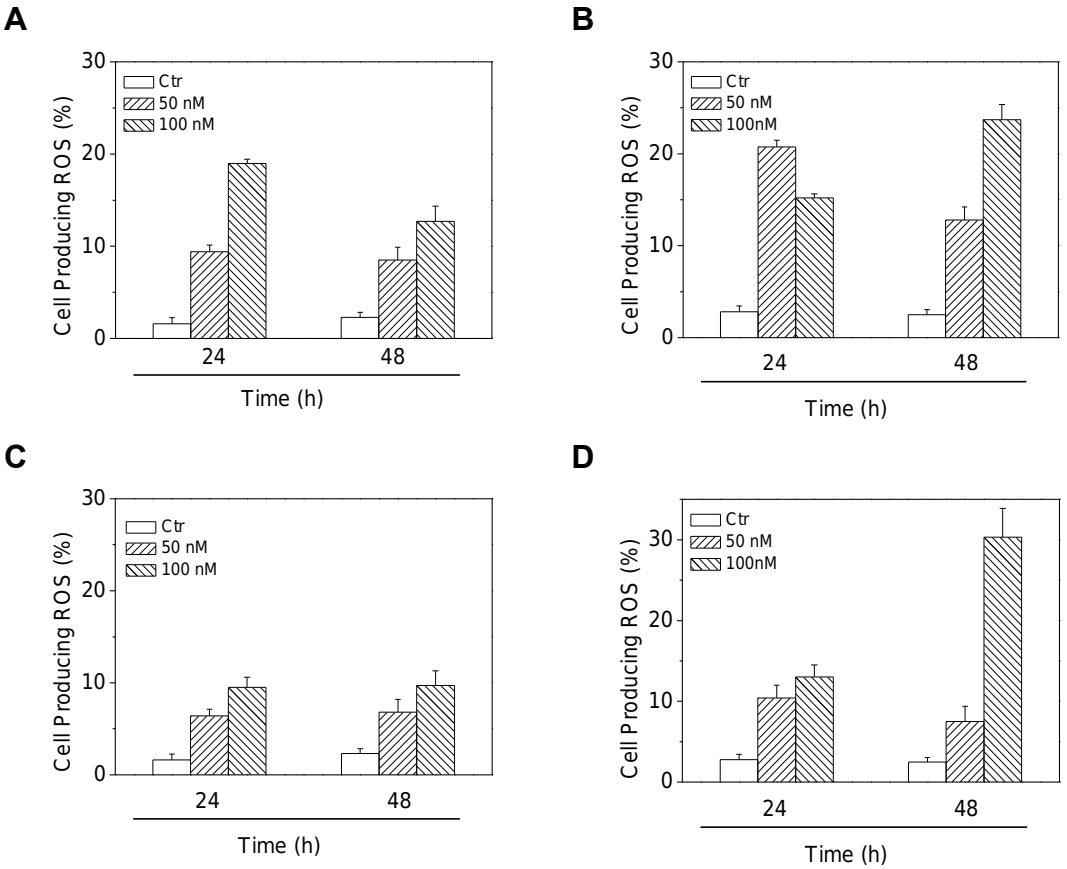

Figure 5 Mitochondrial production of ROS in HeLa cells by compounds **4l** (**A** and **B**) and **5b** (**C** and **D**). After 24 or 48 h of incubation with **4l** or **5b** cells were stained with HE (panel A and C) or H_2-DCFDA (**B** and **D**) and analyzed by flow cytometry. Data are expressed as mean ± S.E.M. of three independent experiments.

Compound 4l induce caspases activation. Caspases are the central executioners of apoptosis mediated by various inducers.[33] Caspases are synthesized as proenzymes that are activated by cleavage. Caspases-2, -8, -9, and -10 are termed apical caspases and are usually the first to be stimulated in the apoptotic process. Their activation in turn leads to their activation of effector caspases, in particular caspase-3.[34]

We observed a clear activation of the effector caspase, caspase-3, and we also observed cleavage of the caspase-3 substrate poly (ADP-ribose) polymerase (PARP) both after 48 h of exposure by compound **4l** (Figure 6, Panels A and

B). In addition, the expression of X-linked inhibitor of apoptosis protein (XIAP), a member of inhibitors of apoptosis protein family, was strongly reduced concomitant with caspases activation. Consistent with the $\Delta\psi_{mt}$ results described above, **4l** treatment induce activation of caspase-9, the major initiator caspase of the intrinsic (mitochondrial) apoptosis pathway.

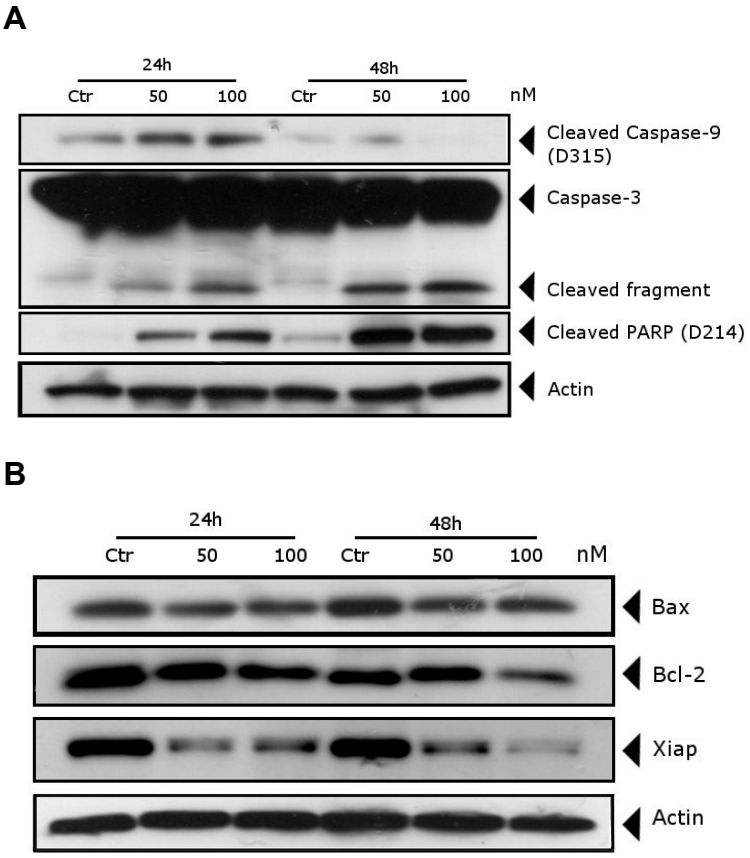

Figure 6 A Western blot analysis of caspase-3, cleaved caspase-9 and cleaved PARP after treatment of HeLa cells by **4l**.
B Western blot analysis of Bcl-2, Bax and XIAP after treatment of HeLa cells by **4l.** To confirm equal protein loading, each membrane was stripped and reprobed with anti-b-actin antibody.

We also examined whether the induction of apoptosis by **4l** is associated with changes in the expression of two proteins of the Bcl-2 family since there is increasing evidence that regulation of protein shares the signaling pathways induced by antimicrotubule compounds.[35] Our results showed (Figure 6, Panel B) that the anti-apoptotic proteins Bcl-2 was only slight affected after 48 h of treatment whereas **4l** treatment had no effect on the expression of the proapoptotic protein Bax.

***In vivo* antitumor activity of compound 4l.** To evaluate the *in vivo* antitumor activity of **4l**, human colon adenocarcinoma xenografts were established by subcutaneous injection of HT29 cells in the backs of nude mice. Once the HT-29 xenografts reached a size of ~300 mm^3, twelve mice were randomly

assigned to one of the two groups. In one of the groups, compound **4l**, prepared in DMSO, was injected intraperitoneally at doses of 100 mg/kg. The compound, as well as a vehicle control, were administered three times a week for one week. As shown in Figure 7, after the observation period, compound **4l** caused a remarkable reduction in tumor growth (66%) as compared with administration of vehicle only. It is worthwhile to note that the reduction of tumor growth is statistically significant just after the third administration of compound suggesting a rapid and efficacious delivery to the tumoral mass. During the whole treatment period, no significant weight changes occurred in the treated animals (Figure 7, panel B), suggesting that macroscopically, **4l** is potentially not toxic.

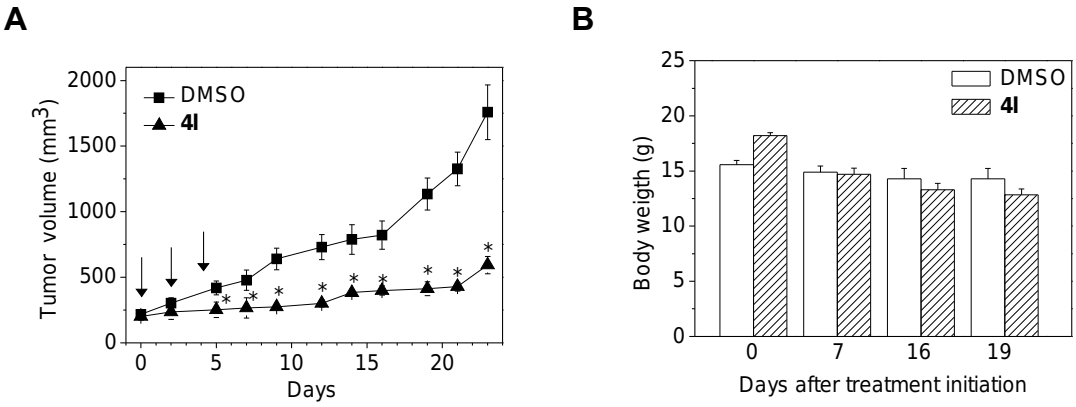

Figure 7 Inhibition of human xenograft growth *in vivo* by compound **4l. A** HT29 tumor-bearing nude mice were administered with vehicle control or 100 mg/kg of **4l** intraperitoneally on days 0, 2 and 4 (indicated by an arrow). The figure shows the tumor volume (**A**) and body weight (**B**) recorded at the indicated days after treatments. Data are expressed as mean ± SEM of tumor volume and body weight at each time point for six animals per group. *p<0.01 *vs*. control.

Conclusions

In conclusion, we have demonstrated that the 1,2,3,4-triazole ring is a suitable mimic for the *cis*-olefinic configuration present in CA-4. *N*-1-(3',4',5'-trimethoxyphenyl)tetrazole was the key intermediate for the preparation of many active compounds via a parallel synthesis. The observed antiproliferative activities depended on the substitution pattern on the phenyl at the 5-position of the tetrazole ring. The methoxy and ethoxy groups at the *para*-position were beneficial for biological activity. The introduction of an additional EWG, such as F or Cl, or weak electron-releasing Me group at the 3'-position of the 4'-methoxy phenyl ring are favourable for the maintenance or improve the activity of **4f,** in

contrast a methoxy group caused an approximate 15- to 150-fold decrease in potency. The *para*-ethoxy phenyl derivative **4l** and its isomeric derivative **5b** showed activities lower than 10 nM, with IC_{50} values ranging from 0.3 to 8.1 nM. Replacement of *para*-ethoxy group with alkoxy groups with a longer alkyl chain was detrimental for activity. The results imply the 3'-hydroxy-4'-methoxyphenyl (corresponding to B-ring) in CA-4 can be replaced by a 4'-ethoxy phenyl. With the exception of A549 cells, the introduction of chlorine into the 3'-position of 4'-ethoxy phenyl ring of **4l**, to furnish **4m**, caused only minor changes in antiproliferative activity. Compound **4l** is a good inhibitor of tubulin polymerization (IC_{50}=1.1 M) and strongly displaced colchicines from its binding site in the tubulin (78% inhibition), showing IC_{50} values comparable to that of CA-4 (IC_{50}=1.3 M for assembly with 10 M tubulin, 99% inhibition of the binding of 1 M tubulin, with the inhibitor and colchicine both at 5 M), We have also showed that the tetrazole system which characterizes compound **4l** retained, or ever improved, the biological activity of 1,2,4-triazole analogue **3a** previously reported. The 3'-chloro-4'-ethoxyphenyl derivative **4m** and the two isomeric 4'-ethoxyphenyl derivatives **4l** and **5b** have been shown to arrest the cell cycle at the G2/M phase and induce apoptosis trough the mitochondrial (intrinsic) pathway. Importantly, the antitumor efficacy of **4l** was demonstrated in a tumor xenograft-bearing mouse in which a significative tumor growth was observed at triple dose of compound without weight loss of the animals. Altogether, these results indicate that **4l** is a promising new tubulin binding agents and is worthy of further development as antitumor drug.

Materials and Methods

Antiproliferative assays. Human T-leukemia (Jurkat) and human promyelocytic leukemia (HL-60) cells were grown in RPMI-1640 medium, (Gibco, Milano, Italy). Breast adenocarcinoma (MCF7), human non-small cell lung carcinoma (A549), human cervix carcinoma (HeLa) and human colon adenocarcinoma (HT-29) cells were grown in DMEM medium (Gibco, Milano, Italy), all supplemented with 115 units/mL of penicillin G (Gibco, Milano, Italy), 115 g/mL streptomycin (Invitrogen, Milano, Italy) and 10% fetal bovine serum (Invitrogen, Milano, Italy). $LoVo^{Doxo}$ cells are a doxorubicin resistant subclone of

LoVo cells[22] and were grown in complete Ham's F12 medium supplemented with doxorubicin (0.1 μg/ml). $CEM^{Vbl-100}$ are a multidrug-resistant line selected against vinblastine.[23] A549-T12 are non-small cell lung carcinoma cells exhibiting resistance to taxol.[24] They were grown in complete DMEM medium supplemented with taxol (12 nM). Stock solutions (10 mM) of the different compounds were obtained by dissolving them in DMSO. Individual wells of a 96-well tissue culture microtiter plate were inoculated with 100 L of complete medium containing $8x10^3$ cells. The plates were incubated at 37 °C in a humidified 5% CO_2 incubator for 18 h prior to the experiments. After medium removal, 100 μL of fresh medium containing the test compound at different concentrations, were added to each well and incubated at 37 °C for 72 h. The percentage of DMSO in the medium never exceed 0.25%. This was also the maximum DMSO concentration in all cell-based assays described below. Cell viability was assayed by the (3-(4,5-dimethylthiazol-2-yl)-2,5-diphenyl tetrazolium bromide test as previously described.[36] The IC_{50} was defined as the compound concentration required to inhibit cell proliferation by 50%, in comparison to cells treated with the maximum amount of DMSO (0.25%) and considered as 100% viability.

Effects on tubulin polymerization and on colchicine binding to tubulin. To evaluate the effect of the compounds on tubulin assembly *in vitro*,[20a] varying concentrations of compounds were preincubated with 10 M bovine brain tubulin in glutamate buffer at 30 ˚C and then cooled to 0 ˚C. After addition of 0.4 mM GTP, the mixtures were transferred to 0 °C cuvettes in a recording spectrophotometer and warmed to 30 °C. Tubulin assembly was followed turbidimetrically at 350 nm. The IC_{50} was defined as the compound concentration that inhibited the extent of assembly by 50% after a 20 min incubation. The capacity of the test compounds to inhibit colchicine binding to tubulin was measured as described,[20b] except that the reaction mixtures contained 1 μM tubulin, 5 μM [^{3}H]colchicine and 1 μM test compound.

Molecular Modelling. Materials and Methods. All molecular modeling studies were performed on a MacPro dual 2.66GHz Xeon running Ubuntu 8. The tubulin structure was downloaded from the PDB data bank (http://www.rcsb.org/ - PDB

code: 1SA0).[37] Hydrogen atoms were added to the protein, using Molecular Operating Environment (MOE),[38] and minimized keeping all the heavy atoms fixed until a RMSD gradient of 0.05 kcal mol^{-1} $Å^{-1}$ was reached. Ligand structures were built with MOE and minimized using the MMFF94x forcefield until a RMSD gradient of 0.05 kcal mol^{-1} $Å^{-1}$ was reached. The docking simulations were performed using PLANTS.[39]

Flow cytometric analysis of cell cycle distribution. For flow cytometric analysis of DNA content, $5x10^5$ HeLa cells in exponential growth were treated with different concentrations of the test compounds for 24 and 48 h. After an incubation period, the cells were collected, centrifuged and fixed with ice-cold ethanol (70%). The cells were then treated with lysis buffer containing RNAse A and 0.1% Triton X-100, and then stained with PI. Samples were analyzed on a Cytomic FC500 flow cytometer (Beckman Coulter). DNA histograms were analyzed using MultiCycle® for Windows (Phoenix Flow Systems).

Annexin-V assay. Surface exposure of PS on apoptotic cells was measured by flow cytometry with a Coulter Cytomics FC500 (Beckman Coulter) by adding Annexin-V-FITC to cells according to the manufacturer's instructions (Annexin-V Fluos, Roche Diagnostic). Simultaneously the cells were stained with PI. Excitation was set at 488 nm, and the emission filters were at 525 nm and 585 nm, respectively.

Assessment of mitochondrial changes. The mitochondrial membrane potential was measured with the lipophilic cation 5,5',6,6'-tetrachlo-1,1',3,3'-tetraethylbenzimidazolcarbocyanine (JC-1, Molecular Probes), as described.[13c] The production of ROS was measured by flow cytometry using either HE (Molecular Probes) or H_2DCFDA (Molecular Probes) as previously described.[13c]

Western Blot Analysis. HeLa cells were incubated in the presence of test compounds and, after different times, were collected, centrifuged and washed two times with ice cold phosphate-buffered saline (PBS). The pellet was then resuspended in lysis buffer. After the cells were lysed on ice for 30 min, lysates were centrifuged at 15000 x g at 4 °C for 10 min. The protein concentration in

the supernatant was determined using BCA protein assay reagents (Pierce, Italy). Equal amounts of protein (20 μg) were resolved using sodium dodecyl sulfate polyacrylamide gel electrophoresis (SDS-PAGE) (7.5-15 % acrylamide gels) and transferred to PVDF Hybond-p membrane (GE Healthcare). Membranes were blocked with I-block (Tropix) the membrane being gently rotated overnight at 4 °C. Membranes were then incubated with primary antibodies against, Bcl-2, Bax, cleaved PARP, cleaved caspase-9, p-Cdc2^{Tyr15}, Cdc25c (Cell Signaling), caspase-3 (Alexis) , Cyclin B (Upstate) or β-actin (Sigma-Aldrich) for 2 hr at room temperature. Membranes were next incubated with peroxidase-labeled secondary antibodies for 60 min. All membranes were visualized using ECL Advance (GE Healthcare) and exposed to Hyperfilm MP (GE Healthcare). To ensure equal protein loading, each membrane was stripped and reprobed with anti-β-actin antibody.

Antitumor activity *in vivo.* 4 weeks old, Female BALB/c-nu nude mice (15–18g) were obtained from Shanghai SLAC Laboratory Animal Co.Ltd (Shanghai, China). The animals were maintained under specific pathogen-free conditions with food and water supplied ad libitum in Zhejiang University of Traditional Chinese Medicine Laboratory Animal Center. Human colon adenocarcinoma, HT-29 cells in the logarithmic growth phase, were resuspend in FBS-free RPMI 1640, at the cell concentration of 1×10^7cells/ mL, and inoculate (0.2 mL) in the hypodermis of the pars dorsalis of each mouse. Once the HT-29 xenografts reached a size of ~300 mm^3, eighteen mice were randomly assigned to three groups: Compound **4l** was prepared in DMSO and injected intraperitoneally at volumes of 0.01 ml/g body weight to give a dose of 100 mg/kg, respectively. The compound were administered three times a week for one week. After completing the treatment schedule, tumor-bearing mice were euthanized. Tumor volume was calculated by the formula: $V=\times(L \times W^2)/2$ where L is the length and W is the width of the tumor nodules measured by vernier caliper. The study was approved by the Institutional Animal Ethical Committee of the second affiliated hospital, school of medicine, Zhejiang University (PRC).

Statistical analysis. Unless indicated differently, the results are presented as mean ± S.E.M. The differences between different treatments were analysed,

using the two-sided Student's *t* test. P values lower than 0.05 were considered significant.

References

1. a) Downing, K.H. Structural basis for the interaction of tubulin with proteins and drugs that affect microtubule dynamics. *Annu. Rev. Cell. Dev. Biol.* **2000**, *16*, 89-111; b) Amos, L. A. Microtubule structure and its stabilisation. *Org. Biomol. Chem.* **2004**, *2*, 2153-2160; c) Honore, S.; Pasquier, E.; Braguer, D. Understanding microtubule dynamics for improved cancer therapy. *Cell. Mol. Life Sci.* **2005**, *62*, 3039-3056.

2. a) Risinger, A. L.; Giles, F. J.; Mooberry, S. L. Microtubule dynamics as a target in oncology. *Cancer Treat. Rev.* **2008**, *35*, 255-261; b) Kingston, D. G.; Tubulin-Interactive natural products as anticancer agents (1). *J. Nat. Prod.* **2009**, *72*, 507-515; c) Dumantet, C.; Jordan, M. A. Microtubule-binding agents: a dynamic field of cancer therapeutics. *Nat. Rev. Drug. Discov.* **2010**, *9*, 790-803; d) Kanthou, C.; Tozer, G. M. Microtubule depolymerizing vascular disrupting agents: novel therapeutic agents for oncology and other pathologies. *Int. J. Exp. Pathol.* **2009**, *90*, 284-294.

3. Pettit, G.R.; Singh, S.B.; Hamel, E.; Lin, C.M.; Alberts, D.S.; Garcia-Kendall, D. Isolation and structure of the strong cell growth and tubulin inhibitor combretastatin A-4. *Experentia* **1989**, *45*, 209-211.

4. Lin, C.M.; Ho, H.H.; Pettit, G.R.; Hamel, E. Antimitotic natural products combretastatin A-4 and combretastatin A-2: studies on the mechanism of their inhibition of the binding of colchicine to tubulin. *Biochemistry* **1989**, *28*, 6984-6991.

5. McGown, A. T.; Fox, B. W. Differential cytotoxicity of combretastatins A1 and A4 in two daunorubucin-resistant P388 cell lines. *Cancer Chemother. Pharmacol.* **1990**, *26*, 79-81.

6. a) Petit, I.; Karajannis, M. A.; Vincent, L.; Young, L.; Butler, J.; Hopper, A. T.; Shido, K.; Steller, H.; Chaplin, D. J.; Feldman, E.; Rafi, S. The microtubule-targeting agent CA4P regresses leukemic xenografts by disrupting interaction with vascular cells and mitochondrial-dependent cell death. *Blood* **2008**, *111*, 1951-1961; b) Siemann, D. W.; Chaplin, D. J.; Walike, P. A. A review and update of the current status of the vasculature-disabling agent combretastatin-A4 phosphate (CA4P). *Expert Opin. Investig. Drugs* **2009**, *18*, 189-197; c) Patterson, D. M.; Rustin, G. J. S. Combretastatin A-4 phosphate. *Drugs Future* **2007**, *32*, 1025-1032.

7. a) Tron, G.C.; Pirali, T.; Sorba, G.; Pagliai, F.; Busacca, S.; Genazzani, A. A. Medicinal chemistry of combretastatin A4: present and future directions. *J. Med. Chem.* **2006**, *49*, 3033-3044; b) Chaudari, A.; Pandeya, S. N.; Kumar, P.; Sharma, P. P.; Gupta, S.; Soni, N.; Verma, K. K.; Bhardwaj, G. Combretastain A-4 analogues as anticancer agents. *Mini Rev. Med. Chem.* **2007**, *12*, 1186–1205; c) Hsieh, H. P.; Liou, J. P.; Mahindroo, N. Pharmaceutical Design of Antimitotic Agents Based on Combretastatins. *Curr. Pharm. Des.* **2005**, *11*, 1655-1677; d) Mahindroo, N; Liou, J.P.; Chang, J.Y.; Hsieh, H.P. Antitubulin agents for the treatment of cancer. A medicinal chemistry update. *Exp. Opin. Ther. Pat.* **2006**, *16*, 647-691.

8. Theeramunkong, S.; Caldarelli, A.; Massarotti, A.; Aprile, S.; Caprifoglio, D.; Zaninetti, R.; Teruggi, A.; Pirali, T.; Grosa, G.; Tron, G. C.; Genazzani, A. A. Regioselective Suzuki coupling of dihaloheteroaromatic compounds as a rapid strategy to synthesize potent rigid combretastatin analogues. *J. Med. Chem.* **2011**, *54*, 4977-4986.

9. a) Ohsumi, K.; Hatanaka, T.; Fujita, K.; Nakagawa, R.; Fukuda, Y.; Nihai, Y.; Suga, Y.; Morinaga, Y.; Akiyama, Y.; Tsuji, T. Synthesis and antitumor activity of cis-restricted combretastatins 5-membered heterocyclic analogues. *Bioorg. Med. Chem. Lett.* **1988**,

8, 3153-3158; b) Wang, L.; Woods, K. W.; Li, Q.; Barr, K. J.; McCroskey, R. W.; Hannick, S. M.; Gherke, L.; Credo, R. B.; Hui, Y.-H.; Marsh, K.; Warner, R.; Lee, J. Y.; Zielinski-Mozng, N.; Frost, D.; Rosenberg, S. H.; Sham, H. L. Potent, orally active heterocycle-based combretastatin A-4 analogues: synthesis, structure-activity relationship, pharmaokinetics, and in vivo antitumor activity evaluation. *J. Med. Chem.* **2002**, *45*, 1697-1711.

10. a) Bonezzi, K.; Taraboletti, G.; Borsotti, P.; Bellina, F.; Rossi, R.; Gavazzi, R. Vascular disrupting activity of tubulin-binding 1,5-diaryl-1H-imidazoles. *J. Med. Chem.* **2009**, *52*, 7906-7910; b) Schobert, R.; Biersack, B.; Dietrich, A.; Effenberger, K.; Knauer, S.; Mueller, T. 4-(3-Halo/amino-4,5-dimethoxyphenyl)-5-aryloxazoles and N-methylimidazoles that are cytotoxic against combretastatin A resistant tumor cels and vascular disrupting in a cis platin resistant germ cell tumor model. *J.Med. Chem.* **2010**, *53*, 6595-6002.

11. a) Kaffy, J.; Pontikis, R.; Carrez, D.; Croisy, A.; Monneret, C.; Florent, J.-C. Isoxazole-type derivatives related to combretastatin A-4, synthesis and biological evaluation. *Bioorg. Med. Chem.* **2006**, *14*, 4067-4077; b) Lee, S.; Kim, J. N.; Lee, H. K.; Yoon, K. S.; Shin, K. D.; Kwon, B.-M.; Han, D. C. Biological evaluation of KRIBB3 analogs as a microtubule polymerization inhibitor. *Bioorg. Med. Chem. Lett.* **201**1, *21*, 977-979.

12. Wu, M.; Li, W.; Yang, C.; Chen, D.; Ding, J.; Chen, Y.; Lin, L.; Xie, Y. Synthesis and activity of combretastatin A-4 analogues: 1,2,3-thiadiazoles as potent antitumor agents. *Bioorg. Med. Chem. Lett.* **2007**, *17*, 869-873.

13. a) Odlo, K.; Hntzen, J.; Fournier dit Chabert, J.; Ducki, S.; Gani, O. A. B. S. M.; Sylte, I. Skrede, M.; Florenes, V. A.; Hansen, T. V. 1,5-Disubstituted 1,2,3-triazoles as cis-restricted analogues of combretastatin A-4: synthesis, molecular modeling and evaluation as cytotoxic agents and inhibitors of tubulin. *Bioorg. Med. Chem.* **2008**, *16*, 4829-4838; b) Zhang, Q.; Peng, Y.; Wang, X. I.; Keeman, S. M.; Aurora. S.; Welsh, W. J. Highly potent triazole-based tubulin polymerization inhibitors. *J. Med. Chem.* **2007**, *50*, 749-754; c) Romagnoli, R.; Baraldi, P. G.; Cruz-Lopez, O.; Lopez-Cara, C.; Carrion, M. D.; Brancale, A.; Hamel, E.; Chen, L.; Bortolozzi, R.; Basso, G.; Viola, G. Synthesis and antitumor activity of 1,5-disubstituted 1,2,4-triazoles as cis-restricted combretastatin analogs, *J. Med. Chem.* **2010**, *53*, 4248-4258.

14. Only one analogue with a tetrazole ring, corresponding to 1-(3,4,5-trimethoxyphenyl)-5-(4-methoxy, 3-aminophenyl)-1*H*-tetrazole has been reported by Otsumi et al. (reference 9a). This compound showed potent antitubulinic activity (IC_{50}=2 M) as well as cytotoxicty (IC_{50}=7.2 nM) against the colon 26 murine tumor cell line.

15. a) Cushman, M.; Nagarathnam, D.; Gopal, D.; He, H.-M.; Lin, C. M.; Hamel, E. Synthesis and evaluation of analogues of (z)-1-(4-methoxyphenyl)-2-(3,4,5-trimethoxyphenyl)ethene as potential cytotoxic and antimitotic agents. *J. Med. Chem.* **1992**, *35*, 2293-2306; b) Gaukroger, K.; Hadfield, J. A.; Lawrence, N. J.; Nlan, S.; McGown, A. T. Structural requirements for the interaction of combretastatins with tubulin: how important is the trimethoxy unit? *Org. Biomol. Chem.* **2003**, *1*, 3033-3037.

16. For compound **7a** see: Potewar, T. M.; Siddiqui, S. A.; Lahoti, R. J.; Srinivasan, K. V. Efficient and rapid synthesis of 1-substituted-1H-1,2,3,4-tetrazoles in the acidic ionic liquid 1-n-butylimidazolium tetrafluoroborate. *Tetrahedron Lett.* **2007**, *48*, 1721-1724. For compound **7b** see: Vorobiov, A. N.; Gaponik, P. N.; Petrov, P. T.; Ivashkevich, O. A. One-pot syntheses of 5-amino-1-aryltetrazole derivatives. *Synthesis*, **2010**, 1307-1312.

17. Satoh, Y.; Marcopulos, N. Application of 5-lithiotetrazoles in organic synthesis. *Tetrahedron Lett.* **1995**, *36*, 1679-1682.

18. Yi, K. Y.; Yoo, S. Synthesis of 5-aryl and vinyl tetrazoles by the palladium-catalyzed cross-coupling reaction. *Tetrahedron Lett.* **1995**, *36*, 1679-1682.

19. Spulak, M.; Lubojacky, R.; Senel, P.; Kunes, J.; Pour, M. Direct C-H arylation and alkenylation of 1-substituted tetrazoles: phosphine as stabilizing factor. *J. Org. Chem.* **2010**, *75*, 241-244.

20. a) Hamel, E. Evaluation of antimitotic agents by quantitative comparisons of their effects on the polymerization of purified tubulin. *Cell Biochem. Biophys.* **2003**, *38*, 1-21; b) Verdier-Pinard, P.; Lai J.-Y.; Yoo, H.-D.; Yu, J.; Marquez, B.; Nagle D.G.; Nambu, M.; White, J.D.; Falck, J.R.; Gerwick, W.H.; Day, B.W.; Hamel, E. Structure-activity analysis of the interaction of curacin A, the potent colchicine site antimitotic agent, with tubulin and effects of analogs on the growth of MCF-7 breast cancer cells. *Mol. Pharmacol.* **1998**, *53*, 62-67.

21. Szakács, G.; Paterson, J.K.; Ludwig, J.A.; Booth-Genthe, C.; Gottesman, M.M. Targeting multidrug resistance in cancer *Nat. Rev. Drug Discov*. **2006**, 5, 219-234.

22. Baguley B.C. Multidrug resistance mechanism in cancer *Mol. Biotechnol.* **2010**, *46*, 308-316.

23. Dupuis, M.; Flego, M.; Molinari, A.; Cianfriglia, M. Saquinavir induces stable and functional expression of the multidrug transporter P-glycoprotein in human CD4 T-lymphoblastoid CEM rev cells. *HIV Medicine* **2003,** *4*, 338–345.

24. Toffoli, G.; Viel, A.; Tuimoto, I.; Bisconti, G.; Rossi, G.; Baoiocchi, M. Pleiotropic-resistant phenotype is a multifactorial phenomenon in human colon carcinoma cell lines. *Br. J. Cancer* **1991**, *63*, 51–56.

25. Martello, L.A.; Verdier-Pinard, P.; Shen, H. J.; He, L.; Torres, K.; Orr, G. A.; Horwitz, S. B. Elevated level of microtubule destabilizing factors in a taxol-resistant/ dependent A549 cell line with an alpha-tubulin mutation *Cancer Res.* **2003**, *63*, 448-454.

26. P.R. Clarke, L. A. Allan. Cell-cycle control in the face of damage- a matter of life or death. *Trends Cell Biol.* **2009**, *19*, 89-98.

27. Donzelli, M., Draetta, GF. Regulating mammalian checkpoints through Cdc25 inactivation. *EMBO Rep.* **2003**, *4*,671-677.

28. Kiyokawa H., Ray, D. In vivo roles of Cdc25 phosphatases: biological insight into the anti-cancer therapeutic targets. *Anticancer Agents Med Chem*. **2008**,*8,* 832-836.

29. Vermes, I.; Haanen, C.; Steffens-Nakken, H.; Reutelingsperger, C. A novel assay for apoptosis. Flow cytometric detection of phosphatidylserine expression on early apoptotic cells using fluorescein labelled annexin V. *J. Immunol. Methods* **1995**, *184*, 39–51.

30. a) Ly, J.D., Grubb D.R., Lawen A. The mitochondrial membrane potential ($\Delta\Psi_m$) in apoptosis: an update. *Apoptosis* **2003,** 3, 115-128; b) Green, D. R.; Kroemer, G. The pathophysiology of mitochondrial cell death. *Science* **2005**, *305*, 626–629.

31. Cai, J.; Jones, D. P. Superoxide in apoptosis. Mitochondrial generation triggered by cytochrome *c* loss. *J. Biol. Chem.* **1998**, *273*,11401-11404.

32. a) Rothe, G.; Valet, G. Flow cytometric analysis of respiratory burst activity in phagocytes with hydroethidine and 2′,7′-dichlorofluorescein. *J. Leukocyte Biol.* **1990**, *47*, 440–448; b) Nohl, H.; Gille, L.; Staniek, K. Intracellular generation of reactive oxygen species by mitochondria. *Biochem. Pharmacol.* **2005**, *69*, 719-723.

33. J.-B. Denault, G. S. Salvesen. Caspases: keys in the ignition of cell death. *Chem. Rev.* **2002**, *102*, 4489-4499.

34. A. G. Porter, R.U. Janicke, Emerging role of caspase-3 in apoptosis. *Cell Death Differ.* **1999**, 6, 99-104.

35. Mollinedo, F.; Gajate, C. Microtubules, microtubule-interfering agents and apoptosis. *Apoptosis* **2003**, 8:413-450.

36. Viola, G.; Fortunato, E.; Cecconet, L.; Del Giudice, L., Dall'Acqua, F.; Basso, G. Central role of mitochondria and p53 in PUVA-induced apoptosis in human keratinocytes cell line NCTC-2544. *Toxicol. Appl. Pharm.* **2008**, *227*, 84-96.

37. Ravelli, R. B. G.; Gigant, B.; Curmi, P. A.; Jourdain, I.; Lachkar, S.; Sobel, A.; Knossow,

M. Insight into tubulin regulation from a complex with colchicine and a stathmin-like domain. *Nature* **2004**, *428*, 198-202.

38. Molecular Operating Environment (MOE 2008.10). Chemical Computing Group, Inc. Montreal, Quebec, Canada. http://www.chemcomp.com.

39. Korb, O.; Stützle, T.; Exner, T. E. PLANTS: Application of ant colony optimization to structure-based drug design. In *Ant Colony Optimization and Swarm Intelligence*, 5th International Workshop, ANTS 2006, Brussels, Belgium, Sep 4−7, 2006; Dorigo, M.; Gambardella, L. M.; Birattari, M.; Martinoli, A.; Poli, R.; Sttzle, T., Eds.; Springer: Berlin, **2006**; LNCS 4150, pp 247− 258.

5. PYRROLOQUINOLINONES DERIVATIVES

Synthesis and in vitro evaluation of 3h-pyrrolo[3,2-f]-quinolin-9-one derivatives that show potent and selective antileukemic activity. Ferlin MG, Bortolozzi R, Brun P, Castagliuolo I, Hamel E, Basso G, Viola G. **ChemMedChem. 2010 Aug 2;5(8):1373-85.**[22]

***MG-2477, a new tubulin inhibitor induces autophagy through inhibition of the Akt/mTOR pathway and delayed apoptosis in A549 cells*.** Viola G, Bortolozzi R, Hamel E, Moro S, Brun P, Castagliuolo I, Ferlin MG, Basso G. **Biochem Pharmacol. 2012 Jan 1;83(1):16-26.**[23]

5.1. Synthesis and in *vitro* biological evaluation of some 3*H*-pyrrolo[3,2-*f*]quinolin-9-one derivatives, showing potent and selective antileukemic activity.

Maria Grazia Ferlin[§], Roberta Bortolozzi[¥], Paola Brun[±], Ignazio Castagliuolo[±], Ernest Hamel[#], Giuseppe Basso[¥], Giampietro Viola[¥]

[§]*Department of Pharmaceutical Sciences*

[¥]*Department of Pediatrics, Laboratory of Oncohematology, University of Padova, Italy*

[±]*Department of Histology, Microbiology and Medical Biotechnologies, University of Padova, Italy*

[#]*Screening Technologies Branch, Developmental Therapeutics Program, Division of Cancer Treatment and Diagnosis, National Cancer Institute at Frederick, National Institutes of Health, Frederick, Maryland 21702, USA*

Abstract

A series of new substituted 7-phenyl-3*H*-pyrrolo[3,2-*f*]quinolin-9-ones were synthesized and evaluated for their antiproliferative activity. The most active derivatives showed high selectivity against human leukemia cell lines and potently inhibited their growth, with nM GI_{50} values. The active compounds strongly inhibited tubulin assembly and colchicine binding to tubulin. Their activities were equal to or greater than that of the reference compound combretastatin A-4 (CA-4). Flow cytometry studies showed that Jurkat cells treated with the most active compounds **11** and **12** were arrested in the G2/M phase of the cell cycle in a concentration-dependent manner. This effect was associated with apoptosis of the cells, mitochondrial depolarization, generation of reactive oxygen species, activation of caspase-3 and cleavage of the enzyme polyADP-ribose polymerase.

Introduction

For several years we have studied the pyrroloquinoline nucleus as a promising scaffold for antiproliferative agents,[1-3] leading to the discovery of the 3*H*-pyrrolo[3,2-*f*]quinoline (PyQ) scaffold (Figure 1) as the most promising framework for the design of potent anticancer compounds. In particular, we found several active agents with *N*-pyrrole alkyl substituents that were derivatives of 7-phenyl-3*H*-pyrrolo[3,2-*f*]quinolin-9-one (7-PPyQs).[3] We showed that 7-PPyQs exhibited strong cytotoxic activity against a wide panel of human tumor cell lines, including MDR-positive cancer cells. Moreover, *in vivo* the 7-PpyQs exhibited significant inhibition of tumor growth (83%) in a syngenic hepatocellular carcinoma model in Balb/c mice.[2]

Structure-activity relationship (SAR) studies of various series of pyrroloquinoline derivatives allowed us to establish some structural features crucial for antitumor activity. First, the [3,2-*f*] angular geometry is essential for significant activity, as is the carbonyl group at the 9 position and the side phenyl ring. Moreover, optimal activity requires the presence of an *N*-alkyl group on the pyrrole ring. Although active compounds had substituents ranging from ethyl to *n*-pentyl groups, as well as a cyclopropylmethyl group, ionizable groups, such as dimethylaminoethyl at position N-3 or oxygen-containing substituents at positions C-2 and C-4, caused severe loss of activity. Since previously synthesized compounds[3] had caused cells to arrest in the G2/M phase of the cell cycle, we suspected that these compounds interacted with tubulin, possibly at the colchicine site. Thus, the SAR observations suggested the presence of a deep hydrophobic pocket near the colchicine site.[3] Substituents on the phenyl ring at C-7, either electron-withdrawing or releasing groups, had only minor effects on activity.

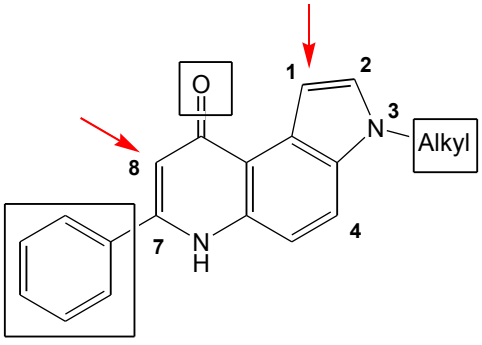

Figure 1. 3*H*-pyrrolo[3,2-*f*]quinolin-9(6*H*)-ones, SARs are described in the text

In an effort to produce additional highly active analogues, we synthesized and evaluated the effects of substitutions at other positions of the 3H-pyrrolo[3,2-*f*]quinolin-9-one nucleus. We describe here 3*H*-PyQ derivatives with small substituents at the C-1 position and with the side phenyl ring shifted from C-7 to C-8. Not only was the simple 8-phenyl-PyQ **30** prepared, but also substituents were introduced onto template **30** to examine their effects on bioactivity. We also focused on making molecules more water soluble in comparison with previous analogues, by inserting suitable substituents at the 1, 3 and 7 positions.[3] Such compounds should be of value for *in vivo* studies on pharmacokinetics, metabolism and toxicity.

The newly prepared agents were assayed for their *in vitro* cytotoxicity against a panel of human solid tumors and leukemic cell lines. The most active compounds were confirmed to be inhibitors of tubulin assembly binding at the colchicine site and were found to have major effects on cell cycle distribution and induction of cellular apoptosis.

Chemistry

The new PPyQs were synthetized as shown in Schemes 1-3.

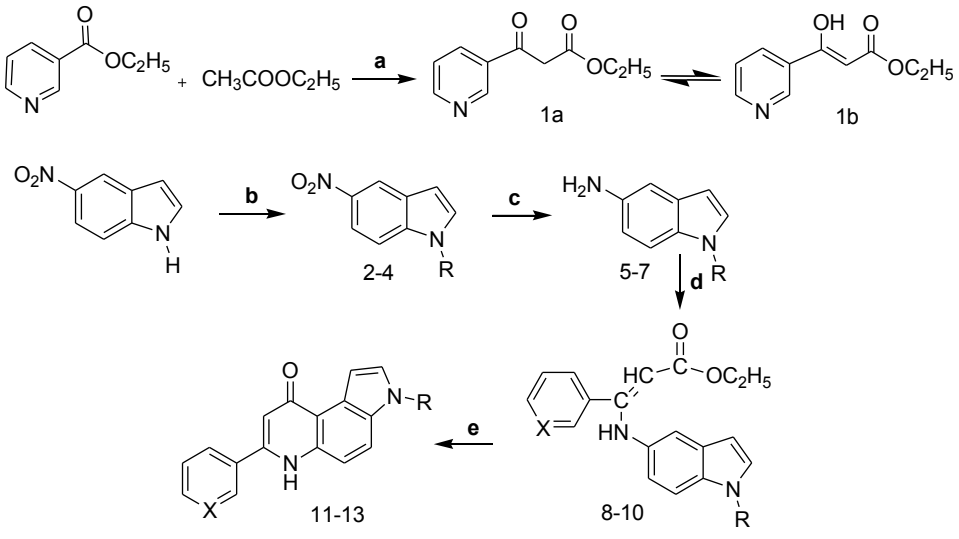

Compds	R	X
2, 5, 8, 11	$-(CH_2)_2-COOC_2H_5$	C
3, 6, 9, 12	$-CH_2$-phenyl$(OCH_3)_3$	C
4, 7, 10, 13	$-C_2H_5$	N

Reagents and conditions:
a) potassium *tert*-butoxide, benzene, 80°C; b) NaH, DMF, 70°C; c) H_2, Pd/C 10%, ethanol; d) ethyl benzoylacetate or 1a, ethanol, drierite, reflux; e) diphenyl ether, reflux

Scheme 1. Synthesis of pyrroloquinolinone derivatives **11-13**

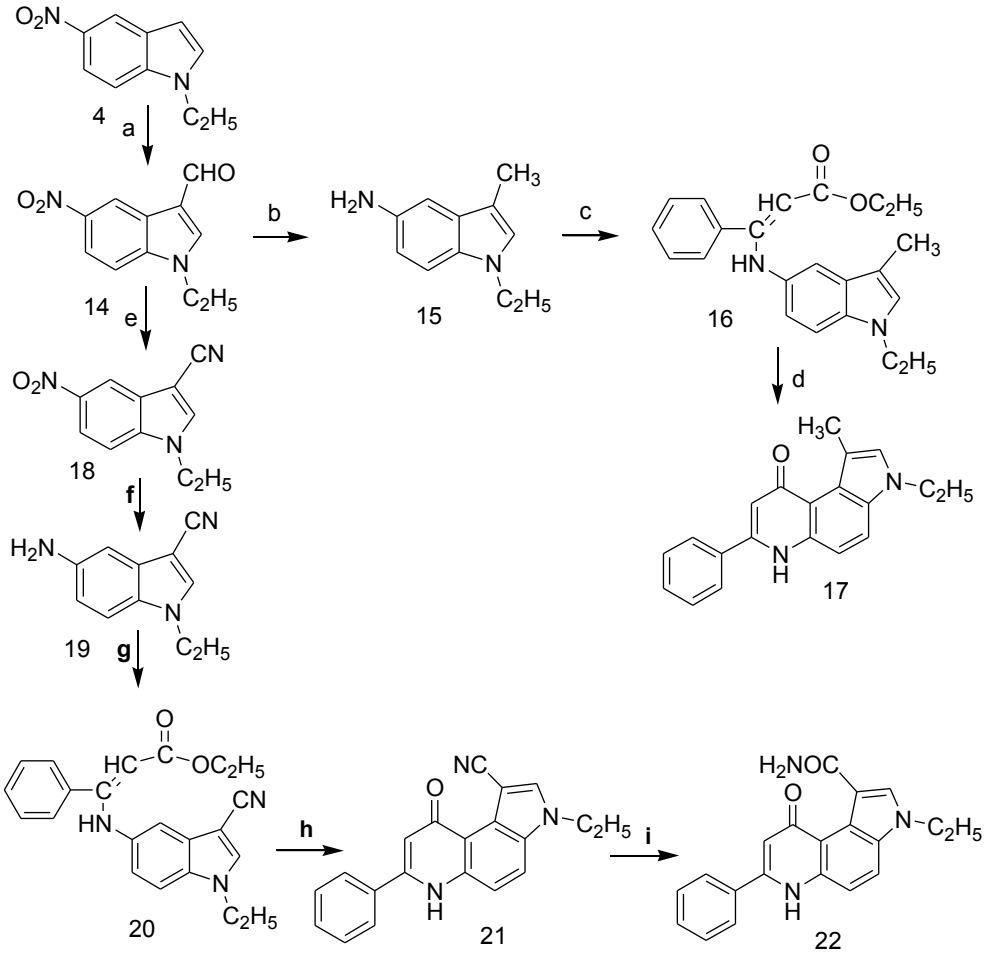

Reagents and conditions:
a) $POCl_3$, DMF, reflux; b) and f) H_2, PD/C, ethyl acetate, 40°C; c) and g) ethyl benzoylacetate, ethanol, drierite, reflux; d) and h) diphenyl ether, reflux; e) NH_2OH HCl, pyridine, SeO_2, Na_2SO_4, DMF; i) CH_3COOH/H_2SO_4,H_2O, reflux

Scheme 2. Synthesis of 7-phenyl-pyrroloquinolinone derivatives **17**, **21** and **22**.

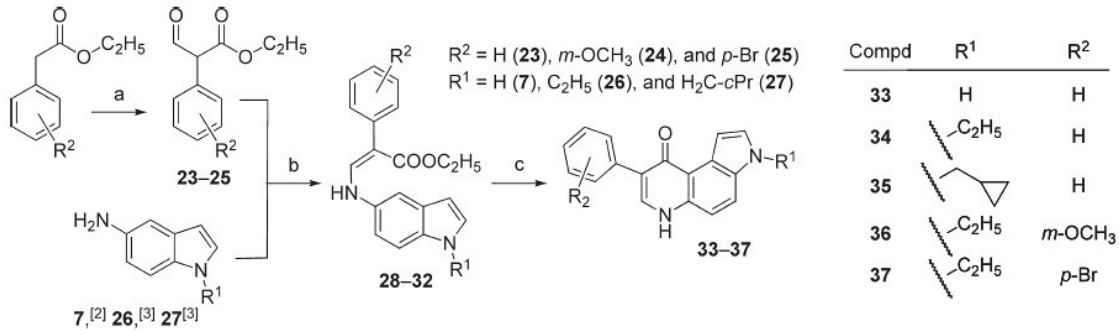

Compd	R^1	R^2
33	H	H
34	C_2H_5	H
35		H
36	C_2H_5	*m*-OCH_3
37	C_2H_5	*p*-Br

Scheme 3. Synthesis of 8-phenyl-pyrroloquinolinone derivatives **33-37**.

The detailed procedure of synthesis of pyrroloquinolinone derivatives is described on the full work published on ChemMedChem (2010 Aug 2).

Results and discussion

***In vitro* antiproliferative activities.** These new synthetics were evaluated for their *in vitro* antiproliferative activity against a panel of human tumor cell lines, including both solid and leukemic lines. The previously described[3] 3-ethyl-7-PPyQ (**38**) was used as a reference compound (Chart 1).

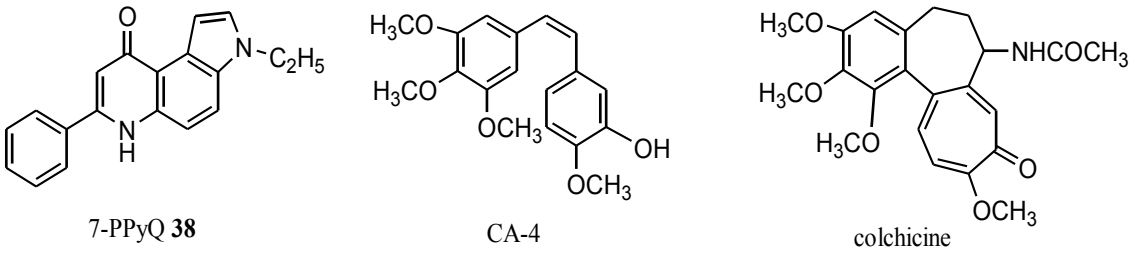

7-PPyQ **38** CA-4 colchicine

Chart 1. Structures of compounds **38**[3]**, CA-4** and **colchicine** taken as references in the assays of antiproliferative activity, inhibition of tubulin polymerization and colchicine binding, respectively.

After 72 h of continuous drug exposure, the concentration required for 50% growth inhibition (GI_{50}) was determined by the MTT colorimetric assay (Table 1).

Compd	GI_{50} (μM)										
	HT-29	ARO	Hep G2	IGROV	MCF-7	HeLa	HL-60	ML2	K562	RS 4;11	Jurkat
11	0.48 ±0.08	0.55 ±0.15	0.52 ±0.10	0.62 ±0.15	0.58 ±0.18	0.45 ±.10	0.002 ±0.0001	0.005 ±0.002	0.19 ±0.06	0.002 ±0.0004	0.0005 ±0.00001
12	0.45 ±0.10	0.58 ±0.15	0.95 ±0.15	0.85 ±0.20	1.40 ±0.50	0.40 ±0.05	0.002 ±0.0001	0.01 ±0.002	0.03 ±0.007	0.001 ±0.0001	0.003 ±0.0001
13	0.85 ±0.14	0.45 ±0.07	0.50 ±0.05	0.65 ±0.15	0.85 ±0,15	0.40 ±0.05	0.03 ±0.002	0.3 ±0.04	0.24 ±0.03	0.04 ±0.007	0.05 ±0.004
17	>50	>50	5.8±1.1	>50	>50	4.5 ±0.8	17.5 ±2.3	14.4 ±2.3	27.3 ±0.34	6.5 ±1.0	8.0 ±1.2
21	>50	>50	>50	>50	>50	>50	0.21 ±0.01	0.55 ±0.03	0.46 ±0.008	0.13 ±0.02	0.3 ±0.01
22	>50	>50	>50	>50	>50	>50	0.32 ±0.03	0.09 ±0.02	1.7 ±0.5	0.03 ±0.002	0.05 ±0.006
33	>50	>50	>50	n.d.	n.d.	>50	>50	>50	>50	n.d.	n.d.
34	>50	>50	>50	n.d.	n.d.	>50	>50	>50	>50	n.d.	n.d.
35	>50	>50	>50	n.d.	n.d.	>50	>50	>50	>50	n.d.	n.d.
36	>50	>50	>50	n.d.	n.d.	>50	>50	>50	>50	n.d.	n.d.
37	>50	>50	>50	n.d.	n.d.	>50	>50	>50	>50	n.d.	n.d.
38 [3]	0.03 ±0.01	0.03 ±0.01	0.05 ±0.01	0.06 ±0.01	0.04 ±0.01	0.01 ±0.008	0.0005 ±0.00002	0.001 0.0003±	0.001 ±0.0001	0.002 ±0.0003	0.0005 ±0.00002

[a]GI_{50}= compound concentration required to inhibit tumor cell proliferation by 50%. Data are expressed as the mean ± SE from the dose-response curves of at least three independent experiments. n.d. not determined. See text for details of the cell lines examined. The first six lines are derived from human solid tumors, the last five from human leukemias.

Table1. In vitro inhibitory effects on cell proliferation by compounds **11-13, 17, 20, 21, 33-37** and **38**

Of the compounds listed, the reference compound **38** showed nM and sub-nM GI_{50} values in all cell lines tested, while its regioisomer 3-ethyl-8-PpyQ **34** was inactive (GI_{50}'s>50 μM), as were the other 8-PPyQ derivatives, **33** and **35-37**. Clearly, either removing the side phenyl from position 7 or placing it at the 8 position of the tricycle nucleus was very deleterious for activity. Three of the new 7-PPyQ compounds, **11**-**13**, were active in all lines, while an additional three (**17**, **21** and **22**) had moderate activity only in the leukemic lines. In fact, compound **38** had GI_{50} values 10-100-fold lower for leukemia cells (GI_{50}'s 0.5-2 nM) in comparison with the solid tumor cells (GI_{50}'s, 0.01-0.06 μM). This difference was even more marked with the two most active new compounds, **11** and **12**, where the GI_{50}'s for the leukemia cells were 0.5-10 nM and for the solid tumor cells, 0.4-1.4 μM. Both of these compounds had more hydrophilic *N*-alkyl side chains than other 7-PPyQs.

Regarding the three compounds bearing a substituent at the 1 position, **21** and **22,** with cyano and carboxyamide groups, respectively, were completely inactive (GI_{50}'s>50 μM) in the solid tumor cells, but they showed activity at sub-μM concentrations in the leukemia lines. Compound **17**, with a lipophilic methyl group, had only modest activity in the leukemia and HeLa cells. We conclude that a substituent at the 1 position does not eliminate antiproliferative activity, as did substituents at position 2.[2] This finding indicated that suitable substituents at the 1 position of 7-PPyQs might result in compounds with high selectivity for leukemic diseases.

Finally, compound **13,** having a pyridine ring in place of the side phenyl and an ethyl group in the N-3 position like **38**, had somewhat less selectivity towards the leukemic lines in comparison with **38**, **11**-**12, 17**, and **21**-**22**.

Inhibition of tubulin polymerization and colchicine binding. In a previous study,[3] we had found that compound **38** and a number of other 7-PpyQs caused cells to arrest at the G2/M phase of the cell cycle. This finding suggests that the target of these agents is likely to be tubulin, as this is a universal observation in cells treated with antitubulin agents. To determine whether this was true, the most active compounds from the current series (**11, 12, 13,** and **22**), together with an active agent from the earlier studies (**38**), were evaluated for their *in vitro* inhibition of tubulin polymerization and for their inhibitory effects on the

binding of [^{3}H]colchicine to tubulin (Table 2).[8,9] For comparison, combretastatin A-4 (CA-4) was examined in contemporaneous experiments.

Compound	Tubulin assembly[a] IC_{50}±SD (μM)	Colchicine binding [b] % inhibition±SD 1 μM 5 μM 50 μM inhibitor
11	0.75±0.04	44±6 75±4 N.d.
12	1.4±0.2	N.d. 30±4 56±2
13	2.4±0.4	N.d. 23±6 65±0.3
22	>40	N.d.
38	0.57±0.02	34±2 73±0.7 N.d.
CA-4	1.2±0.01	84±3 98±0.3 N.d.

[a] Inhibition of tubulin polymerization. Tubulin was at 10 μM.
[b] Inhibition of [^{3}H]colchicine binding. Tubulin and colchicine at 1 and 5 μM, respectively. The tested compounds were at 1, 5 or 50 μM, as indicated. N.d.=not determined.

Table 2. Inhibition of tubulin polymerization and colchicine binding by compounds **11**, **12, 13, 22**, **38**, and **CA-4**

In the assembly assay, compound **11** was found to be the most active (IC_{50}=0.75 μM), and it was almost twice as potent as CA-4 (IC_{50}=1.2 μM). Compound **38** was also more inhibitory than CA-4, while **12** and **13** were less inhibitory than CA-4. Compound **22** showed only minimal inhibitory activity, with less than 50% inhibition of tubulin assembly at the highest concentration (40 μM) examined. These effects on tubulin assembly were in good agreement with the relative antiproliferative activities of the compounds.

In the colchicine binding studies, compounds **11** and **38** were about equally active, but they were less potent than CA-4 despite their greater potency as inhibitors of assembly. Such differences are not infrequently observed, and CA-4 is a particularly potent inhibitor of colchicine binding.[9] Compounds **12** and **13** were much less active as inhibitors of colchicine binding than were CA-4, **11** and **39**, with convincing inhibition only observed when the inhibitor concentration was increased to 50 μM, 10-fold higher than the concentration of [^{3}H]colchicine in the reaction mixtures.

Analysis of cell cycle. The effects of different concentrations of compounds **11, 12, 13** and **22** on cell cycle progression were examined with Jurkat T-leukemia cells (Figure 2). Untreated Jurkat cells showed a classical pattern of proliferating cells, with large numbers of cells in the G1 (47.2%) and S (43.4%) phases and fewer cells in the G2/M (9.4%) phase. As in our earlier study,[3] the

two most active compounds (**11** and **12**) showed a clear G2/M arrest pattern in a concentration-dependent manner, with a concomitant decrease of cells in the other phases of the cell cycle after 24 h of treatment. In particular, as shown in Figure 2, the G2/M cell population increased from 9.4% in the control to 77% with 0.06 μM compound **11**. The G1 cells decreased from 47% in the control to 3%, while the S phase cells decreased from 43 to 20%. A similar behavior was observed for compound **12**, but a comparable arrest (65%) in G2/M phase required 0.25 μM compound **12**. The other two compounds (**13** and **22**) induced a G2/M arrest only at still higher concentrations, in good agreement with their lower potency in the tubulin polymerization assay and their lower antiproliferative activity. Further experiments showed that the accumulation of mitotic cells occurred in a time-dependent manner associated with the appearance of a hypodiploid peak (sub-G1) indicative of apoptosis (data not shown). This observation prompted us to investigate the possible activation of apoptotic mechanisms in the presence of the most active derivatives.

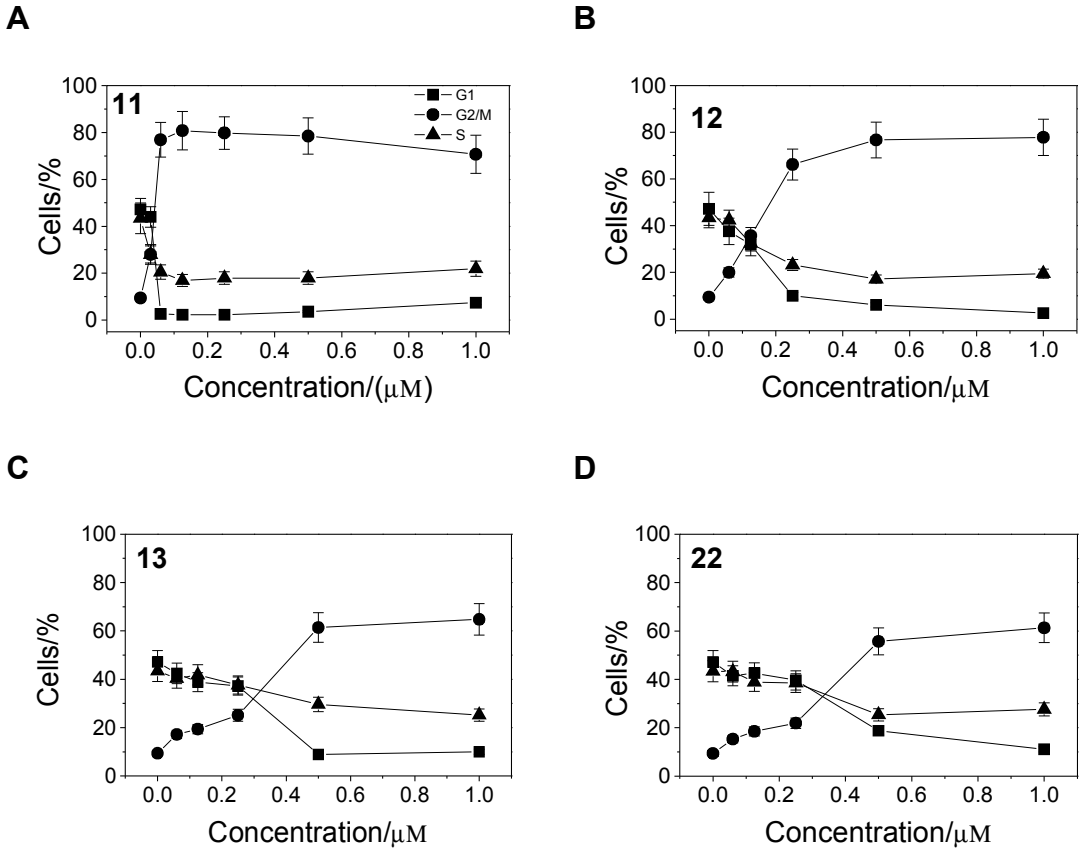

Figure 2. Effects of compounds **11, 12, 13** and **22** on cell cycle distribution and G2/M arrest in Jurkat cells after 24 h of incubation. Cells were treated with different concentrations (0.015 to 1.0 mM) of the test compounds. Then the cells were fixed and stained with propidium iodide (PI) to analyze DNA content by flow cytometry. The data are expressed as mean ± S.E.M. for 2 independent experiments.

Loss of plasma membrane asymmetry during apoptosis. To better characterize drug-induced apoptosis, we performed a biparametric cytofluorimetric analysis using PI and AnnexinV-FITC, which stain DNA and phosphatidylserine (PS) residues, respectively.[10,11] Annexin-V is a Ca^{2+}-dependent phospholipid binding protein with high affinity for PS. Annexin-V staining precedes the loss of membrane integrity that accompanies the final stages of cell death resulting from either apoptotic or necrotic processes. Because the externalization of PS occurs in the earlier stages of apoptosis, annexin-V staining identifies apoptosis at an earlier stage than the appearance of sub-G1 cells. Such cells represent a later stage of cell death involving nuclear changes such as DNA fragmentation.

After drug treatment with different concentrations and for different times, Jurkat cells were labeled with the two dyes, and the resulting red (PI) and green (FITC) fluorescence was monitored by flow cytometry. Compounds 11 and 12 provoked a remarkable induction of apoptotic cells after 24 h of treatment, while the less active compounds 13 and 22 showed a lower efficacy (Figure 3). The percentage of annexin-V positive cells increased further at 48 h. These findings prompted us to further investigate the apoptotic machinery after treatment with compounds 11 and 12.

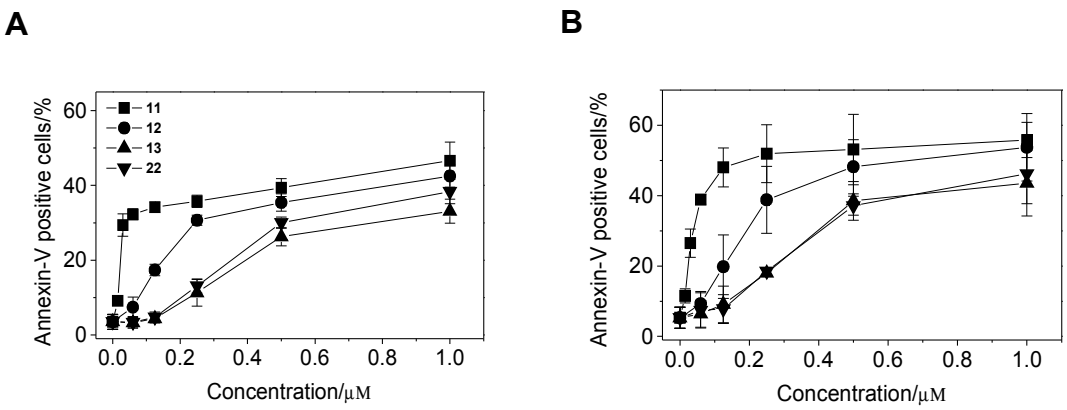

Figure 3. Flow cytometric analysis of apoptotic cells after treatment of Jurkat cells with compounds **11, 12, 13** or **22**. After 24 h (Panel A) and 48 h (panel B) of treatment cell were harvested and labeled with annexin-V-FITC and PI and then analyzed by flow cytometry. The data are expressed as mean of percentage of annexin-V positive cells ± S.E.M. for 3 independent experiments.

Apoptosis is mediated by mitochondrial depolarization. Mitochondria play an essential role in the propagation of apoptosis.[12,13] It is well established that,

at an early stage, apoptotic stimuli alter the mitochondrial transmembrane potential $\Delta\psi_{mt}$. $\Delta\psi_{mt}$ was monitored by the fluorescence of the dye JC-1.[14] In the presence of normal cells (high $\Delta\psi_{mt}$), JC-1 forms fluorescent red (590 nm) aggregates locally and spontaneously that are associated with a large shift in the emission, while, when the mitochondrial membrane is depolarized (low $\Delta\psi_{mt}$), JC-1 forms monomers that emit at 530 nm. Treated Jurkat cells in the presence of derivatives 11 and 12 (0.5 and 0.1 μM) exhibited a significant increase in the percentage of cells with low $\Delta\psi_{mt}$ in a concentration- and time-dependent manner compared with the control cells, indicating depolarization of mitochondrial membrane potential (Figure 4, panels A). The disruption of $\Delta\psi_{mt}$ is associated with the appearance of annexin-V positivity in the treated cells when they are in early apoptotic stage. In fact, the dissipation of $\Delta\psi_{mt}$ is characteristic of apoptosis and has been observed with both microtubule destabilizing and stabilizing agents in various cell types.[15]

Mitochondrial generation of reactive oxygen species (ROS). Mitochondrial membrane depolarization is associated with mitochondrial production of ROS.[16] Therefore, we investigated whether ROS production increased after treatment with compounds 11 and 12. We utilized the fluorescence indicator hydroethidine (HE), whose fluorescence appears if reactive oxygen species are generated.[17,18] HE is oxidized by superoxide anion into ethidium ion, which emits red fluorescence. Superoxide is produced by mitochondria due to a shift from the normal 4-electron reduction of O_2 to a 1-electron reduction when cytochrome c is released from mitochondria. ROS generation was also measured with the dye 2,7-dichlorodihydrofluorescein diacetate (H_2DCFDA) which is oxidized to the fluorescent compound dichlorofluorescein (DCF) by a variety of peroxides including hydrogen peroxide.[18] As shown in Figure 4 (panels B and C), compounds 11 and 12, as expected, induced the production of ROS in comparison with control cells, in agreement with the dissipation of $\Delta\psi_{mt}$.

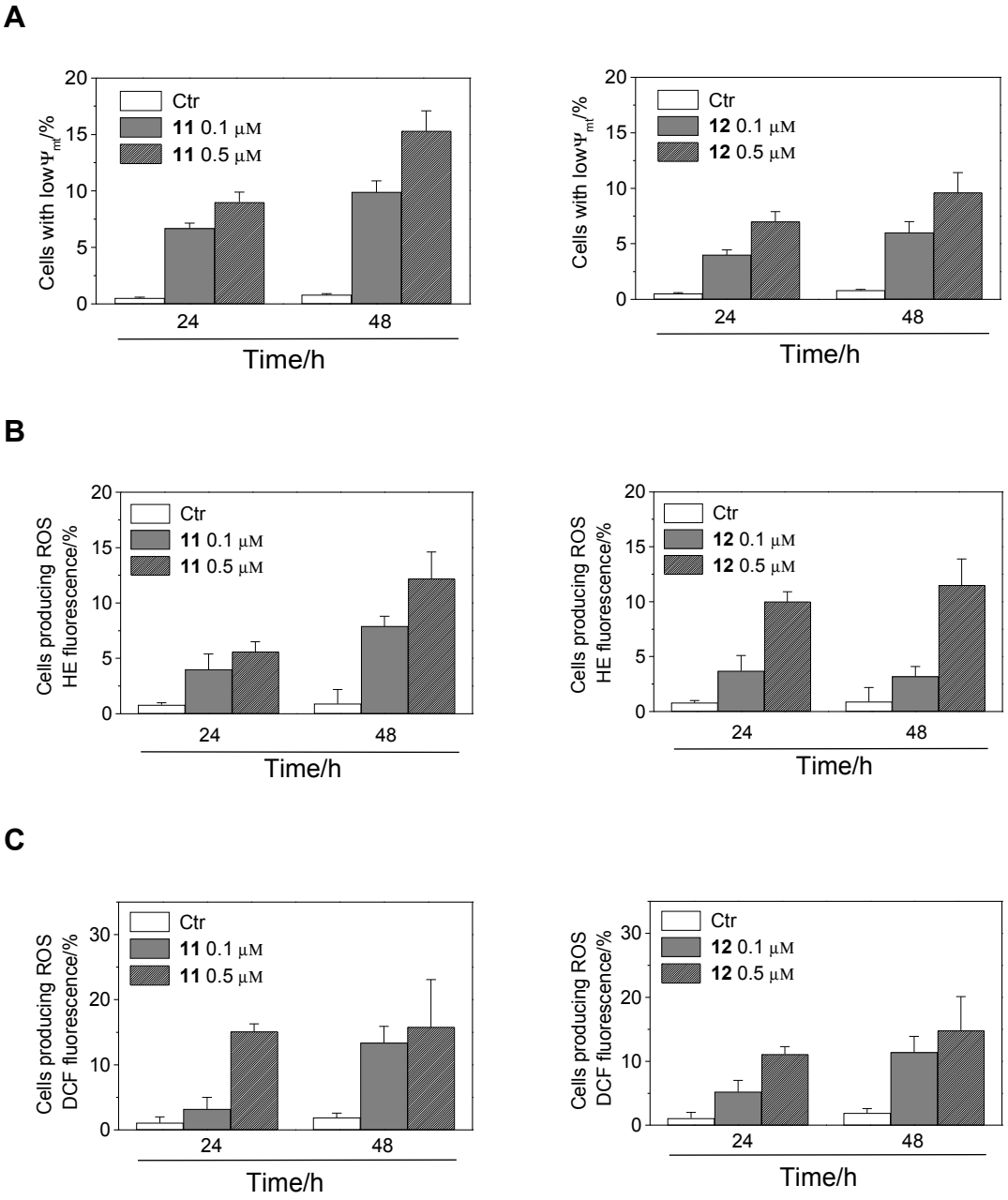

Figure 4. Assessment of mitochondrial dysfunction after treatment with compound 11 or 12. **A**. Induction of loss of mitochondrial membrane potential in Jurkat cells after 24 and 48 h of incubation with compounds 11 and 12 at 0.1 and 0.5 mM. Cells were stained with the fluorescent probe JC-1 and analyzed by flow cytometry. **B** and **C**. Mitochondrial production of ROS in Jurkat cells after 24 and 48 h of incubation with 11 and 12. Cells were stained with HE (**B**) or H_2-DCFDA (**C**) and analyzed by flow cytometry. The results are expressed as percentage of the fluorescence intensity relative to the untreated control. Data are expressed as mean ± S.E.M. of three independent experiments

Caspase-3 activation, PARP cleavage and Bcl-2 downregulation. Caspases are the central executioners of apoptosis mediated by various inducers.[19,20] Caspases are synthesized as proenzymes, which are activated by cleavage. Caspases-2, -8, -9, and -10 are termed apical and are usually the first to be stimulated in the apoptotic process. They in turn activate effector caspases,

such as caspase-3 in particular.[21] Exposure of Jurkat cells to compounds 11 or 12 was found to activate caspase-3, as shown in Figure 5, in a time and concentration dependent manner.

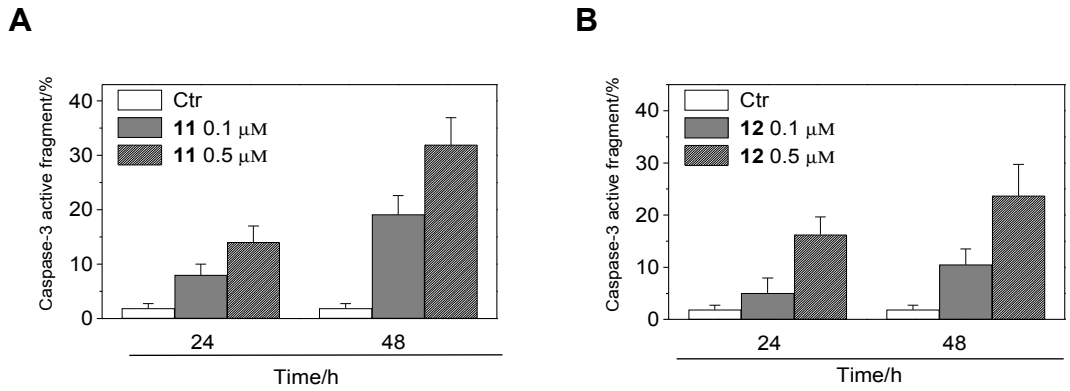

Figure 5. Caspase-3 induced activity by compounds **11** and **12**. Jurkat cells were incubated in the presence of **11** (**A**) or **12** (**B**) at 0.1 and 0.5 mM. After 48 h of treatment, cells were harvested and stained with an anti-human active caspase-3 fragment monoclonal antibody conjugated with FITC. Data obtained by flow cytometry analysis are expressed as percentage of caspase-3 active fragment positive cells. Data are expressed as mean ± S.E.M. of three independent experiments

PARP (poly ADP-ribose polymerase) is a 116 kDa nuclear protein that appears to be involved in apoptosis.[22] This protein is one of the main cleavage targets of caspase-3 both *in vitro* and *in vivo*.[22] As shown in Figure 6 (panel A), immunoblot analysis showed that the typical 89 kDa fragment of PARP increased in treated cells with both compounds in a time-dependent manner. Bcl-2 is a protein extensively investigated as a modulating agent of apoptosis, and it plays a major role in inhibiting apoptosis. Bcl-2 regulates the mitochondrial membrane potential and avoids the subsequent release of cytochrome *c* to prevent caspase activation.[23,24] Therefore, we examined whether the induced apoptosis by 11 and 12 is associated with changes in Bcl-2 expression. As depicted in Figure 6 (panel B), flow cytometric analysis showed that both compounds decreased Bcl-2 expression. Altogether these data indicate that the induction of apoptosis by these new derivatives is mediated through caspase-3 activation, PARP cleavage and Bcl-2 down regulation.

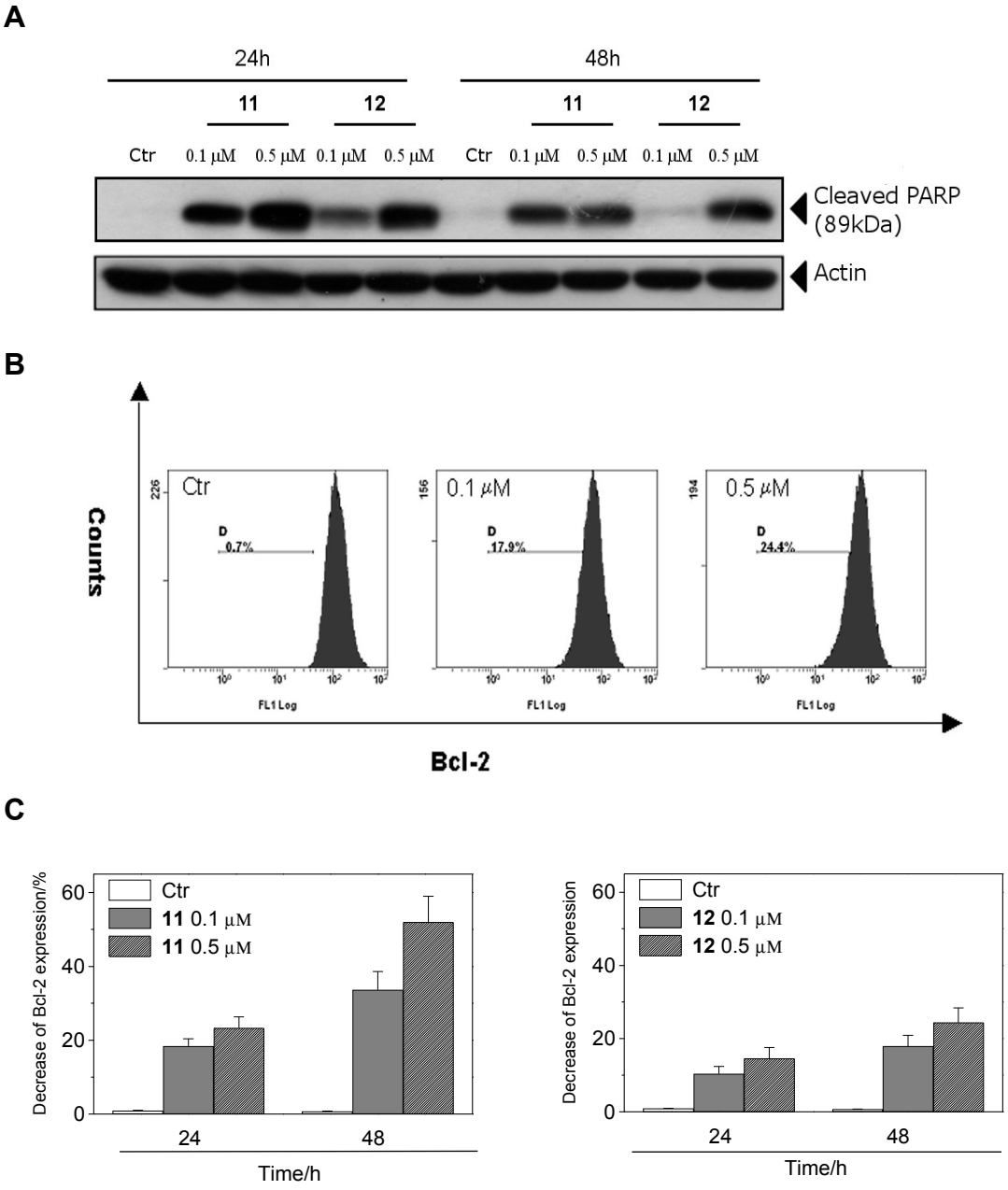

Figure 6. Western blot analysis of PARP and flow cytometric analysis of Bcl-2 expression. **A** Jurkat cells were treated with compounds 11 and 12 at the indicated concentrations for 24 and 48 h. The cells were then subjected to immunoblot analysis. **B** Cells were treated as above and after permeabilization labelled with a Bcl-2 FITC conjugated antibody. Representative histograms after 24 h of treatment with compound 11 at the indicated concentrations. **C** Bcl-2 expression in Jurkat cells after treatment with compounds 11 and 12 at the indicated concentrations for 24 and 48 h. Data are expressed as mean ± S.E.M. of two independent experiments.

Conclusions

Several 7-phenyl- and 8-phenylpyrroloquinolinone derivatives were prepared and assayed for their antiproliferative activity on a panel of solid tumor and

leukemic cell lines. Depending on the position and nature of substitutions, new structure-activity relationships on PPyQs were demonstrated that add to those known previously. Among these, the most surprising was the inactivity of the regioisomer 8-PPyQs **33-37** against all cell lines This indicates that the interaction of the 2-phenyl-quinolin-4-one moiety in the colchicine site of tubulin either requires the C-7 phenyl group or is eliminated with a bulky C-8 substituent.

Another important SAR was the finding that when position 1 of the 3-ethyl-7-PPyQ **38** bears small hydrophilic groups like cyano and carboxyamide as substituents, the resulting compounds **21** and **22** retained good antiproliferative activity, but only for leukemic cells. This should permit the future design of compounds specifically directed against leukemias. Finally, introducing a hydrophilic side chain in the N-3 or C-7 position of the PyQ nucleus provided compounds **11-13** that maintain high activity and an antiproliferative profile similar to the reference compound **38**, all of which have greater cytotoxicity for leukemia cells than for solid tumor cells.

Compound **11**, especially, exhibited potent inhibition of tubulin polymerization and was one of the most potent inhibitors of colchicine binding (IC_{50}=0.76 μM for assembly, 44% inhibition of the binding of [^{3}H]colchicine when equimolar with tubulin and 1/5-th the concentration of colchicine in the reaction mixture). Flow cytometry demonstrated that **11** had cellular effects typical for microtubule-interacting agents, causing accumulation of cells in the G2/M phase of the cell cycle and increased numbers of apoptotic sub-G1 cells Moreover, **11** is a potent inducer of multiple additional markers of apoptosis in the Jurkat cell line. Apoptosis induced by multiple antimitotic agents has been associated with alteration in a variety of cellular signalling pathways, and compound **11** had similar effects. The agent induced Bcl-2 down-regulation after 24 h of treatment. Since Bcl-2 prevents the initiation of the cellular apoptotic program by stabilizing mitochondrial permeability, its loss had multiple consequences. These included loss of mitochondrial Dy_{mt}, which in turn resulted in an uncoupling of the respiratory chain and the efflux from the mitochondria of caspase-9 and the apoptosis-inducing factor (AIF). Thus, the proteolytic activation of caspase-3 occurred with subsequent PARP cleavage. Compound **11**, with its apparent selectivity towards leukemic cell lines, therefore merits further investigation as a

potential chemotherapeutic agent.

Materials and Methods

Growth inhibitory activity. Human T-leukemia (Jurkat), promyelocytic leukemia (HL-60), chronic myelogenous leukemia (K562), myeloid leukemia (ML-2) and acute lymphoblastic leukemia (RS 4;11) cells, the latter with a t(4;11) translocation, were grown in RPMI-1640 medium (Gibco Milano, Italy). Human breast adenocarcinoma (MCF-7), cervix carcinoma (HeLa), ovarian cancer (IGROV), anaplastic thyroid (ARO), hepatoma (HepG2) and colon adenocarcinoma (HT-29) cells were grown in DMEM medium (Gibco Milano, Italy) supplemented with 115 units/mL of penicillin G (Gibco, Milano, Italy), 115 mg/mL streptomycin (Invitrogen, Milano, Italy) and 10% fetal bovine serum (Invitrogen, Milano, Italy). Individual wells of a 96-well tissue culture microtiter plate were inoculated with 100 mL of complete medium containing $8x10^3$ cells. The plates were incubated at 37C° in a humidified 5% CO_2 incubator for 18. At this time, the initial medium was removed from each well, and 100 mL of the drug solutions, dissolved in complete medium, at different concentrations, was added to each well and incubated at 37°C for 72 h. Cell viability was assayed by the MTT [(3-(4,5-dimethylthiazol-2-yl)-2,5 diphenyl tetrazolium bromide) test as previously described.[25] The GI_{50} was defined as the compound concentration required to inhibit cell proliferation by 50%.

Effects on tubulin polymerization and on colchicine binding to tubulin. Bovine brain tubulin was purified as described previously. To evaluate the effect of the compounds on tubulin assembly *in vitro,* varying concentrations were preincubated with 10 mM tubulin in glutamate buffer at 30˚C and then cooled to 0˚C. After addition of GTP, the mixtures were transferred to 0°C cuvettes in a recording spectrophotometer and warmed-up to 30°C, and the assembly of tubulin was observed turbidimetrically. The IC_{50} was defined as the compound concentration that inhibited the extent of assembly by 50% after a 20 min incubation. The capacity of the test compounds to inhibit colchicine binding to tubulin was measured as described,[8,9] except that the reaction mixtures

contained 1 mM tubulin, 5 mM [^{3}H]colchicine and 1 mM test compound.

Flow cytometric analysis of cell cycle distribution and apoptosis. For flow cytometric analysis of DNA content, 5x10^5 Jurkat cells in exponential growth were treated with different concentrations of the test compounds for 24 and 48 h. After an incubation period, the cells were collected, centrifuged and fixed with ice-cold ethanol (70%). The cells were then treated with lysis buffer containing RNAse A and Triton X-100 0.1%, and then stained with PI. Samples were analyzed on a Cytomic FC500 flow cytometer (Beckman Coulter). DNA histograms were analyzed using MultiCycle® for Windows (Phoenix Flow Systems, CA, USA).

Annexin-V assay. Surface exposure of PS by apoptotic cells was measured by flow cytometry with a Coulter Cytomics FC500 (Beckman Coulter, USA) by adding Annexin-V-FITC to cells according to the manufacturer's instructions (Annexin-V Fluos, Roche Diagnostic). Simultaneously the cells were stained with PI. Excitation was set at 488 nm and the emission filters were at 525 nm and 585 nm, respectively.

Assessment of mitochondrial changes. The mitochondrial membrane potential was measured with the lipophilic cation 5,5',6,6'-tetrachlo-1,1',3,3'-tetraethylbenzimidazolcarbocyanine (JC-1, Molecular Probes, USA), as described.[25] Briefly, after different times of treatment, the cells were collected by centrifugation and resuspended in Hank's Balanced Salt Solution (HBSS) containing the JC-1 at the concentration of 1 mM. The cells were then incubated for 10 min at 37°C centrifuged and resuspended in HBSS. The production of ROS was measured by flow cytometry using HE (Molecular Probes, USA) and H_2DCFDA (Molecular Probes, USA).

After different times of treatment, the cells were collected by centrifugation and resuspended in HBSS containing the fluorescence probes HE and H2-DCFDA at the concentrations of 2.5 and 0.1 mM, respectively. The cells were then incubated for 30 min at 37°C, centrifuged and resuspended in HBSS. The fluorescence was directly recorded with the flow cytometer using as excitation wavelength 488 nm and emission at 585 nm and 530 nm for HE and H_2DCFDA,

respectively.

Caspase- 3 assay. Caspase-3 activation in Jurkat cells was evaluated by flow cytometry using a human active caspase-3 fragment antibody conjugated with FITC (BD Pharmingen) as described.[26] Briefly, after different times of incubation in the presence of test compounds, the cells were collected by centrifugation and resuspended in Cytofix™ (BD Pharmingen) buffer for 20 min, washed with Perm/Wash™ (BD Pharmingen) and then incubated for 30 min with the antibody. After this period the cells were washed and analyzed by flow cytometry. The results were expressed as percentage of caspase-3 active fragment positive cells.

Flow cytometric analysis of Bcl-2 expression. Bcl-2 expression was evaluated in Jurkat cells by flow cytometry using a monoclonal antibody conjugated with FITC (DAKO). Briefly, after different times of incubation in the presence of test compounds, the cells were collected by centrifugation and permeabilized using a Fix&Perm cell permeabilization kit (Caltag Laboratories, Burlingame CA). The cells were then labeled with Bcl-2 antibody, washed and analyzed by flow cytometry.

Western Blot Analysis. Jurkat cells were incubated in the presence of test compounds and, after different times, were collected, centrifuged and washed two times with ice cold PBS. The pellet was then resuspended in lysis buffer. After the cells were lysed on ice for 30 min, lysates were centrifuged at 15000 g at 4°C for 10 min. The protein concentration in the supernatant was determined using BCA protein assay reagents (Pierce, Italy). Equal amounts of protein (20 μg) were resolved using SDS-PAGE gels (12% acrylamide) and transferred to PVDF Hybond-p membrane (GE Healthcare). Membranes were blocked with I-block (Tropix) overnight, under rotation at 4°C. Membranes were then incubated with a primary antibody against the cleaved fragment of PARP (rabbit, 1:1000, Cell Signaling), or β-actin (mouse, 1:10,000, Sigma) for 2 h at room temperature. Membranes were next incubated with peroxidase-labeled goat anti-rabbit IgG (1:100,000, Sigma) or peroxidase-labeled goat anti-mouse IgG (1:100,000, Sigma) for 60 min. All membranes were visualized using ECL Advance (GE Healthcare) and exposed to Hyper film MP (GE Healthcare). To

ensure equal protein loading, each membrane was stripped and reprobed with anti-b-actin antibody.

References

1. M. G. Ferlin, G. Chiarelotto, V. Gasparotto, L. Barzon, G. Palù, I. Castagliuolo *J. Med. Chem*. **2005**, *48*, 3417-3427.
2. V. Gasparotto, I. Castagliuolo, G. Chiarellotto, V. Pezzi, D. Montanaro, P. Brun, G. Palù, G. Viola, M. G. Ferlin *J. Med. Chem*. **2006**, *49*, 910-1915.
3. V. Gasparotto, I. Castagliuolo, M. G. Ferlin *J. Med. Chem.* 2007, *50*, 5509-5513.
4. H.O. Burrus, and G. Powell *J. Am. Chem. Soc*., 1945, *67*, 1468-1472
5. T. Owa, H. Yoscino, K. Okauchi, K. Yoshimatsu, Y. Ozawa, N. H. Sugi, T. Nagasu, N. Koyanagi, K. Kitoh *J. Med. Chem.* 1999, *42*, 3789-3799
6. L-J. Huang, M-C. Hsieh, C-M. Teng, K-H. Lee Kuo S-C *Bioorg. & Med. Chem.* 1998, *6*, 1657-1662
7. E. M. Beccalli, C. La Rosa, A. Marchesini *J. Org. Chem.* **1984**, *49*, 4287-4290.
8. E. Hamel *Cell Biochem. Biophys.* **2003**, *38*, 1-21.
9. P. Verdier-Pinard, J.-Y. Lai, H.-D. Yoo, J. Yu, B. Marquez, D. G. Nagle, M. Nambu, J. D. White, J. R. Falck, W. H. Gerwick, B. W. Day, E. Hamel *Mol. Pharmacol.* **1998**, *53*, 62-76
10. I. Vermes, C. Haanen, H. Steffens-Nakken, C. Reutelingsperger *J. Immunol. Methods* **1995**, *184*, 39–51.
11. S.J. Martin, C.P. Reutelingsperger, A.J. McGahon, J.A. Rader, R.C. van Schie, D.M. Laface, D.R. Green *J. Exp. Med.* **1995**, 182,1545-56.
12. D. R. Green, G. Kroemer *Science* **2005**, *305*, 626–629.
13. J.D. Ly, D.R. Grubb, A. Lawen *Apoptosis* **2003**, 3, 115-128.
14. S. Salvioli, A. Ardizzoni, C. Franceschi, A. Cossarizza *FEBS Lett.* **1997,** *411*, 77-82.
15. F. Mollinedo, C. Gajate *Apoptosis* **2003**, *8,* 413-450.
16. N. Zamzami, P. Marchetti, M. Castedo, D. Decaudin, A. Macho, T. Hirsch, S. A. Susin, P. X. Petit, B. Mignotte, G. Kroemer *J. Exp. Med.* **1995**, *182,* 367–377.
17. K. Staniek *Biochem Pharmacol* **2005**, *69*, 719–723.
18. G. Rothe, G. Valet *J. Leukocyte Biol.* **1990**, *47*, 440–448.
19. W. C. Earnshaw, L. M. Martins, S. H. Kaufmann *Annu. Re*v. *Biochem.* **1999**, *68*, 383–424.
20. J.-B. Denault, G. S. Salvesen *Chem. Rev.* **2002**, *102*, 4489-4499.
21. G. Porter, R. U. Janicke *Cell Death Differ*. **1996**, 99-104.
22. C. Soldani, A. I. Scovassi *Apoptosis*. **2002**, *7*, 321-328.
23. R. M. Kluck, E. Bossy-Wetzel, D. R. Green *Science* **1997**, *275*, 1132-1136.
24. C. M. Knudson, S. J. Korsmeyer *Nature Genet* **1997**, *16*, 358-363.
25. G. Viola, L. Cecconet, A. Leszl, P. Brun, A. Salvador, F. Dall'Acqua, G. Basso, P. Diana,

P. Barraja, G. Cirrincione *Cancer Chem. Pharm.* **2009**, *64*, 1235-1251.

26. R. Romagnoli, P.G. Baraldi, M. D. Carrion, O.Cruz-Lopez., C. Lopez Cara, J. Balzarini, E. Hamel, A. Canella, E. Fabbri, R. Gambari, G. Basso, G. Viola *Bioorg. Med. Chem. Lett.* **2009**, *19*, 2022-2028.

5.2. MG-2477, a new tubulin inhibitor, induces autophagy through inhibition of the Akt/mTOR pathway and delayed apoptosis in A549 cells.[23]

Giampietro Viola,[1§*] Roberta Bortolozzi[1§], Ernest Hamel[2], Stefano Moro[3], Paola Brun[4], Ignazio Castagliuolo[4], Maria Grazia Ferlin[3], Giuseppe Basso[1]

[1]Department of Pediatrics, Laboratory of Oncohematology, University of Padova, Italy

[2]Screening Technologies Branch, Developmental Therapeutics Program, Division of Cancer Treatment and Diagnosis, National Cancer Institute at Frederick, National Institutes of Health, Frederick, Maryland 21702, USA

[3]Department of Pharmaceutical Sciences, University of Padova, Italy

[4]Department of Histology, Microbiology and Medical Biotechnologie, University of Padova, Italy

§ These authors contributed equally to this work

Abstract

We previously demonstrated that MG-2477 (3-cyclopropylmethyl-7-phenyl-3*H*-pyrrolo[3,2-*f*]quinolin-9(6*H*)-one) inhibits the growth of several cancer cell lines *in vitro*. Here we show that MG-2477 inhibited tubulin polymerization and caused cells to arrest in metaphase. The detailed mechanism of action of MG-2477 was investigated in a non-small cell lung carcinoma cell line (A549). Treatment of A549 cells with MG-2477 caused the cells to arrest in the G2/M phase of the cell cycle, with a concomitant accumulation of cyclin B. Moreover, the compound induced autophagy, which was followed at later times by apoptotic cell death. Autophagy was detected as early as 12 h by the conversion of microtubule associated protein 1 light chain 3 (LC3-I) to LC3-II, following cleavage and lipid addition to LC3-I. After 48 h of MG-2477 exposure, phosphatidylserine externalization on the cell membrane, caspase-3 activation, and PARP cleavage occurred, revealing that apoptotic cell death had begun. Pharmacological inhibition of autophagy with 3-methyladenine or bafilomycin A1 increased apoptotic cell death, suggesting that the autophagy caused by MG-2477 played a protective role and delayed apoptotic cell death. Additional studies revealed that MG-2477 inhibited survival signaling by blocking activation of Akt and its downstream targets, including mTOR, and FHKR. Treatment with

MG-2477 also reduced phosphorylation of mTOR downstream targets p70 ribosomal S6 kinase and 4E-BP1. Overexpression of Akt by transfection with a myr-Akt vector decreased MG-2477 induced autophagy, indicating that Akt is involved. Taken together, these results indicated that the autophagy induced by MG-2477 delayed apoptosis by exerting an adaptive response following microtubule damage.

Introduction

Antimitotic agents, primarily of natural origin, are a class of compounds that have been used for the treatment of a variety of malignancies for many years. Although they are sometimes considered “old chemotherapeutics” with respect to current anticancer approaches[1,2], at the present time they still represent valuable drugs that retain high scientific interest. Their impressive success in patients is due to their potent anti-proliferative effects and to their particular mechanism of action of altering microtubule dynamics, whether their detailed mechanism of action involves inhibition of tubulin assembly (vinca alkaloids, eribulin, estramustine) or inhibition of microtubule disassembly (taxoids, epothilones). The importance of microtubules in mitosis and cell division, as well as the clinical success of microtubule targeting drugs, has made these dynamic organelles one of the most attractive targets for anticancer therapy[3].

As with many anticancer drugs, the mode of action of antitubulin agents involves the induction of programmed cell death (PCD)[4]. Apoptosis (Type I PCD) is characterized by chromatin condensation, DNA fragmentation and activation of caspases. In recent years, it became evident that other forms of cell death, alternatives to apoptosis, are also “programmed”. Among them, autophagy (Type II PCD) is now recognized as an important process involved in different human pathologies, such as neurodegenerative diseases, aging and cancer[5,6]. Recent studies have suggested that, like apoptosis, autophagy is important in the regulation of cancer development and progression and in determining the response of tumor cells to anticancer therapy. In fact, autophagy has been observed as a novel response to some anticancer agents,

such as temozolomide, dexamethasone, 6-thioguanine, and camptothecin, as well as to ionizing radiation[7-11]. In this context, very few studies report the possibility that antimitotic drugs might induce autophagy[12-14]. From a molecular point of view, several cell signaling pathways have been implicated in regulating autophagy, including phosphatidyl inositol 3-kinase (PI3K)/Akt/mammalian target of rapamycin (mTOR). Recent studies have shown that the inhibition of Akt and its downstream target mTOR contribute to the initiation of autophagy[15,16].

Recently, we identified MG-2477 (3-cyclopropylmethyl-7-phenyl-3*H*-pyrrolo[3,2-*f*]quinolin-9(6*H*)-one) (structure shown in Figure 1, Panel A), as a potent growth inhibitor of human tumor cell lines that might interfere with microtubules[17]. The current investigation was designed to characterize the action of MG-2477 in a human tumor cell line (A549 non-small cell lung carcinoma cells) and to characterize the molecular mechanisms by which MG-2477 caused cell death. We focused our attention on this cell line due to the poor prognosis and lack of effective therapies in treating lung carcinoma patients. We show here that MG-2477 was a potent cytotoxic antimicrotubule agent that induced autophagy in A549 cells. Autophagy was followed by apoptotic cell death that was caspase-dependent but did not involve mitochondrial dysfunction.

Results

MG-2477 Binds to the Colchicine Site of Tubulin and Inhibits the Polymerization of Tubulin into Microtubules. To evaluate if MG-2477 interfered with the microtubule network, we first examined its effects on cultured cells by immunofluorescence microscopy. Shown in Figure 1, Panel B, is the normal microtubule network of untreated cells. Following 24 h of treatment with MG-2477 at 1.0 μM, there was extensive disruption of the microtubule network. Treated cells showed a characteristic “rounded up” morphology caused by loss of microtubules in both interphase and mitotic cells. We also examined cells for arrest in mitosis following treatment with MG-2477 (Figure 1, Panel C). Large numbers of cells arrested in metaphase were apparent from their condensed chromosomes and lost nuclear membrane. The percentage of mitotic cells (the mitotic index) increased in a concentration dependent manner following

treatment with MG-2477.

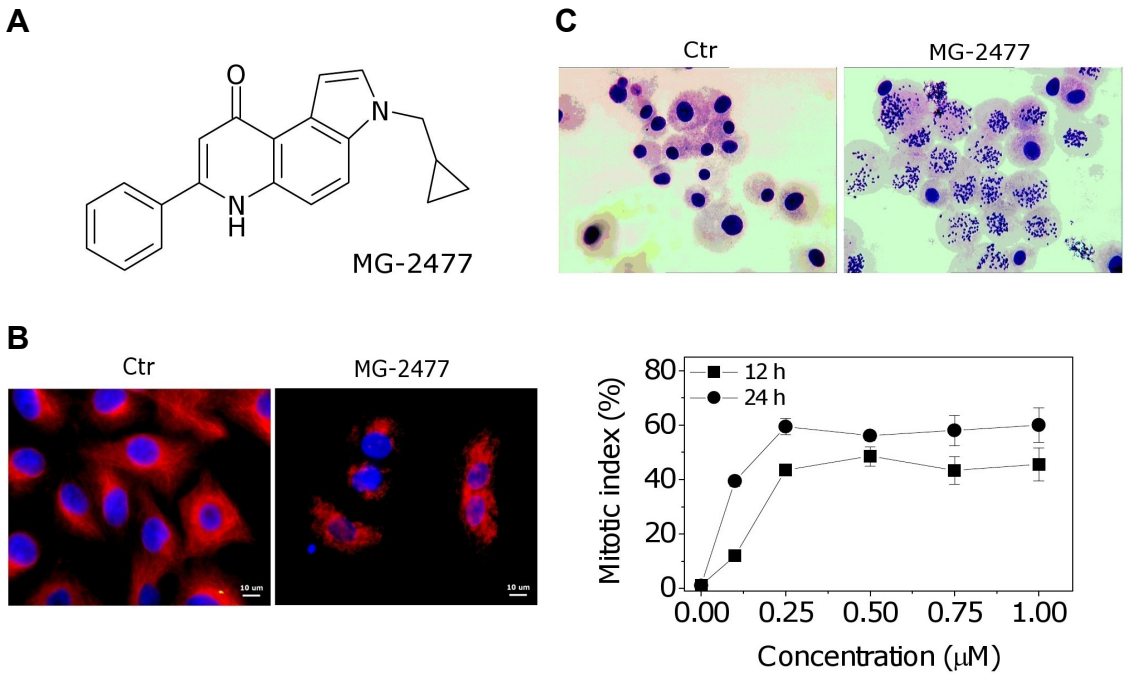

Figure 1. MG2477 inhibits tubulin assembly and destabilizes microtubules by acting at the colchicine site of tubulin. **A** Chemical structure of MG-2477. **B** Immunofluorescence images of A549 cells treated with anti-β-tubulin antibody and with a TRITC-conjugated secondary antibody and then observed by confocal microscopy. Cells were untreated or exposed to 1 mM MG-2477 for 24 h. **C** Quantitative assessment of mitotic arrest by MG-2477. A549 cells were treated with MG-2477. Two hundred cells/treatment were scored for the presence of mitotic figures by contrast phase microscopy, and the mitotic index was calculated as the proportion of cells with mitotic figures. Data are expressed as mean ± S.E.M. of three independent experiments.

These cellular effects implied that MG-2477 interfered with tubulin polymerization. We therefore examined its effects on the assembly of purified tubulin [19]. We added different concentrations of MG-2477 to 10 μM αβ-tubulin and compared its effects with those of two reference compounds, combretastatin A-4 (CA4) and thiocolchicine. MG-2477 inhibited tubulin polymerization with an IC_{50} value of 0.9 μM (Figure 2, Panel A), a value lower than that of CA4 (IC_{50}, 1.2 μM) but similar to that of thiocolchicine (IC_{50}, 0.8 μM). To determine if MG-2477 interacted with tubulin at the colchicine site, we determined whether it inhibited binding of 5 μM [^{3}H]colchicine to 1 μM tubulin, again in comparison with CA4 and thiocolchicine. The inhibitors were used at both 1 and 5 μM. MG-2477 significantly inhibited [^{3}H]colchicine binding to tubulin, indicating that it acts at the colchicine site. Its inhibitory effect, however, was lower than that of CA4 but greater than that of thiocolchicine (Figure 2, Panel B).

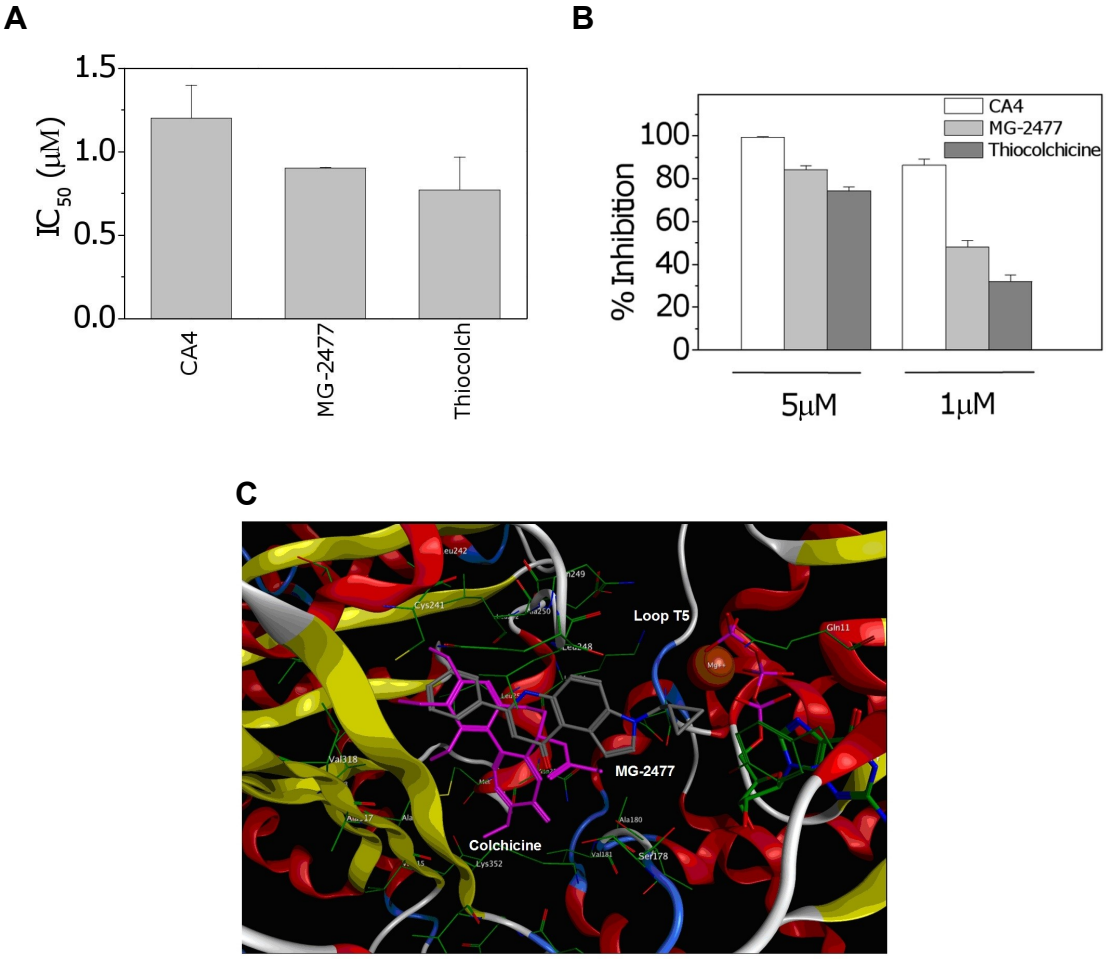

Figure 2. Inhibition of microtubule assembly and colchicine binding. **A** To evaluate the effect of the compound on tubulin assembly in vitro, varying concentrations of compound were preincubated with 10 mM bovine brain tubulin. Following addition of GTP, tubulin assembly at 30 °C was followed turbidimetrically at 350 nm. The IC_{50} was defined as the compound concentration that inhibited the extent of assembly by 50% after a 20 min incubation. **B** The capacity of the test compound to inhibit colchicine binding to tubulin was measured in reaction mixtures that contained 1 mM tubulin, 5 mM [^{3}H]colchicine and 1 or 5 mM MG-2477, as indicated. Thiocolchicine and CA4 were used as reference compounds. Data are expressed as mean ± SD of two independent experiments. **C** Docked pose of MG-2477 (gray), overlapped with colchicine (pink) in the tubulin binding site.

The 1SA0 tubulin structure[21] was used for computer-based automated docking of MG-2477 in comparison with colchicine. This was performed using the MOE-Dock program. Figure 2 (Panel C) depicts the binding mode of MG-2477 in the colchicine site. The colchicine site is largely buried in the intermediate domain of the β-subunit, although colchicine also interacts with loop T5 of the neighboring α-subunit (Figure 2, Panel C), consistent with the observation that colchicine stabilizes the tubulin heterodimer[21]. Docking simulations showed that, like colchicine, MG-2477 can be accommodated in the same hydrophobic cleft, adopting an energetically stable conformation. Moreover, the most stable conformation of MG-2477 displayed the same chemical interactions as

colchicine, predominantly hydrophobic interactions with Val 181, Ala 250, Cys 241, Val 318, and Ile 378. Again, like colchicine, MG-2477 interacted with the neighboring α-tubulin T5 loop, consistent with a competitive mechanism of action at the colchicine site.

MG-2477 Induces Cell Cycle Arrest at the G2/M Phase of the Cell Cycle. The effect of MG-2477 on cell cycle progression was examined by flow cytometry. MG-2477 treatment resulted in the accumulation of cells in the G2/M phase, with a concomitant reduction in the proportion of cells in the G1 phase. A small decrease of cells in the S phase was also observed (Figure 3, Panels A and B). The accumulation in G2/M cells began after 12 h of treatment and is concentration dependent until the concentration of 0.25 μM, after which a plateau was reached. The characteristic hypodipolid peak (subG1), indicating apoptotic cells, did not appear until after 48 h of treatment (Figure 3, Panel C).

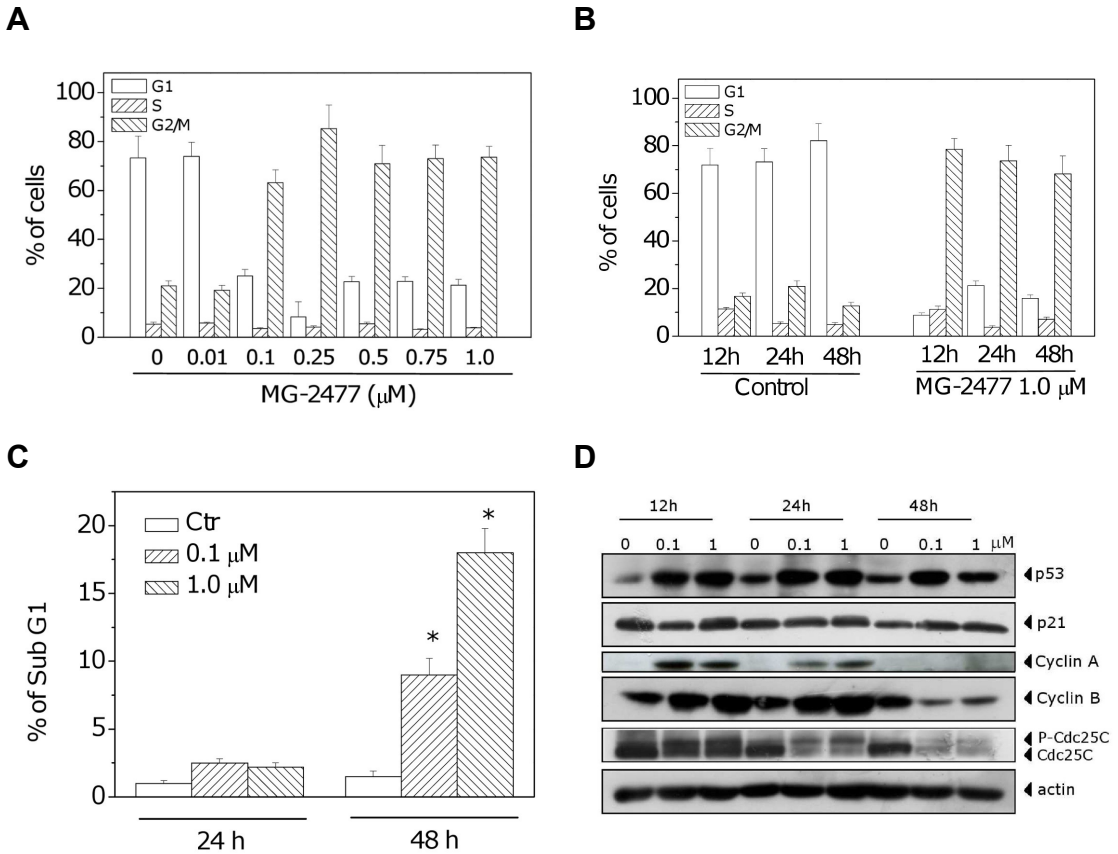

Figure 3. Effects of MG-2477-induced G2/M phase arrest in A549 cells. **A** Cells were treated with MG-2477 for 24 h, and cell cycle distribution was analyzed by flow cytometry after staining the cells with PI. **B** Cells were treated with MG-2477, and cell cycle distribution was analyzed. Data are expressed as mean ± SEM of three independent experiments **C** Percentage of cells in the SubG1 peak. Cells were treated with MG-2477 at 0.1 and 1.0 μM for 24 and 48 h. Data are expressed as mean ± SEM of three independent experiments. * $p<0.01$ vs control. **D** Cells were treated with MG-2477 for 24 and 48h. Whole cell lysates were subjected to Western blot.

Next, we investigated the association between MG-2477-induced G2/M arrest and alterations in G2/M regulatory protein expression. As shown in Figure 3 (Panel D), MG-2477 caused an increase in cyclin B1 expression after 12 and 24 h, followed by a decrease at 48 h. Similar effects occurred in the expression of cyclin A. At 24 h, a slower migrating form of phosphatase cdc25C appeared, indicating changes in the phosphorylation status of this protein. As early as 12 h, increased levels of p53 protein were expressed in response to treatment with MG-2477, but there was little change in expression of $p21^{waf/Cip1}$.

MG-2477 Induces Growth Inhibition and Delayed Apoptotic Response in A549 Cells. A549 cells exposed to 1 μM MG-2477 were analyzed for viability at 24, 48 and 72 h by the MTT assay. Cells exhibited a lag period lasting over 24 h in their response to MG-2477, while a significant decrease in viability occurred at 48 and 72 h (Figure 4, Panel A).

To characterize the mode of cell death, we performed a biparametric cytofluorimetric analysis using PI and AnnexinV-FITC, which stain DNA and PS residues, respectively[28]. After drug treatment for 12, 24 or 48 h, A549 cells were labeled with the two dyes and washed, and the resulting red (PI) and green (FITC) fluorescence was monitored by flow cytometry. We observed the appearance of Annexin-V^+/PI^-cells, indicative of apoptosis, as shown in the representative histograms depicted in Figure 4 (Panel B, upper). Quantitatively, MG-2477 treatment resulted in a significant induction of apoptotic cells only after 48 h of treatment (Figure 4, Panel B, lower), consistent with the appearance of subG1 cells described above.

It is well established that, at an early stage, apoptotic stimuli alter the mitochondrial transmembrane potential ($\Delta\psi_{mt}$)[29,30]. To address whether MG-2477 affected the $\Delta\psi_{mt}$, we examined treated cells for fluorescence of the dye JC-1. No significant changes in mitochondrial potential were observed (Figure 4, Panel C). To confirm that mitochondria were not involved in the mechanism of apoptosis, we also evaluated the mitochondrial production of ROS by two fluorescent probes, HE and H_2DCFDA, using flow cytometry. In agreement with the low levels of mitochondrial depolarization, only a slight increase of ROS production was observed in cells treated with MG-2477 (Figure 4, Panel C).

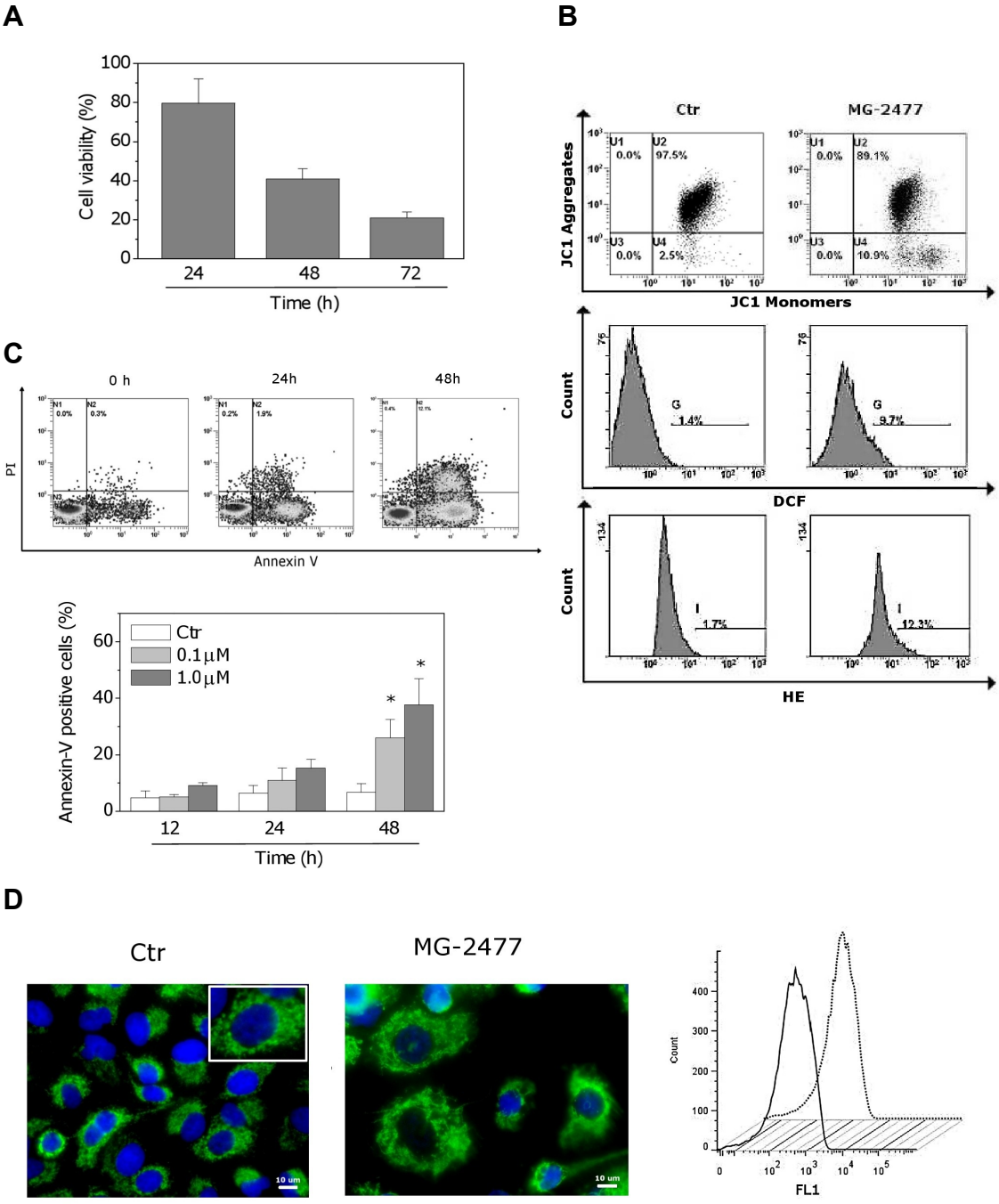

Figure 4. MG-2477 induced delayed apoptosis in A549 cells. **A** Cells were incubated with 1 µM MG-2477. Cell viability was quantified by the MTT assay. **B** Representative histograms of A549 cells treated with MG-2477 (upper panel) and analyzed by flow cytometry after staining with Annexin-V-FITC and PI(lower panel). Data are expressed as mean ± SEM of six independent experiments. * $p<0.01$ vs control. **C** Analysis of mitochondrial dysfunction in cells treated with 1 µM MG-2477 for 48 h and analyzed by flow cytometry with JC-1. ROS production was measured by flow cytometry with H_2DCFDA and HE. **D** Representative confocal images of control A549 cells and cells treated with 1 µM MG-2477 for 48 h, showing cytochrome *c* labeled with a monoclonal antibody conjugated to FITC. The nuclei were stained blue with DAPI. Scale bar, 10 µm. Inset in the control cells image: an enlargement of one cell for a better comparison with the treated cells. **E** Flow cytometric analysis of cytochrome *c* after treatment with MG-2477 (1 µM) for 48 h. Cells were stained with a FTIC-conjugated monoclonal antibody directed against cytochrome *c*. Straight line: control cells; dotted line: MG-2477 treated cells.

Furthermore, immunofluorescence and flow cytometric analysis of cells treated with the compound did not show any release of cytochrome *c* (Figure 4, Panels D and E), indicating that the late apoptosis induced by MG-2477 did not follow a mitochondrial pathway.

The activation of caspases plays a central role in the process of apoptotic cell death[31]. We therefore wondered whether inhibition of caspases with the pan-caspase inhibitor z-VAD.fmk would prevent cell death. Our results showed that z-VAD.fmk significantly reduced cell mortality as assessed by flow cytometry after double staining with PI and Annexin-V (Figure 5, Panel A), indicating that cell death induced by MG-2477 is caspase-dependent.

To determine which caspases were involved in MG-2477-induced cell death, the expression of caspases was measured by immunoblot analysis and flow cytometry. We observed a clear activation of two effector caspases, caspase-7 and caspase-3, and we also observed cleavage of the caspase-3 substrate PARP after 48 h of MG-2477 exposure (Figure 5, Panels B and C). In addition, the expression of XIAP, a member of the inhibitors of apoptosis protein family, was strongly reduced concomitant with caspase activation. Consistent with the $\Delta\psi_{mt}$ results described above, MG-2477 treatment did not induce activation of caspase-9, the major initiator caspase of the intrinsic (mitochondrial) apoptosis pathway, nor of caspase-8. As shown in Figure 5, Panel C, expressed levels of these proteins did not change significantly following treatment with MG-2477. Caspase-2 is a unique caspase with characteristics of both initiator and effector caspases[32]. Recently, its key role in several apoptosis signaling cascades has emerged. In particular, caspase-2 has been implicated in the cell death induced by different antimitotic agents[33,34]. Western blot analysis showed an early activation of caspase-2 following treatment with MG-2477 that occurred prior to caspase 3/7 activation (Figure 5, Panel C). In agreement with these data, the caspase-9 inhibitor z-LEDH.fmk did not prevent apoptosis, while the selective caspase-2 inhibitor z-VDVAD.fmk, significantly reduced cell death induced by MG-2477(Figure 5, Panel A).

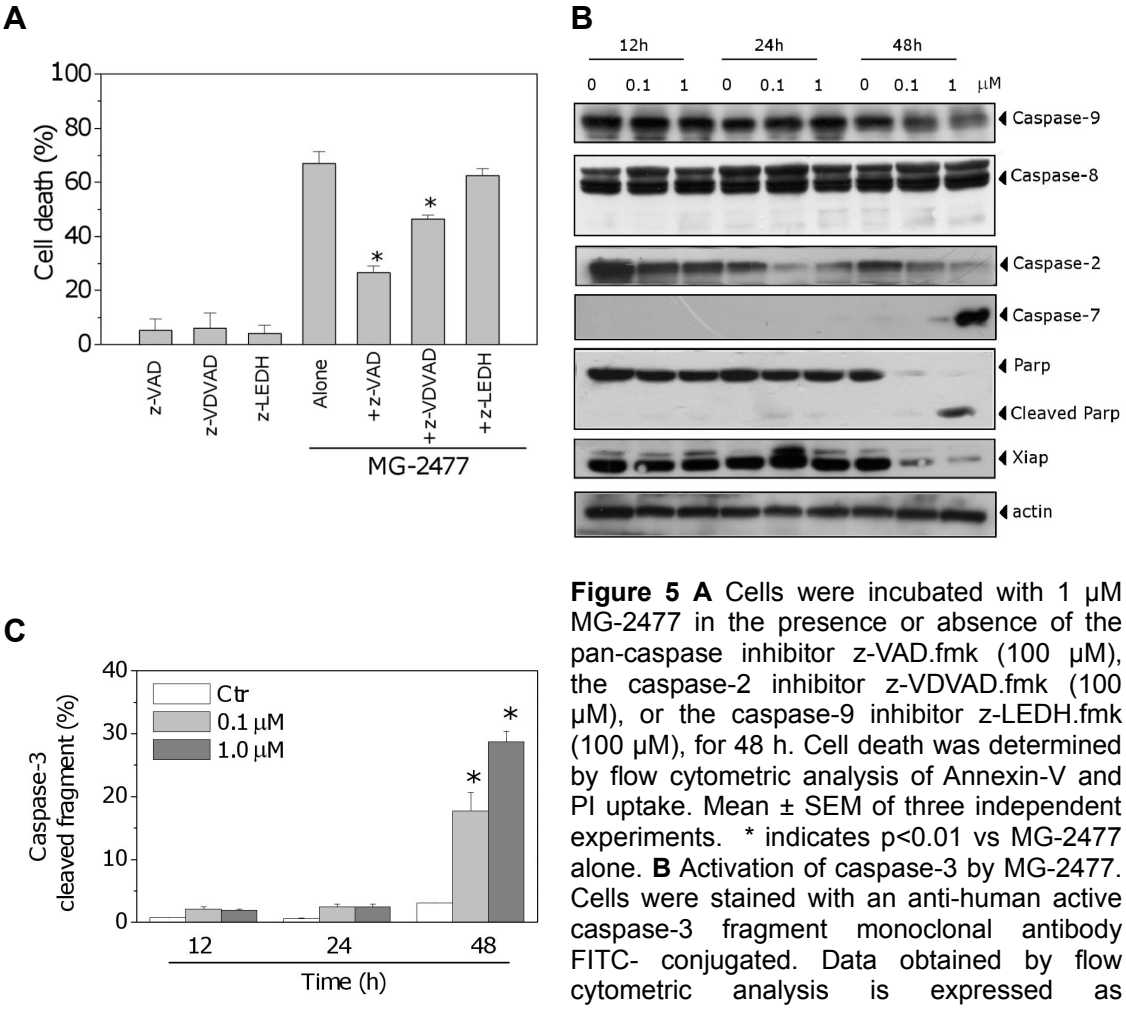

Figure 5 A Cells were incubated with 1 μM MG-2477 in the presence or absence of the pan-caspase inhibitor z-VAD.fmk (100 μM), the caspase-2 inhibitor z-VDVAD.fmk (100 μM), or the caspase-9 inhibitor z-LEDH.fmk (100 μM), for 48 h. Cell death was determined by flow cytometric analysis of Annexin-V and PI uptake. Mean ± SEM of three independent experiments. * indicates $p<0.01$ vs MG-2477 alone. **B** Activation of caspase-3 by MG-2477. Cells were stained with an anti-human active caspase-3 fragment monoclonal antibody FITC- conjugated. Data obtained by flow cytometric analysis is expressed as percentage of caspase-3 active fragment positive cells. Mean ± SEM of five independent experiments. * $p<0.01$ vs control. **C** Expression of caspases, PARP and XIAP following treatment with MG-2477.

Effect of MG-2477 on Bcl-2 Family Proteins. There is increasing evidence that regulation of the Bcl-2 family of protein shares the signaling pathways induced by antimicrotubule compounds[4]. Our results showed (Figure 6, Panel A) that the anti-apoptotic proteins Bcl-2 and Bcl-XL were phosphorylated in the first 12-24 h of treatment, as demonstrated by band shifts, followed by reduction in expression of the proteins at 48 h. Mcl-1, an anti-apoptotic member of the Bcl-2 family, was also phosphorylated in response to MG-2477 treatment. The Mcl-1 band then disappeared at 48 h with the occurrence of apoptosis, following treatment with 1μM MG-2477. MG-2477 treatment had little or no effect on the expression of proapoptotic proteins such as Bax or Bak (Figure 6, Panel B).

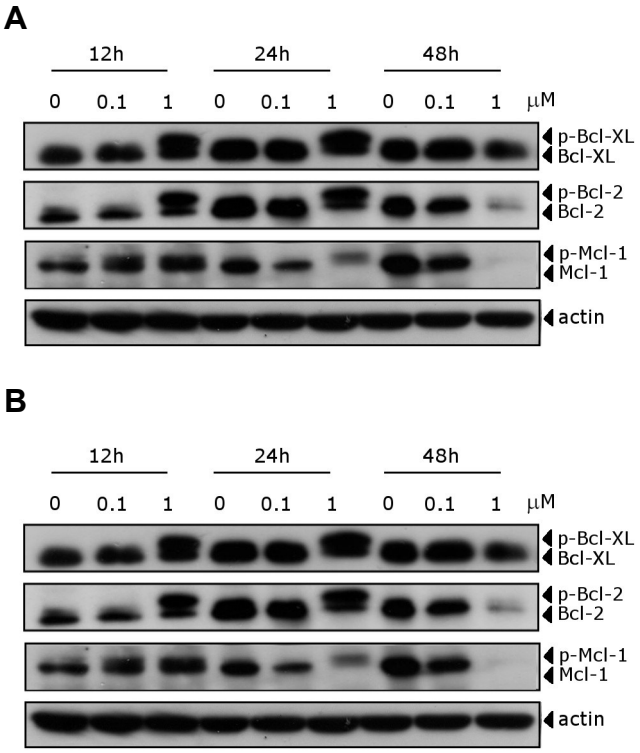

Figure 6
Effect of MG-2477 treatment, as indicated, on the expression of anti-apoptotic **A** and pro-apoptotic **B** member proteins of the Bcl-2 family.

MG-2477 Induces Autophagy in A549 Cells. In view of the minimal level of apoptosis observed following 12-24 h of treatment with MG-2477, we examined whether autophagy was induced in A549 cells with MG-2477 treatment. We first examined levels of LC3-II induced by MG-2477 treatment, since this protein is a good indicator of autophagosome formation[35]. As shown in Figure 7 (Panel A), MG-2477 induced, in a time-dependent manner, an increase in the amount of LC3-II. This effect was already evident after 12 h of treatment, in contrast to the low levels of apoptosis at this time point. We next used monodansyl cadaverine (MDC), a dye that stains autophagosomes[35]. As shown in Figure 7 (Panel B), MDC-positive vacuoles were detected after MG-2477 treatment.

A typical characteristic of autophagy is the development of AVOs[10]. Observations with fluorescence microscopy of A549 cell treated with MG-2477 and stained with the fluorescent probe AO showed an increase in cell size and cytoplasmic acidic vacuolization, as shown in Figure 7 (Panel B). To quantify the appearance of AVOs after treatment with MG-2477, we performed flow cytometric analysis after staining of the cells with AO. In good agreement with the early appearance of LC3-II, there was also a significant increase in red fluorescence after 24 h of treatment (Figure 7, Panel C). A recent study[36] reports that vincristine disruption of the microtubule cytoskeleton may interfere with the

fusion of autophagosomes with lysosomes. We therefore visualized autophagosome formation in A549 cells by using a cell line expressing the autophagosome-associated LC3 protein fused to green fluorescent protein (GFP-LC3). MG-2477 induced a redistribution of GFP-LC3 from a diffuse to a vacuolar pattern when autophagosomes were formed (Figure 7, Panel D). More importantly, these autophagosomes co-localized with the lysosomotropic dye LysoTracker RED, indicating the effective formation of autophagolysosomes.

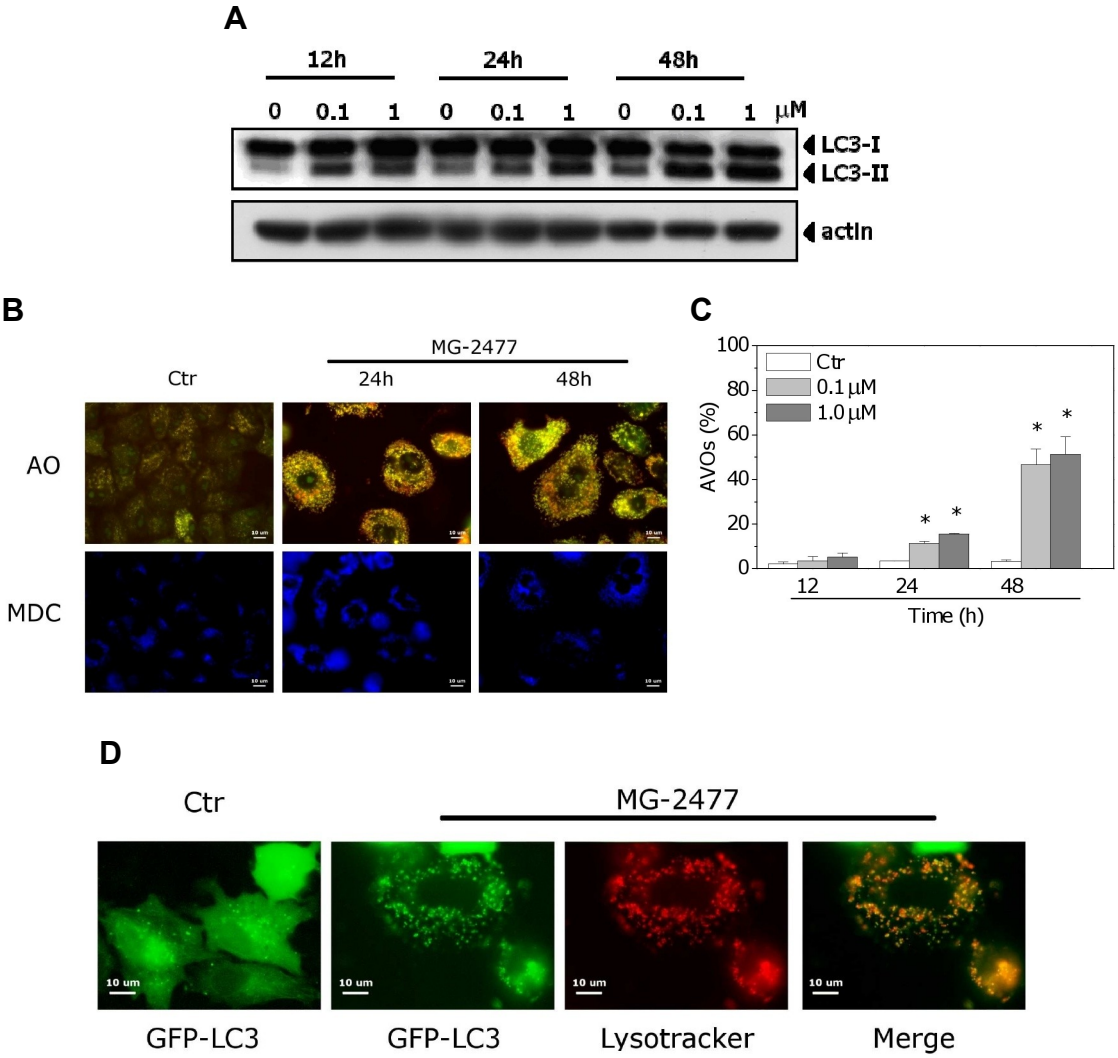

Figure 7. A Immunoblot analysis of LC3 after treatment with MG-2477. **B** Fluorescence microscopic analysis of A549 cells treated with 1 μM MG-2477 for 24 or 48 h and then stained with AO or MDC. **C** Detection of MG-2477-induced AVO formation in A549 cells. Cells were treated with MG-2477, stained with AO and analyzed by flow cytometry. Mean ± SEM of four independent experiments. * $p<0.01$ vs non-treated cells. **D** A549 cells were transiently transfected with GFP-LC3 and treated with 1 μM MG-2477 for 24 h. Lysosomes were stained with LysoTracker RED, and cells were analyzed by confocal microscopy.

Inhibition of Autophagy Potentiates MG-2477-induced Apoptotic Cell Death. To investigate whether inhibition of autophagy would affect the cytotoxicity of MG-2477, A549 cells were treated with 1 μM MG-2477 in the

presence of 3-MA or bafilomycin A1, two well known inhibitors of autophagy[37,38].

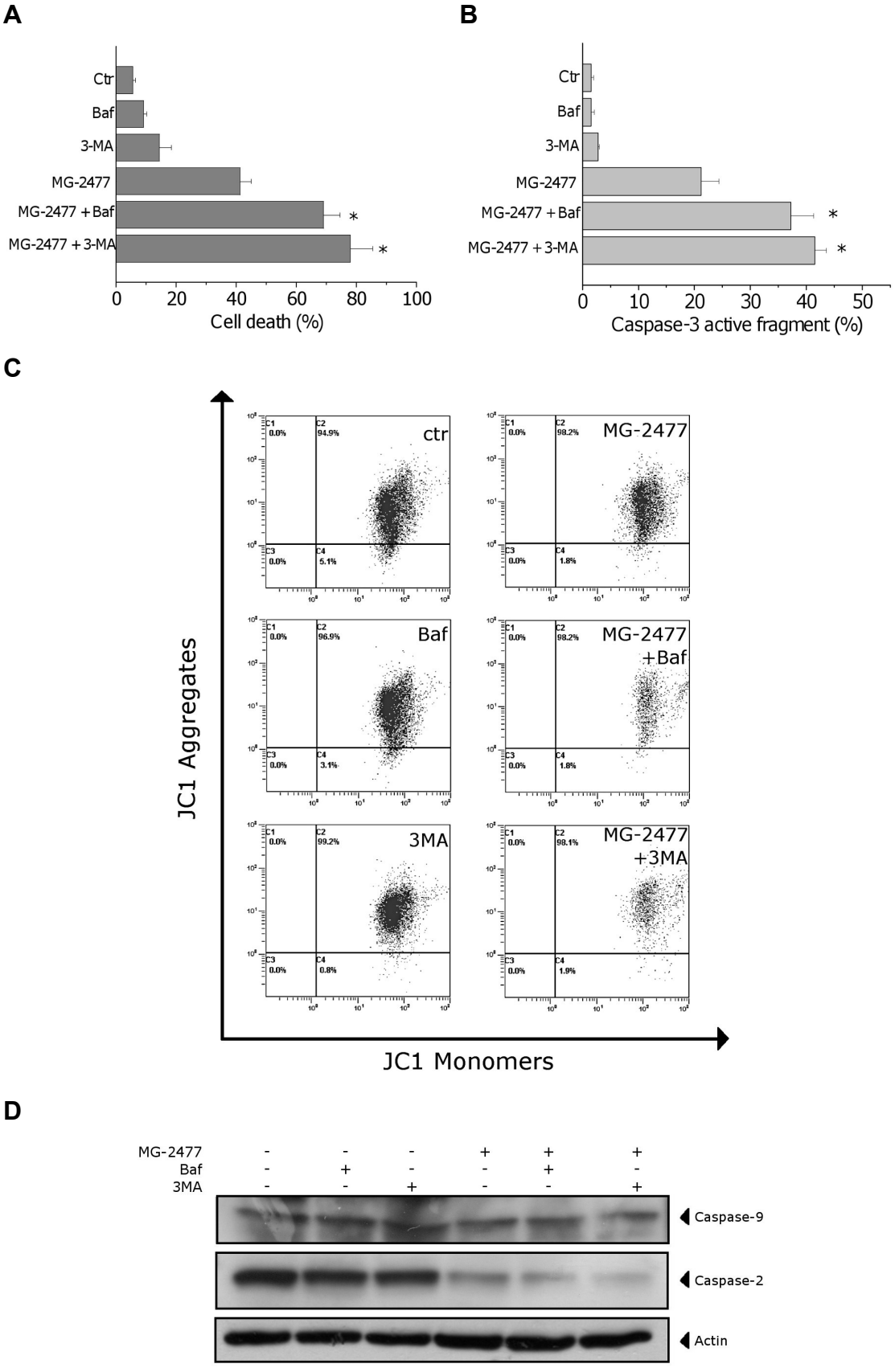

Figure 8. A Cells were incubated with 1 μM MG-2477 in the presence or absence of 3-MA (1 mM) or bafilomycin A1 (2 nM) for 48 h. Cell death was determined by flow cytometric analysis of Annexin-V and PI uptake. Mean ± SEM of three independent experiments. * $p<0.01$ vs MG-2477 alone. **B** Cells were incubated with 1 μM MG-2477 in the presence or absence of 3-MA (1 mM) or bafilomycin A1 (2 nM) for 48 h. Cells were stained with an anti-human active caspase-3 fragment monoclonal antibody conjugated to FITC. Data obtained by flow cytometric analysis is expressed as the percentage of caspase-3 active fragment positive cells. Mean ± SEM of three independent experiments. *$p<0.01$ vs MG-2477 alone. **C** Representative histograms of flow cytometric analysis of mitochondrial depolarization after treatment of A549 cells with MG-2477 (1 μM) for 48 h in the presence of 3-MA or bafilomycin A1. **D** Western blot analysis of pro-caspase-9 and pro-caspase-2 after 48 h of MG-2477 (1 μM) in the presence of of 3-MA or bafilomycin A1.

As shown in Figure 8 (Panel A), the presence of bafilomycin A1 or 3-MA significantly increased the percentage of apoptotic cells as detected by the Annexin-V assay. Furthermore, the activation of caspase-3 was also enhanced in the presence of either 3-MA or bafilomycin A1 (Figure 8, Panel B). Importantly, to explore the role of mitochondria when autophagy was inhibited, we analyzed the mitochondrial potential and the activation of caspase-9 in the presence of 3-MA and bafilomycin A1. We did not observe significant variations with respect to the cells treated in the absence of the two inhibitors either of the mitochondrial depolarization (Figure 8, panel C) or of caspase-9 activation (Figure 8, Panel D). In contrast, a potentiation of caspase-2 was observed after treatment of the cells with MG-2477 in the presence of either of the autophagy inhibitors (Figure 8, Panel D).

MG-2477 Induces Inhibition of the PI3K/Akt/mTOR Pathway. PI3K/Akt/mTOR signaling is one of the major pathways activated in cancer cells, including lung cancer cells. This pathway plays a variety of physiological roles, including regulation of cell growth, of the cell cycle and of cell survival. Recent studies have indicated that inhibition of the PI3K/Akt/mTOR pathway is associated with triggering autophagy in cancer cells[15,16].

As shown in Figure 9 (Panel A), treatment with MG-2477 reduced the expression of p85, the regulatory subunit of PI3K after 24 h of treatment and, at the same time, caused a decrease in the phosphorylation (at Ser^{473}) of the Akt protein. Similar responses were observed for the phosphorylated forms of the Akt downstream protein FKHR (Ser^{256}).

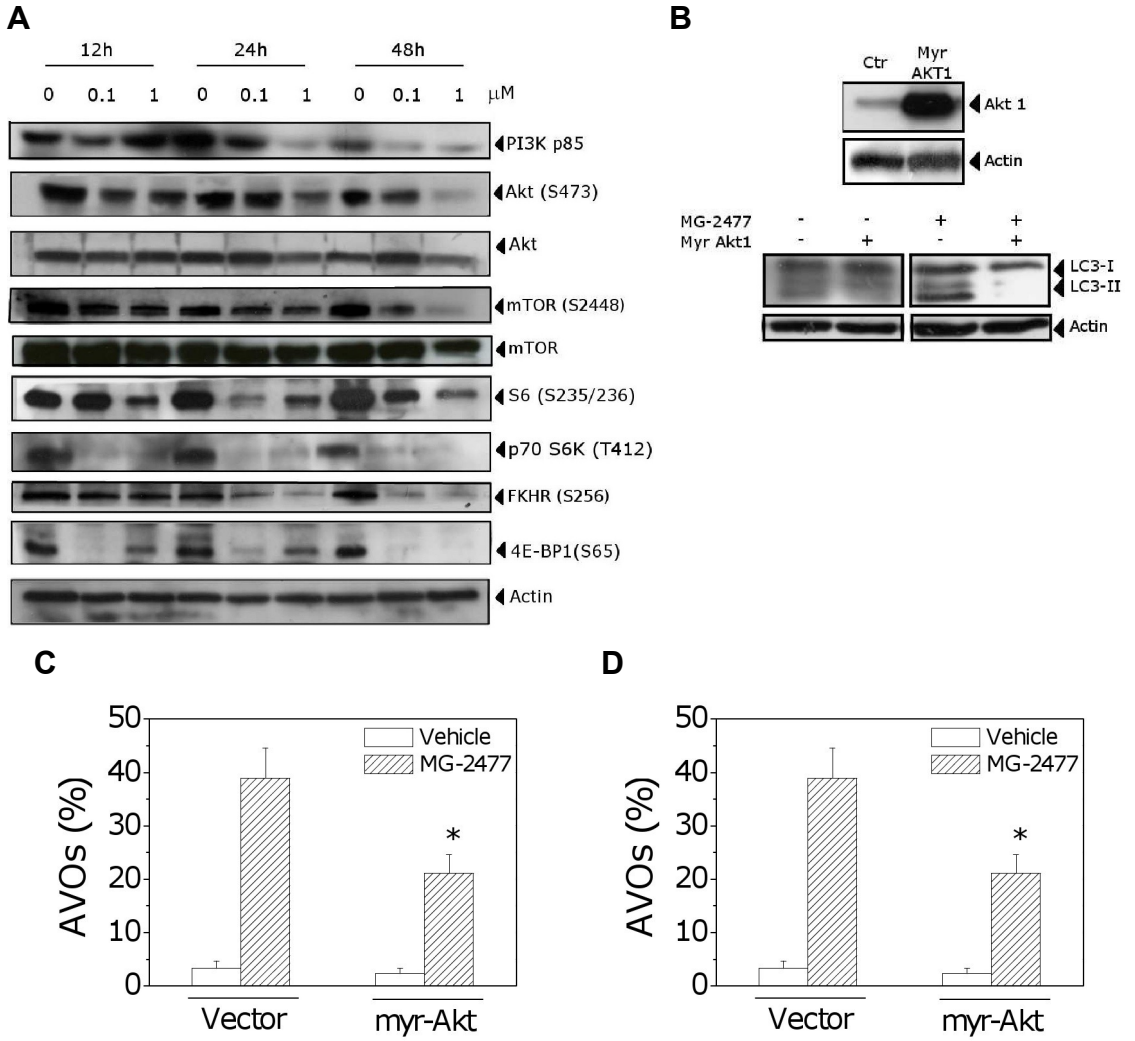

Figure 9. A Effect of MG-2477 treatment on the PI3K/Akt/mTOR pathway. Cells were treated with MG-2477, harvested and subjected to Western blot analysis. **B** A549 cells overexpressing Akt after Myr-Akt transfection (upper). Immunoblot analysis of LC-3 in Myr-Akt transfected cells treated with MG-2477 (1 μM) (lower). **C** Detection of AVO formation in Myr-Akt transfected cells treated with 1 μM MG-2477. Cells were treated for 48 h, stained with AO and analyzed by flow cytometry. Mean ± SEM of three independent experiments. *p<0.01 vs the cells with the empty vector treated with MG-2477. **D** Percentage of viable cells in Myr-Akt transfected cells treated with MG-2477 (1 μM) for 48 h. Mean ± SEM of three independent experiments.

We further investigated the effect of MG-2477 treatment on mTOR activity. Exposure of A549 cells to MG-2477 resulted in diminished levels of the phosphorylated (activated) form of mTOR (Ser^{2448}), while total mTOR levels were not affected by the treatment. MG-2477 treatment also induced a sharp decrease in the phosphorylation of the mTOR targets p70 ribosomal protein S6 kinase and 4E-BP1, revealing a potent inhibitory effect of MG-2477 treatment on Akt/mTOR signaling.

To evaluate the relationship between MG-2477-induced autophagy and the Akt pathway, we transiently transfected A549 cells with a Myr-Akt plasmid, coding

for an active form of Akt. Compared with the control cells, in cells transfected with the vector plasmid the expression of Akt was dramatically increased (Figure 9, Panel B, upper). Then we evaluated the effects of MG-2477 treatment on these cells. As shown in Figure 9 (Panel C), cells overexpressing Akt were refractory to MG-2477-induced autophagy as compared with cells transfected with the empty vector. The cells overexpressing Akt and treated with MG-2477 showed a significant reduction in LC3-II expression (Figure 9, Panel B, lower) and in formation of AVOs (Figure 9, Panel C). In addition, no significant variation in cell viability was observed in the Akt overexpressing cells (Figure 7, Panel D), in good agreement with the data reported by Vanderweele et al. [39] and Asnaghi et al. [40], which showed that Akt up-regulation promotes a selective resistance to different antimicrotubule agents but not other chemotherapic drugs.

Discussion

Previous studies demonstrated that MG-2477 displayed effective antiproliferative activity in numerous cell lines derived from human solid tumors, including multidrug resistant cell lines[17]. In this study we showed that MG-2477 induced depolymerization of tubulin and inhibited normal spindle formation in A549 cells, resulting in mitotic arrest and cell death. The inhibition of tubulin polymerization was similar to that observed with reference compounds such as CA4. Examination of the effects of MG-2477 on [^{3}H]colchicine binding to tubulin revealed that colchicine binding was efficiently inhibited, indicating that MG-2477 binds in the colchicine site. These data were supported by molecular docking analysis.

From the point of view of the cytotoxic mechanism of action of MG-2477, we provided evidence that the compound induced autophagy in A549 cells, followed by apoptotic cell death. Autophagy was morphologically and biochemically characterized, including the appearance in treated A549 cells expressing GFP-LC3 of cytoplasmic vacuoles that displayed punctuate fluorescence indicative of LC3 recruitment to the autophagosome.

Our results showed that MG-2477 treatment decreased the expression of the PI3K p85 regulatory subunit, followed by Akt dephosphorylation on Ser^{473}. The

inhibitory effects of MG-2477 on PI3K/Akt were correlated with the dephosphorylation of FKHR, an Akt downstream protein target. Moreover, exposure of cells to MG-2477 also inactivated mTOR and reduced phosphorylation of its downstream targets p706K and 4E-BP1. Thus, these results are consistent with many recent studies indicating that inhibition of the Akt/mTOR pathway is associated with induction of autophagy in cancer cells[16,41,42].

At present, the precise molecular mechanism that switches between autophagy and apoptosis is not clear. Autophagy and apoptosis can be induced in response to different cellular stresses, and the induction of autophagy/apoptosis can occur sequentially, simultaneously or in a mutually exclusive manner[43]. Our observations indicate that pharmacological inhibition of autophagy with 3-MA or bafilomycin A1 does not activate, but only enhances, apoptotic death, suggesting that autophagy induced by MG-2477 is an adaptive response in A549 cells.

It has been suggested that microtubules are essential for the endocytic and autophagic pathways of membrane trafficking and facilitate autophagosome formation and serve to direct mature autophagosomes for degradation in lysosomes[44]. However, a number of studies have shown that in mammalian cells, the disruption of the microtubule network provokes a delay in autophagy rather than a complete block of this process[45-47]. In particular, Köchl et al.[47] demonstrated this in rat hepatocytes expressing green fluorescent protein (GFP)-LC3. When these cells were pre-treated with the antimitotic agents nocodazole and vinblastine, prior to inducing autophagy, the formation of autophagosomes was facilitated by but did not require microtubules. Moreover, analysis of LC3-II turnover and of the overlap of GFP-LC3-positive vesicles with lysotracker Red-positive lysosomes confirmed that intact microtubules contributed to the fusion of autophagosomes with lysosomes.

Our results are in good agreement with those of Köchl et al. [47] since they showed a co-localization between GFP-LC3 autophagosomes and Lysotracker-positive vesicles that occurred following treatment with MG-2477, suggesting an accumulation of autophagolysosomes. Thus our data indicated that intact microtubules are not essential for targeting and for fusion with lysosomes.

Furthermore, our data indicated that cell death following MG-2477 treatment is

caspase-dependent, as demonstrated by a significant increase in cell viability in the presence of the pan-caspase inhibitor z-VAD.fmk. Some studies, using different drugs, report that autophagy may precede mitochondrial-activated apoptosis [9,48]. An unexpected finding in our study was that mitochondrial functions such as mitochondrial polarization and release of cytochrome *c* were only slightly affected by treatment with MG-2477. This suggested that with MG-2477 treatment mitochondria were not involved in the cell death process. Of note, MG-2477 treatment did not induce activation of caspase-9, one of the major initiator caspases in the mitochondrial apoptosis pathway. Interestingly, caspase-2 seemed to be activated prior to caspase-3 and caspase-7, and the prevention of cell death induced by the selective caspase-2 inhibitor z-VDVAD.fmk indicated the major role played by this caspase. Newer evidence about the functions and activation mechanisms involved in apoptosis indicate that caspase-2 is unique among the caspases, displaying features of both initiator and executioner. Moreover, many recent studies indicate that activation of caspase-2 is fundamental for the induction of apoptosis induced by antimitotic drugs[33,34].

Several lines of evidence suggest that Bcl-2 phosphorylation is associated with the loss of antiapoptotic functions, although, in contrast, many other studies show that Bcl-2 is only a biochemical marker of G2/M phase events[4]. In addition, modulation of Bcl-2 expression can affect the induction of autophagy[49,50]. Our results showed that Bcl-2 is phosphorylated in A549 cells treated with MG-2477 at early time points when hallmarks of apoptosis were not yet evident.

Asnaghi et al.[40] showed that Bcl-2 phosphorylation by antimitotic drugs is regulated by Akt and mTOR. They demonstrated this phenomenon by inhibiting mTOR signaling by inducing the expression of a dominant negative mutant of the Akt kinase in HEK293 cells. The levels of Bcl-2 phosphorylation after nocodazole treatment were higher in comparison with cells transfected with the empty vector. Interestingly, sensitivity to nocodazole was also significant increased. Opposite findings were obtained in HEK293 cells expressing constitutively active Akt. Thus, these results suggest that the level of activity of Akt may regulate Bcl-2 phosphorylation and the apoptotic threshold through the mTOR kinase. Other studies showed that, in cells where Akt is constitutively

activated, the cytotoxic effects of different antimicrotubule agents are reduced[39,51]. However, the effects of these compounds are enhanced when a specific blockade of the Akt signaling pathway is produced. In our study, we did not observe any increase in MG-2477 induced cell death in A549 cells transiently transfected with a constitutively active form of Akt (Myr-Akt), but, at the same time, the cells were considerably more resistant to MG-2477 induced autophagy than cells transfected with the empty vector. Thus, these results strongly indicate that MG-2477-induced autophagy could be mediated by a block of the Akt pathway.

In summary, the findings presented here indicate that MG-2477 is highly effective in reducing cell viability and that the reduced survival of A549 cells is associated with an initial autophagy that may be mediated by inhibition of the Akt/mTOR pathway. Autophagy is not the major cause of cell death but represents an adaptive early response to cellular stress that could enhance cell survival by retarding apoptosis. These results indicate that inhibition of autophagy might increase the efficacy of MG-2477 and that it could be a potential strategy for enhancing the chemotherapeutic effects of this compound.

Materials and Methods

Chemicals. 3-cyclopropylmethyl-7-phenylpyrrolo[3,2-*f*]quinolinone, abbreviated MG-2477, was synthesized at the Department of Pharmaceutical Sciences, University of Padova, Italy, as previously described [17]. 3-Methyladenine (3-MA), *N*-benzyloxycarbonyl-Val-Ala-DL-Asp-fluoromethylketone (z-VAD.fmk), *N*-benzyloxycarbonyl-Val-Asp-Val-Ala-Asp-fluoromethylketone (z-VDVAD.fmk) and bafilomycin A1 were purchased from Sigma-Aldrich (Milano, Italy), *N*-benzyloxycarbonyl-Leu-Glu-His-Asp-fluoromethylketone (z-LEHD.fmk), was purchased from Vinci-Biochem (Vinci, Italy).

Cell Lines and Growth Inhibition Assay. The human non-small cell lung carcinoma (A549) cell line was purchased from the American Type Culture Collection . The cells were grown in Dulbecco's modified Eagle's medium (Invitrogen, Milano, Italy), supplemented with 10% heat-inactivated fetal bovine serum, 100 U/mL penicillin G and 10 µg/mL streptomycin at 37 °C in a

humidified incubator with 5% CO_2.

The cytotoxic activity of MG-2477 was determined using a standard 3-[4,5-dimethylthiazol-2-yl]-2,5-diphenyltetrazodium bromide (MTT) based colorimetric assay (Sigma-Aldrich, Milano, Italy). Briefly, A549 cells were seeded at a density of $8x10^3$ cells/well in 96-well microtiter plates. After 24 h, cells were exposed to the test compound. After different times, cell survival was determined by the addition of an MTT solution as described previously[18].

In Vitro Microtubule Assembly Assay and Colchicine Binding to Tubulin. To evaluate the effect of MG-2477 on tubulin assembly *in vitro*, varying concentrations were preincubated with 10 μM tubulin in glutamate buffer at 30˚C and then cooled to 0 ˚C. After addition of GTP, the mixtures were transferred to 0 °C cuvettes in a recording spectrophotometer and warmed to 30 °C, and the assembly of tubulin was observed turbidimetrically at 350 nm. The IC_{50} was defined as the compound concentration that inhibited the extent of assembly by 50% after a 20 min incubation[19]. The capacity of compound MG-2477 to inhibit colchicine binding to tubulin was measured as described [20], except that the reaction mixtures contained 1 μM tubulin, 5 μM [^{3}H]colchicine (Amersham) and 1 μM test compound.

Mitotic Index Determination. A549 cells were incubated with MG-2477 for 12 and 24 h prior to centrifugation, and the cell pellet was resuspended in 10 mL of 75 mM KCl at room temperature. After 10 min, 1 mL of methanol–acetic acid (3:l) as fixative was slowly added with mild agitation of the mixture.

Slides were prepared after cells were repelleted, washed twice with 10 mL of the fixative, and resuspended in fixative. After drying, samples were stained with Giemsa solution. Two hundred cells/treatment were scored for the presence of mitotic figures by optical microscopy, and the mitotic index was calculated as the proportion of cells with mitotic figures.

Molecular Docking Simulations-Target Structures. Tubulin complexed with colchicine was retrieved from the PDB (PDB code: 1SA0)[21]. Hydrogen atoms were added, using standard geometries, to the protein structure with the Molecular Operation Environment (MOE, version 2009.10) program[22].

Molecular Docking Protocol. MG-2477 was built using the "Builder" module of MOE, and it was docked into the putative colchicine site using flexible MOE-Dock methodology. The purpose of MOE-Dock is to search for favorable binding configurations between a small, flexible ligand and a rigid macromolecular target. Searching is conducted within a user-specified 3D docking box, using the "tabù search" protocol[23] and the MMFF94 force field[24]. Charges for ligands were imported from the MOPAC program[25] output files. MOE-Dock performs a user-specified number of independent docking runs (50 in the present case) and writes the resulting conformations and their energies to a molecular database file. The resulting MG-2477/tubulin complexes were subjected to MMFF94 all-atom energy minimization until the *rms* of the conjugate gradient was <0.1 kcal mol^{-1} $Å^{-1}$. GB/SA approximation[26] was used to model the electrostatic contribution to the free energy of solvation in a continuum solvent model. The interaction energy values were calculated as the energy of the complex minus the energy of the ligand minus the energy of tubulin: $DE_{inter} = E_{(complex)} - (E_{(L)} + E_{(Tubulin)})$.

Immunocytochemistry. A549 cells ($5x10^3$/well) were seeded on chamber slides. After 24 h, MG-2477 (0.1-1 μM) was added to the culture medium, and cells were incubated for a further 24-48 h. As described previously[27], cells were fixed in cold 4% paraformaldehyde for 15 min, rinsed and stored prior to analysis. Primary antibody staining was performed for β-tubulin (Millipore, Billerica, MA). After incubation, cells were washed and incubated with a secondary antibody conjugated to Alexa Fluor 594 (1:2000, Invitrogen, Milano, Italy). Cells were counterstained with 4',6-diamidino-2-phenylindole (DAPI) (Sigma-Aldrich, Milano, Italy). Cells were examined by fluorescence microscopy (Nikon Eclipse 80i, Melville, NY, USA).

Externalization of Phosphatidylserine (PS). Surface exposure of PS by apoptotic cells was measured by flow cytometry with a Coulter Cytomics FC500 (Beckmann Coulter, USA) instrument by adding Annexin V-FITC to cells according to the manufacturer's instructions (Annexin-V Fluos, Roche Diagnostic, Monza, Italy). Simultaneously, the cells were stained with propidium iodide (PI).

Analysis of Cell Cycle Distribution. $5x10^5$ A549 cells in exponential growth were treated with different concentrations of MG-2477 for different times. After the incubation , cells were collected, centrifuged and fixed with ice-cold ethanol (70%) and analyzed as described previously[18].

Assessment of Mitochondrial Changes and Release of Cytochrome C. The mitochondrial membrane potential was measured with the lipophilic cation 5,5',6,6'-tetrachlo-1,1',3,3'-tetraethylbenzimidazol-carbocyanine (JC-1, Molecular Probes, Eugene, OR, USA),while the production of reactive oxygen species (ROS) was followed by flow cytometry using the fluorescent dyes hydroethidine (HE, Molecular Probes, Eugene, OR, USA) and 2',7'-dichlorodihydrofluorescein diacetate (H_2DCFDA, Molecular Probes, Eugene, OR, USA), as previously described[18]. Cytochrome *c* release was analyzed by immunocytochemistry using a commercial kit (Innocyte flow cytometric cytochrome c release kit, from Calbiochem, Milano Italy) following the manufacturer's instructions.

Flow Cytometric Analysis of Caspase-3. Caspase-3 activation in A549 cells was evaluated by flow cytometry using a human active caspase-3 fragment antibody conjugated to FITC (BD Biosciences, Milano, Italy). Briefly, after treatment, the cells were collected by centrifugation and resuspended in Perm/Wash™ (BD Biosciences, Milano, Italy) buffer for 20 min, washed and then incubated for 30 min with the antibody. After this period, the cells were washed and analyzed by flow cytometry.

Examination of LC3 Translocation. A549 cells were cultured on 6 well dishes in a complete medium for 24 h. Cells were transfected with green fluorescent protein labeled LC3 (GFP-LC3) using Effectene Transfection Reagent (Qiagen, Milano, Italy) and incubated for another 24 h to permit expression of the GFP-LC3 fusion protein. The localization of LC3 in transfected cells after treatment with MG-2477 was determined by fluorescence microscopy.

Detection of Acidic Vesicular Organelles (AVOs) and Autophagic Vacuoles. To detect and quantitate AVOs in treated cells, we performed flow

cytometric analysis of acridine orange (AO, Molecular Probes, Eugene, OR, USA) stained cells as described[10]. The formation of AVOs was also visualized by confocal microscopy. Briefly, at the appropriate time points following treatment with MG-2477, cells were incubated for 15 min with medium containing 0.5 μg /mL of AO. The AO was removed, and fluorescent micrographs were taken with a video confocal microscope (Nikon Eclipse 80i, Melville, NY, USA), using a Nikon Nir Apo 60X/1.0W water immersion objective. Autophagic vacuoles were detected with monodansylcadaverine (MDC, Invitrogen Milano, Italy). After incubation of the cells with MG-2477, cells were incubated with MDC (50 μM) in HBSS at 37 °C for 15 min, then washed, and micrographs were prepared as described above.

Western Blot Analysis. Cells were treated with MG-2477 and, after different times, were collected, centrifuged and washed two times with ice cold phosphate-buffered saline (PBS). The pellet was then resuspended in lysis buffer as described[27]. The protein concentration in the supernatant was determined using the BCA protein assay (Pierce, Milano, Italy). Equal amounts of protein (10-20 μg) were resolved using SDS-PAGE gel electrophoresis and transferred to PVDF Hybond-p membranes (GE Healthcare, Milano, Italy). Membranes were blocked with ECL-Blocking Solution (GE Healthcare, Milano, Italy) overnight, with rotation at 4 °C. Membranes were then incubated with primary antibodies against cyclin A (Upstate) , cyclin B1(BD), p53, Bcl-2, Bcl-XL, Bax, X-linked inhibitor of apoptosis protein (XIAP), PARP, procaspase-9, procaspase-8, procaspase-2, cleaved caspase-7, Akt, p-Akt^{Ser473}, mTOR, p-mTor^{Ser2448} (Cell Signaling, Milano, Italy), p21$^{cip1/waf1}$, β-actin (Sigma Aldrich, Milano, Italy), and LC-3 (Novus Biologicals, Milano, Italy) overnight. Membranes were next incubated with peroxidase-conjugated secondary antibodies for 60 min. All membranes were visualized using ECL Advance (GE Healthcare, Milano, Italy) and exposed to Hyperfilm MP (GE Healthcare, Milano, Italy). To ensure equal protein loading, each membrane was stripped and reprobed with anti-b-actin antibody.

Plasmids and Transfection. Myrystoylated Akt (Myr-Akt) plasmid was purchased from Addgene (Cambridge, MA, USA). Cells were seeded into 6

well-plates the day before transfection. Transfection of Myr-Akt was performed with Effectene Transfection Reagent (Qiagen, Milano, Italy) according to the manufacturer's protocol.

Statistical Analysis. Unless indicated otherwise, results are presented as mean ± S.E.M. The differences between different treatments were analyzed using the two-sided Student's *t* test. P values lower than 0.05 were considered significant.

References

1. Hadfield JA, Ducki S, Hirst N, McGrow AT. Tubulin and microtubules as targets for anticancer drugs. Prog Cell Cyc Res 2003; 5:309-325.
2. Jordan MA, Wilson L. Microtubules as a target for anticancer drugs. Nature Rev Cancer 2004;4:253-265
3. Dumontet C, Jordan MA. Microtubule-binding agents: a dynamic field of cancer therapeutics. Nat Rev Drug Discov 2010; 9:790-803.
4. Mollinedo F, Gajate C. Microtubules, microtubule-interfering agents and apoptosis. Apoptosis 2003; 8:413-50.
5. Klionsky DJ. Autophagy: from phenomenology to molecular understanding in less than a decade. Nat Rev Mol Cell Biol 2007; 8:931-7.
6. Rubinsztein DC, Gestwicki JE, Murphy LO, Klionsky DJ. Potential therapeutic applications of autophagy. Nat Rev Drug Discov 2007; 6:304-12.
7. Kanzawa T, Germano IM, Komata T, Ito H, Kondo Y, Kondo S. Role of autophagy in temozolomide-induced cytotoxicity for malignant glioma cells. Cell Death Differ 2004; 11:448-57.
8. Laane E, Tamm Pokrovskaja K, Buentke , Ito K, Kharazina P, Oscarsson J et al. Cell death induced by dexamethasone in lymphoid leukemia is mediated through initiation of autophagy. Cell Death Differ 2009 1018-1029.
9. Abedin MJ, Wang D, McDonnell MA, Lehmann U, Kelekar A. Autophagy delays apoptotic death in breast cancer cells following DNA damage. Cell Death Differ 2007; 14:500-10.
10. Paglin S, Hollister T, Delohery T, Hackett N, McMahill M, Sphicas E, et al. A novel response of cancer cells to radiation involves autophagy and formation of acidic vesicles. Cancer Res 2001;61: 439–444.
11. Zeng X, Kinsella TJ. Mammalian target of rapamycin and S6 kinase 1 positively regulate 6-thioguanine-induced autophagy. Cancer Res 2008;68: 2384-89.
12. Arthur CR, Gupton JT, Kellogg GE, Yeudall WA, Cabot MC, Newsham IF, et al. Autophagic cell death, polyploidy and senescence induced in breast tumor cells by the substituted pyrrole JG-03-14, a novel microtubule poison. Biochem Pharmacol 2007; 74:981-91.

13. Eum KH, Lee M. Crosstalk between autophagy and apoptosis in the regulation of paclitaxel-induced cell death in v-Ha-ras-transformed fibroblasts. Mol Cell Biochem 2011; 348:61-68.

14. Karna P, Zughaier S, Pannu V, Simmons R, Narayan S, Aneja R. Induction of reactive oxygen species-mediated autophagy by a novel microtubule-modulating agent. J Biol Chem 2010; 285: 18737-48

15. Guertin DA, Sabatini DM. Defining the role of mTOR in cancer. Cancer Cell 2007;1:9-22.

16. Takeuchi H, KondoY, Fujiwara K, Kanzawa T, Aoki H, Mills GB et al. Synergistic augmentation of rapamycin-induced autophagy in malignant glioma cells by phosphatydilinoditol 3-kinase/protein kinase B inhibitors. Cancer Res 2005;65:3336-46.

17. Gasparotto V, Castagliuolo I, Ferlin MG. 3-substituted 7-phenyl-pyrroloquinolinones show potent cytotoxic activity in human cancer cell lines. J Med Chem 2007;50: 5509-5513.

18. Viola G, Fortunato E, Cecconet L, Del Giudice L, Dall'Acqua F, Basso G. Central role of mitochondria and p53 in PUVA-induced apoptosis in human keratinocytes cell line NCTC-2544. Tox Appl Pharmacol 2008;227:84-96.

19. Hamel, E. Evaluation of antimitotic agents by quantitative comparisons of their effects on the polymerization of purified tubulin. Cell Biochem Biophys 2003; 38:1-22.

20. Verdier-Pinard, P.; Lai J.-Y.; Yoo, H.-D.; Yu, J.; Marquez, B.; Nagle D. G.; et al. Structure-activity analysis of the interaction of curacin A, the potent colchicine site antimitotic agent with tubulin and effects of analogs on the growth of MCF-7 breast cancer cells. Mol Pharmacol 1998; 53:62-76

21. Ravelli RB, Gigant B, Curmi PA, Jourdain I, Lachkar S, Sobel A, et al. Insight into tubulin regulation from a complex with colchicine and a stathmin-like domain. Nature 2004; 428: 198-202.

22. MOE (Molecular Operating Environment), version 2008.10; software available from Chemical Computing Group Inc. (1010 Sherbrooke Street West, Suite 910, Montreal, Quebec, Canada H3A 2R7); http://www.chemcomp.com

23. Baxter C.A, Murray CW, Clark DE, Westhead DR, Eldridge MD. Flexible docking using tabù search and an empirical estimate of binding affinity. Proteins: Structure, Function and Genetics 1998; 33: 367-382.

24. Halgren T. Merck Molecular Force Field. I. Basis, form, scope, parameterization, and performance of MMFF94. J Comput Chem 1996; 17: 490-519.

25. Stewart, J. J. P. MOPAC 7; Fujitsu Limited: Tokyo, Japan, 1993.

26. Wojciechowski M, Lesyng B. Generalized Born Model: analysis, refinement and applications to proteins. J Phys Chem B 2004; 108: 18368-376.

27. Pistollato F, Abbadi S, Rampazzo E, Viola G, Della Puppa A, Cavallini L, et al. Succinate and hypoxia antagonizes 2-deoxyglucose effects on glioblastoma. Biochem Pharm 2010; 80:1517-27.

28. Vermes I, Haanen C, Steffens-Nakken H, Reutelingsperger C. A novel assay for apoptosis. Flow cytometric detection of phosphatidylserine expression on early apoptotic cells using fluorescein labelled Annexin V. J Immun Method 1995; 184:39-51.

29. Ly, J. D, Grubb, D. R. Lawen, A. The mitochondrial membrane potential (□□m) in apotosis. Apoptosis 2003;3:115-128.

30. Green DR, Kroemer G. The pathophysiology of mitochondrial cell death. Science 2005; 305:626-29.

31. Kumar S. Caspase function in programmed cell death. Cell Death Differ 2007;14:32-43.

32. Vakifahmetoglu-Norberg H, Zhivotovsky B. The unpredictable caspase-2: what can it do? Trends Cell Biol 2010; 20:150-159.

33. Mhaidat NM, Wang Y, Kiejda KA, Zang XD, Hersey P. Docetaxel-induced apoptosis in melanoma cells is dependent on activation of caspase-2. Mol Cancer Ther 2007;6:752-761.

34. Ho LH, Read SH, Dorstyn L, Lambrusco L, Kumar S. Caspase-2 is required for cell death induced by cytoskeletal disruption. Oncogene 2008; 27:3393-3404.

35. Klionsky DJ, Abeliovich H, Agostinis P, Agrawal DK, Allev G, Askew DS et al. Guidelines for the use and interpretation of assay for monitoring autophagy in higher eukaryotes. Autophagy 2008; 4:151-175

36. Groth-Pedersen L, Ostenfeld MS, Hoyer-Hansen M, Nylandsted J, Jaattela M. Vincristine induces dramatic lysosomal changes and sensitizes cancer cells to lysosome-destabilizing siramesine. Cancer Res 2007;67:2217-25.

37. Boya P, Gonzalez-Polo RA, Casares N, Perfettini JL, Dessen P, Metiver D., et al. Inhibition of macroautophagy triggers apoptosis. Mol Cell Biol 2005; 25:1025-40.

38. Gonzalez-Polo R.A., Boya P., Pauleau A.L., Jalil A., Larochette N., Souquere S., et al. The apoptosis/autophagic paradox: autophagic vacuolisation before apoptotic cell death. J Cell Sci 2005; 118:3091-3102.

39. VanderWeele DJ, Zhou R, Rudin CM. Akt up-regulation increases resistance to microtubule-directed chemotherapeutic agents through mammalian target of rapamycin. Mol Cancer Ther 2004; 3:1605-13.

40. Asnaghi L, Calastretti A, Bevilacqua A, D'Agnano I, Gatti G, Canti G, et al. Bcl-2 phosphorylation and apoptosis activated by damaged microtubules require mTOR and are regulated by Akt. Oncogene 2004; 23:5781-91.

41. Saiki S, Sasazawa Y, Imamichi Y, Kawajiri S, Fujimaki T, Tanida I. Caffeine induces apoptosis by enhancement of autophagy via PI3K/Akt/mTOR/p70S6K inhibition. Autophagy 2011; 7:176-87.

42. Degtyarev M, De Mazière A, Orr C, Lin J, Lee BB, Tien JY, et al. Akt inhibition promotes autophagy and sensitizes PTEN-null tumors to lysosomotropic agents. J Cell Biol 2008; 183: 101-116.

43. Eisenberg-Lerner A, Bialik S, Simon HU, Kimchi A. Life and death partners: apoptosis, autophagy and the cross-talk between them. Cell Death Differ 2009; 16: 966-975.

44. Monastyrska I, Rieter E, Klionsky DJ, Reggiori F. Multiple roles of the cytoskeleton in autophagy. Biol Rev 2009;84:431-448.

45. Fass E, Shvets E., Degani I., Hirschberg K., Elazar Z. Microtubules support production of starvation-induced autophagosomes but not their targeting and fusion with lysosomes. J Biol Chem 2006;281:36303–16.

46. Jahreiss L, Menzies FM, Rubinsztein, DC The itinerary of autophagosomes: from peripheral formation to kiss-and-run fusion with lysosomes. Traffic 2008;9,574–87.

47. Köchl R, Hu XW, Chan EY, Tooze SA Microtubules facilitate autophagosome formation and fusion of autophagosomes with endosomes. Traffic 2006;7:129–45.

48. Sy LK, Yan SC, Lok CN, Man RYK, Che CM. Timosaponin AIII induces autophagy preceding mitochondria-mediated apoptosis in HeLa cancer cells. Cancer Res 2008;68: 10229-237.

49. Pettingre S, Tassa A, Qu X, Liang XH, Mizushima N, Packer M et al. Bcl-2 antiapototic proteins inhibit Beclin 1-dependent autophagy. Cell 2005;122:927-939.

50. Levine B, Sinha S, Kroemer G. Bcl-2 family members: dual regulator of apoptosis and autophagy. Autophagy 2008;4:600-606.

51. Fuijiwara Y, Hosokawa Y, Watanabe K, Tanimura S, Ozaki K, Kohno M. Blockade of the phosphatidylinositol-3-kinase-Akt signaling pathway enhances the induction of apoptosis by microtubule-destabilizing agents in tumor cells in which the pathway is constitutively activated. Mol Cancer Ther 2007;6:1133-142.

6. CONCLUSIONS

We proposed the mechanisms of action of three classes of tubulin polymerization inhibitors, colchicine site binders, with similar or higher antiproliferative activity than the respective lead compounds.

About combretastatin A4 derivatives, we show that molecular structures that retain the bioactive configuration, afforded by the cis-double bond present in CA-4, increase their stability and their efficacy as tubulin binding agents and as antiproliferative compounds. In particular, the new restricted molecules contain an heterocycles ring such as diaryl-triazole ring, aroylthiazoles, benzo-thiopenes, and an amino-thiazole ring system in place of the ethylene bridge. SAR studies show that the substitution pattern on the phenyl at the 5-position of the thiazole-, tetrazole-, triazole- ring system plays an important role for antitubulin and antiproliferative activities, and this is supported by the molecular docking studies.

All the series synthesized presented at least one compound comparable to CA-4, as inhibitor of tubulin polymerization, and that showed antiproliferative activity derived from a interference with microtubule assembly.

As general mechanisms of action, the interaction of such compounds with tubulin colchicine site leads to cell cycle arrest in the G2/M phase with a consequent mitotic block; treatment of HeLa cells induces increased expression of cyclin B1, which then phosphorylates cdc25c. The mitotic arrest caused by antimitotic agents is described in association with the loss of mitochondrial membrane potential, generation of ROS, activation of caspase-3 with cleavage of PARP and consequent induction of apoptosis. In particular, in all of the combretastatin derivatives studied but amino-thiazoles, flow cytometry analysis show ROS production, depolarization of mitochondrial potential and thus the activation of intrinsic pathway of apoptosis, typical of antimitotc agent. We also demonstrated that the 1,5-Disubstituted Tetrazoles induce a decrease of X-linked inhibitor of apoptosis (XIAP). However, 2-amino-4-(3',4',5'-trimethoxyphenyl)-5-(4'-ethoxyphenyl) thiazole induces apoptosis only partially dependent on caspase activation and without involving mitochondrial depolarization. Preliminary experiments suggest that, in addition to apoptosis, cells are also killed by mitotic catastrophe as indicated by morphological

changes including formation of giant cells and multinucleated cells. Mitotic catastrophe has been described as a mechanism of cell death that occurs in response to treatment with antimitotic agents.

Several compounds of the described series are also active in suppressing the growth of drug resistant cells overexpressing the efflux pump glycoprotein P and cells with mutant tubulin, suggesting that these derivatives might be useful in treating drug-refractory patients.

Even more importantly, 2-(pyrrolidinin-1-yl)-4-amino-5-(3',4',5'-trimethoxybenzoyl)thiazole and 1-(3',4',5'-trimetoxiphenyl)-5-aryltetrazole has higher significant *in vivo* activity in a colon cancer xenograft than the reference compound CA-4.

These findings suggest this derivatives, that retain the bioactive configuration of combretastatin-A4, are promising new antimitotic compounds for the potential treatment of cancer.

Similar mechanisms of action has been described for chalcones series of molecules, which are able to induce cell cycle arrest in G2/M phase and cell death by the activation of the intrinsic pathway with mitochondrial involvement. Further analysis of the molecular mechanism of action of these compounds and their efficacy in *in vivo* models are needed.

Pyrroloquinolinones derivatives exibit potent inhibition of tubulin polymerization and high affinity to colchicine binding site too. SAR studies show that the phenyl in position 7 and a hydrophobic group at the N-pyrrole are essential structural features for potent cytotoxic activity. Several compounds of this series have cellular effects typical for microtubule interacting agents, causing accumulation of cell in G2/M phase of the cell cycle and cytotoxicity cells at sub-micromolar concentration. Moreover we found these compounds to be potent inducers of apoptosis markers associated with alteration in many cellular signalling pathways, such as the proteolitic activation of caspase-3 occoured with subsequent PARP cleavage and the downregulation of Bcl-2. Interestingly these compounds present a stronger antiproliferative activity in a series of leukemia cell lines compared to solid tumors. Although still unexplored this effect is worthwhile to further investigation in the next future.

The detailed mechanism of action of MG-2477 (3-cyclopropylmethyl-7-phenyl-3*H*-pyrrolo[3,2-*f*]quinolin-9(6*H*)-one), the most cytotoxic and tubulin inhibitor

between pyrroloquinolinones agents, was investigated in a non-small cell lung carcinoma cell line (A549). MG-2477 displayed effective antiproliferative activity in numerous cell lines derived from human solid tumors, including multidrug resistant cell lines. In particular this compound induces depolymerization of tubulin, inhibits normal spindle formation and, as a late event, leads to the activation of caspase-dependent cell death. Differently by the classical antimitotic agents, treatment with MG-2477 only slightly affects mitochondrial functions such as mitochondrial polarization and release of cytochrome *c.* The treatment doesn't induce activation of caspase-9, thus canonical intrinsic pathway is not followed to activate apoptosis and we found caspase 2 as the main actress of the apoptotic process. Our findings indicate that MG-2477 is highly effective in reducing cell viability, and that the reduced survival of A549 cells is associated with an initial autophagy that may be mediated by inhibition of the Akt/mTOR pathway. We described autophagy not as the major cause of cell death but as an adaptive early response to cellular stress, that could enhance cell survival by retarding apoptosis.

Resistance to Vincristine mediated by AKT activity[13], and the activation of autophagy in response to Paclitaxel treatment[9] have been described, but this is the first evidence of a microtubule binding compound able to modulate Akt signalling and to directly induce autophagy. These results indicate that inhibition of autophagy might increase the efficacy of MG-2477 and that it could be a potential strategy for enhancing the chemotherapeutic effects of this compound. Further analysis are needed to study the efficacy and the mechanism of action of this compound *in vivo* models.

7. REFERENCES

1. Dumontet C, Jordan MA. *Microtubule-binding agents: a dynamic field of cancer therapeutics.* Nat Rev Drug Discov. 2010 Oct;9(10):790-803

2. Conde C, Cáceres A. *Microtubule assembly, organization and dynamics in axons and dendrites.* Nat Rev Neurosci. 2009 May;10(5):319-32.

3. Stanton RA, Gernert KM, Nettles JH, Aneja R. *Drugs that target dynamic microtubules: a new molecular perspective.* Med Res Rev. 2011 May;31(3):443-81.

4. Kavallaris M. *Microtubules and resistance to tubulin-binding agents.* Nat Rev Cancer. 2010 Mar;10(3):194-204.

5. Ecsedy JA, Manfredi M, Chakravarty A, and D'Amore N. *Current and next generation antimitotic therapies in cancer*, Signaling Pathways in Cancer Pathogenesis and Therapy, 1st edition (Ed.) D.A. Frank, 2012, pp.5-21.

6. Honore S, Pasquier E, Braguer D. *Understanding microtubule dynamics for improved cancer therapy.* Cell Mol Life Sci. 2005 Dec;62(24):3039-56.

7. Haldar S, Basu A, Croce CM. *Bcl2 is the guardian of microtubule integrity.* Cancer Res. 1997 Jan 15;57(2):229-33.

8. Wei Y, Sinha S, Levine B. *Dual role of JNK1-mediated phosphorylation of Bcl-2 in autophagy and apoptosis regulation.* Autophagy. 2008 Oct;4(7):949-51.

9. Eum KH, Lee M. *Crosstalk between autophagy and apoptosis in the regulation of paclitaxel-induced cell death in v-Ha-ras-transformed fibroblasts.* Mol Cell Biochem. 2011 Feb;348(1-2):61-8.

10. Vakifahmetoglu H, Olsson M, Zhivotovsky B. *Death through a tragedy: mitotic catastrophe.* Cell Death Differ. 2008 Jul;15(7):1153-62.

11. Galmarini CM, Kamath K, Vanier-Viornery A, Hervieu V, Peiller E, Falette

N, Puisieux A, Ann Jordan M, Dumontet C. *Drug resistance associated with loss of p53 involves extensive alterations in microtubule composition and dynamics.* Br J Cancer. 2003 Jun 2;88(11):1793-9.

12. Asnaghi L, Calastretti A, Bevilacqua A, D'Agnano I, Gatti G, Canti G, Delia D, Capaccioli S, Nicolin A. *Bcl-2 phosphorylation and apoptosis activated by damaged microtubules require mTOR and are regulated by Akt.* Oncogene. 2004 Jul 29;23(34):5781-91.

13. VanderWeele DJ, Zhou R, Rudin CM. *Akt up-regulation increases resistance to microtubule-directed chemotherapeutic agents through mammalian target rapamycin.* Mol Cancer Ther. 2004 Dec;3(12):1605-13.

14. Romagnoli R, Baraldi PG, Carrion MD, Cruz-Lopez O, Cara CL, Basso G, Viola G, Khedr M, Balzarini J, Mahboobi S, Sellmer A, Brancale A, Hamel E. *2-Arylamino-4-amino-5-aroylthiazoles. "One-pot" synthesis and biological evaluation of a new class of inhibitors of tubulin polymerization.* J Med Chem. *2009 Sep 10;52(17):5551-5.*

15. Gasparotto V, Castagliuolo I, FerlinMG. *3-substituted 7-phenyl-pyrroloquinolinones show potent cytotoxic activity in human cancer cell lines.* J Med Chem. 2007 Nov 1;50(22):5509-13.

16. Romagnoli R, Baraldi PG, Cruz-Lopez O, Lopez Cara C, Carrion MD, Balzarini J, Hamel E, Basso G, Bortolozzi R, Viola G. *Symmetrical alpha-bromoacryloylamido diaryldienone derivatives as a novel series of antiproliferative agents. Design, synthesis and biological evaluation.* Bioorg Med Chem Lett. 2010 May 1;20(9):2733-9.

17. Romagnoli R, Baraldi PG, Cruz-Lopez O, Lopez Cara C, Carrion MD, Brancale A, Hamel E, Chen L, Bortolozzi R, Basso G, Viola G. *Synthesis and antitumor activity of 1,5-disubstituted 1,2,4-triazoles as cis-restricted combretastatin analogues.* J Med Chem. 2010 May 27;53(10):4248-58.

18. Romagnoli R, Baraldi PG, Cara CL, Hamel E, Basso G, Bortolozzi R, Viola G. *Synthesis and biological evaluation of 2-(3',4',5'-*

trimethoxybenzoyl)-3-aryl/arylaminobenzo[b]thiophene derivatives as a novel class of antiproliferative agents. Eur J Med Chem. 2010 Dec;45(12):5781-91.

19. Romagnoli R, Baraldi PG, Brancale A, Ricci A, Hamel E, Bortolozzi R, Basso G, Viola G. *Convergent synthesis and biological evaluation of 2-amino-4-(3',4',5'-trimethoxyphenyl)-5-aryl thiazoles as microtubule targeting agents.* J Med Chem. 2011 Jul 28;54(14):5144-53.

20. Romagnoli R, Baraldi PG, Lopez Cara C, Salvador MK, Bortolozzi R, Basso G, Viola G, Balzarini J, Brancale A, Fu XH, Li J, Zhang SZ, Hamel E.*One-Pot Synthesis and Biological Evaluation of 2-Pyrrolidinyl-4-Amino-5-(3',4',5'-Trimethoxybenzoyl)Thiazole: a Unique, Highly Active Antimicrotubule Agent.* Eur J Med Chem. 2011 Dec;46(12):6015-24.

21. Romagnoli R, Baraldi PG, Salvador MK, Preti D, Tabrizi MA, Brancale A, Fu XH, Li J, Zhang SZ, Hamel E, Basso G, Bortolozzi R, and Viola G. *Synthesis and Evaluation of 1,5-Disubstituted Tetrazoles as Rigid Analogues of Combretastatin A-4 with Potent Antiproliferative and Antitumor Activity*. J Med Chem. 2012 Jan 12;55(1):475-88.

22. Ferlin MG, Bortolozzi R, Brun P, Castagliuolo I, Hamel E, Basso G, Viola G. *Synthesis and in vitro evaluation of 3h-pyrrolo[3,2-f]-quinolin-9-one derivatives that show potent and selective antileukemic activity.* ChemMedChem. 2010 Aug 2;5(8):1373-85.

23. Viola G, Bortolozzi R, Hamel E, Moro S, Brun P, Castagliuolo I, Ferlin MG, Basso G. *MG-2477, a new tubulin inhibitor induces autophagy through inhibition of the Akt/mTOR pathway and delayed apoptosis in A549 cells*. Biochem Pharmacol. 2012 Jan 1;83(1):16-26.